APPLICATION OF EARTH OBSERVATIONS AND CHEMICAL TRANSPORT MODELLING TO INVESTIGATE AIR QUALITY AND HEALTH FROM THE CITY TO THE GLOBAL SCALE

by

KARN VOHRA

A thesis submitted to
the University of Birmingham
for the degree of
DOCTOR OF PHILOSOPHY

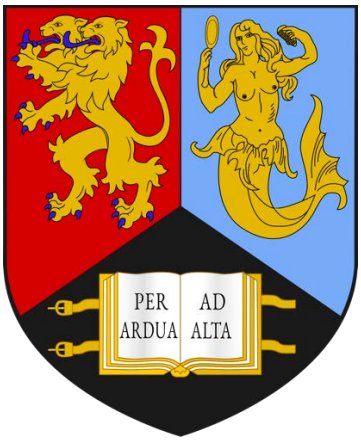

School of Geography, Earth and Environmental Sciences
College of Life and Environmental Sciences
University of Birmingham
September 2021

ABSTRACT

Ambient air pollution is responsible for 4-9 million premature deaths worldwide each year. Routine ground-based monitoring of air quality in cities is sparse and expensive and only includes a handful of pollutants. Most health risk assessment models are derived with limited health outcomes and cover a narrow range (2.4-35 μg m^{-3}) of fine particulate ($PM_{2.5}$) concentrations. Satellites provide daily global coverage of a dynamic range of pollutants for more than a decade and there are updated health risk assessment models that account for the increasing number of health outcomes that have been associated with air pollution and that cover a wider exposure range than previous models. In this work, the skill of satellite observations at reproducing variability in surface air quality in the UK and Indian cities was assessed. Temporal consistency ($R>0.5$) occurred between space-based and surface observations of nitrogen dioxide (NO_2) and ammonia (NH_3), whereas measurements of aerosol optical depth (AOD) have weak month-to-month variability ($R<0.4$) with surface $PM_{2.5}$, but do replicate long-term trends in $PM_{2.5}$. This provided the confidence to use satellite observations to determine recent (2000s-2010s) long-term trends in NO_2, NH_3, formaldehyde (HCHO) as a marker for reactive non-methane volatile organic compounds (NMVOCs), and AOD as a marker for $PM_{2.5}$ in London and Birmingham in the UK, and Delhi and Kanpur in India. Trends in most pollutants declined in UK cities because of successful control on vehicular emissions but increased in Indian cities despite recent pollution control measures. These validated satellite observations were then used to quantify long-term trends in air quality over 46 tropical cities which are growing at an unprecedented pace (1-10 % a^{-1}) and that lack routine, reliable and accessible ground-based air quality measurements. Most pollutants in almost all tropical cities increased, driven almost exclusively by increase in anthropogenic activity rather than traditional biomass burning. Population exposure to hazardous pollutants $PM_{2.5}$ and NO_2

increased by up to 23 % a^{-1} for NO_2 and 18 % a^{-1} for $PM_{2.5}$ due to the combined increase in emerging anthropogenic air pollution and population. This suggests an impending health crisis that demands further analysis to determine the increase in health burden from increased exposure to these hazardous pollutants. This was followed by examining the health burden from exposure to $PM_{2.5}$ produced exclusively from fossil fuel combustion, a dominant and controllable anthropogenic source of $PM_{2.5}$. The health burden was estimated using the chemical transport model GEOS-Chem, validated with satellite and surface observations, and a recent meta-analysis that accounted for a wider exposure range than previous approaches. 10.2 million adult premature deaths were estimated to be from fossil fuel related $PM_{2.5}$ in 2012 with 62 % of these in China and India. These estimates are more than double than those obtained from the Global Burden of Disease and other studies because of the updated health risk assessment model and a finer spatial resolution chemical transport model. These estimates decline to 8.7 million in 2018 due to substantial decline in fossil fuel emissions in China, demonstrating the efficacy of air quality policies that target fossil fuel sources. Fossil fuel combustion can be more readily controlled than other primary and secondary sources of $PM_{2.5}$ and transitioning towards cleaner sources of energy can mitigate these premature deaths. These results highlight the immediate health crisis due to ongoing reliance on fossil fuels to complement the longer term and potentially more severe effects these will have on climate. The thesis demonstrates the application of satellite observations, ground-based measurements, chemical transport models, emission inventories and health risk assessment models and statistical techniques to determine trends and drivers of these trends in air quality in cities and estimate the health burden at different spatial scales. This is crucial information that policymakers and stakeholders require to make informed decisions and develop prescient policies.

ACKNOWLEDGEMENTS

First and foremost, I would like to thank my supervisors, Eloïse Ann Marais and William James Bloss for providing me the opportunity to pursue a PhD in an area I am passionate about and making my transition from corporate life back to academia smooth. Their continued guidance, support, and encouragement throughout my PhD research has made this one of the most challenging, exciting, and rewarding experiences I have encountered so far.

I would also like to express my gratitude to all my collaborators at University of Birmingham, University College London, Harvard University, Université libre de Bruxelles, Birmingham City Council and IIT Kanpur. Thank you to NASA, BIRA-IASB, Defra, London Air Quality Network, EMEP, AERONET, SPARTAN, GFED, $CEDS_{GBD\text{-}MAPS}$ team, World Bank, UN, IHME, CDC WONDER and Statistics Canada for making the datasets publicly available for use.

I am grateful to the University of Birmingham for awarding me the Global Challenges PhD studentship without which this research work wouldn't have been possible. Thank you to Birmingham Environment for Academic Research (BEAR) for letting me store and process terabytes of data, Birmingham International Academy (BIA), University Graduate School, Westmere and Library Services for plethora of workshops and sessions to enhance my presentation and writing skills. Thank you to Rosie, Gretchel, Jamie, Lesley, and Claire for being patient with my countless emails and helping me out with admin-related tasks.

I am thankful to my Master's supervisor Professor Sachchida Nand Tripathi for always encouraging me to strive for excellence and also supporting me during my PhD research. My mentors and friends at IIT Kanpur, Deepika, Abhishek, Shamjad, Shikhar, Sonali, Evy, Vaibhav, Akhil, Kshitij, Bharath and friends back in my hometown Dehradun, Sanchi, Shilpi and Supriya have constantly motivated me and specially since the pandemic. I am eternally grateful to my former colleagues at Mckinsey and Company and in Gurgaon, Ganesh, Jani, Jiten, Mihir, Rishabh, Suhani, Tushar, Deepak, Guneet and Rut who have supported my decisions to pursue PhD. Thank you to my friends and colleagues at University of Birmingham, University of Leicester and University College London for the problem-solving sessions, peer-to-peer feedback sessions and socials especially Gongda and Alfred for our biweekly trips to Leicester. I feel blessed to have met Bala, Proma, Gippi, Shashi, Rajat, Saubhik, Vysakh, Siva, Shahryr, Govind, Samar, Yash, Madhav and Manik in the UK who have made my experience in Birmingham enjoyable.

Lastly and most importantly, I would like to thank my parents for believing in me, Diana for being there by my side and God Almighty for making all this possible.

Thank you everyone for being a part of my journey!

AUTHOR'S CONTRIBUTION

This thesis is based on three manuscripts two of which have undergone peer-review and one is in preparation for submission.

CHAPTER 1: INTRODUCTION, is unique to this thesis.

CHAPTER 2: LONG-TERM TRENDS IN AIR QUALITY IN MAJOR CITIES IN THE UK AND INDIA: A VIEW FROM SPACE

Published in **Atmospheric Chemistry and Physics** as:
K. Vohra, E. A. Marais, S. Suckra, L. Kramer, W. J. Bloss, R. Sahu, A. Gaur, S. N. Tripathi, M. Van Damme, L. Clarisse, P.-F. Coheur, Long-term trends in air quality in major cities in the UK and India: A view from space, Atmos. Chem. Phys., 21, 6275–6296, doi:10.5194/acp-21-6275-2021.

KV analysed and interpreted the data and prepared the manuscript, and EAM assisted in the writing and provided supervisory guidance, with co-supervision from WJB. LK provided data analysis and usage guidance. ShS derived the relationship between hourly PM_{10} and $PM_{2.5}$ for Birmingham. Observations are from RS, AG, and SNT for the surface site in Kanpur and from MVD, LC, and PFC for IASI NH_3.

CHAPTER 3: LARGE AND SIGNIFICANT INCREASES IN EXPOSURE TO AIR POLLUTION DETRIMENTAL TO HEALTH IN TROPICAL FUTURE MEGACITIES

To be submitted as:
K. Vohra, E. A. Marais, W. J. Bloss, M. Van Damme, L. Clarisse, P.-F. Coheur, Large and significant increases in exposure to air pollution detrimental to health in tropical future megacities.

KV and EAM designed the research, with input from WJB. New data products were provided by MVD, LC, and PFC. KV analysed the data. KV and EAM wrote the paper, with input from all co-authors.

CHAPTER 4: GLOBAL MORTALITY FROM OUTDOOR FINE PARTICLE POLLUTION GENERATED BY FOSSIL FUEL COMBUSTION: RESULTS FROM GEOS-CHEM

Published in **Environmental Research** as:
K. Vohra, A. Vodonos, J. Schwartz, E. A. Marais, M. P. Sulprizio, L. J. Mickley, Global mortality from outdoor fine particle pollution generated by fossil fuel combustion: Results from GEOS-Chem, Environ. Res., 195, 110754, doi:10.1016/j.envres.2021.110754.

KV and AV carried out the health impact calculations guided by JS. EAM and MPS performed GEOS-Chem simulations. LJM oversaw the project. All authors contributed to writing the manuscript.

CHAPTER 5: SYNTHESIS, is unique to this thesis.

TABLE OF CONTENTS

LIST OF FIGURES

LIST OF TABLES

LIST OF ABBREVIATIONS

AOD	Aerosol Optical Depth
AERONET	AErosol RObotic NETwork
AMF	Air Mass Factor
AQEG	Air Quality Expert Group
NH3	Ammonia
AF	Attributable Fraction
AURN	Automatic Urban and Rural Network
AEIC	Aviation Emissions Inventory Code
BCC	Birmingham City Council
CANSIM	Canadian Socio-Economic Information Management System
CO	Carbon monoxide
CIESIN	Center for International Earth Science Information Network
CDC	Centers for Disease Control and Prevention
CPCB	Central Pollution Control Board
CTM	Chemical Transport Model
CEDS	Community Emissions Data System
CMAQ	Community Multiscale Air Quality Model
CRF	Concentration-Response Function
CIs	Confidence Intervals
COVID-19	COronaVIrus Disease of 2019
CrIS	Cross-track Infrared Sounder
DT	Dark Target
GADM	Database of Global Administrative Areas
DJF	December-February
DB	Deep Blue
DPCC	Delhi Pollution Control Committee
Defra	Department for Environment, Food and Rural Affairs
DICE	Diffuse and Inefficient Combustion Emissions
DALY	Disability-Adjusted Life-Years
DEAD	Dust Entrainment And Deposition

EO	Earth Observations
ERA5	ECMWF Reanalysis v5
EDGAR	Emission Database for Global Atmospheric Research
ECMWF	European Centre for Medium-Range Weather Forecasts
EMEP	European Monitoring and Evaluation Programme
$PM_{2.5}$	Fine particulate matter
HCHO	Formaldehyde
GEMS	Geostationary Environment Monitoring Spectrometer
GEO	Geostationary Orbit
GBD	Global Burden of Disease
GBD-MAPS	Global Burden of Disease – Major Air Pollution Sources
GEIA	Global Emissions InitiAtive
GEMM	Global Exposure Mortality Model
GFED	Global Fire Emissions Database
GMAO	Global Modeling and Assimilation Office
GOME	Global Ozone Monitoring Experiment
GEOS	Goddard Earth Observing System
GPWv4.11	Gridded Population of the World, Version 4 Revision 11
HEMCO	Harvard-NASA Emission Component
HEI	Health Effects Institute
HO_2	Hydroperoxyl radical
HARP-2	Hyper Angular Rainbow Polarimeter
HRI	Hyperspectral Range Index
IMD	India Meteorological Department
IIT	Indian Institute of Technology
IGP	Indo-Gangetic Plain
IASI	Infrared Atmospheric Sounder Interferometer
IASI-NG	Infrared Atmospheric Sounder Interferometer - New Generation
IHME	Institute for Health Metrics and Evaluation
IER	Integrated Exposure-Response
ICOADS	International Comprehensive Ocean-Atmosphere Data Set
LST	Local Solar Time

LT	Local Time
LAQN	London Air Quality Network
LUT	Look-Up Table
LEO	Low-Earth Orbit
LRI	Lower Respiratory Infection
MAPS	Major Air Pollution Sources
CH4	Methane
MEGAN	Model of Emissions of Gases and Aerosols from Nature
MODIS	MODerate-resolution Imaging Spectroradiometer
MISR	Multi-angle Imaging Spectro-Radiometer
3MI	Multi-viewing Multi-channel Multi-polarisation Imager
NASA	National Aeronautics and Space Administration
NAEI	National Atmospheric Emission Inventory
NEI	National Emissions Inventory
NERC	Natural Environment Research Council
NO	Nitric oxide
NO_2	Nitrogen dioxide
NO_x	Nitrogen oxides
NMVOCs	Non-Methane Volatile Organic Compounds
OVOCs	Oxygenated Volatile Organic Compounds
O_3	Ozone
OMPS	Ozone Mapping and Profiler Suite
OMI	Ozone Monitoring Instrument
PARANOX	PARAmetrization of emitted NOX
PM	Particulate Matter
E_{pop}	Population Exposure
QA4ECV	Quality Assurance for Essential Climate Variables
RETRO	REanalysis of the TROposhperic chemical composition
RMA	Reduced Major Axis regression
RH	Relative Humidity
RR	Relative Risk

SCIAMACHY	Scanning Imaging Absorption Spectrometer for Atmospheric Cartography
SDS	Scientific Data Set
SOA	Secondary Organic Aerosol
SCD	Slant Column Density
SES	Socio-Economic Status
SZA	Solar Zenith Angle
SPEXone	Spectro-Polarimeter for Planetary Exploration
SMA	Standard Major Axis regression
SP	Standard Product
SNA	Sulfate, Nitrate and Ammonium
SO_2	Sulfur dioxide
SPARTAN	Surface Particulate Matter Network
TEMPO	Tropospheric Emissions: Monitoring of Pollution
TROPOMI	TROPOspheric Monitoring Instrument
UKEAP	UK Eutrophying and Acidifying Pollutants Network
UV	Ultraviolet
UN	United Nations
UoB	University of Birmingham
USEPA	US Environmental Protection Agency
UPPCB	Uttar Pradesh Pollution Control Board
VCD	Vertical Column Density
VOCs	Volatile Organic Compounds
WONDER	Wide-ranging Online Data for Epidemiologic Research
WHO	World Health Organization

THESIS OVERVIEW

This thesis uses ground-based measurements and Earth observations of atmospheric composition, emission inventories, chemical transport models and health risk assessment models to examine trends in air pollution and impact on human health at different spatial scales.

Chapter 1 provides an introduction to the thesis. It describes the challenges of developing air quality policies, and the existing and future air pollution monitoring capabilities.

Chapter 2 assesses the ability of satellite observations to reproduce variability in surface air pollution and quantify long-term trends in air quality in major cities in the UK (London and Birmingham) and India (Delhi and Kanpur). The work described in this chapter is published as:

K. Vohra, E. A. Marais, S. Suckra, L. Kramer, W. J. Bloss, R. Sahu, A. Gaur, S. N. Tripathi, M. Van Damme, L. Clarisse, P.-F. Coheur, Long-term trends in air quality in major cities in the UK and India: A view from space, Atmos. Chem. Phys., 21, 6275–6296, doi:10.5194/acp-21-6275-2021.

Chapter 3 extends the methodology developed in Chapter 2 to quantify long-term trends in fastest growing cities in the tropics, assesses the relative contribution of anthropogenic activity and biomass burning to these trends and examines the combined effect of increase in population and air pollutants hazardous to human health. The findings of this chapter are in preparation for submission to peer-reviewed journal as:

K. Vohra, E. A. Marais, W. J. Bloss, M. Van Damme, L. Clarisse, P.-F. Coheur, Large and significant increases in exposure to air pollution detrimental to health in tropical future megacities.

Chapter 4 investigates global premature mortality burden from fossil fuel related $PM_{2.5}$ using the state-of-the-art chemical transport model GEOS-Chem. The findings from this chapter have been published as:

K. Vohra, A. Vodonos, J. Schwartz, E. A. Marais, M. P. Sulprizio, L. J. Mickley, Global mortality from outdoor fine particle pollution generated by fossil fuel combustion: Results from GEOS-Chem, Environ. Res., 195, 110754, doi:10.1016/j.envres.2021.110754.

Chapter 5 summarises the key research findings and states some opportunities for future research.

CHAPTER 1

INTRODUCTION

1.1 **Challenges of developing air quality policies**

Air pollution adversely affects human health and the environment. Long-term exposure to air pollutants is linked to a range of adverse health outcomes, such as respiratory and cardiovascular diseases, dementia, loss of fertility and eyesight (Cacciottolo et al., 2017; WHO, 2018; Schraufnagel et al., 2019b, 2019a; Chua et al., 2021; Li et al., 2021). More than 90 % of the world's population resides in areas where air quality levels exceed World Health Organization (WHO) recommended guidelines (WHO, 2018). Air quality policy decisions depend on multiple factors that influence air pollution. These include but are not limited to natural and anthropogenic emission sources, meteorology, chemical and physical processing of pollutants and precursors in the atmosphere, and adoption of mitigation measures. Under current legislation in the UK and many other countries, local emission sources such as power plants are relatively easier to control than transboundary pollution such as widespread areal sources that cross political boundaries like open burning of biomass (Andreae, 1991) and persistent pollutants such as mercury and microplastics that can be transported long distances (Hung et al., 2021; Zhang et al., 2021). Countries typically target large point sources to address air pollution before moving to mobile and areal and diffuse sources.

Each year 4-9 million premature deaths are attributed to ambient air pollution (Burnett et al., 2014; 2018; Cohen et al., 2018; WHO, 2018; Lelieveld et al., 2019; 2020; McDuffie et al., 2021). Policies and mitigation measures such as adoption of emission control technologies and increasing energy efficiency can be effective at reducing air pollution and adverse health outcomes. Due to policy measures in the US and Europe, premature deaths decreased by 29.8 % in the US and 36.3 % in Europe in 2009 compared to 1990 (Pope et al., 2009; Correia et al., 2013; Butt et al., 2017; Cohen et al., 2018; Stanaway et al., 2018). The greatest premature

mortality burden occurs in developing countries which are densely populated and lack effective air quality policies. These include China, India, Pakistan and Bangladesh in Asia and Nigeria in Africa (Cohen et al., 2018; Stanaway et al., 2018; McDuffie et al., 2021). Alarming statistics on premature mortality attributable to exposure to air pollution have attracted the attention of policy makers and has led to the creation of action plans to improve air quality in China and India (Chinese State Council, 2013; Ganguly et al., 2020).

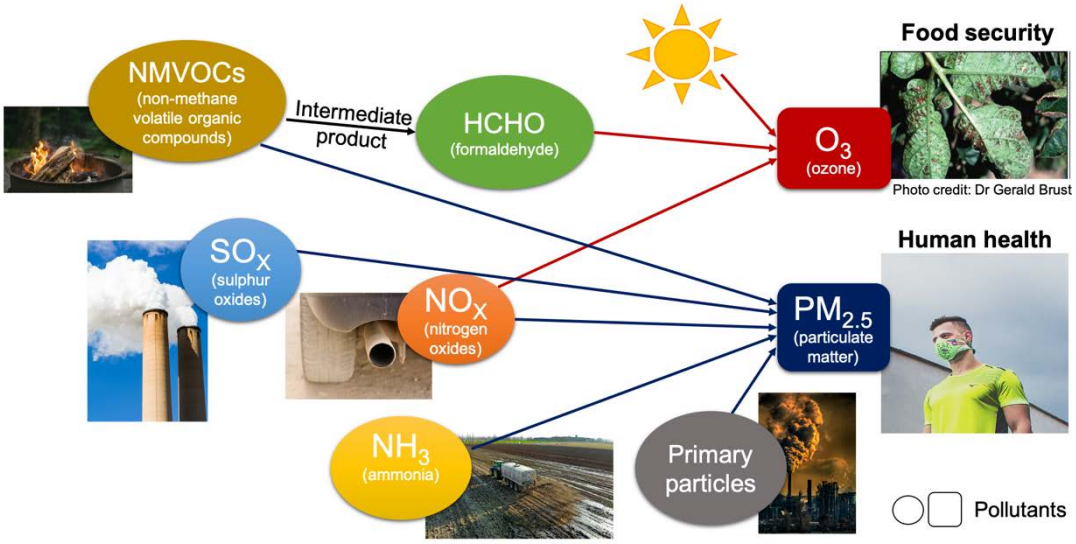

Figure 1.1 Schematic diagram showing the pathways from precursor emissions to hazardous pollutants.

In addition to the health impacts of air pollution, variable emission sources, atmospheric chemistry, and the spatiotemporal variability of air pollutants also influence the decisions of policymakers and stakeholders. The emission sources can be biogenic, anthropogenic or pyrogenic and can vary with the extent of urbanization. Transportation is a dominant pollution source in urban areas (Badami, 2005) and agriculture in rural areas (Defra, 2019). These sources also vary geographically and with economic development. Fossil fuels are a dominant energy source in Asia (Hanif, 2018) compared to solid fuels such as charcoal in Africa (Bockarie et

al., 2020). Bottom-up emission inventories are used to identify the dominant sources of air pollution but these emission inventories are costly to maintain and keep up-to-date, and are prone to large errors in regions where activity data and emission factors are lacking, unreliable or only available at coarse spatial resolutions (Marais and Wiedinmyer, 2016; Elguindi et al., 2020).

Figure 1.1 shows common air pollutants such as nitrogen oxides (NO_x = NO + NO_2) mostly emitted as nitric oxide (NO), sulfur dioxide (SO_2), carbon monoxide (CO), volatile organic compounds (VOCs), ammonia (NH_3) and primary particulate matter ($PM_{2.5}$). Primary particles include black carbon and organic aerosols. Gaseous emissions can undergo chemical reactions to form secondary pollutants such as ozone (O_3) and secondary inorganic and organic $PM_{2.5}$. Secondary inorganic $PM_{2.5}$ consists of nitrate from uptake of nitric acid formed from oxidation of NO_x, sulfate from oxidation of SO_2 and ammonium from uptake of the acid buffer NH_3. Secondary organic $PM_{2.5}$ originates from partitioning of semi-volatile organic compounds or reactive uptake of oxidation products of non-methane VOCs (Behera and Sharma, 2010; Li et al., 2017; Weagle et al., 2018).

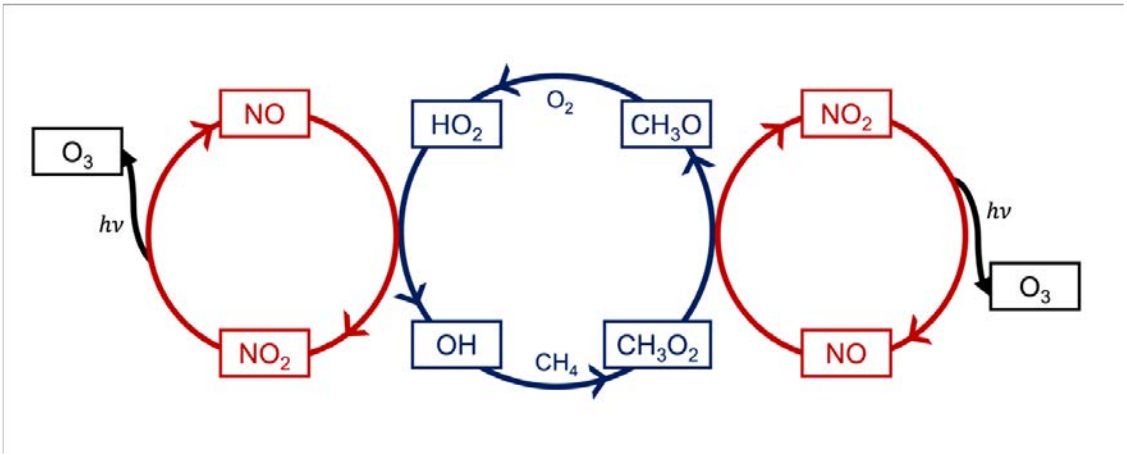

Figure 1.2 Methane oxidation mechanism to show ozone production in the presence of NO_x and sunlight.

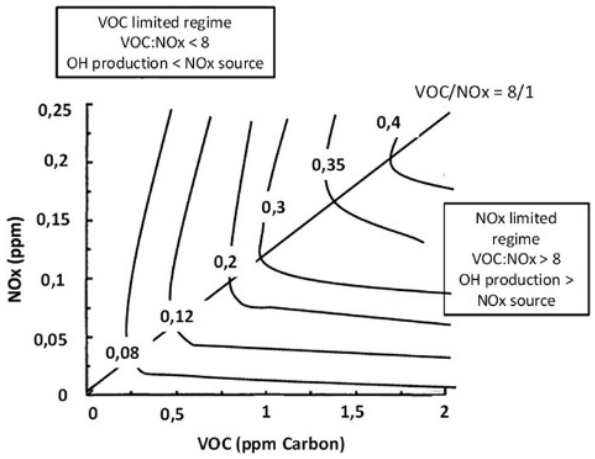

Figure 1.3 Ozone isopleth plot showing the dependence of ozone concentration (contours with maximum daily ozone concentration in ppmv) on NO_x and VOCs concentrations. Source: Melkonyan and Kuttler (2012)

Ozone is formed from chemical reactions of precursor emissions of NO_x and VOCs in the presence of sunlight (Jacob et al., 1993; Loughlin et al., 2000). Figure 1.2 shows the chemistry forming ozone from oxidation of methane in the presence of NO_x and sunlight (Wang et al., 2017; Fitzky et al., 2019). Methane is oxidised by the hydroxyl radical (OH) to form the methyl radical (CH_3) which reacts with O_2 to form the methyl peroxy radical (CH_3O_2). CH_3O_2 reacts with NO and O_2 to form the hydroperoxy radical (HO_2) and NO_2. HO_2 reacts with NO recycling the OH radical and forming NO_2 (Wang et al., 2017; Fitzky et al., 2019). The NO_2 formed is then photolysed in the presence of O_2 to form ozone. CH_3O_2 also reacts with the HO_2 radical to form methyl hydroperoxide (CH_3OOH), the loss pathways of which can terminate the methane oxidation chain. Oxidation of the CH_3O_2 radical also forms formaldehyde (HCHO) and CO which contribute to ozone formation following the same processes shown in Figure 1.2. This chemistry is non-linear and depends on the relative abundance of NO_x and VOCs as in Figure 1.3 (Martin et al., 2004; Duncan et al., 2010). Ozone formation decreases when NO_x emissions decrease in a NO_x-limited (VOC-saturated) regime and remains relatively stable when NO_x emissions decrease in a VOC-limited (NO_x-saturated) regime (Martin et al., 2004; Duncan et

al., 2010). Ozone formation is equally sensitive to emissions of both NO_x and VOCs at the ozone ridgeline separating the NO_x-limited and VOC-limited regimes (Melkonyan and Kuttler, 2012). This makes it challenging to regulate ozone pollution, as measurements of ozone alone are insufficient and knowledge of the ozone formation regime is needed to identify which sources to target to develop policies (Loughlin et al., 2000).

Figure 1.4 shows the atmospheric lifetimes of common air pollutants ranging from a few seconds for NO to months for CO to years for methane (CH_4), and so these pollutants can be found near the emission sources such as NO from vehicles (Gentner and Xiong, 2017) or be transported long distances such as CO from incomplete combustion of traditional solid fuels (Ludwig et al., 2003). The major sink for $PM_{2.5}$ is wet deposition, but other factors like particle growth and dry deposition contribute (Feichter and Leisner, 2009). For trace gases loss pathways include physical deposition to surfaces (dry deposition) as is the case for ozone, and chemical loss by atmospheric oxidants such as the OH radical, the nitrate radical (NO_3) and ozone (Ng et al., 2017; Shah et al., 2020; Yang et al., 2020). The OH radical is formed from the photolysis of ozone in the presence of water vapour and thus is the key oxidant during daytime. The OH radical controls lifetime of trace gases by forming long-term reservoir species like nitric acid for NO_x or from conversion of formaldehyde to CO and the HO_2 radical (Shah et al., 2020; Yang et al., 2020). At night, in the absence of photolysis, the oxidation is driven by the NO_3 radical formed from the reaction of NO_2 with ozone (Ng et al., 2017; Shah et al., 2020; Yang et al., 2020). The NO_3 radical reacts with NO_2 to form dinitrogen pentoxide (N_2O_5) and with unsaturated VOCs such as isoprene to form the peroxy radical (Ng et al., 2017; Iyer et al., 2018; Yang et al., 2020). Convective transport of these pollutants from the boundary layer (the layer where pollutants are well-mixed and extends from the Earth's surface to 1-2 km altitude)

is particularly efficient in tropical countries and alters the atmospheric composition in the free troposphere (extends beyond the boundary layer to the tropopause at around 12-18 km altitude) and lower stratosphere (extends to about 10 km above the tropopause) by transporting air containing relatively depleted ozone or precursors of pollutants that are efficient at forming ozone in the upper troposphere (Thompson et al., 1997; Fueglistaler et al., 2009). These pollutants not only vary in space but can also vary with season and time of day in response to seasonality and diurnal variability of emission sources, atmospheric chemistry and meteorological factors (Guttikunda and Gurjar, 2012; Gil-Alana et al., 2020; Shah et al., 2020). This adds another layer of complexity for policymakers to decide if the policies targeting these pollutants should vary seasonally and temporally.

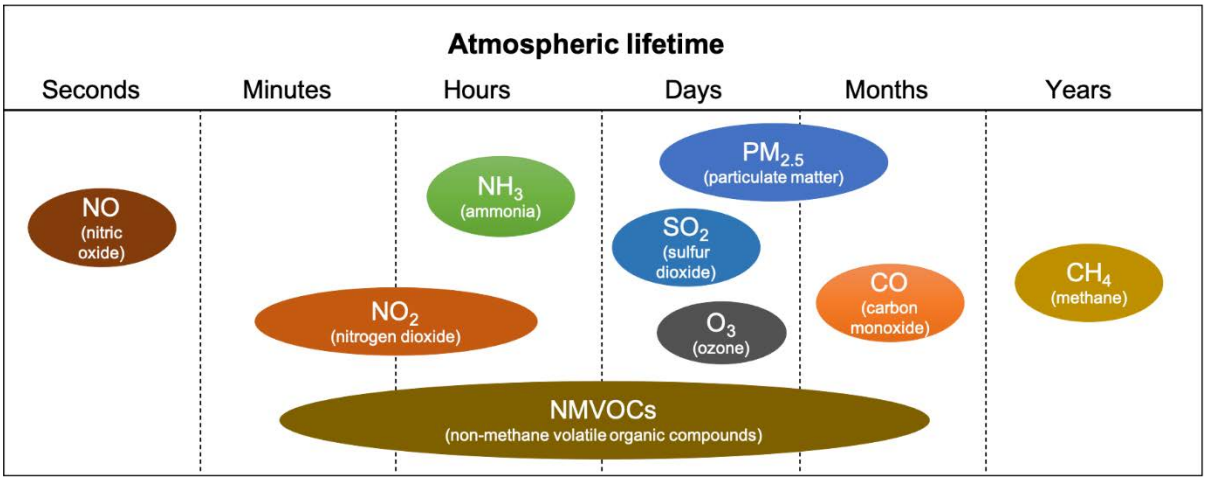

Figure 1.4 The range in atmospheric lifetimes of dominant air pollutants.

A major challenge is in assessing the efficacy of policies, as this requires appropriate tools and resources to assess compliance with regional or national emissions targets and air quality standards. For example, in the UK compliance assessment is with monitoring (Defra, 2020) and dispersion modelling (Carslaw et al., 2013) despite poor agreement between modelled and roadside NO_2 measurements (Barnes et al., 2018). Results derived from models versus from

measurements can also lead to inconsistent outcomes that suggest either compliance or non-compliance (Barnes et al., 2018).

1.2 **Existing and future air pollution monitoring capabilities**

The regional, national and local authorities have deployed reference grade sensors for decades to provide us with valuable information about the temporal variability of air pollutants and assess compliance against air quality standards (AQEG, 2015). Reference grade sensors often provide continuous air quality measurements of criteria pollutants that are typically NO_x, SO_2, O_3, CO, $PM_{2.5}$ and a range of VOCs (often mostly hydrocarbons) throughout the day at high temporal resolution such as every 15 minutes or 1 hour (AQEG, 2015). In the UK, comprehensive surface measurement networks are established and operated by national authorities such as the Department for Environment, Food and Rural Affairs (Defra), local authorities such as Birmingham City Council (BCC), and more recently, include research institutions such as the Natural Environment Research Council (NERC) funded fixed air quality supersites of comprehensive measurements of air pollution and environmental variables that influence air pollution. These are in Birmingham, London and Manchester. An innovative upcoming development to monitor air quality in the UK is establishment of two mobile supersites to make measurements of roadside and urban atmospheric composition (UoB, 2021). Intensive ground-based and aircraft field campaigns led by agencies such as NASA also allow us to investigate the complexities of air pollution throughout the troposphere (Wolfe et al., 2019). Reference monitors are typically expensive to purchase, establish and maintain, and so are non-existent or sparse in many developing countries and thus have limited spatial coverage worldwide. There are well established networks deploying reference grade sensors in the US, Western Europe, China and India, but still there are data gaps. Surface monitoring equipment can be sparse and periodic (Zhu et al., 2020), and are often relocated due to shifts in policy

priorities, or simply because the infrastructure housing it is no longer available for use (Walker et al., 2019). This makes it challenging to monitor long-term trends in city-wide air quality to determine whether mitigation measures have a net positive effect on the urban airshed. For example, Figure 1.5 shows the trends in surface NO_2 from reference grade sensors operational in Birmingham during 2005-2017. The sites are sparsely distributed and operate for different time periods. Only 1 of the 7 sites provides air quality data for all 13 years and this single location may not be representative of city-wide air quality (Zhu et al., 2020).

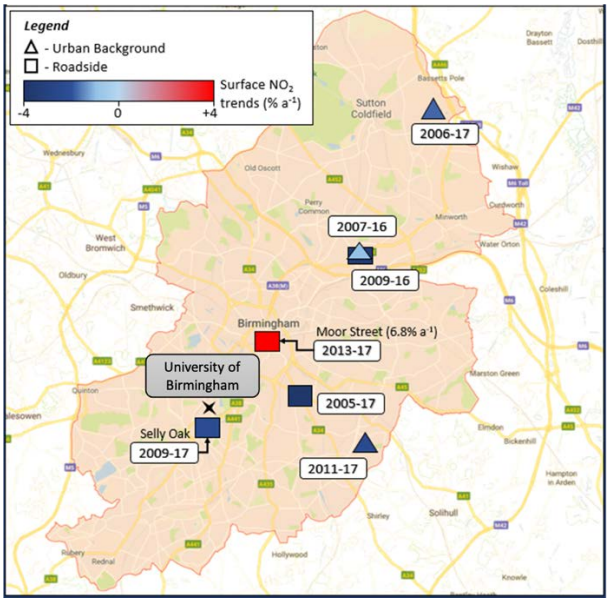

Figure 1.5 Locations of reference grade sensors operational between 2005 and 2017 in Birmingham. The colour shows the trends in monthly mean surface NO_2 for the time period in the callouts.

Low-cost sensors are another innovation in monitoring air quality. These are easy-to-use and portable, and networks of these are being established at a fast pace to address monitoring gaps from existing surface monitors, most notably in Africa, Asia and Latin America where reference monitors are exceedingly sparse (Snyder et al., 2013; Sahu et al., 2021). However, there are issues with data quality, as these measurements can stray from the truth under different atmospheric conditions. This requires regular field calibration with reference grade monitors or corrections to the data using machine learning techniques (Castell et al., 2017; Williams, 2019).

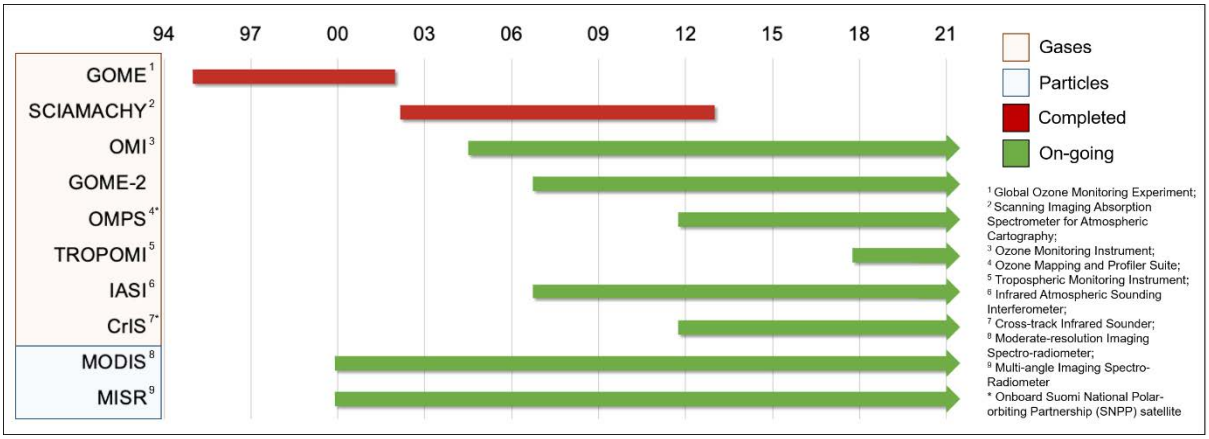

Figure 1.6 Length of record available from sensors measuring trace gases and particles from completed and on-going LEO instruments.

Low-Earth orbit (LEO) satellites have been in space for decades and provide terabytes of atmospheric composition data each day (Streets et al., 2013; Duncan et al., 2014). LEO satellites are 750 km above the Earth's surface and sensors aboard these satellites provide measurements of numerous trace gases and particle abundances and properties (Streets et al., 2013; Duncan et al., 2014). Figure 1.6 shows the length of the satellite data record from space-based instruments onboard completed and on-going LEO satellite missions. The long record of consistent observations from these have been extensively used to determine long-term trends in air pollutants (De Smedt et al., 2010; Alpert et al., 2012; Hilboll et al., 2013; Geddes et al., 2016; Van Damme et al., 2020). These offer the opportunity to assess the impact of economic development as observed from the increasing trends in pollutants that are effective markers of development, such as NO_2 as a proxy for adoption of fossil fuels for energy generation, in rapidly developing countries. Other applications are demonstrating the effectiveness of air quality related policies, as seen from decreasing NO_2 trends in cities in the US (Russell et al., 2012; Lamsal et al., 2015), NO_2 trend reversal from positive (unabated development) to negative (policy adoption) in China (Liu et al., 2017) and individual cities (Lelieveld et al., 2015; Georgoulias et al., 2019). These long-term trends aid in predicting future air quality

trends in case no action plans are setup. Ratios of Earth observations (EO) of HCHO and NO_2 are also used to assess sensitivity of ozone formation to precursor emissions of VOCs (using HCHO as a proxy) and NO_x (using NO_2 as a proxy) (Martin et al., 2004; Duncan et al., 2010; Jin et al., 2020).

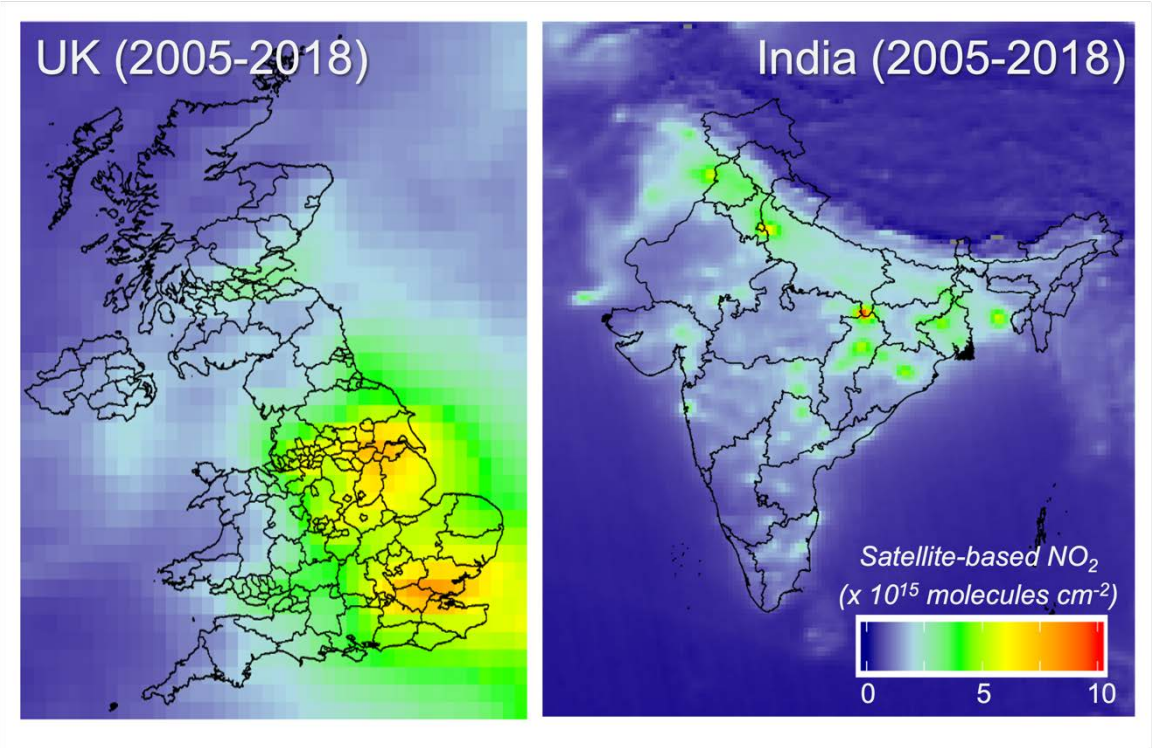

Figure 1.7 Multiyear mean tropospheric column NO_2 from OMI for 2005-2018 for the UK (left) and India (right).

EO from LEO satellites provide complete global coverage. Figure 1.7 shows mean tropospheric column NO_2 from the Ozone Monitoring Instrument (OMI) for the UK and India in 2005-2018. This figure demonstrates the ability of EO to provide extensive coverage of air quality measurements notably in regions with limited surface monitoring capabilities. Also evident are the hotspots of NO_2 pollution in these two countries such as major cities London and Delhi, and coal-mining industries in east India. The extensive coverage of EO can guide policymakers to assess which regions need to be targeted for air quality improvements.

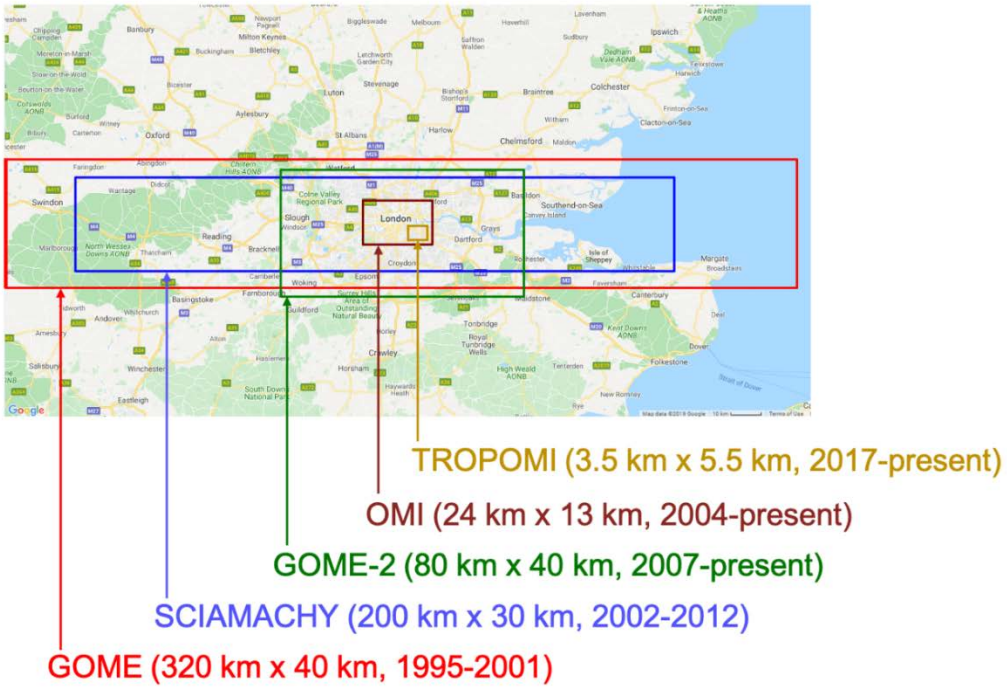

Figure 1.8 Evolution of nadir spatial resolution (across-track × along-track) of UV-visible LEO satellite sensors measuring trace gases. Background map is Greater London and surrounding area. Nadir spatial resolution for TROPOMI is from August 2019.

Figure 1.8 shows the spatial resolution achieved over Greater London at nadir (the portion of the Earth directly below the satellite at the centre of the swath or cross-track extent covered on the Earth's surface as in Figure 1.9a) from different UV-visible LEO satellite sensors that measure trace gases such as NO_2, SO_2, O_3 and HCHO. Figure 1.9a illustrates the finer spatial resolution at nadir and its degradation towards the edges of the swath (off-nadir) due to viewing geometry and instrument configuration. The spatial resolution of individual pixels has improved with time from hundreds of km for Global Ozone Monitoring Experiment (GOME) and Scanning Imaging Absorption Spectrometer for Atmospheric Cartography (SCIAMACHY) to tens of km for OMI and Tropospheric Monitoring Instrument (TROPOMI). This has led to the transition from one piece of broad regional information for a few counties from GOME to individual London boroughs from TROPOMI. Even though the spatial

resolution is still relatively coarse for satellite observations, these are more consistent with the spatial resolution of the models used to inform policy than are point measurements from reference grade instruments and so can be used to assess these models and in combination with these models to derive additional information about surface air quality and precursor emissions, as is now standard (Duncan et al., 2016).

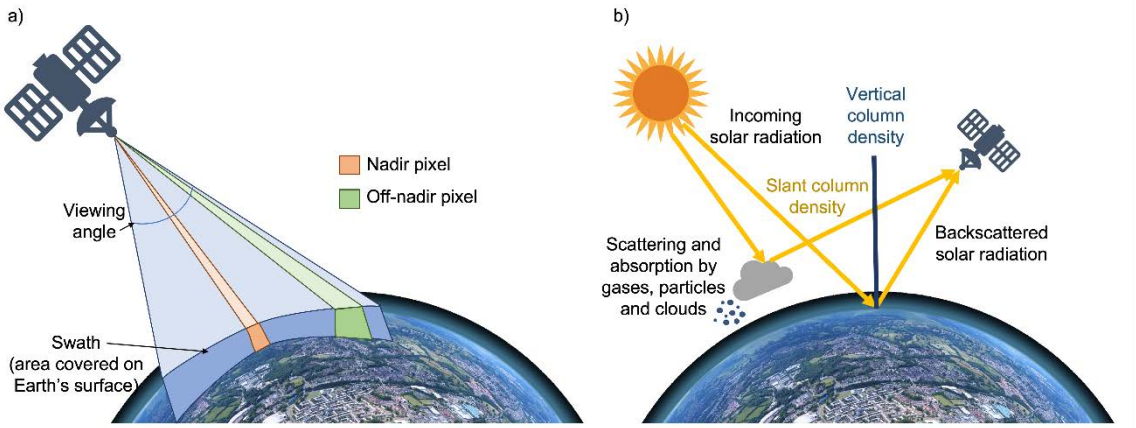

Figure 1.9 LEO swath and slant column configurations. Panels are degradation of spatial resolution from centre towards edge of swath (a), and schematic representation of slant column path from the incoming solar radiation and backscattered radiation from the Earth's surface, clouds and aerosols, and vertical column for UV-visible instruments (b).

Sun-synchronous LEO satellites have nighttime and daytime overpasses and provide measurements of atmospheric composition during the daytime for UV-visible instruments that rely on the sun as the light source such as OMI and during the daytime and nighttime for infrared instruments such as Infrared Atmospheric Sounder Interferometer (IASI) that rely on the temperature difference between the Earth's surface and overlying atmosphere. For example, OMI provides NO_2 measurements during daytime at the satellite overpass time of 13h30 local solar time (LST) and IASI provides NH_3 measurements in the morning (09h30 LST) and night (21h30 LST), though there are concerns that the daytime and night-time measurements from IASI are not consistent and most of the validation of application of IASI NH_3 measurements uses daytime retrievals (Van Damme et al., 2015).

UV-visible space-based instruments measure solar backscattered radiation that has traversed the whole atmospheric column, as shown in Figure 1.9b. Most of the air pollutants and precursors measured by LEO instruments, with the exception of ozone, typically have peak concentrations near the Earth's surface, so the variability in the column is sensitive to changes in surface air pollution. NO_2 exists in large amounts in the stratosphere and the retrieval algorithms remove this stratospheric contribution to isolate tropospheric column NO_2. There are some exceptional events, such as volcanic ash (Sandrini et al., 2014) or large dust events from the Sahara Desert (Heft-Neal et al., 2020) or deep pyrogenic uplift of biomass burning plumes (Kablick III et al., 2020) that can enhance concentrations of aerosols in the free troposphere, but often these events can be easily identified and removed for research that focuses on constraining surface sources.

The retrieval algorithms vary with the atmospheric component and the satellite sensor. For example, OMI observations of column densities of NO_2 (number of molecules of trace gas per unit area along a line of sight) are retrieved within the spectral range of 405-465 nm and those for HCHO are obtained at 328.5-359.0 nm (De Smedt et al., 2018; Lamsal et al., 2021). The retrieval algorithm converts these spectral signatures to a slant column density (SCD) which is the number of molecules in the entire viewing path from the sun to the Earth's surface and reflected back up to the satellite (Figure 1.9b) (Krotkov et al., 2017; Lamsal et al., 2021). This SCD is converted to a vertical column density (VCD), the number of molecules in the vertical atmospheric column (Figure 1.9b), using an air mass factor (AMF). The AMF accounts for the viewing geometry of the instrument, surface reflectivity, atmospheric scattering and absorption by clouds, gases and aerosols, and the vertical profile of the species of interest. The AMF is

calculated using a radiative transfer model and typically uses information about clouds from the same or a nearby sensor, and the vertical profile of the species of interest and abundances of other relevant aerosols and trace gases from a chemical transport model (CTM) (Palmer et al., 2001; Bucsela et al., 2006). The VCD throughout the atmosphere is derived after dividing the SCD by the AMF and, for NO_2, this follows subtraction of the stratospheric component from the total column SCD to isolate the tropospheric SCD (Bucsela et al., 2013; Krotkov et al., 2017; Lamsal et al., 2021).

The IASI is an infrared spectrometer which measures total column NH_3 in the spectral range 812–1126 cm^{-1} (Van Damme et al., 2014; 2020). The product that is mostly widely used and validated involves conversion of the spectral signature into a hyperspectral range index (HRI) which is a measure of the strength of the NH_3 spectral signal and depends on the abundance of NH_3 and the thermal contrast between the Earth's surface and the boundary layer (Van Damme et al., 2014; Whitburn et al., 2016). This HRI is converted to total column NH_3 using a neural network that is trained with information about the vertical profile of NH_3 derived using a Gaussian function with three input parameters representative of NH_3 near emission sources and transported from nearby or distant sources, surface emissivity, satellite viewing angles and meteorological parameters such as temperature, pressure and humidity (Whitburn et al., 2016; Van Damme et al., 2017).

The MODerate-resolution Imaging Spectroradiometer (MODIS) has multiple bands in the visible and infrared wavelength regions. Outgoing radiances in these bands are used to retrieve the amount of light attenuated by aerosols in the atmosphere, the aerosol optical depth (AOD) (Levy et al., 2013; Munchak et al., 2013). This is done by matching the top-of-atmosphere

spectral reflectance from the quality assured pixels to values of spectral reflectance in a look-up table (LUT). The quality assured pixels are those not impacted by clouds or that do not occur over surfaces unsuitable for aerosol retrieval (such as ice and snow). The LUT includes values of AOD for a representative range of aerosol types and properties under different environmental conditions (Levy et al., 2013; Remer et al., 2013). There are separate algorithms to retrieve AOD over dark surfaces such as tropical forests known as the Dark Target (DT) algorithm and over bright surfaces such as deserts known as Deep-Blue (DB) algorithm (Levy et al., 2013; Munchak et al., 2013; Remer et al., 2013). The DT algorithm uses surface reflectance at 670 nm, but the surface reflectance at this wavelength is high over bright areas, making it difficult to distinguish the bright surface from the aerosols above (Levy et al., 2013; Sayer et al., 2014). To address this, a separate DB algorithm is used. This uses surface reflectances on the deep blue end of the spectrum at 412 nm where the surface reflectance over the bright surface is darker and can be distinguished from the aerosols above (Hsu et al., 2004; Sayer et al., 2014).

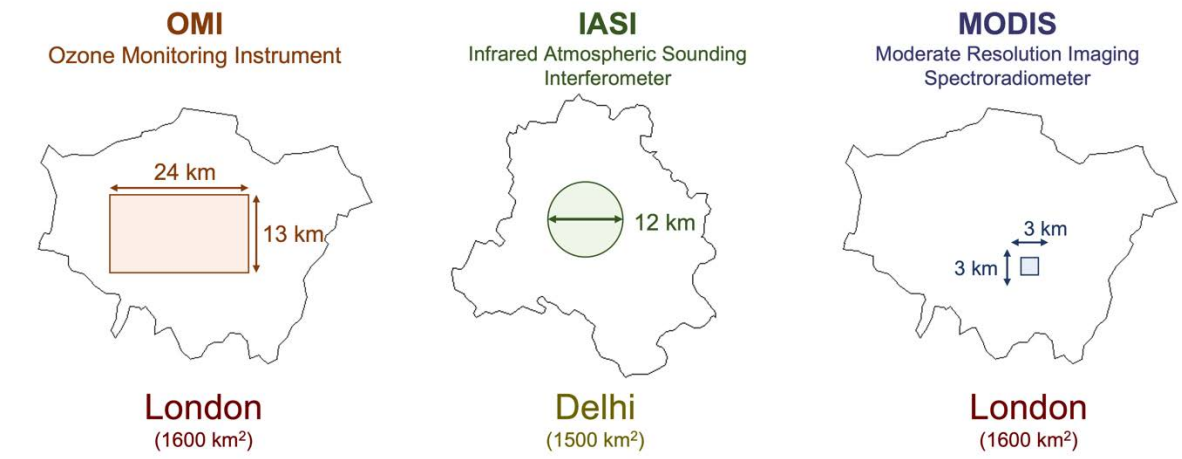

Figure 1.10 Schematic diagram showing the spatial resolution at nadir from different satellite sensors relative to size of the cities London and Delhi.

EO provide consistent and continuous long-term global measurements of multiple atmospheric constituents simultaneously. Column measurements can often be easily related to the

underlying emissions and so are used to provide near real-time information about emissions (Lamsal et al., 2011; Streets et al., 2013). However, it is important to understand the limitations and uncertainties in EO to appropriately use these. EO provide measurements throughout the troposphere or atmosphere, often with just one piece of information about the vertical distribution. The retrieval of trace gases may also be affected by the presence of aerosols and clouds which contribute to uncertainties in the AMF depending on the altitude at which these occur (Palmer et al., 2001; Vasilkov et al., 2021). For example, clouds or thick aerosol layers prevent light from reaching the trace gases below and also leads to spurious retrieval of AOD (Wei et al., 2020; Vasilkov et al., 2021). For this reason, AOD is only retrieved for cloud-free scenes, leading to substantial data loss over the tropics and in locations with intense monsoon seasons like India and West Africa (Levy et al., 2013; Remer et al., 2013; Sogacheva et al., 2017). EO represent the column measurements around the satellite overpass time only and do not capture the diurnal variability of the target pollutant. The spatial resolution of the LEO observations has improved since the 1990s and is a few kms now (Figure 1.8), but it is still too coarse to resolve very local fine-scale emission sources such as individual road networks or shipping lanes beyond major shipping routes or capture sub-city variability for small cities (< 100 km^2). Figure 1.10 illustrates the nadir spatial resolution of OMI, IASI and MODIS with respect to the size of large cities such as London and Delhi. The nadir spatial resolution of OMI and IASI limits our ability to use these observations at sub-city-scale. MODIS has finer spatial resolution than both OMI and IASI (Figure 1.10), but fewer observations are retrieved due to stricter cloud filtering.

Surface observations from reference grade and low-cost sensors and EO from space-based satellites that provide measurements of atmospheric composition require a CTM to augment

their use in policy. CTMs are numerical models which include detailed formation about the loss pathways for gases and particles. These solve mass balance equations to simulate pollutant concentrations. CTMs represent our best understanding of atmospheric chemistry and transport, and can aid in determining the implication of rapid development and policy decisions on the environment and human health. CTMs such as Goddard Earth Observing System (GEOS)-Chem are extensively used for global (Sherwen et al., 2016; Jo et al., 2019) and regional (Marais et al., 2019; Bockarie et al., 2020; Potts et al., 2021) studies. CTMs, following extensive validation against ground- and space-based observations, can be used with health risk assessment models to determine the contribution of individual emission sources and sectors such as fossil fuels to total $PM_{2.5}$ and the consequent impact on health (Marais et al., 2012; Vinken et al., 2014; Weagle et al., 2018; Bockarie et al., 2020) for targeted policy. Health risk assessment models are statistical relationships between premature mortality and long-term exposure to hazardous pollutants such as $PM_{2.5}$. These are derived using epidemiological data from cohort studies for a range of exposures, health outcomes, age ranges and geographical locations. The models most widely used to estimate the premature mortality burden from long-term pollutant exposure at global, regional and national scales (Cohen et al., 2017; Stanaway et al., 2018; Lelieveld et al., 2020) are the Integrated Exposure-Response (IER) model (Burnett et al., 2014) and the Global Exposure Mortality Model (GEMM) (Burnett et al., 2018; Lelieveld et al., 2019). Development of these models is challenging and requires assumptions to fill data gaps because of limited cohort studies covering the wide range of health endpoints, age groups, and exposures. These assumptions include but are not limited to active and second-hand smoking data as proxy for high $PM_{2.5}$ (>50 $\mu g\ m^{-3}$) concentrations and cohort studies from a few countries (typically in North America and Europe) used to represent the world (Burnett et

al., 2014; 2018). This can lead to large uncertainties in the health risk assessment models that then propagate to the premature mortality estimates.

1.3 **Research gaps**

The following are key research gaps that this thesis seeks to address.

1. Previous studies have focused only on application of EO of one or two pollutants with the underlying assumption that EO and surface observations of atmospheric composition have consistent month-to-month variability. A focus on multiple pollutants simultaneously to understand long-term changes in air quality in cities with EO requires systematic assessment of the skill of EO datasets at replicating temporal variability in city-wide surface air pollution before using EO to assess the efficacy of policies and the deleterious effects of rapid unabated development on city-wide air quality (Chapter 2).
2. Following validation of EO as a constraint on long-term trends in air quality, it is crucial to estimate long-term air quality trends using EO in tropical cities. The tropics represents an increasingly larger proportion of the global population and there are few to no ground monitors. These trends can then be used to determine the threat of rapid growth to air quality and develop timely regulatory measures (Chapter 3).
3. Health impact assessments typically estimate premature mortality burden related to $PM_{2.5}$ from all sources, including those that can (anthropogenic) and cannot (natural) be regulated. Estimation of premature mortality from air pollution resulting from fossil-fuel combustion is critical for guiding policymakers and motivating political leaders to take immediate action against sources that have an immediate effect of health and long-term impact on climate (Chapter 4).

References

Alpert, P., Shvainshtein, O., and Kishcha, P., AOD trends over megacities based on space monitoring using MODIS and MISR, Am. J. Clim. Change, 1, doi:10.4236/ajcc.2012.13010, 2012.

Andreae, M. O., Biomass Burning - Its History, Use, and Distribution and Its Impact on Environmental-Quality and Global Climate, Global Biomass Burning, 3-21, 1991.

AQEG, Evidential value of Defra air quality compliance monitoring, Air Quality Expert Group, 2015.

Badami, M. G., Transport and urban air pollution in India, Environ Manage, 36, 195-204, doi:10.1007/s00267-004-0106-x, 2005.

Barnes, J. H., Hayes, E. T., Chatterton, T. J., and Longhurst, J. W. S., Policy disconnect: A critical review of UK air quality policy in relation to EU and LAQM responsibilities over the last 20 years, Environ Sci Policy, 85, 28-39, doi:10.1016/j.envsci.2018.03.024, 2018.

Behera, S. N., and Sharma, M., Reconstructing Primary and Secondary Components of PM2.5 Composition for an Urban Atmosphere, Aerosol Science and Technology, 44, 983-992, doi:10.1080/02786826.2010.504245, 2010.

Bockarie, A. S., Marais, E. A., and MacKenzie, A. R., Air pollution and climate forcing of the charcoal industry in Africa, Environ. Sci. Technol., 54, 13429-13438, doi:10.1021/acs.est.0c03754, 2020.

Bucsela, E. J., Celarier, E. A., Wenig, M. O., Gleason, J. F., Veefkind, J. P., Boersma, K. F., and Brinksma, E. J., Algorithm for NO_2 vertical column retrieval from the ozone monitoring instrument, Ieee T Geosci Remote, 44, 1245-1258, doi:10.1109/Tgrs.2005.863715, 2006.

Bucsela, E. J., Krotkov, N. A., Celarier, E. A., Lamsal, L. N., Swartz, W. H., Bhartia, P. K., Boersma, K. F., Veefkind, J. P., Gleason, J. F., and Pickering, K. E., A new stratospheric and tropospheric NO_2 retrieval algorithm for nadir-viewing satellite instruments: applications to OMI, Atmos. Meas. Tech., 6, 2607-2626, doi:10.5194/amt-6-2607-2013, 2013.

Burnett, R., Pope, C. A., Ezzati, M., Olives, C., Lim, S. S., Mehta, S., Shin, H. H., Singh, G., Hubbell, B., Brauer, M., et al., An Integrated Risk Function for Estimating the Global Burden of Disease Attributable to Ambient Fine Particulate Matter Exposure, Environ. Health Persp., 122, 397-403, doi:10.1289/ehp.1307049, 2014.

Burnett, R., Chen, H., Szyszkowicz, M., Fann, N., Hubbell, B., Pope, C. A., Apte, J. S., Brauer, M., Cohen, A., Weichenthal, S., et al., Global estimates of mortality associated with long-term exposure to outdoor fine particulate matter, Proc. Natl. Acad. Sci. U.S.A., 115, 9592-9597, doi:10.1073/pnas.1803222115, 2018.

Butt, E. W., Turnock, S. T., Rigby, R., Reddington, C. L., Yoshioka, M., Johnson, J. S., Regayre, L. A., Pringle, K. J., Mann, G. W., and Spracklen, D. V., Global and regional trends

in particulate air pollution and attributable health burden over the past 50 years, Environ. Res. Lett., 12, doi:10.1088/1748-9326/aa87be, 2017.

Cacciottolo, M., Wang, X., Driscoll, I., Woodward, N., Saffari, A., Reyes, J., Serre, M. L., Vizuete, W., Sioutas, C., Morgan, T. E., et al., Particulate air pollutants, APOE alleles and their contributions to cognitive impairment in older women and to amyloidogenesis in experimental models, Transl. Psychiat., 7, doi:10.1038/tp.2016.280, 2017.

Carslaw, D., Williams, M., and Stedman, J.; Environmental Research Group, S. o. B. a. H. S., London, An Investigation of Different Approaches to Compliance Assessment in the Air Quality Directive 2008/50/EC, https://uk-air.defra.gov.uk/assets/documents/reports/cat05/1302150859_130213_Compliance_Assessment_Final.pdf, 2013.

Castell, N., Dauge, F. R., Schneider, P., Vogt, M., Lerner, U., Fishbain, B., Broday, D., and Bartonova, A., Can commercial low-cost sensor platforms contribute to air quality monitoring and exposure estimates?, Environ. Int., 99, 293-302, doi:10.1016/j.envint.2016.12.007, 2017.

Action Plan on Air Pollution Prevention and Control, http://www.gov.cn/zwgk/2013-09/12/content_2486773.htm, Last accessed: 07 June 2021, 2013.

Chua, S. Y. L., Warwick, A., Peto, T., Balaskas, K., Moore, A. T., Reisman, C., Desai, P., Lotery, A. J., Dhillon, B., Khaw, P. T., et al., Association of ambient air pollution with age-related macular degeneration and retinal thickness in UK Biobank, Br. J. Ophthalmol., doi:10.1136/bjophthalmol-2020-316218, 2021.

Cohen, A. J., Brauer, M., Burnett, R., Anderson, H. R., Frostad, J., Estep, K., Balakrishnan, K., Brunekreef, B., Dandona, L., Dandona, R., et al., Estimates and 25-year trends of the global burden of disease attributable to ambient air pollution: an analysis of data from the Global Burden of Diseases Study 2015, Lancet, 389, 1907-1918, doi:10.1016/S0140-6736(17)30505-6, 2017.

Cohen, A. J., Brauer, M., and Burnett, R., Estimates and 25-year trends of the global burden of disease attributable to ambient air pollution: an analysis of data from the Global Burden of Diseases Study 2015 (vol 389, pg 1907, 2017), Lancet, 391, 1576-1576, doi:10.1016/S0140-6736(18)30900-0, 2018.

Correia, A. W., Pope, C. A., Dockery, D. W., Wang, Y., Ezzati, M., and Dominici, F., Effect of Air Pollution Control on Life Expectancy in the United States An Analysis of 545 US Counties for the Period from 2000 to 2007, Epidemiology, 24, 23-31, doi:10.1097/EDE.0b013e3182770237, 2013.

De Smedt, I., Stavrakou, T., Muller, J. F., van der A, R. J., and Van Roozendael, M., Trend detection in satellite observations of formaldehyde tropospheric columns, Geophys. Res. Lett., 37, doi:10.1029/2010gl044245, 2010.

De Smedt, I., Theys, N., Yu, H., Danckaert, T., Lerot, C., Compernolle, S., Van Roozendael, M., Richter, A., Hilboll, A., Peters, E., et al., Algorithm theoretical baseline for formaldehyde

retrievals from S5P TROPOMI and from the QA4ECV project, Atmos. Meas. Tech., 11, 2395-2426, doi:10.5194/amt-11-2395-2018, 2018.

Clean Air Strategy, https://assets.publishing.service.gov.uk/government/uploads/system/uploads/attachment_data/file/770715/clean-air-strategy-2019.pdf, Last accessed: 06 June 2021, 2019.

Defra; Department for Environment, F. R. A., Air Pollution in the UK 2019, https://uk-air.defra.gov.uk/library/annualreport/viewonline?year=2019_issue_1&jump=tp#report_pdf, 2020.

Duncan, B. N., Yoshida, Y., Olson, J. R., Sillman, S., Martin, R. V., Lamsal, L., Hu, Y. T., Pickering, K. E., Retscher, C., Allen, D. J., et al., Application of OMI observations to a space-based indicator of NO_x and VOC controls on surface ozone formation, Atmos. Environ., 44, 2213-2223, doi:10.1016/j.atmosenv.2010.03.010, 2010.

Duncan, B. N., Prados, A. I., Lamsal, L. N., Liu, Y., Streets, D. G., Gupta, P., Hilsenrath, E., Kahn, R. A., Nielsen, J. E., Beyersdorf, A. J., et al., Satellite data of atmospheric pollution for US air quality applications: Examples of applications, summary of data end-user resources, answers to FAQs, and common mistakes to avoid, Atmos. Environ., 94, 647-662, doi:10.1016/j.atmosenv.2014.05.061, 2014.

Duncan, B. N., Lamsal, L. N., Thompson, A. M., Yoshida, Y., Lu, Z. F., Streets, D. G., Hurwitz, M. M., and Pickering, K. E., A space-based, high-resolution view of notable changes in urban NO_x pollution around the world (2005-2014), J. Geophys. Res.-Atmos., 121, 976-996, doi:10.1002/2015jd024121, 2016.

Elguindi, N., Granier, C., Stavrakou, T., Darras, S., Bauwens, M., Cao, H., Chen, C., van der Gon, H. A. C. D., Dubovik, O., Fu, T. M., et al., Intercomparison of Magnitudes and Trends in Anthropogenic Surface Emissions From Bottom-Up Inventories, Top-Down Estimates, and Emission Scenarios, Earths Future, 8, doi:10.1029/2020EF001520, 2020.

Feichter, J., and Leisner, T., Climate engineering: A critical review of approaches to modify the global energy balance, The European Physical Journal Special Topics, 176, 81-92, doi:10.1140/epjst/e2009-01149-8, 2009.

Fitzky, A. C., Sandén, H., Karl, T., Fares, S., Calfapietra, C., Grote, R., Saunier, A., and Rewald, B., The Interplay Between Ozone and Urban Vegetation—BVOC Emissions, Ozone Deposition, and Tree Ecophysiology, Frontiers in Forests and Global Change, 2, doi:10.3389/ffgc.2019.00050, 2019.

Fueglistaler, S., Dessler, A. E., Dunkerton, T. J., Folkins, I., Fu, Q., and Mote, P. W., Tropical Tropopause Layer, Rev Geophys, 47, doi:10.1029/2008rg000267, 2009.

Ganguly, T., Selvaraj, K. L., and Guttikunda, S. K., National Clean Air Programme (NCAP) for Indian cities: Review and outlook of clean air action plans, Atmos. Environ.-X, 8, doi:10.1016/j.aeaoa.2020.100096, 2020.

Geddes, J. A., Martin, R. V., Boys, B. L., and van Donkelaar, A., Long-Term Trends Worldwide in Ambient NO_2 Concentrations Inferred from Satellite Observations, Environ. Health Persp., 124, 281-289, doi:10.1289/ehp.1409567, 2016.

Gentner, D. R., and Xiong, F. L. Z., Tracking pollutant emissions, Nat. Geosci., 10, 883-884, doi:10.1038/s41561-017-0027-y, 2017.

Georgoulias, A. K., van der A, R. J., Stammes, P., Boersma, K. F., and Eskes, H. J., Trends and trend reversal detection in 2 decades of tropospheric NO_2 satellite observations, Atmos. Chem. Phys., 19, 6269-6294, doi:10.5194/acp-19-6269-2019, 2019.

Gil-Alana, L. A., Yaya, O. S., and Carmona-Gonzalez, N., Air quality in London: evidence of persistence, seasonality and trends, Theor Appl Climatol, 142, 103-115, doi:10.1007/s00704-020-03305-1, 2020.

Guttikunda, S. K., and Gurjar, B. R., Role of meteorology in seasonality of air pollution in megacity Delhi, India, Environ Monit Assess, 184, 3199-3211, doi:10.1007/s10661-011-2182-8, 2012.

Hanif, I., Impact of fossil fuels energy consumption, energy policies, and urban sprawl on carbon emissions in East Asia and the Pacific: A panel investigation, Energy Strateg Rev, 21, 16-24, doi:10.1016/j.esr.2018.04.006, 2018.

Heft-Neal, S., Burney, J., Bendavid, E., Voss, K. K., and Burke, M., Dust pollution from the Sahara and African infant mortality, Nature Sustainability, 3, 863-871, doi:10.1038/s41893-020-0562-1, 2020.

Hilboll, A., Richter, A., and Burrows, J. P., Long-term changes of tropospheric NO_2 over megacities derived from multiple satellite instruments, Atmos. Chem. Phys., 13, 4145-4169, doi:10.5194/acp-13-4145-2013, 2013.

Hsu, N. C., Tsay, S. C., King, M. D., and Herman, J. R., Aerosol properties over bright-reflecting source regions, Ieee T Geosci Remote, 42, 557-569, doi:10.1109/Tgrs.2004.824067, 2004.

Hung, K. N., Yuan, C. S., Lee, C. E., Ie, I. R., Yeh, M. J., Soong, K. Y., and Fang, S. C., Spatiotemporal distribution and long-range transport of atmospheric speciated mercury at three remote islands in Taiwan Strait and South China Sea, Atmos Res, 248, doi:10.1016/j.atmosres.2020.105193, 2021.

Iyer, S., Reiman, H., Møller, K. H., Rissanen, M. P., Kjaergaard, H. G., and Kurtén, T., Computational Investigation of $RO_2 + HO_2$ and $RO_2 + RO_2$ Reactions of Monoterpene Derived First-Generation Peroxy Radicals Leading to Radical Recycling, The Journal of Physical Chemistry A, 122, 9542-9552, doi:10.1021/acs.jpca.8b09241, 2018.

Jacob, D. J., Logan, J. A., Yevich, R. M., Gardner, G. M., Spivakovsky, C. M., Wofsy, S. C., Munger, J. W., Sillman, S., Prather, M. J., Rodgers, M. O., et al., Simulation of Summertime

Ozone over North-America, J. Geophys. Res.-Atmos., 98, 14797-14816, doi:10.1029/93jd01223, 1993.

Jin, X. M., Fiore, A., Boersma, K. F., De Smedt, I., and Valin, L., Inferring Changes in Summertime Surface Ozone-NO_x-VOC Chemistry over US Urban Areas from Two Decades of Satellite and Ground-Based Observations, Environ. Sci. Technol., 54, 6518-6529, doi:10.1021/acs.est.9b07785, 2020.

Jo, D. S., Hodzic, A., Emmons, L. K., Marais, E. A., Peng, Z., Nault, B. A., Hu, W. W., Campuzano-Jost, P., and Jimenez, J. L., A simplified parameterization of isoprene-epoxydiol-derived secondary organic aerosol (IEPOX-SOA) for global chemistry and climate models: a case study with GEOS-Chem v11-02-rc, Geosci. Model Dev., 12, 2983-3000, doi:10.5194/gmd-12-2983-2019, 2019.

Kablick III, G. P., Allen, D. R., Fromm, M. D., and Nedoluha, G. E., Australian PyroCb Smoke Generates Synoptic-Scale Stratospheric Anticyclones, Geophys. Res. Lett., 47, e2020GL088101, doi:https://doi.org/10.1029/2020GL088101, 2020.

Krotkov, N. A., Lamsal, L. N., Celarier, E. A., Swartz, W. H., Marchenko, S. V., Bucsela, E. J., Chan, K. L., Wenig, M., and Zara, M., The version 3 OMI NO_2 standard product, Atmos. Meas. Tech., 10, 3133-3149, doi:10.5194/amt-10-3133-2017, 2017.

Lamsal, L. N., Martin, R. V., Padmanabhan, A., van Donkelaar, A., Zhang, Q., Sioris, C. E., Chance, K., Kurosu, T. P., and Newchurch, M. J., Application of satellite observations for timely updates to global anthropogenic NO_x emission inventories, Geophys. Res. Lett., 38, doi:10.1029/2010gl046476, 2011.

Lamsal, L. N., Duncan, B. N., Yoshida, Y., Krotkov, N. A., Pickering, K. E., Streets, D. G., and Lu, Z. F., U.S. NO_2 trends (2005-2013): EPA Air Quality System (AQS) data versus improved observations from the Ozone Monitoring Instrument (OMI), Atmos. Environ., 110, 130-143, doi:10.1016/j.atmosenv.2015.03.055, 2015.

Lamsal, L. N., Krotkov, N. A., Vasilkov, A., Marchenko, S., Qin, W. H., Yang, E. S., Fasnacht, Z., Joiner, J., Choi, S., Haffner, D., et al., Ozone Monitoring Instrument (OMI) Aura nitrogen dioxide standard product version 4.0 with improved surface and cloud treatments, Atmos. Meas. Tech., 14, 455-479, doi:10.5194/amt-14-455-2021, 2021.

Lelieveld, J., Beirle, S., Hormann, C., Stenchikov, G., and Wagner, T., Abrupt recent trend changes in atmospheric nitrogen dioxide over the Middle East, Sci. Adv., 1, doi:10.1126/sciadv.1500498, 2015.

Lelieveld, J., Klingmuller, K., Pozzer, A., Poschl, U., Fnais, M., Daiber, A., and Munzel, T., Cardiovascular disease burden from ambient air pollution in Europe reassessed using novel hazard ratio functions, Eur Heart J, 40, 1590-1596, doi:10.1093/eurheartj/ehz135, 2019.

Lelieveld, J., Pozzer, A., Poschl, U., Fnais, M., Haines, A., and Munzel, T., Loss of life expectancy from air pollution compared to other risk factors: a worldwide perspective, Cardiovasc Res, 116, 1910-1917, doi:10.1093/cvr/cvaa025, 2020.

Levy, R. C., Mattoo, S., Munchak, L. A., Remer, L. A., Sayer, A. M., Patadia, F., and Hsu, N. C., The Collection 6 MODIS aerosol products over land and ocean, Atmos. Meas. Tech., 6, 2989-3034, doi:10.5194/amt-6-2989-2013, 2013.

Li, C., Martin, R. V., van Donkelaar, A., Boys, B. L., Hammer, M. S., Xu, J. W., Marais, E. A., Reff, A., Strum, M., Ridley, D. A., et al., Trends in chemical composition of global and regional population-weighted fine particulate matter estimated for 25 years, Environ. Sci. Technol., 51, 11185-11195, doi:10.1021/acs.est.7b02530, 2017.

Li, Q., Zheng, D. N., Wang, Y. Y., Li, R., Wu, H. P., Xu, S. X., Kang, Y. F., Cao, Y. X., Chen, X. J., Zhu, Y. M., et al., Association between exposure to airborne particulate matter less than 2.5 μm and human fecundity in China, Environ. Int., 146, doi:10.1016/j.envint.2020.106231, 2021.

Liu, F., Beirle, S., Zhang, Q., van der A, R. J., Zheng, B., Tong, D., and He, K. B., NO_x emission trends over Chinese cities estimated from OMI observations during 2005 to 2015, Atmos. Chem. Phys., 17, 9261-9275, doi:10.5194/acp-17-9261-2017, 2017.

Loughlin, D. H., Ranjithan, S. R., Baugh, J. W., and Brill, E. D., Application of genetic algorithms for the design of ozone control strategies, J Air Waste Manage, 50, 1050-1063, doi:10.1080/10473289.2000.10464133, 2000.

Ludwig, J., Marufu, L. T., Huber, B., Andreae, M. O., and Helas, G., Domestic combustion of biomass fuels in developing countries: A major source of atmospheric pollutants, J Atmos Chem, 44, 23-37, doi:10.1023/A:1022159910667, 2003.

Marais, E. A., Jacob, D. J., Kurosu, T. P., Chance, K., Murphy, J. G., Reeves, C., Mills, G., Casadio, S., Millet, D. B., Barkley, M. P., et al., Isoprene emissions in Africa inferred from OMI observations of formaldehyde columns, Atmos. Chem. Phys., 12, 6219-6235, doi:10.5194/acp-12-6219-2012, 2012.

Marais, E. A., and Wiedinmyer, C., Air quality impact of Diffuse and Inefficient Combustion Emissions in Africa (DICE-Africa), Environ. Sci. Technol., 50, 10739-10745, doi:10.1021/acs.est.6b02602, 2016.

Marais, E. A., Silvern, R. F., Vodonos, A., Dupin, E., Bockarie, A. S., Mickley, L. J., and Schwartz, J., Air Quality and Health Impact of Future Fossil Fuel Use for Electricity Generation and Transport in Africa, Environ. Sci. Technol., 53, 13524-13534, doi:10.1021/acs.est.9b04958, 2019.

Martin, R. V., Fiore, A. M., and Van Donkelaar, A., Space-based diagnosis of surface ozone sensitivity to anthropogenic emissions, Geophys. Res. Lett., 31, doi:10.1029/2004gl019416, 2004.

McDuffie, E. E., Martin, R. V., Spadaro, J. V., Burnett, R., Smith, S. J., O'Rourke, P., Hammer, M. S., van Donkelaar, A., Bindle, L., Shah, V., et al., Source sector and fuel

contributions to ambient $PM_{2.5}$ and attributable mortality across multiple spatial scales, Nat. Commun., 12, 3594, doi:10.1038/s41467-021-23853-y, 2021.

Melkonyan, A., and Kuttler, W., Long-term analysis of NO, NO_2 and O_3 concentrations in North Rhine-Westphalia, Germany, Atmos. Environ., 60, 316-326, doi:10.1016/j.atmosenv.2012.06.048, 2012.

Munchak, L. A., Levy, R. C., Mattoo, S., Remer, L. A., Holben, B. N., Schafer, J. S., Hostetler, C. A., and Ferrare, R. A., MODIS 3 km aerosol product: applications over land in an urban/suburban region, Atmos. Meas. Tech., 6, 1747-1759, doi:10.5194/amt-6-1747-2013, 2013.

Ng, N. L., Brown, S. S., Archibald, A. T., Atlas, E., Cohen, R. C., Crowley, J. N., Day, D. A., Donahue, N. M., Fry, J. L., Fuchs, H., et al., Nitrate radicals and biogenic volatile organic compounds: oxidation, mechanisms, and organic aerosol, Atmos. Chem. Phys., 17, 2103-2162, doi:10.5194/acp-17-2103-2017, 2017.

Palmer, P. I., Jacob, D. J., Chance, K., Martin, R. V., Spurr, R. J. D., Kurosu, T. P., Bey, I., Yantosca, R., Fiore, A., and Li, Q. B., Air mass factor formulation for spectroscopic measurements from satellites: Application to formaldehyde retrievals from the Global Ozone Monitoring Experiment, J. Geophys. Res.-Atmos., 106, 14539-14550, doi:10.1029/2000jd900772, 2001.

Pope, C. A., Ezzati, M., and Dockery, D. W., Fine-Particulate Air Pollution and Life Expectancy in the United States., New Engl J Med, 360, 376-386, doi:10.1056/NEJMsa0805646, 2009.

Potts, D. A., Marais, E. A., Boesch, H., Pope, R. J., Lee, J., Drysdale, W., Chipperfield, M. P., Kerridge, B., Siddans, R., Moore, D. P., et al., Diagnosing air quality changes in the UK during the COVID-19 lockdown using TROPOMI and GEOS-Chem, Environ. Res. Lett., 16, doi:10.1088/1748-9326/abde5d, 2021.

Remer, L. A., Mattoo, S., Levy, R. C., and Munchak, L. A., MODIS 3 km aerosol product: algorithm and global perspective, Atmos. Meas. Tech., 6, 1829-1844, doi:10.5194/amt-6-1829-2013, 2013.

Russell, A. R., Valin, L. C., and Cohen, R. C., Trends in OMI NO_2 observations over the United States: effects of emission control technology and the economic recession, Atmos. Chem. Phys., 12, 12197-12209, doi:10.5194/acp-12-12197-2012, 2012.

Sahu, R., Nagal, A., Dixit, K. K., Unnibhavi, H., Mantravadi, S., Nair, S., Simmhan, Y., Mishra, B., Zele, R., Sutaria, R., et al., Robust statistical calibration and characterization of portable low-cost air quality monitoring sensors to quantify real-time O_3 and NO_2 concentrations in diverse environments, Atmos. Meas. Tech., 14, 37-52, doi:10.5194/amt-14-37-2021, 2021.

Sandrini, S., Giulianelli, L., Decesari, S., Fuzzi, S., Cristofanelli, P., Marinoni, A., Bonasoni, P., Chiari, M., Calzolai, G., Canepari, S., et al., In situ physical and chemical characterisation

of the Eyjafjallajökull aerosol plume in the free troposphere over Italy, Atmos. Chem. Phys., 14, 1075-1092, doi:10.5194/acp-14-1075-2014, 2014.

Sayer, A. M., Munchak, L. A., Hsu, N. C., Levy, R. C., Bettenhausen, C., and Jeong, M. J., MODIS Collection 6 aerosol products: Comparison between Aqua's e-Deep Blue, Dark Target, and "merged" data sets, and usage recommendations, J. Geophys. Res.-Atmos., 119, 13965-13989, doi:10.1002/2014jd022453, 2014.

Schraufnagel, D. E., Balmes, J. R., Cowl, C. T., De Matteis, S., Jung, S. H., Mortimer, K., Perez-Padilla, R., Rice, M. B., Riojas-Rodriguez, H., Sood, A., et al., Air pollution and noncommunicable diseases A review by the Forum of International Respiratory Societies' Environmental Committee, Part 1: The damaging effects of air pollution, Chest, 155, 409-416, doi:10.1016/j.chest.2018.10.042, 2019a.

Schraufnagel, D. E., Balmes, J. R., Cowl, C. T., De Matteis, S., Jung, S. H., Mortimer, K., Perez-Padilla, R., Rice, M. B., Riojas-Rodriguez, H., Sood, A., et al., Air Pollution and Noncommunicable Diseases A Review by the Forum of International Respiratory Societies' Environmental Committee, Part 2: Air Pollution and Organ Systems, Chest, 155, 417-426, doi:10.1016/j.chest.2018.10.041, 2019b.

Shah, V., Jacob, D. J., Li, K., Silvern, R. F., Zhai, S. X., Liu, M. Y., Lin, J. T., and Zhang, Q., Effect of changing NO_x lifetime on the seasonality and long-term trends of satellite-observed tropospheric NO_2 columns over China, Atmos. Chem. Phys., 20, 1483-1495, doi:10.5194/acp-20-1483-2020, 2020.

Sherwen, T., Evans, M. J., Carpenter, L. J., Andrews, S. J., Lidster, R. T., Dix, B., Koenig, T. K., Sinreich, R., Ortega, I., Volkamer, R., et al., Iodine's impact on tropospheric oxidants: a global model study in GEOS-Chem, Atmos. Chem. Phys., 16, 1161-1186, doi:10.5194/acp-16-1161-2016, 2016.

Snyder, E. G., Watkins, T. H., Solomon, P. A., Thoma, E. D., Williams, R. W., Hagler, G. S. W., Shelow, D., Hindin, D. A., Kilaru, V. J., and Preuss, P. W., The Changing Paradigm of Air Pollution Monitoring, Environ. Sci. Technol., 47, 11369-11377, doi:10.1021/es4022602, 2013.

Sogacheva, L., Kolmonen, P., Virtanen, T. H., Rodriguez, E., Saponaro, G., and de Leeuw, G., Post-processing to remove residual clouds from aerosol optical depth retrieved using the Advanced Along Track Scanning Radiometer, Atmos. Meas. Tech., 10, doi:10.5194/amt-10-491-2017, 2017.

Stanaway, J. D., Afshin, A., Gakidou, E., Lim, S. S., Abate, D., Abate, K. H., Abbafati, C., Abbasi, N., Abbastabar, H., Abd-Allah, F., et al., Global, regional, and national comparative risk assessment of 84 behavioural, environmental and occupational, and metabolic risks or clusters of risks for 195 countries and territories, 1990-2017: a systematic analysis for the Global Burden of Disease Study 2017, Lancet, 392, 1923-1994, doi:10.1016/S0140-6736(18)32225-6, 2018.

Streets, D. G., Canty, T., Carmichael, G. R., de Foy, B., Dickerson, R. R., Duncan, B. N., Edwards, D. P., Haynes, J. A., Henze, D. K., Houyoux, M. R., et al., Emissions estimation from satellite retrievals: A review of current capability, Atmos. Environ., 77, 1011-1042, doi:10.1016/j.atmosenv.2013.05.051, 2013.

Thompson, A. M., Tao, W. K., Pickering, K. E., Scala, J. R., and Simpson, J., Tropical deep convection and ozone formation, B. Am. Meteorol. Soc., 78, 1043-1054, doi:10.1175/1520-0477(1997)078<1043:TDCAOF>2.0.CO;2, 1997.

Mobile research laboratories will keep track of UK air pollution, https://www.birmingham.ac.uk/news/latest/2021/03/mobile-research-laboratories-will-keep-track-of-uk-air-pollution.aspx, Last accessed: 15 August 2021, 2021.

Van Damme, M., Clarisse, L., Heald, C. L., Hurtmans, D., Ngadi, Y., Clerbaux, C., Dolman, A. J., Erisman, J. W., and Coheur, P. F., Global distributions, time series and error characterization of atmospheric ammonia (NH_3) from IASI satellite observations, Atmos. Chem. Phys., 14, 2905-2922, doi:10.5194/acp-14-2905-2014, 2014.

Van Damme, M., Clarisse, L., Dammers, E., Liu, X., Nowak, J. B., Clerbaux, C., Flechard, C. R., Galy-Lacaux, C., Xu, W., Neuman, J. A., et al., Towards validation of ammonia (NH_3) measurements from the IASI satellite, Atmos. Meas. Tech., 8, 1575-1591, doi:10.5194/amt-8-1575-2015, 2015.

Van Damme, M., Whitburn, S., Clarisse, L., Clerbaux, C., Hurtmans, D., and Coheur, P. F., Version 2 of the IASI NH_3 neural network retrieval algorithm: near-real-time and reanalysed datasets, Atmos. Meas. Tech., 10, 4905-4914, doi:10.5194/amt-10-4905-2017, 2017.

Van Damme, M., Clarisse, L., Franco, B., Sutton, M. A., Erisman, J. W., Kruit, R. W., van Zanten, M., Whitburn, S., Hadji-Lazaro, J., Hurtmans, D., et al., Global, regional and national trends of atmospheric ammonia derived from a decadal (2008-2018) satellite record, Environ. Res. Lett., doi:10.1088/1748-9326/abd5e0, 2020.

Vasilkov, A., Krotkov, N., Yang, E. S., Lamsal, L., Joiner, J., Castellanos, P., Fasnacht, Z., and Spurr, R., Explicit and consistent aerosol correction for visible wavelength satellite cloud and nitrogen dioxide retrievals based on optical properties from a global aerosol analysis, Atmos. Meas. Tech., 14, 2857-2871, doi:10.5194/amt-14-2857-2021, 2021.

Vinken, G. C. M., Boersma, K. F., van Donkelaar, A., and Zhang, L., Constraints on ship NO_x emissions in Europe using GEOS-Chem and OMI satellite NO_2 observations, Atmos. Chem. Phys., 14, 1353-1369, doi:10.5194/acp-14-1353-2014, 2014.

Walker, H. L., Heal, M. R., Braban, C. F., Ritchie, S., Conolly, C., Sanocka, A., Dragosits, U., and Twigg, M. M., Changing supersites: assessing the impact of the southern UK EMEP supersite relocation on measured atmospheric composition, Environ Res Commun, 1, doi:10.1088/2515-7620/ab1a6f, 2019.

Wang, T., Xue, L., Brimblecombe, P., Lam, Y. F., Li, L., and Zhang, L., Ozone pollution in China: A review of concentrations, meteorological influences, chemical precursors, and effects, Sci. Total. Environ., 575, 1582-1596, doi:10.1016/j.scitotenv.2016.10.081, 2017.

Weagle, C. L., Snider, G., Li, C., van Donkelaar, A., Philip, S., Bissonnette, P., Burke, I., Jackson, J., Latimer, R., Stone, E., et al., Global Sources of Fine Particulate Matter: Interpretation of $PM_{2.5}$ Chemical Composition Observed by SPARTAN using a Global Chemical Transport Model, Environ. Sci. Technol., 52, 11670-11681, doi:10.1021/acs.est.8b01658, 2018.

Wei, J., Li, Z. Q., Sun, L., Peng, Y. R., Liu, L., He, L. J., Qin, W. M., and Cribb, M., MODIS Collection 6.1 3 km resolution aerosol optical depth product: global evaluation and uncertainty analysis, Atmos. Environ., 240, doi:10.1016/j.atmosenv.2020.117768, 2020.

Whitburn, S., Van Damme, M., Clarisse, L., Bauduin, S., Heald, C. L., Hadji-Lazaro, J., Hurtmans, D., Zondlo, M. A., Clerbaux, C., and Coheur, P. F., A flexible and robust neural network IASI-NH_3 retrieval algorithm, J. Geophys. Res.-Atmos., 121, 6581-6599, doi:10.1002/2016jd024828, 2016.

Ambient air pollution, https://www.who.int/teams/environment-climate-change-and-health/air-quality-and-health/ambient-air-pollution, Last accessed: 06 June 2021, 2018.

Williams, D. E., Low Cost Sensor Networks: How Do We Know the Data Are Reliable?, ACS Sensors, 4, 2558-2565, doi:10.1021/acssensors.9b01455, 2019.

Wolfe, G. M., Nicely, J. M., Clair, J. M. S., Hanisco, T. F., Liao, J., Oman, L. D., Brune, W. B., Miller, D., Thames, A., Abad, G. G., et al., Mapping hydroxyl variability throughout the global remote troposphere via synthesis of airborne and satellite formaldehyde observations, Proc. Natl. Acad. Sci. U.S.A., 116, 11171-11180, doi:10.1073/pnas.1821661116, 2019.

Yang, Y., Wang, Y., Zhou, P., Yao, D., Ji, D., Sun, J., Wang, Y., Zhao, S., Huang, W., Yang, S., et al., Atmospheric reactivity and oxidation capacity during summer at a suburban site between Beijing and Tianjin, Atmos. Chem. Phys., 20, 8181-8200, doi:10.5194/acp-20-8181-2020, 2020.

Zhang, Y. L., Gao, T. G., Kang, S. C., Allen, S., Luo, X., and Allen, D., Microplastics in glaciers of the Tibetan Plateau: Evidence for the long-range transport of microplastics, Sci. Total. Environ., 758, doi:10.1016/j.scitotenv.2020.143634, 2021.

Zhu, Y., Chen, J., Bi, X., Kuhlmann, G., Chan, K. L., Dietrich, F., Brunner, D., Ye, S., and Wenig, M., Spatial and temporal representativeness of point measurements for nitrogen dioxide pollution levels in cities, Atmos. Chem. Phys., 20, 13241-13251, doi:10.5194/acp-20-13241-2020, 2020.

CHAPTER 2

LONG-TERM TRENDS IN AIR QUALITY IN MAJOR CITIES IN THE UK AND INDIA: A VIEW FROM SPACE

Abstract

Air quality networks in cities can be costly, inconsistent, and typically monitor a few pollutants. Space-based instruments provide global coverage spanning more than a decade to determine trends in air quality, augmenting surface networks. Here we target cities in the UK (London and Birmingham) and India (Delhi and Kanpur) and use observations of nitrogen dioxide (NO_2) from the Ozone Monitoring Instrument (OMI), ammonia (NH_3) from the Infrared Atmospheric Sounding Interferometer (IASI), formaldehyde (HCHO) from OMI as a proxy for non-methane volatile organic compounds (NMVOCs), and aerosol optical depth (AOD) from the Moderate Resolution Imaging Spectroradiometer (MODIS) for $PM_{2.5}$. We assess the skill of these products at reproducing monthly variability in surface concentrations of air pollutants where available. We find temporal consistency between column and surface NO_2 in cities in the UK and India ($R = 0.5$-0.7) and NH_3 at two of three rural sites in the UK ($R = 0.5$-0.7), but not between AOD and surface $PM_{2.5}$ ($R < 0.4$). MODIS AOD is consistent with AERONET at sites in the UK and India ($R \geq 0.8$) and reproduces significant decline in surface $PM_{2.5}$ in London (2.7 % a^{-1}) and Birmingham (3.7 % a^{-1}) since 2009. We derive long-term trends in the four cities for 2005-2018 from OMI and MODIS and for 2008-2018 from IASI. Trends of all pollutants are positive in Delhi, suggesting no air quality improvements there, despite rollout of controls on industrial and transport sectors. Kanpur, identified by the WHO as the most polluted city in the world in 2018, experiences a significant and substantial (3.1 % a^{-1}) increase in $PM_{2.5}$. NO_2, NH_3 and $PM_{2.5}$ decline in London and Birmingham are likely due in large part to emissions controls on vehicles. Trends are significant only for NO_2 and $PM_{2.5}$. Reactive NMVOCs decline in Birmingham, but the trend is not significant. There is a recent (2012-2018) steep (> 9 % a^{-1}) increase in reactive NMVOCs in London. The cause for this rapid increase is uncertain, but may reflect increased contribution of oxygenated VOCs from household products, the food and

beverage industry, and domestic wood burning, with implications for formation of ozone in a VOC-limited city.

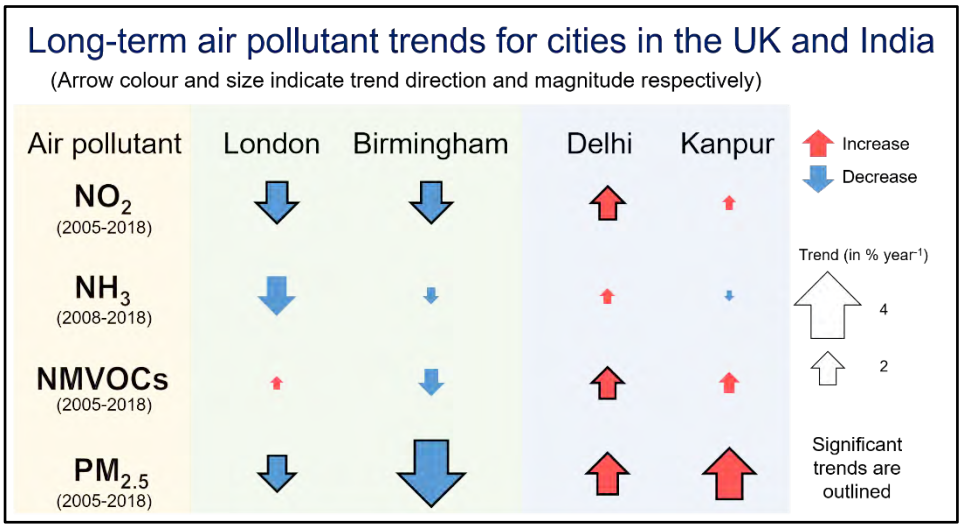

2.1 Introduction

More than 55 % of people live in urban areas and this is projected to increase to 68 % by 2050 (UN, 2019). Air pollution in cities routinely exceeds levels safe for human health (Landrigan et al., 2018). Regulatory air quality monitoring networks, such as those employed in cities in the UK and India, provide detailed data concerning individual species and specific locations, but are labour intensive to operate and maintain, with potential gaps in spatial coverage and discontinuities hindering longer-term trend discovery. Here we assess the ability to use the long record of satellite observations of atmospheric composition to monitor long-term trends in surface air quality in cities in the UK (London, Birmingham) and India (Delhi, Kanpur) of variable size, at a range of development stages, and with air pollutant concentrations that pose greater risk to health than previously thought (Vodonos et al., 2018).

Our study focuses on two large cities in the UK (London and Birmingham) and two in India (Delhi and Kanpur). Each is at a different stage of development: London is well developed, Birmingham is undergoing urban renewal, Delhi is experiencing rapid development (Singh and Grover, 2015), and Kanpur is a rapidly industrialising city (World Bank, 2014). Air quality policy is well established in the UK and the rapid decline in regulated air pollutants and their precursors has been monitored since 1970. According to the National Atmospheric Emission Inventory (NAEI), precursor emissions of fine particles with aerodynamic diameter < 2.5 μm ($PM_{2.5}$) decreased in 1970-2017 by 1.5 % a^{-1} for nitrogen oxides ($NO_x \equiv NO + NO_2$), 2.0 % a^{-1} for sulfur dioxide (SO_2), and 1.4 % a^{-1} for non-methane volatile organic compounds (NMVOCs). Primary $PM_{2.5}$ emissions decreased by 1.6 % a^{-1} over the same time period compared to a decline of just 0.2 % a^{-1} for ammonia (NH_3) emissions during 1980-2017 (Defra, 2019a). In UK cities, vehicles make a large contribution to air pollution year-round, with seasonal contributions from residential fuelwood burning, agricultural activity, and construction, and sporadic contributions from long-range transport of Saharan dust (Fuller et al., 2014; Crilley et al., 2015; 2017; Harrison et al., 2018; Ots et al., 2018; Carnell et al., 2019). Despite the decline in emissions, many areas in the UK still exceed the legal annual mean limit of NO_2 of 40 μg m^{-3} (Barnes et al., 2018), a threshold that may not adequately protect against health effects of long-term exposure to NO_2 (Lyons et al., 2020). Many areas will also exceed the annual mean $PM_{2.5}$ standard, if updated from 25 to 10 μg m^{-3}, the WHO guideline (Defra, 2019b). Reported annual mean $PM_{2.5}$ in 2016, obtained as the surface monitoring network average, is 12 μg m^{-3} for London and 10 μg m^{-3} for Birmingham (WHO, 2018). There is increasing concern over emissions of the important $PM_{2.5}$ precursor, NH_3, as there are no direct controls on the agricultural sector, the dominant NH_3 source (Carnell et al., 2019). There has

even been a recent increase in NH_3 emissions of 1.9 % a^{-1} in 2013-2017 (Defra, 2019a), attributed to agriculture (Carnell et al., 2019).

Air quality policy in India is in its infancy compared to the UK. The first air pollution act was passed in 1981; 30 years after the equivalent in the UK. There has been a steady rollout of European-style (Euro VI) vehicle emission standards, starting with Delhi in 2018 and scaling up to the whole country by 2020 (Govt. of India, 2016). Strict controls on coal-fired power plants have been in place since December 2015, but most power plants are non-compliant (Sugathan et al., 2018). National $PM_{2.5}$ concentration targets have been set at 20-30 % reductions by 2024 relative to 2017 levels (Govt. of India, 2019), but in 2016 measured annual mean $PM_{2.5}$ in Delhi and Kanpur exceeded the national standard (40 μg m^{-3}) by about a factor of 4: 143 μg m^{-3} for Delhi; 173 μg m^{-3} for Kanpur (WHO, 2018). In Delhi and Kanpur year-round emissions are dominated by vehicles, construction and household biofuel use in the city and industrial activity and coal combustion nearby (Guttikunda and Jawahar, 2014; Venkataraman et al., 2018). Seasonal enhancements come from intense agricultural fires along the Indo-Gangetic Plain (IGP) north of Delhi, frequent firework festivals, and dust storms originating from the Thar Desert and Arabian Peninsula (Ghosh et al., 2014; Parkhi et al., 2016; Yadav et al., 2017; Cusworth et al., 2018; Liu et al., 2018). Like the UK, the agricultural sector is not directly regulated and intense agricultural activity in the IGP contributes to the largest global NH_3 hotspot (Warner et al., 2017; Van Damme et al., 2018; Wang et al., 2019).

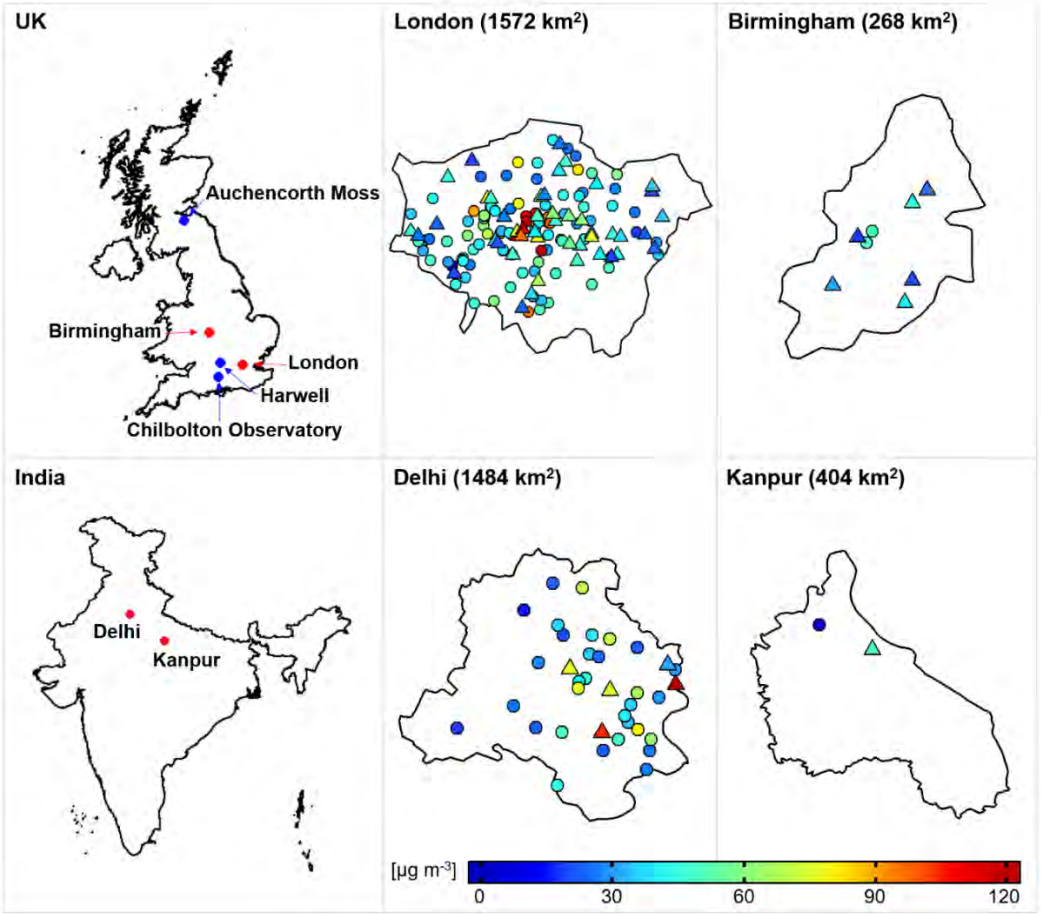

Figure 2.1 Spatial extent of surface NO_2 monitoring stations in London, Birmingham, Delhi, and Kanpur. The left panel shows the location of the target cities (red) and UK sites that are part of the European Monitoring and Evaluation Programme (EMEP) (blue). The centre and right panels show the locations of local authority regulatory NO_2 monitoring stations within the administrative boundaries of each city, coloured by mean midday NO_2 for 2005-2018, and separated into sites used (triangles) and not used (circles) to assess satellite observations of NO_2 (see text for details). The surface area of each city is indicated. Country and city boundaries are from GADM version 3.6 (GADM, 2018) and DataMeet (DataMeet, 2018).

Surface monitoring networks in cities in the UK and India needed to evaluate city-wide trends in air pollutant concentrations and precursor emissions can be exceedingly sparse and are often short term. To illustrate this, we show in Figure 2.1 the coverage of surface sites in the four cities that continuously monitor NO_2, the most widely monitored air pollutant in both countries. There are also diffusion tubes and emerging technologies that measure NO_2 at low cost, but these are susceptible to biases (Heal et al., 1999; Castell et al., 2017) and so are excluded. The

points in Figure 2.1 show sites established and maintained by national agencies, local city councils, and academic institutions. These are coloured by multi-year mean NO_2 around the satellite midday overpass (12h00-15h00 local time or LT) for our period of interest (2005-2018). London has the most extensive surface coverage. There can be more than 100 sites operating simultaneously, but many of these are short-term. Most long-term sites are in central London, and southeast London is devoid of stations. Birmingham has eight monitoring stations, but only two operated for the majority of 2005-2018. There are recently established comprehensive air quality monitoring sites in London and Birmingham, but these started operating in late 2018. More than 40 % of the NO_2 monitoring stations in Delhi were established in 2018 and there are concerns over data access and quality (Cusworth et al., 2018). Fewer stations in the four cities monitor $PM_{2.5}$ than NO_2 and measurements of NMVOCs are limited to a few short-term intensive campaigns and long-term sites that only measure light (short-chain) non-methane hydrocarbons. Long-term continuous monitoring of NH_3 in the UK is limited to hourly measurements at rural European Monitoring and Evaluation Programme (EMEP) sites (Figure 2.1) and monthly measurements at UK Eutrophying and Acidifying Pollutants (UKEAP) Network sites.

Satellite observations of atmospheric composition (Earth observations) provide consistent, long records (> 10 years) and global coverage of multiple air pollutants, complementing surface monitoring networks with limited spatial coverage and temporal records (Streets et al., 2013; Duncan et al., 2014). These have been used extensively as constraints on temporal changes in surface concentrations of air pollutants and precursor emissions (Kim et al., 2006; Lamsal et al., 2011; Zhu et al., 2014), but typically just targeting 1-2 pollutants. In this work, we consider Earth observations of NO_2, formaldehyde (HCHO), NH_3, and aerosol optical depth (AOD).

HCHO is a prompt, high-yield, ubiquitous oxidation product of NMVOCs used as a constraint on NMVOCs emissions (Miller et al., 2008; De Smedt et al., 2010; Marais et al., 2012; 2014b; 2014a). AOD has been used to derive surface concentrations of $PM_{2.5}$ for global assessment of the impact of air pollution on health (van Donkelaar et al., 2006; 2010; Brauer et al., 2016; Anenberg et al., 2019).

Here we conduct a systematic evaluation of the ability of satellite observations of NO_2, NH_3, HCHO and AOD to reproduce temporal variability of surface air pollution in the UK and India before going on to apply these satellite observations to estimate long-term changes in air pollution to assess the efficacy of air quality policies in the four cities of interest.

2.2 Space-Based and Surface Air Quality Observations

Earth observations of NO_2 and HCHO are from the Ozone Monitoring Instrument (OMI), NH_3 from the Infrared Atmospheric Sounding Interferometer (IASI), and AOD from the Moderate Resolution Imaging Spectroradiometer (MODIS). There are also observations of SO_2 and the secondary pollutant ozone from OMI, but SO_2 is below or close to the detection limit year-round for all cities, except in some months in Delhi, and UV measurements of tropospheric column ozone have limited sensitivity to ozone in the boundary layer (Zoogman et al., 2011). TROPOspheric Monitoring Instrument (TROPOMI) sensitivity to SO_2 is 4-fold better than OMI, but the observation record is short (October 2017 launch) (Theys et al., 2019). We use hourly observations of NO_2 and $PM_{2.5}$ from the network of surface sites in the four target cities and NH_3 from the rural EMEP sites in the UK, to assess whether satellite observations of NO_2, AOD, and NH_3 reproduce temporal variability of surface air quality. There are no direct reliable measurements of HCHO in the UK and measurements of NMVOCs are limited to a few sites that only measure light (≤ C9) hydrocarbons.

Figure 2.1 shows locations of EMEP sites in Harwell, England, south of Oxford (51.57° N, 1.32° W), Chilbolton Observatory, England, 40 miles south of Harwell (51.15° N, 1.44° W) and Auchencorth Moss, Scotland, south of Edinburgh (55.79° N, 3.24° W) (Malley et al., 2015; 2016; Walker et al., 2019). Instruments at the Harwell site were relocated to Chilbolton Observatory in 2016, providing the opportunity to assess the satellite data at sites with distinct agricultural activity and anthropogenic influence (Walker et al., 2019). There are also passive NH_3 samplers in the UK, but these have coarse temporal (monthly) resolution (Tang et al., 2018) and no temporal correlation ($R < 0.1$) with a previous version of the IASI NH_3 product (Van Damme et al., 2015).

2.2.1 Surface Monitoring Networks in the UK and India

Surface sites in the UK with continuous (hourly) observations of air pollutants typically use chemiluminescence instruments for NO_2, ion chromatography instruments for NH_3 (Stieger et al., 2018), and a range of reference instruments for PM_{10} and $PM_{2.5}$. Sites used here in London and Birmingham are from the national Department for Environment, Food and Rural Affairs (Defra) Automatic Urban and Rural Network (AURN) (https://uk-air.defra.gov.uk/data/data_selector; last accessed 28 January 2020) with additional sites in London from the King's College London Air Quality Network (LAQN) (https://www.londonair.org.uk/london/asp/datadownload.asp; last accessed 9 March 2019), and in Birmingham from Ricardo Energy & Environment (https://www.airqualityengland.co.uk/local-authority/data?la_id=407; last accessed 24 January 2020) and Birmingham City Council. Observations at the UK EMEP sites are from the EMEP Chemical Coordinating Centre (http://ebas.nilu.no/; last accessed 9 March 2019).

Measurements in India are limited to NO_2, PM_{10} and $PM_{2.5}$ monitoring sites maintained in Delhi by the Central Pollution Control Board (CPCB), India Meteorological Department (IMD) and Delhi Pollution Control Committee (DPCC), and in Kanpur by the Uttar Pradesh Pollution Control Board (UPPCB) and the Indian Institute of Technology (IIT) Kanpur (Gaur et al., 2014). $PM_{2.5}$ measurements at IIT Kanpur form part of the international Surface Particulate Matter Network (SPARTAN) (Snider et al., 2015; Weagle et al., 2018). Data from CPCB, IMD, DPCC, and UPPCB were downloaded from the CPCB site (https://app.cpcbccr.com/ccr/#/caaqm-dashboard/caaqm-landing; last accessed 5 February 2020). NASA AErosol RObotic NETwork (AERONET) sun photometer AOD measurements (version 3.0, Level 2.0; https://aeronet.gsfc.nasa.gov/; last accessed 5 February 2020) are used to validate MODIS AOD at Chilbolton (UK) and Kanpur (India) (Holben et al., 1998; Giles et al., 2019).

2.2.2 Earth Observations of Air Pollution

OMI onboard the NASA Aura satellite, launched in October 2004, has a nadir spatial resolution of 13 km × 24 km, a swath width of 2600 km, and passes overhead twice each day. OMI is a UV-visible spectrometer and so only provides daytime observations (13h30 LT). Global coverage was daily in 2005-2009 and is every 2 days thereafter due to the row anomaly (http://projects.knmi.nl/omi/research/product/rowanomaly-background.php). We use the operational NASA OMI Level 2 product of tropospheric column NO_2 for 2005-2018 (version 3.0; doi:10.5067/Aura/OMI/DATA2017; last accessed 29 February 2020) (Krotkov et al., 2017). Total columns of HCHO are from the Quality Assurance for Essential Climate Variables (QA4ECV) OMI Level 2 product for 2005-2018 (version 1.1; http://doi.org/10.18758/71021031; last accessed 15 February 2020) (De Smedt et al., 2018). We remove OMI NO_2 scenes with cloud radiance fraction ≥ 50 %, terrain reflectivity ≥ 30 %

and solar zenith angle (SZA) ≥ 85° (Lamsal et al., 2010) and OMI HCHO scenes with processing errors and processing quality flags not equal to zero (De Smedt et al., 2017). This removes scenes with cloud radiance fraction > 60 % and SZA > 80°. We apply additional filtering to remove scenes with cloud radiance fraction ≥ 50 % to be consistent with the threshold applied to OMI NO_2. This additional filtering removes 16 % of the data for London, 19 % for Birmingham, 7 % for Delhi, and 8 % for Kanpur.

IASI on the polar sun-synchronous Metop-A satellite, launched in October 2006 is an infrared instrument with a morning (09h30 LT) and nighttime (21h30 LT) overpass. It provides global coverage twice a day with circular 12 km diameter pixels at nadir and a swath width of 2200 km. We use observations for the morning only, when the thermal contrast and sensitivity to the boundary layer is greatest (Clarisse et al., 2010; Van Damme et al., 2014). We use the Level 2 reanalysis product of total column NH_3 (version 3R) obtained with consistent meteorology (ERA5) for clear-sky conditions (cloud fraction < 10 %) (Van Damme et al., 2020). The earlier IASI NH_3 product version (version 2R) was shown to be consistent with ground-based measurements of total column NH_3 at 9 global sites (Dammers et al., 2016).

The MODIS sensor onboard NASA's Aqua satellite, launched in May 2002, has a swath width of 2330 km, crosses the Equator at 13h30 LT and provides near-daily global coverage. We use the Level 2 Collection 6.1 Dark Target daily AOD product at 550 nm and 3 km resolution (Remer et al., 2013; Wei et al., 2019) (https://ladsweb.modaps.eosdis.nasa.gov/; last accessed 29 February 2020). We use only the highest quality AOD data (quality assurance flag of 3) (Munchak et al., 2013; Remer et al., 2013; Gupta et al., 2018).

2.3 Consistency between Earth Observations and Surface Air Pollution

Earth observation products retrieve column densities of pollutants throughout the atmospheric column (total for HCHO, AOD and NH_3; troposphere for NO_2), and are compared in what follows to surface concentrations from the surface monitoring network sites. This is to evaluate whether monthly variability in the column reproduces variability in surface concentrations before going on to use the satellite observations to quantify long-term trends in air pollution in the four cities. The majority of the enhancement in the column, with the exception of events like long-range transport, is near the surface (Fishman et al., 2008; Duncan et al., 2014). Sources of errors in retrieval of HCHO and NO_2 column densities include uncertainties in simulated vertical profiles, and presence of clouds and aerosols (Boersma et al., 2004; Lin et al., 2015; Zhu et al., 2016; Silvern et al., 2018). Retrieval of NH_3 column densities from IASI relies on thermal contrast between the Earth's surface and atmosphere and a sufficiently large training dataset (Whitburn et al., 2016; Van Damme et al., 2017). Errors in retrieval of AOD include uncertainties in aerosol properties and atmospheric conditions in matching simulated and observed top-of-atmosphere radiances from single viewing angle instruments like MODIS (Remer et al., 2005; Levy et al., 2007; 2013). To the extent that errors are random, these are reduced with temporal and spatial averaging.

In what follows, city-average OMI NO_2 and MODIS AOD are compared to representative city-average surface concentrations of NO_2 in all four cities, and $PM_{2.5}$ in London and Birmingham. IASI NH_3 is compared to coincident surface observations of NH_3 at UK EMEP sites (Figure 2.1).

2.3.1 Assessment of OMI NO_2

Data for NO_2 in the UK include 152 monitoring sites in London, 8 in Birmingham, 37 in Delhi, and 2 in Kanpur (Figure 2.1). The data we use for London and Birmingham have been independently ratified, but we still find and remove spurious NO_2 observations. These include persistent (> 24 hours) low (< 1 μg m^{-3}) values that do not exhibit diurnal variability. This occurs at fewer than 10 % of the sites and accounts for at most 1 % of the data at these sites. We identified that NO_2 data from DPCC and CPCB (Delhi) and from UPPCB (Kanpur) networks are inconsistently reported in either ppbv or μg m^{-3}. As information on the units of the individual data are not provided, we determine whether NO_2 is reported in ppbv or μg m^{-3} by regressing total NO_x (reported throughout in ppbv, following the CPCB protocol (CPCB, 2015)) against the sum of the reported NO and NO_2. We identify that NO_2 reported in ppbv (29 % of DPCC, 10 % of CPCB and 74 % of UPPCB data) populates along the 1:1 line and so we convert these to μg m^{-3} using 1.88 μg m^{-3} $ppbv^{-1}$. The same unit inconsistency does not exist for the IMD NO_2 data. These are reported throughout in ppbv and so are converted to μg m^{-3}.

We only consider surface observations coincident with the OMI record (2005-2018), around the satellite overpass (12h00-15h00 LT). We find that NO_2 declines at most sites in London (ranging from -0.8 to -3.6 % a^{-1}) and Birmingham (-1.1 to -3.8 % a^{-1}), with the exception of a few sites influenced by local sources. These include Marylebone Road in central London and Moor Street in Birmingham City Centre. Both are impacted by dense traffic and development projects (Carslaw et al., 2016; Harrison and Beddows, 2017). We find that NO_2 increases in Moor Street by 6.8 % a^{-1} from 2013 to 2017. There are too few long-term sites in Delhi and Kanpur to determine trends at individual sites. We do not filter out sites based on site classification, as this information is not readily available for sites in India. Instead, we remove

sites influenced by local effects and not consistent with month-to-month variability representative of the city. This we do by detrending surface NO_2 at each site, cross-correlating the detrended data for each site, and selecting sites with consistent month-to-month variability ($R > 0.5$) in the detrended data. The original surface NO_2 (including the trend) at the selected sites are then used to obtain city-average monthly mean NO_2 for comparison to OMI NO_2.

The selected sites are shown as triangles in Figure 2.1. Filtering for spurious data and selection of consistent sites leads to 14 years of data at 46 sites in London, 5.5 years of data at 6 sites in Birmingham, and 8 years of data at 5 sites in Delhi. There are only 2 sites in Kanpur, but these are not consistent for the brief period of overlap ($R < 0.5$ for 2011-2012), so we choose the site with the longest record (2011-2018). For the period of overlap for London and Birmingham (2011-2016), mean city-average midday NO_2 is 42.8 μg m^{-3} for London and 26.5 μg m^{-3} for Birmingham. For Delhi and Kanpur (2011-2018 overlap), mean city-average midday NO_2 is 91.9 μg m^{-3} for Delhi and 48.4 μg m^{-3} for Kanpur.

We sample satellite observations within the administrative boundaries of the four cities (Figure 2.1) to capture the domain that policymakers would target and assess. This is extended a few km beyond the administrative boundary for Birmingham, as otherwise there are too few observations due to frequent clouds and small city size (~300 km^2). Error-weighted OMI NO_2 monthly means are estimated for individual pixels centred within the administrative boundaries (including 6.5 km beyond for Birmingham). Months with < 5 observations are removed. The number of months retained is 77 % for Birmingham, > 90 % for London, and > 95 % for Delhi and Kanpur.

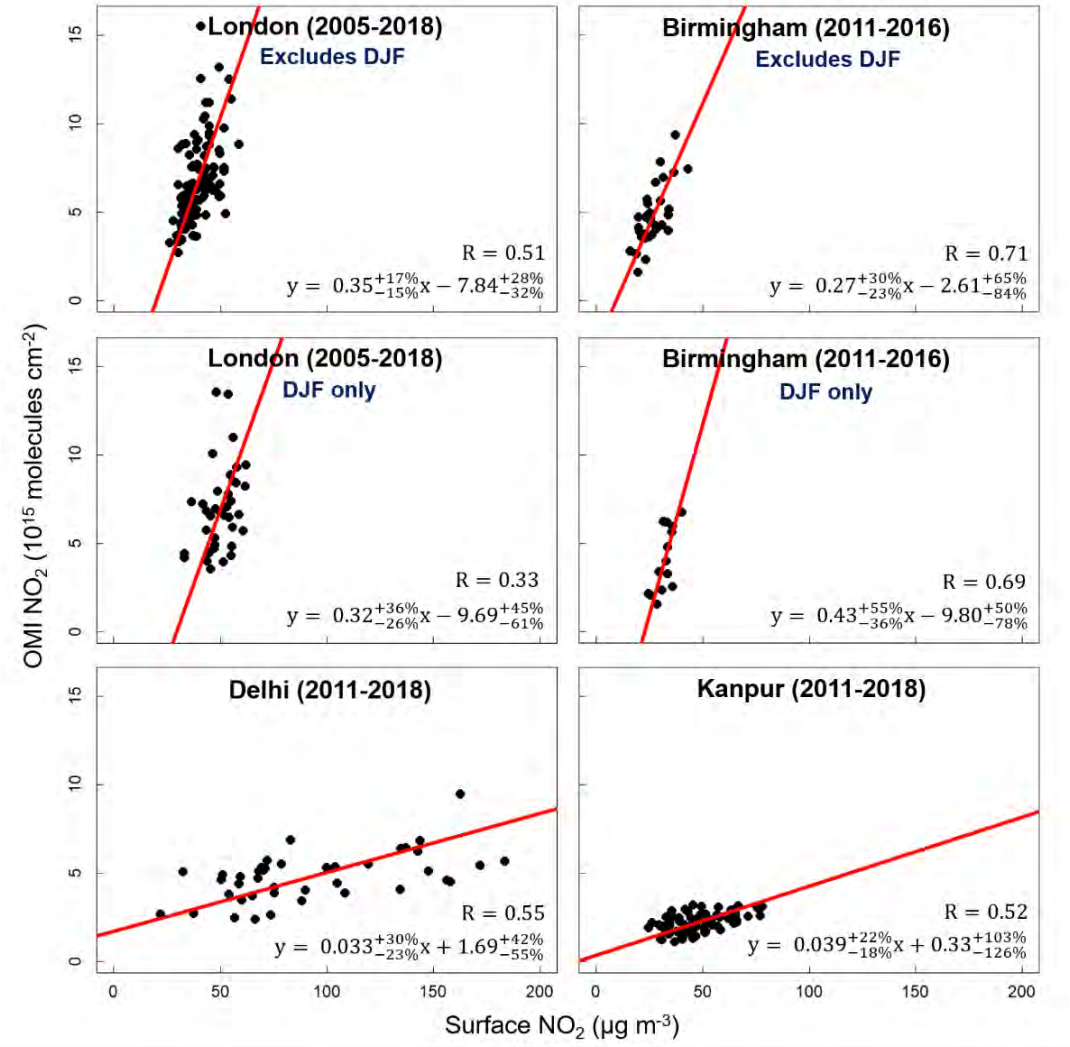

Figure 2.2 Assessment of OMI NO_2 with ground-based NO_2. Points are monthly means of city-average NO_2 from OMI and the surface networks for London (top and centre left), Birmingham (top and centre right), Delhi (bottom left), and Kanpur (bottom right). UK cities include panels with all months except December-February (DJF) (top) and DJF only (centre). Data for all months are given for cities in India. The red line is the standard major axis (SMA) regression. Values inset are Pearson's correlation coefficients and regression statistics. Relative errors on the slopes and intercepts are the 95 % confidence intervals (CI).

Figure 2.2 compares OMI and surface NO_2. The comparison for London and Birmingham is divided into months excluding winter (December-February) and winter months only. Factors that contribute to seasonality in the relationship between tropospheric column and surface NO_2 in locations with large seasonal shifts in temperature and solar insolation include reduced photolysis rates leading to longer NO_x lifetime in winter than summer (Boersma et al., 2009; Kenagy et al., 2018; Shah et al., 2020) and a lower mixed layer height in winter than summer

contributing to accumulation of pollution. Maximum mixed layer height for London is 900 m in winter compared to 1500 m in summer (Kotthaus and Grimmond, 2018). The slope for Birmingham in winter (0.43×10^{15} molecules cm^{-2} $(\mu g\ m^{-3})^{-1}$) is steeper than that for non-winter months (0.27×10^{15} molecules cm^{-2} $(\mu g\ m^{-3})^{-1}$), but the difference is not significant. The surface NO_2 measurements are also susceptible to interferences (positive biases) from thermal decomposition of NO_x reservoir compounds such as peroxyacetyl nitrates in chemiluminescence instruments that use heated molybdenum catalysts (Dunlea et al., 2007; Reed et al., 2016). The effect is worse in winter than summer in London and Birmingham due to abundance of NO_x reservoir compounds in winter (Lamsal et al., 2010). OMI and surface NO_2 monthly variability is consistent (R = 0.51-0.71), except for London in winter (R = 0.33). The correlation degrades (R = 0.40 for London, R = 0.54 for Birmingham) if all months are considered. The seasonal dependence of the relationship between satellite and surface NO_2 affects the ability to use OMI NO_2 to infer seasonality in the underlying NO_x emissions. The same consistency in monthly mean OMI and surface NO_2 in non-winter months ($R \geq 0.6$) has also been found over the UK city Leicester (surface area 73 km^2) (Kramer et al., 2008). Data for all months are used for Delhi and Kanpur, as there is less variability in mixed layer height in India than the UK. Seasonal mean maximum planetary boundary layer height in Delhi varies from 1200 m in winter to 1400 m during monsoon months (Nakoudi et al., 2019). Month-to-month variability in tropospheric column and surface NO_2 (Figure 2.2) is consistent in Delhi (R = 0.55) and Kanpur (R = 0.52). OMI NO_2 exhibits much greater variability for an increment change in surface NO_2 in the UK than in India, resulting in order-of-magnitude lower slopes for Delhi and Kanpur (0.033 and 0.039×10^{15} molecules cm^{-2} $(\mu g\ m^{-3})^{-1}$) than for London and Birmingham (0.35 and 0.27×10^{15} molecules cm^{-2} $(\mu g\ m^{-3})^{-1}$) (Figure 2.2). This difference is likely due to a combination of representativeness of surface sites and systematic biases in the

OMI NO_2 retrieval. In Delhi, the proportion of sites used in Figure 2.2 that measure the relatively lower concentration range of NO_2 (annual mean NO_2 < 50 μg m^{-3}) is just 20 % compared to 74 % for London, leading to a positive bias in city-average surface NO_2 in Delhi. In Kanpur, we use only one site located 600 m from a national highway. Aerosols are not explicitly accounted for in the OMI NO_2 retrieval (Krotkov et al., 2017). For very polluted cities like Delhi and Kanpur, this can lead to ~20% underestimate in OMI NO_2 (Choi et al., 2020; Vasilkov et al., 2020).

2.3.2 Assessment of IASI NH_3

Figure 2.3 compares monthly mean IASI and surface NH_3 at the three UK EMEP sites. IASI is sampled up to 20 km around the surface site following the approach of Dammers et al. (2016) and surface observations are sampled around the IASI morning overpass (08h00-11h00 LT) on days with coincident IASI observations. As with NO_2, only months with more than 5 observations are used. 38 % of months are retained for Auchencorth Moss, 62 % for Harwell and 61 % for Chilbolton Observatory. For the months retained, average NH_3 is 1.6 μg nitrogen (N) m^{-3} for Auchencorth Moss, 2.5 μg N m^{-3} for Harwell and 6.1 μg N m^{-3} for Chilbolton Observatory. Chilbolton is southwest of mixed farmland, contributing to levels of NH_3 about 3 times higher than at Harwell (Walker et al., 2019). Harwell has more dynamic range in NH_3 and stronger correlation (R = 0.69) than the other two sites (R = 0.37 for Auchencorth Moss; R = 0.50 for Chilbolton Observatory). Weak correlation at Auchencorth Moss may be because surface NH_3 concentrations are near the instrument detection limit (monthly mean NH_3 < 2.0 μg N m^{-3}) and also because of low thermal contrast between the surface and overlying atmosphere (Van Damme et al., 2015; Dammers et al., 2016). The slope for Auchencorth Moss (4.02×10^{15} molecules cm^{-2} (μg N m^{-3})$^{-1}$) is steeper than the slopes observed at sites with greater surface concentrations of NH_3 (Harwell = 2.23×10^{15} molecules cm^{-2} (μg N m^{-3})$^{-1}$ and

Chilbolton = 2.07 × 10^{15} molecules cm^{-2} (µg N m^{-3})$^{-1}$). Steeper slopes for sites with relatively low NH_3 concentrations is consistent with assessment of earlier IASI NH_3 product versions (Van Damme et al., 2015; Dammers et al., 2016).

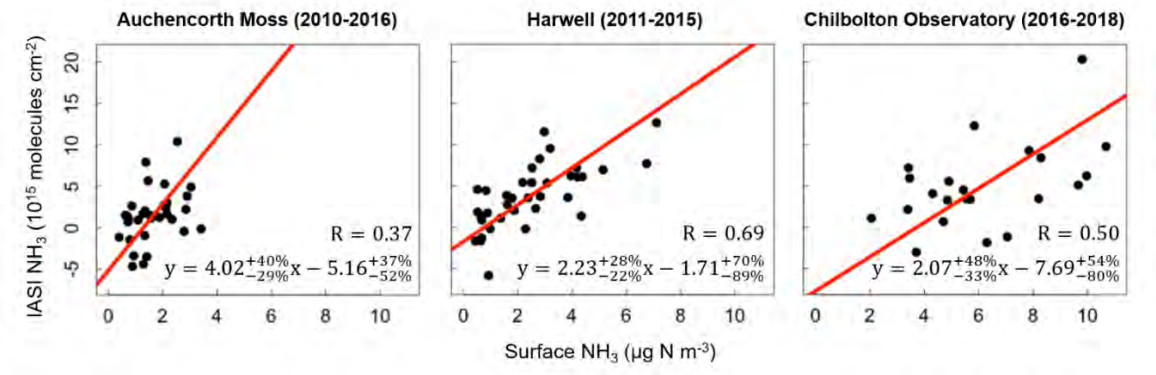

Figure 2.3 Assessment of IASI NH_3 with ground-based NH_3 at UK EMEP sites. Points are monthly means from IASI and the surface sites Auchencorth Moss (left), Harwell (middle) and Chilbolton Observatory (right). The red line is the SMA regression. Values inset are Pearson's correlation coefficients and regression statistics. Relative errors on the slope and intercept are the 95 % CI. Locations of UK EMEP sites are indicated in Figure 2.1.

2.3.3 Assessment of MODIS AOD

Figure 2.4 compares city-average monthly means of MODIS AOD and $PM_{2.5}$ for London in 2009-2018 and for Birmingham in 2009-2017. We use $PM_{2.5}$ data from 24 sites in London and 8 sites in Birmingham. We add 2 more Birmingham sites by deriving $PM_{2.5}$ from PM_{10} at 2 sites with only PM_{10} measurements. We use a conversion factor of 0.85 ($PM_{2.5}$ = 0.85 × PM_{10}) that we obtain from the slope of SMA regression of hourly $PM_{2.5}$ and PM_{10} at 6 sites in Birmingham with both measurements. We use a similar approach as applied to NO_2 to assess AOD. Only surface observations around the satellite overpass (12h00-15h00 LT) and with consistent detrended month-to-month variability (R > 0.5) are retained to obtain city-wide monthly mean $PM_{2.5}$. This results in 20 sites in London for 2009-2018 and 5 sites in Birmingham for 2009-2017. Mean midday city-average $PM_{2.5}$ for the period of overlap (2009-2017) is 13.7 µg m^{-3} in London and 11.3 µg m^{-3} in Birmingham. MODIS AOD monthly means are estimated for

London by averaging the pixels centred within its administrative boundary and for Birmingham within and 6.5 km beyond the administrative boundary, as with OMI NO_2 (Section 3.1). We remove months with < 160 observations; equivalent in spatial coverage to 5 OMI pixels at nadir (the threshold used for OMI). After filtering, 53 % of months are removed for London and 72 % for Birmingham, mostly in winter. Fewer months than OMI are retained, as MODIS uses stricter cloud filtering. The correlations in Figure 2.4 are weak (R = 0.34 for London, R = 0.23 for Birmingham) and do not improve if we apply a less strict threshold for the number of observations required to calculate monthly means. The poor correlation may be due to environmental factors that complicate the relationship between AOD and surface $PM_{2.5}$, such as variability in meteorological conditions, aerosol composition, enhancements in aerosols above the boundary layer, and the aerosol radiative properties (Schaap et al., 2009; van Donkelaar et al., 2016; Shaddick et al., 2018; Sathe et al., 2019). We find that the same assessment is not feasible for Delhi or Kanpur as the record of surface $PM_{2.5}$ and PM_{10} in these cities is too short.

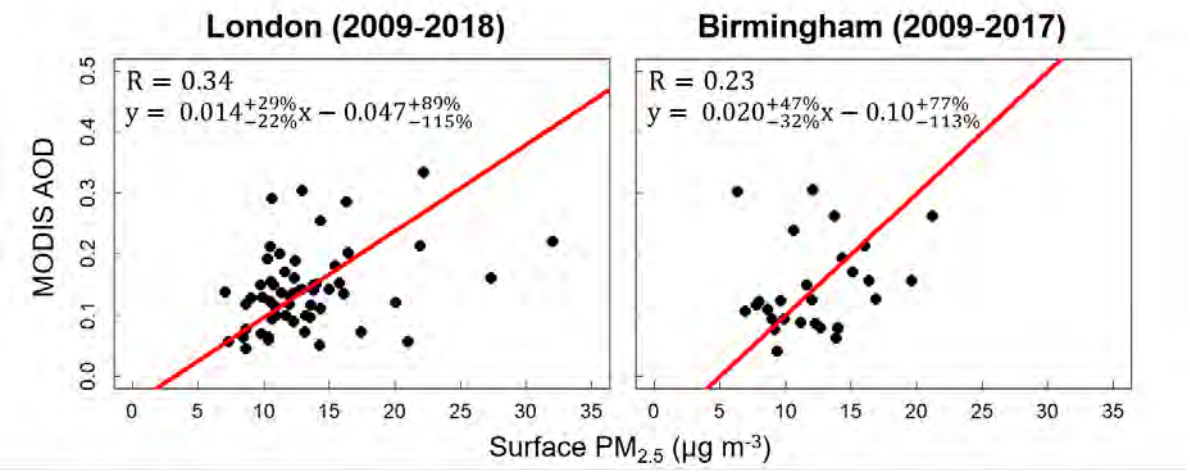

Figure 2.4 Assessment of MODIS AOD with surface $PM_{2.5}$ in London and Birmingham. Points are monthly means of city-average AOD from MODIS and $PM_{2.5}$ from surface networks for London (left) and Birmingham (right). The red line is the SMA regression. Values inset are Pearson's correlation coefficients and regression statistics. Relative errors on the slopes and intercepts are the 95 % CI.

Figure 2.5 compares time series of monthly mean city-average MODIS AOD and surface $PM_{2.5}$ in London (2009-2018) and Birmingham (2009-2017) to assess whether the weak correlation in Figure 2.4 affects agreement in trends of the two quantities. $PM_{2.5}$ is longer lived than NO_2, so trends in $PM_{2.5}$ (lifetime order weeks) for the limited number of sites mostly located in central London should be more representative of variability across the city than the surface sites of NO_2 (lifetime order hours against conversion to temporary reservoirs). The steeper decline in surface $PM_{2.5}$ in Birmingham (3.7 % a^{-1}) than in London (2.7 % a^{-1}) is reproduced in the AOD record (3.7 % a^{-1} in Birmingham; 2.5 % a^{-1} in London), although the AOD trends are not significant. In the two UK cities, surface $PM_{2.5}$ peaks in spring, whereas AOD peaks in the summer, determined from multiyear monthly means (not shown). There are too few $PM_{2.5}$ measurements in Delhi and Kanpur to compare long-term trends.

We compare the MODIS AOD product against ground-truth AOD from AERONET at long-term sites in Kanpur and Chilbolton to assess whether errors in satellite retrieval of AOD contribute to the weak temporal correlation between MODIS AOD and surface $PM_{2.5}$. Daily AERONET AOD at 550 nm is estimated by interpolation using the second-order polynomial relationship between the logarithmic AOD and logarithmic wavelengths at 440, 500, 675 and 870 nm (Kaufman, 1993; Eck et al., 1999; Levy et al., 2010; Li et al., 2012; Georgoulias et al., 2016). AERONET is sampled 30 minutes around the MODIS overpass and MODIS is sampled 27.5 km around the AERONET site (Levy et al., 2010; Petrenko et al., 2012; Georgoulias et al., 2016; McPhetres and Aggarwal, 2018). Months with fewer than 160 MODIS observations are removed.

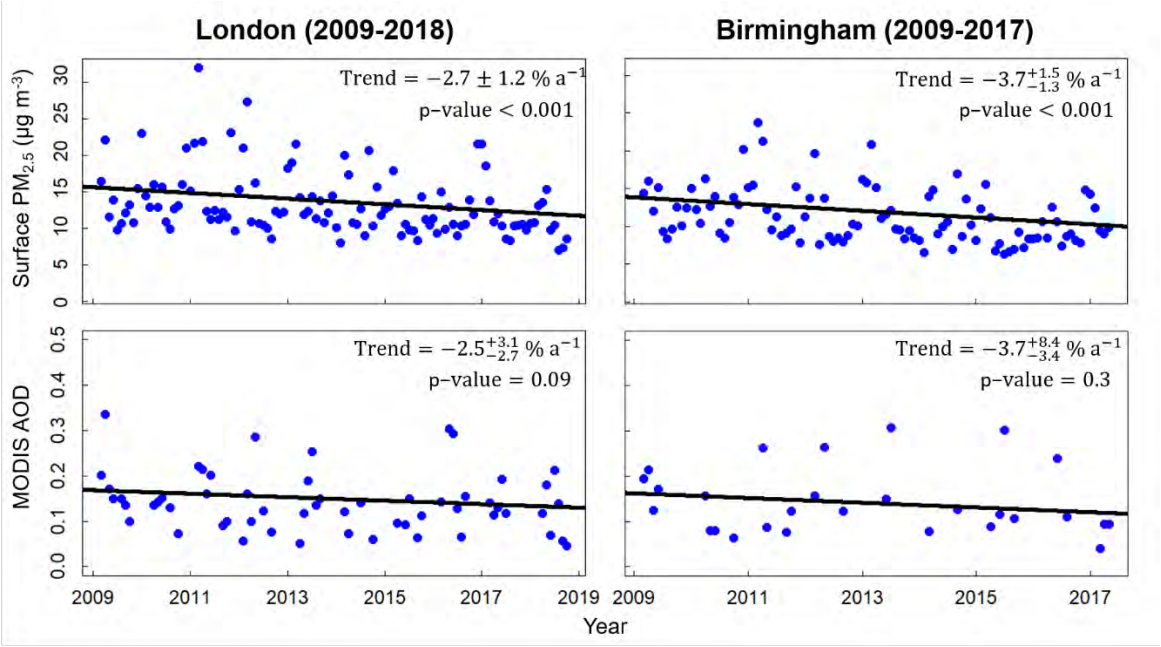

Figure 2.5 Time series of surface $PM_{2.5}$ and MODIS AOD in 2009-2018 for London (left) and 2009-2017 for Birmingham (right). Points are city-average monthly means of $PM_{2.5}$ from the surface network (top) and AOD from MODIS (bottom). Black lines are trends obtained with the Theil-Sen single median estimator. Values inset are annual trends and p-values. Absolute errors on the trends are 95 % CI. Trends are considered significant at the 95 % CI (p-value < 0.05).

Figure 2.6 compares coincident AOD monthly means from MODIS and AERONET for Kanpur and Chilbolton. Monthly variability in MODIS and AERONET AOD is consistent at both sites ($R \geq 0.8$). MODIS exhibits no appreciable bias at Kanpur. There is positive variance (slope = 1.4) at Chilbolton that may result from sensitivity to errors in surface reflectivity at low AOD (Remer et al., 2013; Bilal et al., 2018) and residual cloud contamination (Wei et al., 2018; 2020). Mhawish et al. (2017) obtained similarly strong correlation ($R = 0.8$), but positive bias (26 %), of MODIS AOD at Kanpur from an earlier 3 km MODIS AOD product (Collection 6).

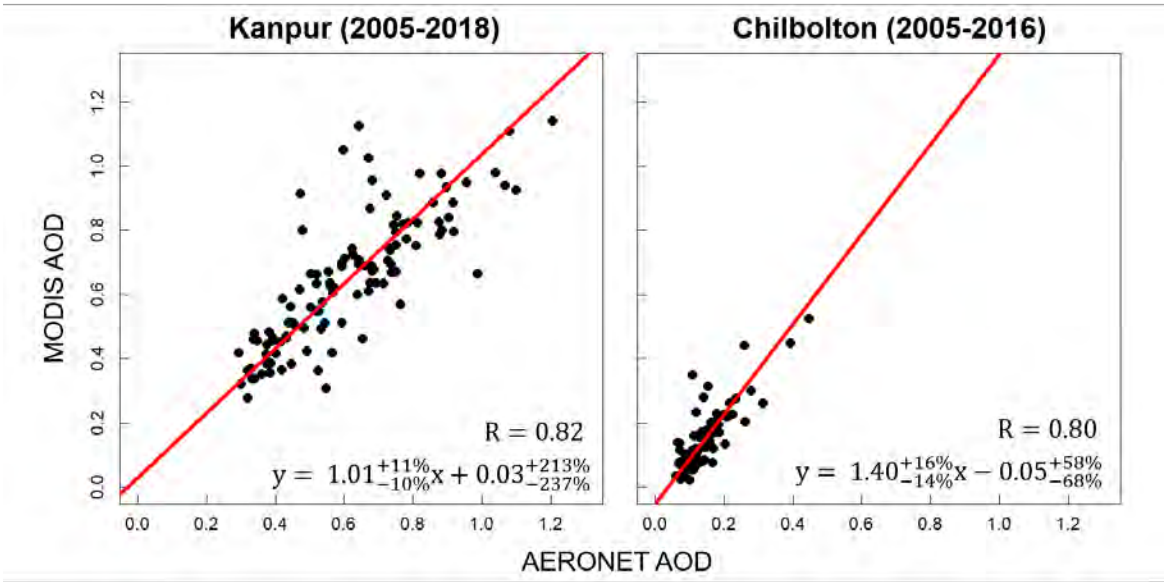

Figure 2.6 Validation of MODIS AOD with AERONET AOD in Kanpur and Chilbolton. Points are monthly means of MODIS and AERONET AOD for Kanpur (left) and Chilbolton (right). The red line is the SMA regression. Values inset are Pearson's correlation coefficients and regression statistics. Relative errors on the slopes and intercepts are the 95 % CI.

2.4 Air Quality Trends in London, Birmingham, Delhi, and Kanpur

The consistency we find between satellite and ground-based monthly mean city-average NO_2 (Figure 2.2) and rural NH_3 (Figure 2.3), and trends in city-average $PM_{2.5}$ (Figure 2.5) supports the use of the satellite record to constraint surface air quality. Variability in NO_2, HCHO, and NH_3 columns can also be related to precursor emissions of NO_x, NMVOCs, and NH_3 (Martin et al., 2003; Lamsal et al., 2011; Marais et al., 2012; Zhu et al., 2014; Dammers et al., 2019), as their lifetimes against conversion to temporary or permanent sinks are relatively short, varying from 1-12 hours depending on photochemical activity, abundance of pre-existing acidic aerosols, and proximity to large sources (Jones et al., 2009; Richter, 2009; Paulot et al., 2017; Van Damme et al., 2018). We adopt the same sampling approach as used to evaluate OMI NO_2. That is, we sample the satellite observations within the city administrative boundaries for

London, Delhi and Kanpur, and extend the sampling domain for Birmingham beyond the administrative boundary by 6.5 km for OMI and MODIS and 10 km for IASI.

We apply the Theil-Sen single median estimator to the time series and also test the effect of fitting a non-linear function (Weatherhead et al., 1998; van der A et al., 2006; Pope et al., 2018) to account explicitly for seasonality:

$$Y_m = A + BX_m + C\sin(\omega X_m + \emptyset) \quad (2\text{-}1)$$

Y_m is city-average satellite observations for month m, X_m is the number of months from the start month (January 2005 for OMI and MODIS, and January 2008 for IASI), and A, B, C and $\emptyset$ are fit parameters. A is the city-average satellite observations in the start month, B is the linear trend, and $[C\sin(\omega X_m + \emptyset)]$ is the seasonal component that includes the amplitude C, frequency ω (fixed to 12 months) and phase shift $\emptyset$. We only show the fit in Equation 2.1 if the trend B is different to that obtained with the Theil-Sen approach. The confidence intervals (CIs) for the Theil-Sen trends are estimated using bootstrap resampling and trends are considered significant for p-value < 0.05, that is, if the 95 % CI range does not intersect zero.

Figure 2.7 shows the time series of monthly means of city-average OMI NO_2 in the four cities for 2005-2018. Decline in OMI NO_2 in both London and Birmingham is 2.5 % a^{-1} and is significant. In Delhi, the OMI NO_2 increase is 2.0 % a^{-1} and is significant (p-value = 0.003), whereas the increase in Kanpur of 0.9 % a^{-1} is not (p-value = 0.06). The relationship between tropospheric column and surface NO_2 in London and Birmingham exhibits seasonality (Figure 2.2). This is in part due to seasonality in mixing depth. We find that excluding the winter months

in the time series has only a small effect on the trend. NO_2 should exhibit seasonality in all cities due to seasonal variability in its lifetime and sources (van der A et al., 2008). The fit in Equation 2.1 yields significant seasonality for all cities (p-value < 0.05 for the amplitude of the seasonality, C), but the linear trends are similar to those in Figure 2.7: -2.4 % a^{-1} for London and Birmingham; unchanged for Delhi and Kanpur.

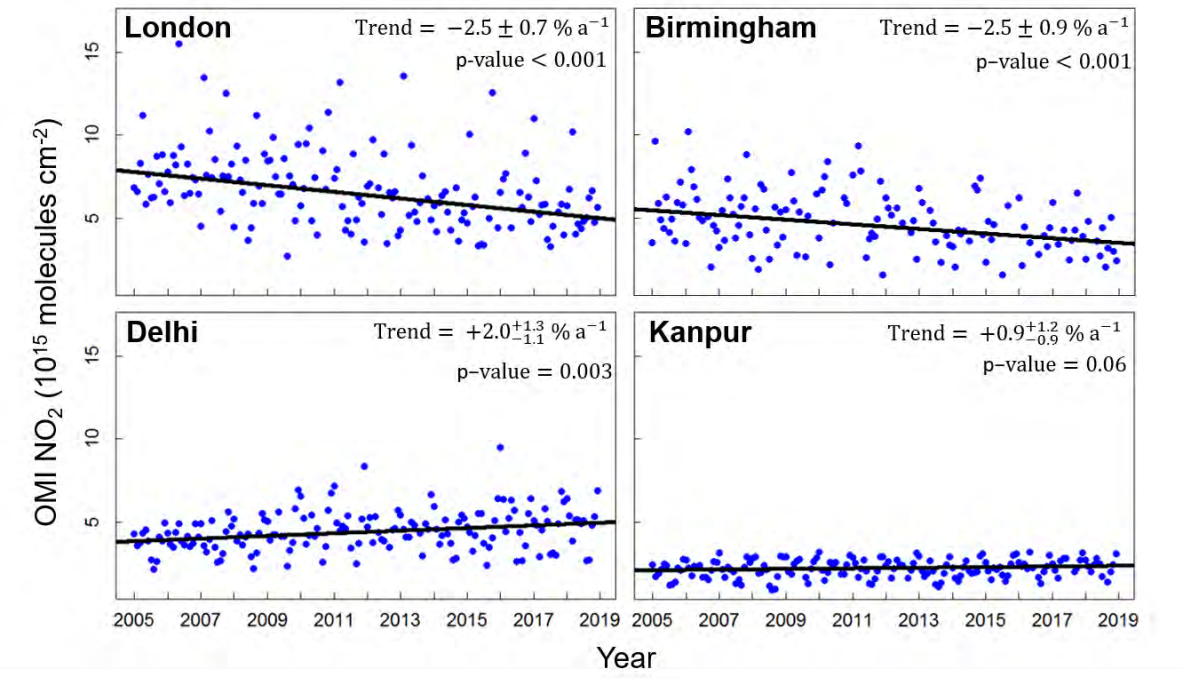

Figure 2.7 Time series of OMI NO_2 in 2005-2018 for London, Birmingham, Delhi and Kanpur. Points are city-average monthly means. Black lines are trends obtained with the Theil-Sen single median estimator. Values inset are annual trends and p-values. Absolute errors on the trends are 95 % CI.

Comparison of the OMI NO_2 trends in Figure 2.7 to surface observations is only possible for London, where there are 46 sites with consistent month-to-month variability representative of the city that operated continuously from 2005 to 2018. The trend obtained for OMI NO_2 in London (-2.5 % a^{-1}) is steeper than we estimate with the surface monitoring sites shown as triangles in Figure 2.1 (1.8 % a^{-1} for 2005-2018). Most sites are in central London, and NO_2 trends in outer London are 1.6 times steeper than in central London (Carslaw et al., 2011). The

decline in NO_2 in the two UK cities is less than the rate of decline in national NO_x emissions (3.8 % a^{-1}) for 2005-2017 from the national bottom-up emission inventory (Defra, 2019a). This may reflect a combination of factors. There is less steep decline in NO_x emissions in London compared to the national total that may in part be due to discrepancies between real-world and reported diesel NO_x emissions (Fontaras et al., 2014), sustained heavy traffic in central London, and an increase in NO_2-to-NO_x emission ratios dampening decline in NO_2 (Grange et al., 2017). There is also weakened sensitivity of the tropospheric column to changes in surface NO_2 due to a gradual increase in the relative contribution of the free tropospheric background to the tropospheric column (Silvern et al., 2019). This weakening of the trend in the tropospheric column will likely be less in London than in Birmingham, due to greater local surface emissions in large cities such as London (Zara et al., 2021). The positive trends in Delhi and Kanpur likely reflect a 2-fold increase in vehicle ownership in Delhi (Govt. of Delhi, 2019), rapid industrialisation in Kanpur (Nagar et al., 2019), and limited effect of air quality policies on pollution sources. This is corroborated by NO_x emissions compliance failures at more than 50 % of coal-fired power plants in Delhi and the surrounding area (Pathania et al., 2018). The lack of trend reversal in Delhi, despite implementation of air quality policies, is consistent with the lack of trend reversal reported by Georgoulias et al. (2019). They used a 21-year record (1996-2017) of multiple space-based sensors to estimate a significant and sustained increase in NO_2 of 3.1 % a^{-1} in Delhi. By the end of 2018, tropospheric column NO_2 is similar in London and Delhi (5.7×10^{15} molecules cm^{-2}; Figure 2.7) but OMI NO_2 over India may be biased low, due to the presence of optically thick aerosols (AOD > 0.4; Figure 2.6) that are not explicitly accounted for in the retrieval (Section 3.1).

The direction of the trends for all four cities is consistent with other trend studies, with differences in the absolute size of the trend due to differences in instruments, time periods, and sampling domains. Pope et al. (2018) observed declines in OMI NO_2 for 2005-2015 of 2.3 ± 0.5 × 10^{14} molecules cm^{-2} a^{-1} for London and 1.1 ± 0.5 × 10^{14} molecules cm^{-2} a^{-1} for Birmingham. We obtain a similar trend for Birmingham but a steeper decline for London of 2.6 × 10^{14} molecules cm^{-2} a^{-1} using our sampling domain for 2005-2015, though the difference is not significant. Schneider et al. (2015) obtained less steep and non-significant changes in NO_2 in London (-1.7 ± 1.2 % a^{-1}) and Delhi (1.4 ± 1.2 % a^{-1}) from the SCanning Imaging Absorption spectroMeter for Atmospheric CHartographY (SCIAMACHY) for 2002-2013. Trends in OMI NO_2 for 2005-2014 from ul-Haq et al. (2015) are similar to ours for Delhi (2.0 % a^{-1}) but lower for Kanpur (0.2 % a^{-1}). Studies have also combined multiple instruments to derive trends since the mid-1990s. These find decreases in NO_2 over London of 0.7 % a^{-1} for 1996-2006 (van der A et al., 2008) and 1.7 % a^{-1} for a longer observing period (1996-2011) (Hilboll et al., 2013), and a consistent increase for Delhi of 7.4 % a^{-1} in 1996-2006 (van der A et al., 2008) and 1996-2011 (Hilboll et al., 2013); much steeper than ours in Figure 2.7.

Figure 2.8 shows time series of monthly means of city-average IASI NH_3 in the four cities for 2008-2018. Mean IASI NH_3 is 15-20 times more in Delhi and Kanpur than in London and Birmingham due to larger emissions of NH_3 in the IGP, higher ambient temperatures promoting volatilization of NH_3, and greater sensitivity of IASI to NH_3 due to greater thermal contrast between the surface and the atmosphere over India (Van Damme et al., 2015; Dammers et al., 2016; Wang et al., 2019). IASI NH_3 decreases by 0.1 % a^{-1} in Kanpur, 0.6 % a^{-1} in Birmingham and 2.4 % a^{-1} in London, and increases by 0.5 % a^{-1} in Delhi. None of the trends are significant. Measurements of surface NH_3 from continuous monitors deployed in Delhi in April 2010 to

July 2011 exhibit the same seasonality as IASI NH_3, peaking in the monsoon season (July-September) (Singh and Kulshrestha, 2012). We investigated the effect of NH_3 seasonality on the trend using Equation 2.1 (grey solid lines in Figure 2.8). Similar to NO_2, all four cities show significant seasonality (p-value < 0.05 for the amplitude of the seasonality, C). The linear trends (grey dashed lines in Figure 2.8) are more positive than those obtained with Theil-Sen for all four cities, but are still not significant. This leads to a trend reversal in Kanpur (+1.0 % a^{-1}) and Birmingham (+2.1 % a^{-1}), steeper increase in Delhi (+3.7 % a^{-1}), and a less negative trend in London (-0.6 % a^{-1}).

Relating trends in NH_3 columns to trends in NH_3 emissions is complicated by partitioning of NH_3 to aerosols to form ammonium and dependence of this process on pre-existing aerosols that have declined in abundance across the UK due largely to controls on precursor emissions of SO_2 (Vieno et al., 2014). Harwell and Auchencorth Moss include measurements of gas-phase NH_3 and aerosol-phase ammonium in $PM_{2.5}$. These exhibit large and distinct seasonality, so we use Equation 2.1 to estimate changes of -0.096 μg N m^{-3} a^{-1} for ammonium and +0.031 μg N m^{-3} a^{-1} for NH_3 at Auchencorth Moss in 2008-2012 and similar changes at Harwell in 2012-2015 of -0.10 μg N m^{-3} a^{-1} for ammonium and +0.035 μg N m^{-3} a^{-1} for NH_3. Only the decline in ammonium at Auchencorth Moss is significant. This suggests the increase in rural NH_3 includes contributions from unregulated agricultural emissions and reduced partitioning of NH_3 to pre-existing aerosols. The opposite trend (decline) in NH_3 in London obtained with Theil-Sen and Equation 2.1 (Figure 2.8) may be because decline in local vehicular emissions of NH_3 with a shift in catalytic converter technology (Richmond et al., 2020) outweighs the increase in NH_3 from waste and domestic combustion (Defra, 2019a), and nearby agriculture (Vieno et al., 2016) and offsets reduced partitioning of NH_3 to acidic aerosols with decline in sulfate. The

opposite effect would be expected in Delhi due to nation-wide increases in SO_2 emissions and sulfate abundance (Klimont et al., 2013; Aas et al., 2019). That is, the increase in NH_3 emissions may be steeper than the increase in NH_3 columns in Figure 2.8 due to a corresponding increase in partitioning of NH_3 to pre-existing aerosols as these become more abundant.

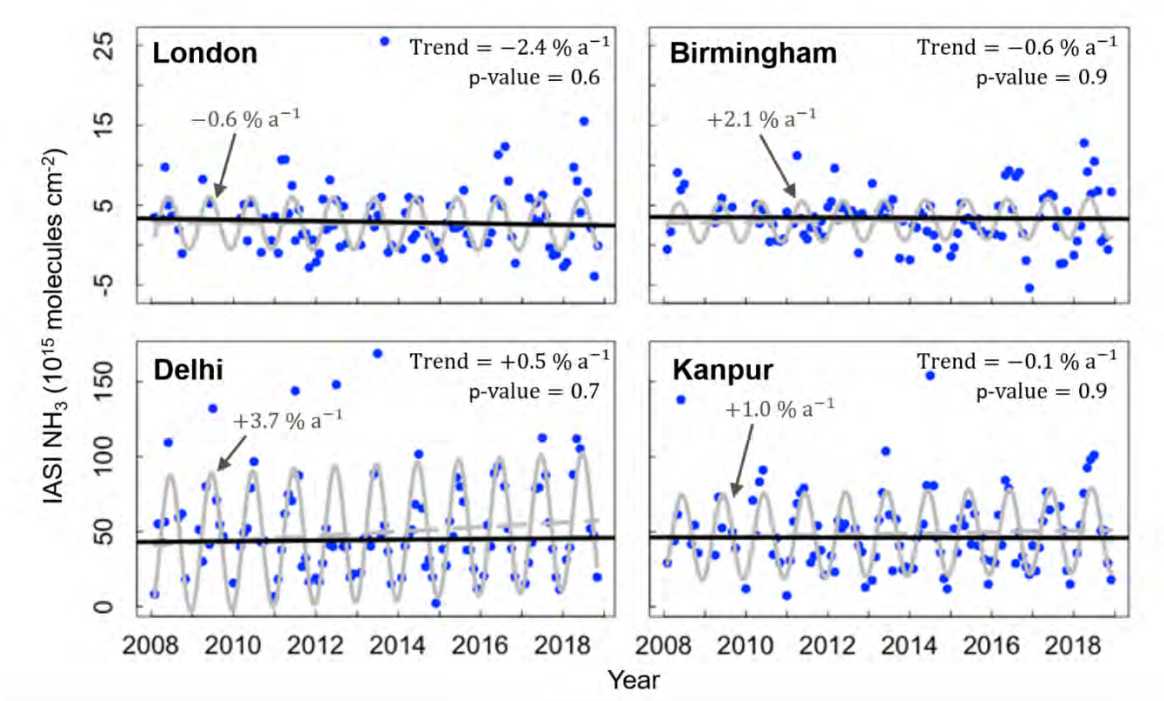

Figure 2.8 Time series of IASI NH_3 in 2008-2018 for London, Birmingham, Delhi and Kanpur. Points are city-average monthly means. Black lines are trends obtained with the Theil-Sen single median estimator. The grey lines are the fit (solid) and trend component (*B*) (dashed) obtained with Equation 2.1. Values inset are annual trends and p-values for the Theil-Sen fit (in black) and annual trends obtained with Equation 2.1 (grey). Trend errors (not shown) exceed ±150 % in all cities.

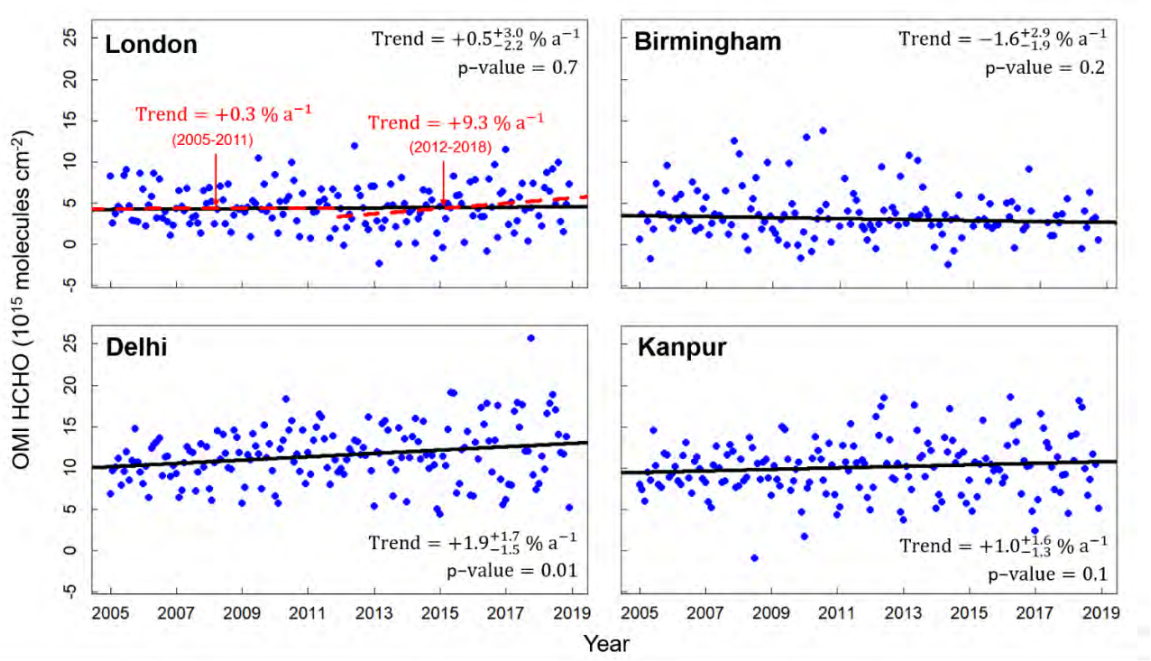

Figure 2.9 Time series of OMI HCHO for London, Birmingham, Delhi and Kanpur. Points are city-average monthly means of OMI HCHO after removing the background contribution (see text for details). Solid black lines are trends for 2005-2018 obtained with the Theil-Sen single median estimator. Values inset are annual trends and p-values. Absolute errors on the trends are 95 % CI. Dashed red lines show trend lines for London in 2005-2011 and 2012-2018 and red text are corresponding annual trends.

Figure 2.9 shows the time series of city-average monthly mean OMI HCHO for the four cities for 2005-2018 after removing the background contribution from oxidation of methane and other long-lived VOCs to isolate variability in the column due to reactive NMVOCs (Zhu et al., 2016). A representative background is obtained as monthly mean OMI HCHO over the remote Atlantic Ocean (25-35° N, 35-45° W) for the UK and the remote Indian Ocean (10-20° S, 70-80° E) for India. The non-linear function in Equation 2.1 is fit to these background HCHO values and used to subtract the background contribution, as in Marais et al. (2012), from the city-average monthly means. OMI HCHO columns from oxidation of reactive NMVOCs in Delhi and Kanpur are almost twice those in London and Birmingham due to a combination of unregulated sources (Venkataraman et al., 2018) and high temperatures enhancing emissions of isoprene, a dominant HCHO precursor in India (Surl et al., 2018; Chalilyakunnel et al.,

2019). The trends suggest reactive NMVOCs emissions have decreased in Birmingham (1.6 % a^{-1}) and increased in London (0.5 % a^{-1}), Delhi (1.9 % a^{-1}) and Kanpur (1.0 % a^{-1}). Only Delhi has a significant trend. The spread in values increases for Delhi and Kanpur from 19-24 % relative to the trend line in 2005 to 31-40 % in 2018. The change in the spread of values does not appear to be due to loss of data resulting from the row anomaly, as the change in the spread of HCHO over time is similar if we remove all pixels affected by the row anomaly for the entire data record (2005-2018). OMI HCHO slant columns (HCHO along the instrument viewing path) remain relatively stable throughout the OMI record (Zara et al., 2018), so the increase in variability may reflect more extreme emissions from seasonal sources like open fires in the IGP (Jethva et al., 2019). The trends from satellite observations of HCHO in megacities obtained by De Smedt et al. (2010) using multiple instruments for 1997-2009 are consistent with ours for Delhi (1.6 ± 0.7 % a^{-1}), but opposite for London (-0.4 ± 2.1 % a^{-1}). There is a shift in the magnitude of the HCHO trend for London around 2011 (Figure 2.9) from an increase of 0.3 % a^{-1} (p-value = 0.9) in 2005-2011 to a rapid increase of 9.3 % a^{-1} (95% CI: 0-26% a^{-1}) in 2012-2018. Visually the data suggest a decline in OMI HCHO in 2005-2011, as in De Smedt et al. (2010), but our trend estimate for 2005-2011 is affected by a limited analysis period and large interannual variability.

According to the UK bottom-up emission inventory, national NMVOCs emissions decreased by 2.4 % a^{-1} from 2005 to 2017 (Defra, 2019a). This is supported by decline in short-chain hydrocarbons measured at Harwell from 2-3 μg m^{-3} in 2008 to 0.8-0.9 μg m^{-3} in 2015. These include hydrocarbons from vegetation (isoprene and monoterpenes) and vehicles (light alkanes and aromatics), but exclude oxygenated VOCs (OVOCs) that in the UK include increasing contributions from domestic combustion, the food and beverage industry, and household

products (Defra, 2019a). OVOCs have relatively high HCHO yields (Millet et al., 2006) and VOC concentrations measured during field campaigns in London and cities in India, including Delhi, are dominated by OVOCs (> 60 % in London) (Valach et al., 2014; Sahu et al., 2016; Wang et al., 2020). In London, OVOCs also dominate inferred fluxes of VOCs (Langford et al., 2010) and reactivity of VOCs with the main atmospheric oxidant, OH (Whalley et al., 2016). The rapid increase in HCHO also has implications for ozone air pollution and the radical budget in London, as ozone formation is VOC-limited and HCHO photolysis is the second largest source of hydrogen oxide radicals ($HO_x \equiv OH + HO_2$) in London (Whalley et al., 2018).

Figure 2.10 shows the time series of city-average MODIS AOD monthly means in the four cities for 2005-2018. Trends in AOD are significant in all four cities and range from a decline of 4.2 % a^{-1} in Birmingham to an increase of 3.1 % a^{-1} in Kanpur. Mean AOD in Delhi and Kanpur is on average 5-6 times more than in London and Birmingham, due to large local anthropogenic emissions, nearby agricultural emissions of $PM_{2.5}$ and its precursors in the IGP, and long-range transport of desert dust (David et al., 2018). Our results, as absolute AOD trends for London (-0.004 a^{-1}) and Birmingham (-0.007 a^{-1}) for 2005-2018, are similar to trends obtained by Pope et al. (2018) for 2005-2015 (-0.006 a^{-1} for London; -0.005 a^{-1} for Birmingham). Our trends for both cities in India are less steep than the increase for Delhi (4.9 % a^{-1}) obtained for 2000-2010 with the MODIS 10 km AOD product (Ramachandran et al., 2012) and for Kanpur (10.3 % a^{-1}) obtained for 2001-2010 with AERONET AOD at the Kanpur AERONET site (Kaskaoutis et al., 2012). This may reflect a recent dampening of the trend or differences in data products and sampling domain/period. Sulfate from coal-fired power plants in India makes a large contribution to $PM_{2.5}$ (Weagle et al., 2018) and emissions from these nearly doubled from 2004 to 2015 (Fioletov et al., 2016).

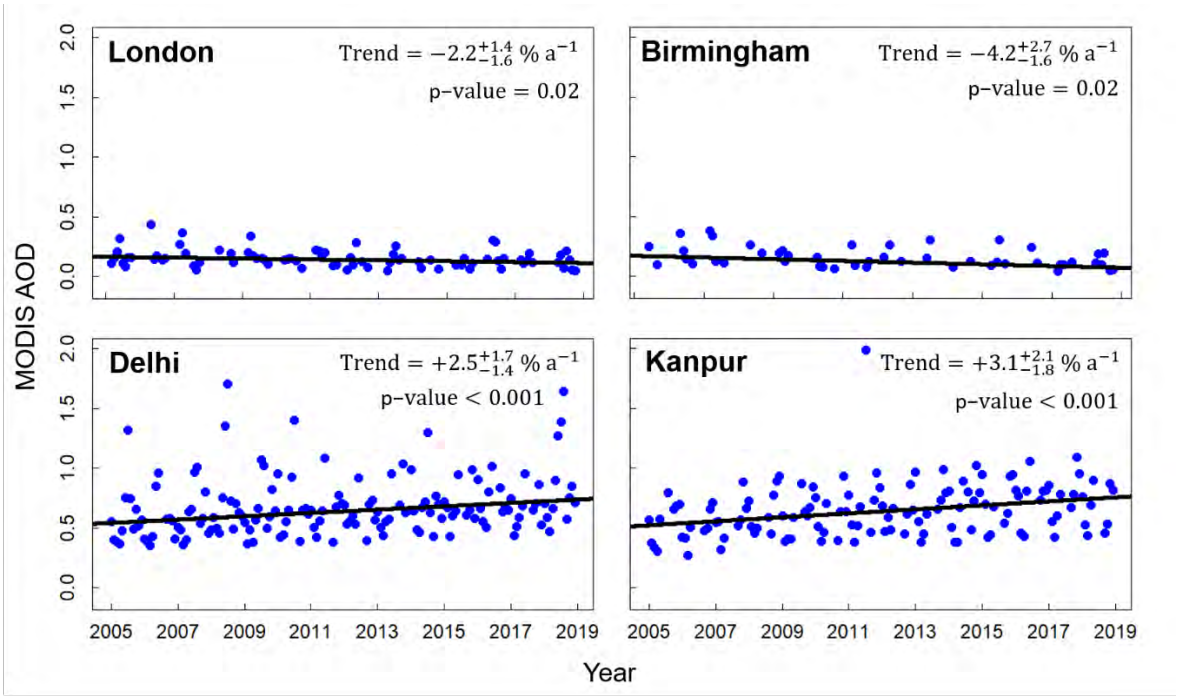

Figure 2.10 Time series of MODIS AOD for London, Birmingham, Delhi and Kanpur. Points are city-average monthly means. Black lines are trends obtained with the Theil-Sen single median estimator. Values inset are annual trends and p-values. Absolute errors on the trends are 95 % CI.

2.5 Conclusions

Satellite observations of atmospheric composition provide long-term and consistent global coverage of air pollutants. We assessed the ability of satellite observations of nitrogen dioxide (NO_2) and formaldehyde (HCHO) from OMI for 2005-2018, ammonia (NH_3) from IASI for 2008-2018, and aerosol optical depth (AOD) from MODIS for 2005-2018 to provide constraints on long-term changes in city-average NO_2, reactive NMVOCs, NH_3, and $PM_{2.5}$, respectively in four cities: 2 in the UK (London and Birmingham) and 2 in India (Delhi and Kanpur).

Assessment of satellite observations against ground-based measurements followed careful screening of the in-situ measurements for poor quality data, correcting NO_2 data reported in inconsistent units at monitoring sites in Delhi and Kanpur, and removing sites influenced by local sources. OMI NO_2 reproduces monthly variability in surface concentrations of NO_2 in

cities, whereas satellite AOD reproduces trends, but not monthly variability, in $PM_{2.5}$ in cities. MODIS and AERONET AOD are consistent at long-term monitoring sites in Kanpur and a UK EMEP site in southern England. IASI NH_3 is consistent with monthly variability in surface NH_3 concentrations at two of three rural UK EMEP sites. There were no appropriate measurements of reactive NMVOCs to compare to OMI HCHO.

According to the long-term record from Earth observations, NO_2, $PM_{2.5}$, and NMVOCs increased in Delhi and Kanpur. There is no reversal in the increase in NO_2 or $PM_{2.5}$ in Delhi or Kanpur, as would be expected from successful implementation of air pollution mitigation measures. In all four cities, the magnitude and direction of trends in NH_3 is sensitive to treatment of NH_3 seasonality and none of the NH_3 trends are significant. In London and Birmingham, NO_2 and $PM_{2.5}$ decrease, and HCHO, a proxy for reactive NMVOCs emissions, decreases in Birmingham, but exhibits a recent (2012-2018) sharp (> 9 % a^{-1}) increase in London. This may reflect increased emissions of oxygenated VOCs and long-chain hydrocarbons from household products, the food and beverage industry, and residential fuelwood burning. This would have implications for formation of secondary organic aerosols (SOA) contributing to $PM_{2.5}$, the radical (HO_x) budget that includes large contribution from HCHO photolysis, and formation of surface ozone that is VOC-limited in London.

References

Aas, W., Mortier, A., Bowersox, V., Cherian, R., Faluvegi, G., Fagerli, H., Hand, J., Klimont, Z., Galy-Lacaux, C., Lehmann, C. M. B., et al., Global and regional trends of atmospheric sulfur, Sci. Rep.-Uk, 9, doi:10.1038/s41598-018-37304-0, 2019.

Anenberg, S. C., Achakulwisut, P., Brauer, M., Moran, D., Apte, J. S., and Henze, D. K., Particulate matter-attributable mortality and relationships with carbon dioxide in 250 urban areas worldwide, Sci. Rep.-Uk, 9, doi:10.1038/s41598-019-48057-9, 2019.

Barnes, J. H., Hayes, E. T., Chatterton, T. J., and Longhurst, J. W. S., Policy disconnect: A critical review of UK air quality policy in relation to EU and LAQM responsibilities over the last 20 years, Environ. Sci. Policy, 85, 28-39, doi:10.1016/j.envsci.2018.03.024, 2018.

Bilal, M., Qiu, Z. F., Campbell, J. R., Spak, S. N., Shen, X. J., and Nazeer, M., A New MODIS C6 Dark Target and Deep Blue Merged Aerosol Product on a 3 km Spatial Grid, Remote Sens.-Basel, 10, doi:10.3390/rs10030463, 2018.

Boersma, K. F., Eskes, H. J., and Brinksma, E. J., Error analysis for tropospheric NO_2 retrieval from space, J. Geophys. Res.-Atmos., 109, doi:10.1029/2003jd003962, 2004.

Boersma, K. F., Jacob, D. J., Trainic, M., Rudich, Y., DeSmedt, I., Dirksen, R., and Eskes, H. J., Validation of urban NO_2 concentrations and their diurnal and seasonal variations observed from the SCIAMACHY and OMI sensors using in situ surface measurements in Israeli cities, Atmos. Chem. Phys., 9, 3867-3879, doi:10.5194/acp-9-3867-2009, 2009.

Brauer, M., Freedman, G., Frostad, J., van Donkelaar, A., Martin, R. V., Dentener, F., van Dingenen, R., Estep, K., Amini, H., Apte, J. S., et al., Ambient Air Pollution Exposure Estimation for the Global Burden of Disease 2013, Environ. Sci. Technol., 50, 79-88, doi:10.1021/acs.est.5b03709, 2016.

Carnell, E., Vieno, M., Vardoulakis, S., Beck, R., Heaviside, C., Tomlinson, S., Dragosits, U., Heal, M. R., and Reis, S., Modelling public health improvements as a result of air pollution control policies in the UK over four decades—1970 to 2010, Environ. Res. Lett., 14, doi:10.1088/1748-9326/ab1542, 2019.

Carslaw, D. C., Beevers, S. D., Westmoreland, E., Williams, M. L., Tate, J. E., Murrells, T., Stedman, J., Li, Y., Grice, S., Kent, A., et al., Trends in NO_x and NO_2 emissions and ambient measurements in the UK, 2011.

Carslaw, D. C., Murrells, T. P., Andersson, J., and Keenan, M., Have vehicle emissions of primary NO_2 peaked?, Faraday Discuss., 189, 439-454, doi:10.1039/c5fd00162e, 2016.

Castell, N., Dauge, F. R., Schneider, P., Vogt, M., Lerner, U., Fishbain, B., Broday, D., and Bartonova, A., Can commercial low-cost sensor platforms contribute to air quality monitoring and exposure estimates?, Environ. Int., 99, 293-302, doi:10.1016/j.envint.2016.12.007, 2017.

Chalilyakunnel, S., Millet, D. B., and Chen, X., Constraining emissions of volatile organic compounds over the Indian subcontinent using spacebased formaldehyde measurements, J. Geophys. Res., 124, 10525-10545, doi:10.1029/2019JD031262, 2019.

Choi, S., Lamsal, L. N., Follette-Cook, M., Joiner, J., Krotkov, N. A., Swartz, W. H., Pickering, K. E., Loughner, C. P., Appel, W., Pfister, G., et al., Assessment of NO_2 observations during DISCOVER-AQ and KORUS-AQ field campaigns, Atmos. Meas. Tech., 13, 2523-2546, doi:10.5194/amt-13-2523-2020, 2020.

Clarisse, L., Shephard, M. W., Dentener, F., Hurtmans, D., Cady-Pereira, K., Karagulian, F., Van Damme, M., Clerbaux, C., and Coheur, P. F., Satellite monitoring of ammonia: A case study of the San Joaquin Valley, J. Geophys. Res.-Atmos., 115, doi:10.1029/2009jd013291, 2010.

CPCB; Central Pollution Control Board, India, Protocol for Data Transmission from CAAQM Stations Existing as on Date, https://app.cpcbccr.com/ccr_docs/Protocol_CAAQM.pdf, 2015.

Crilley, L. R., Bloss, W. J., Yin, J., Beddows, D. C. S., Harrison, R. M., Allan, J. D., Young, D. E., Flynn, M., Williams, P., Zotter, P., et al., Sources and contributions of wood smoke during winter in London: assessing local and regional influences, Atmos. Chem. Phys., 15, 3149-3171, doi:10.5194/acp-15-3149-2015, 2015.

Crilley, L. R., Lucarelli, F., Bloss, W. J., Harrison, R. M., Beddows, D. C., Calzolai, G., Nava, S., Valli, G., Bernardoni, V., and Vecchi, R., Source apportionment of fine and coarse particles at a roadside and urban background site in London during the 2012 summer ClearfLo campaign, Environ. Pollut., 220, 766-778, doi:10.1016/j.envpol.2016.06.002, 2017.

Cusworth, D. H., Mickley, L. J., Sulprizio, M. P., Liu, T. J., Marlier, M. E., DeFries, R. S., Guttikunda, S. K., and Gupta, P., Quantifying the influence of agricultural fires in northwest India on urban air pollution in Delhi, India, Environ. Res. Lett., 13, doi:10.1088/1748-9326/aab303, 2018.

Dammers, E., Palm, M., Van Damme, M., Vigouroux, C., Smale, D., Conway, S., Toon, G. C., Jones, N., Nussbaumer, E., Warneke, T., et al., An evaluation of IASI-NH_3 with ground-based Fourier transform infrared spectroscopy measurements, Atmos. Chem. Phys., 16, 10351-10368, doi:10.5194/acp-16-10351-2016, 2016.

Dammers, E., McLinden, C. A., Griffin, D., Shephard, M. W., Van der Graaf, S., Lutsch, E., Schaap, M., Gainairu-Matz, Y., Fioletov, V., Van Damme, M., et al., NH_3 emissions from large point sources derived from CrIS and IASI satellite observations, Atmos. Chem. Phys., 19, 12261-12293, doi:10.5194/acp-19-12261-2019, 2019.

Datameet India Community data, https://github.com/datameet/maps/tree/master/Country, Last accessed: 12 March 2021, 2018.

David, L. M., Ravishankara, A. R., Kodros, J. K., Venkataraman, C., Sadavarte, P., Pierce, J. R., Chaliyakunnel, S., and Millet, D. B., Aerosol Optical Depth Over India, J. Geophys. Res.-Atmos., 123, 3688-3703, doi:10.1002/2017jd027719, 2018.

De Smedt, I., Stavrakou, T., Muller, J. F., van der A, R. J., and Van Roozendael, M., Trend detection in satellite observations of formaldehyde tropospheric columns, Geophys. Res. Lett., 37, doi:10.1029/2010gl044245, 2010.

De Smedt, I., van Geffen, J., Richter, A., Beirle, S., Yu, H., Vlietinck, J., Roozendael, M. V., A, R. v. d., Lorente, A., Scanlon, T., et al., Product User Guide for HCHO (Version 1.0), doi:10.18758/71021031, 2017.

De Smedt, I., Theys, N., Yu, H., Danckaert, T., Lerot, C., Compernolle, S., Van Roozendael, M., Richter, A., Hilboll, A., Peters, E., et al., Algorithm theoretical baseline for formaldehyde retrievals from S5P TROPOMI and from the QA4ECV project, Atmos. Meas. Tech., 11, 2395-2426, doi:10.5194/amt-11-2395-2018, 2018.

Defra; Department for Environment Food & Rural Affairs, United Kingdom, Emissions of air pollutants in the UK, 1970 to 2017, https://assets.publishing.service.gov.uk/government/uploads/system/uploads/attachment_data/file/778483/Emissions_of_air_pollutants_1990_2017.pdf, 2019a.

Defra; Department for Environment Food & Rural Affairs, United Kingdom, Clean Air Strategy, https://assets.publishing.service.gov.uk/government/uploads/system/uploads/attachment_data/file/770715/clean-air-strategy-2019.pdf, 2019b.

Duncan, B. N., Prados, A. I., Lamsal, L. N., Liu, Y., Streets, D. G., Gupta, P., Hilsenrath, E., Kahn, R. A., Nielsen, J. E., Beyersdorf, A. J., et al., Satellite data of atmospheric pollution for US air quality applications: Examples of applications, summary of data end-user resources, answers to FAQs, and common mistakes to avoid, Atmos. Environ., 94, 647-662, doi:10.1016/j.atmosenv.2014.05.061, 2014.

Dunlea, E. J., Herndon, S. C., Nelson, D. D., Volkamer, R. M., San Martini, F., Sheehy, P. M., Zahniser, M. S., Shorter, J. H., Wormhoudt, J. C., Lamb, B. K., et al., Evaluation of nitrogen dioxide chemiluminescence monitors in a polluted urban environment, Atmos. Chem. Phys., 7, 2691-2704, doi:10.5194/acp-7-2691-2007, 2007.

Eck, T. F., Holben, B. N., Reid, J. S., Dubovik, O., Smirnov, A., O'Neill, N. T., Slutsker, I., and Kinne, S., Wavelength dependence of the optical depth of biomass burning, urban, and desert dust aerosols, J. Geophys. Res.-Atmos., 104, 31333-31349, doi:10.1029/1999jd900923, 1999.

Fioletov, V. E., McLinden, C. A., Krotkov, N., Li, C., Joiner, J., Theys, N., Carn, S., and Moran, M. D., A global catalogue of large SO_2 sources and emissions derived from the Ozone Monitoring Instrument, Atmos. Chem. Phys., 16, 11497-11519, doi:10.5194/acp-16-11497-2016, 2016.

Fishman, J., Bowman, K. W., Burrows, J. P., Richter, A., Chance, K. V., Edwards, D. P., Martin, R. V., Morris, G. A., Pierce, R. B., Ziemke, J. R., et al., Remote sensing of

tropospheric pollution from space, B. Am. Meteorol. Soc., 89, 805-821, doi:10.1175/2008bams2526.1, 2008.

Fontaras, G., Franco, V., Dilara, P., Martini, G., and Manfredi, U., Development and review of Euro 5 passenger car emission factors based on experimental results over various driving cycles, Sci. Total Environ., 468, 1034-1042, doi:10.1016/j.scitotenv.2013.09.043, 2014.

Fuller, G. W., Tremper, A. H., Baker, T. D., Yttri, K. E., and Butterfield, D., Contribution of wood burning to PM_{10} in London, Atmos. Environ., 87, 87-94, doi:10.1016/j.atmosenv.2013.12.037, 2014.

GADM Data, https://gadm.org/, Last accessed: 12 March 2021, 2018.

Gaur, A., Tripathi, S. N., Kanawade, V. P., Tare, V., and Shukla, S. P., Four-year measurements of trace gases (SO_2, NO_x, CO, and O_3) at an urban location, Kanpur, in Northern India, J. Atmos. Chem., 71, 283-301, doi:10.1007/s10874-014-9295-8, 2014.

Georgoulias, A. K., Alexandri, G., Kourtidis, K. A., Lelieveld, J., Zanis, P., Poschl, U., Levy, R., Amiridis, V., Marinou, E., and Tsikerdekis, A., Spatiotemporal variability and contribution of different aerosol types to the aerosol optical depth over the Eastern Mediterranean, Atmos. Chem. Phys., 16, 13853-13884, doi:10.5194/acp-16-13853-2016, 2016.

Georgoulias, A. K., van der A, R. J., Stammes, P., Boersma, K. F., and Eskes, H. J., Trends and trend reversal detection in 2 decades of tropospheric NO_2 satellite observations, Atmos. Chem. Phys., 19, 6269-6294, doi:10.5194/acp-19-6269-2019, 2019.

Ghosh, S., Gupta, T., Rastogi, N., Gaur, A., Misra, A., Tripathi, S. N., Paul, D., Tare, V., Prakash, O., Bhattu, D., et al., Chemical Characterization of Summertime Dust Events at Kanpur: Insight into the Sources and Level of Mixing with Anthropogenic Emissions, Aerosol Air Qual. Res., 14, 879-891, doi:10.4209/aaqr.2013.07.0240, 2014.

Giles, D. M., Sinyuk, A., Sorokin, M. G., Schafer, J. S., Smirnov, A., Slutsker, I., Eck, T. F., Holben, B. N., Lewis, J. R., Campbell, J. R., et al., Advancements in the Aerosol Robotic Network (AERONET) Version 3 database - automated near-real-time quality control algorithm with improved cloud screening for Sun photometer aerosol optical depth (AOD) measurements, Atmos. Meas. Tech., 12, 169-209, doi:10.5194/amt-12-169-2019, 2019.

Govt. of Delhi; Planning Department, Delhi, Economic Survey of Delhi, 2018-2019, 2019.

Govt. of India; Ministry of Road Transport and Highways, India, Notification, http://egazette.nic.in/WriteReadData/2016/168300.pdf, 2016.

Govt. of India; Ministry of Environment Forest & Climate Change, India, National Clean Air Program, 2019.

Grange, S. K., Lewis, A. C., Moller, S. J., and Carslaw, D. C., Lower vehicular primary emissions of NO_2 in Europe than assumed in policy projections, Nat. Geosci., 10, 914-918, doi:10.1038/s41561-017-0009-0, 2017.

Gupta, P., Remer, L. A., Levy, R. C., and Mattoo, S., Validation of MODIS 3 km land aerosol optical depth from NASA's EOS Terra and Aqua missions, Atmos. Meas. Tech., 11, 3145-3159, doi:10.5194/amt-11-3145-2018, 2018.

Guttikunda, S. K., and Jawahar, P., Atmospheric emissions and pollution from the coal-fired thermal power plants in India, Atmos. Environ., 92, 449-460, doi:10.1016/j.atmosenv.2014.04.057, 2014.

Harrison, R. G., Nicoll, K. A., Marlton, G. J., Ryder, C. L., and Bennett, A. J., Saharan dust plume charging observed over the UK, Environ. Res. Lett., 13, doi:10.1088/1748-9326/aabcd9, 2018.

Harrison, R. M., and Beddows, D. C., Efficacy of Recent Emissions Controls on Road Vehicles in Europe and Implications for Public Health, Sci. Rep.-Uk, 7, doi:10.1038/s41598-017-01135-2, 2017.

Heal, M. R., O'Donoghue, M. A., and Cape, J. N., Overestimation of urban nitrogen dioxide by passive diffusion tubes: a comparative exposure and model study, Atmos. Environ., 33, 513-524, doi:10.1016/S1352-2310(98)00290-8, 1999.

Hilboll, A., Richter, A., and Burrows, J. P., Long-term changes of tropospheric NO_2 over megacities derived from multiple satellite instruments, Atmos. Chem. Phys., 13, 4145-4169, doi:10.5194/acp-13-4145-2013, 2013.

Holben, B. N., Eck, T. F., Slutsker, I., Tanre, D., Buis, J. P., Setzer, A., Vermote, E., Reagan, J. A., Kaufman, Y. J., Nakajima, T., et al., AERONET - A federated instrument network and data archive for aerosol characterization, Remote Sens. Environ., 66, 1-16, doi:10.1016/S0034-4257(98)00031-5, 1998.

Jethva, H., Torres, O., Field, R. D., Lyapustin, A., Gautam, R., and Kayetha, V., Connecting Crop Productivity, Residue Fires, and Air Quality over Northern India, Sci. Rep.-Uk, 9, doi:10.1038/s41598-019-52799-x, 2019.

Jones, N. B., Riedel, K., Allan, W., Wood, S., Palmer, P. I., Chance, K., and Notholt, J., Long-term tropospheric formaldehyde concentrations deduced from ground-based fourier transform solar infrared measurements, Atmos. Chem. Phys., 9, 7131-7142, doi:10.5194/acp-9-7131-2009, 2009.

Kaskaoutis, D. G., Singh, R. P., Gautam, R., Sharma, M., Kosmopoulos, P. G., and Tripathi, S. N., Variability and trends of aerosol properties over Kanpur, northern India using AERONET data (2001-10), Environ. Res. Lett., 7, doi:10.1088/1748-9326/7/2/024003, 2012.

Kaufman, Y. J., Aerosol Optical-Thickness and Atmospheric Path Radiance, J. Geophys. Res.-Atmos., 98, 2677-2692, doi:10.1029/92jd02427, 1993.

Kenagy, H. S., Sparks, T. L., Ebben, C. J., Wooldrige, P. J., Lopez-Hilfiker, F. D., Lee, B. H., Thornton, J. A., McDuffie, E. E., Fibiger, D. L., Brown, S. S., et al., NO_x Lifetime and NO_y Partitioning During WINTER, J. Geophys. Res.-Atmos., 123, 9813-9827, doi:10.1029/2018jd028736, 2018.

Kim, S. W., Heckel, A., McKeen, S. A., Frost, G. J., Hsie, E. Y., Trainer, M. K., Richter, A., Burrows, J. P., Peckham, S. E., and Grell, G. A., Satellite-observed US power plant NO_x emission reductions and their impact on air quality, Geophys. Res. Lett., 33, doi:10.1029/2006gl027749, 2006.

Klimont, Z., Smith, S. J., and Cofala, J., The last decade of global anthropogenic sulfur dioxide: 2000-2011 emissions, Environ. Res. Lett., 8, doi:10.1088/1748-9326/8/1/014003, 2013.

Kotthaus, S., and Grimmond, C. S. B., Atmospheric boundary-layer characteristics from ceilometer measurements. Part 2: Application to London's urban boundary layer, Q. J. Roy. Meteor. Soc., 144, 1511-1524, doi:10.1002/qj.3298, 2018.

Kramer, L. J., Leigh, R. J., Remedios, J. J., and Monks, P. S., Comparison of OMI and ground-based in situ and MAX-DOAS measurements of tropospheric nitrogen dioxide in an urban area, J. Geophys. Res.-Atmos., 113, doi:10.1029/2007jd009168, 2008.

Krotkov, N. A., Lamsal, L. N., Celarier, E. A., Swartz, W. H., Marchenko, S. V., Bucsela, E. J., Chan, K. L., Wenig, M., and Zara, M., The version 3 OMI NO_2 standard product, Atmos. Meas. Tech., 10, 3133-3149, doi:10.5194/amt-10-3133-2017, 2017.

Lamsal, L. N., Martin, R. V., van Donkelaar, A., Celarier, E. A., Bucsela, E. J., Boersma, K. F., Dirksen, R., Luo, C., and Wang, Y., Indirect validation of tropospheric nitrogen dioxide retrieved from the OMI satellite instrument: Insight into the seasonal variation of nitrogen oxides at northern midlatitudes, J. Geophys. Res.-Atmos., 115, doi:10.1029/2009jd013351, 2010.

Lamsal, L. N., Martin, R. V., Padmanabhan, A., van Donkelaar, A., Zhang, Q., Sioris, C. E., Chance, K., Kurosu, T. P., and Newchurch, M. J., Application of satellite observations for timely updates to global anthropogenic NO_x emission inventories, Geophys. Res. Lett., 38, doi:10.1029/2010gl046476, 2011.

Landrigan, P. J., Fuller, R., Acosta, N. J. R., Adeyi, O., Arnold, R., Basu, N., Balde, A. B., Bertollini, R., Bose-O'Reilly, S., Boufford, J. I., et al., The Lancet Commission on pollution and health, Lancet, 391, 462-512, doi:10.1016/S0140-6736(17)32345-0, 2018.

Langford, B., Nemitz, E., House, E., Phillips, G. J., Famulari, D., Davison, B., Hopkins, J. R., Lewis, A. C., and Hewitt, C. N., Fluxes and concentrations of volatile organic compounds above central London, UK, Atmos. Chem. Phys., 10, 627–645, doi:10.5194/acp-10-627-2010, 2010.

Levy, R. C., Remer, L. A., and Dubovik, O., Global aerosol optical properties and application to Moderate Resolution Imaging Spectroradiometer aerosol retrieval over land, J. Geophys. Res.-Atmos., 112, doi:10.1029/2006jd007815, 2007.

Levy, R. C., Remer, L. A., Kleidman, R. G., Mattoo, S., Ichoku, C., Kahn, R., and Eck, T. F., Global evaluation of the Collection 5 MODIS dark-target aerosol products over land, Atmos. Chem. Phys., 10, 10399-10420, doi:10.5194/acp-10-10399-2010, 2010.

Levy, R. C., Mattoo, S., Munchak, L. A., Remer, L. A., Sayer, A. M., Patadia, F., and Hsu, N. C., The Collection 6 MODIS aerosol products over land and ocean, Atmos. Meas. Tech., 6, 2989-3034, doi:10.5194/amt-6-2989-2013, 2013.

Li, Q., Li, C. C., and Mao, J. T., Evaluation of Atmospheric Aerosol Optical Depth Products at Ultraviolet Bands Derived from MODIS Products, Aerosol Sci. Tech., 46, 1025-1034, doi:10.1080/02786826.2012.687475, 2012.

Lin, J. T., Liu, M. Y., Xin, J. Y., Boersma, K. F., Spurr, R., Martin, R., and Zhang, Q., Influence of aerosols and surface reflectance on satellite NO_2 retrieval: seasonal and spatial characteristics and implications for NO_x emission constraints, Atmos. Chem. Phys., 15, 11217-11241, doi:10.5194/acp-15-11217-2015, 2015.

Liu, T. J., Marlier, M. E., DeFries, R. S., Westervelt, D. M., Xia, K. R., Fiore, A. M., Mickley, L. J., Cusworth, D. H., and Milly, G., Seasonal impact of regional outdoor biomass burning on air pollution in three Indian cities: Delhi, Bengaluru, and Pune, Atmos. Environ., 172, 83-92, doi:10.1016/j.atmosenv.2017.10.024, 2018.

Lyons, R., Doherty, R., Reay, D., and Shackley, S., Legal but lethal: Lessons from NO_2 related mortality in a city compliant with EU limit value, Atmos. Pollut. Res., doi:10.1016/j.apr.2020.02.016, 2020.

Malley, C. S., Braban, C. F., Dumitrean, P., Cape, J. N., and Heal, M. R., The impact of speciated VOCs on regional ozone increment derived from measurements at the UK EMEP supersites between 1999 and 2012, Atmos. Chem. Phys., 15, 8361-8380, doi:10.5194/acp-15-8361-2015, 2015.

Malley, C. S., Heal, M. R., Braban, C. F., Kentisbeer, J., Leeson, S. R., Malcolm, H., Lingard, J. J. N., Ritchie, S., Maggs, R., Beccaceci, S., et al., The contributions to long-term health-relevant particulate matter at the UK EMEP supersites between 2010 and 2013: Quantifying the mitigation challenge, Environ. Int., 95, 98-111, doi:10.1016/j.envint.2016.08.005, 2016.

Marais, E. A., Jacob, D. J., Kurosu, T. P., Chance, K., Murphy, J. G., Reeves, C., Mills, G., Casadio, S., Millet, D. B., Barkley, M. P., et al., Isoprene emissions in Africa inferred from OMI observations of formaldehyde columns, Atmos. Chem. Phys., 12, 6219-6235, doi:10.5194/acp-12-6219-2012, 2012.

Marais, E. A., Jacob, D. J., Wecht, K., Lerot, C., Zhang, L., Yu, K., Kurosu, T. P., Chance, K., and Sauvage, B., Anthropogenic emissions in Nigeria and implications for atmospheric

ozone pollution: A view from space, Atmos. Environ., 99, 32-40, doi:10.1016/j.atmosenv.2014.09.055, 2014a.

Marais, E. A., Jacob, D. J., Guenther, A., Chance, K., Kurosu, T. P., Murphy, J. G., Reeves, C. E., and Pye, H. O. T., Improved model of isoprene emissions in Africa using Ozone Monitoring Instrument (OMI) satellite observations of formaldehyde: implications for oxidants and particulate matter, Atmos. Chem. Phys., 14, 7693-7703, doi:10.5194/acp-14-7693-2014, 2014b.

Martin, R. V., Jacob, D. J., Chance, K., Kurosu, T. P., Palmer, P. I., and Evans, M. J., Global inventory of nitrogen oxide emissions constrained by space-based observations of NO_2 columns, J. Geophys. Res.-Atmos., 108, doi:10.1029/2003jd003453, 2003.

McPhetres, A., and Aggarwal, S., An Evaluation of MODIS-Retrieved Aerosol Optical Depth over AERONET Sites in Alaska, Remote Sens.-Basel, 10, doi:10.3390/rs10091384, 2018.

Mhawish, A., Banerjee, T., Broday, D. M., Misra, A., and Tripathi, S. N., Evaluation of MODIS Collection 6 aerosol retrieval algorithms over Indo-Gangetic Plain: Implications of aerosols types and mass loading, Remote Sens. Environ., 201, 297-313, doi:10.1016/j.rse.2017.09.016, 2017.

Miller, S. M., Matross, D. M., Andrews, A. E., Millet, D. B., Longo, M., Gottlieb, E. W., Hirsch, A. I., Gerbig, C., Lin, J. C., Daube, B. C., et al., Sources of carbon monoxide and formaldehyde in North America determined from high-resolution atmospheric data, Atmos. Chem. Phys., 8, 7673-7696, doi:10.5194/acp-8-7673-2008, 2008.

Millet, D. B., Jacob, D. J., Turquety, S., Hudman, R. C., Wu, S. L., Fried, A., Walega, J., Heikes, B. G., Blake, D. R., Singh, H. B., et al., Formaldehyde distribution over North America: Implications for satellite retrievals of formaldehyde columns and isoprene emission, J. Geophys. Res.-Atmos., 111, doi:10.1029/2005jd006853, 2006.

Munchak, L. A., Levy, R. C., Mattoo, S., Remer, L. A., Holben, B. N., Schafer, J. S., Hostetler, C. A., and Ferrare, R. A., MODIS 3 km aerosol product: applications over land in an urban/suburban region, Atmos. Meas. Tech., 6, 1747-1759, doi:10.5194/amt-6-1747-2013, 2013.

Nagar, P. K., Sharma, M., and Das, D., A new method for trend analyses in PM_{10} and impact of crop residue burning in Delhi, Kanpur and Jaipur, India, Urban Clim., 27, 193-203, doi:10.1016/j.uclim.2018.12.003, 2019.

Nakoudi, K., Giannakaki, E., Dandou, A., Tombrou, M., and Komppula, M., Planetary boundary layer height by means of lidar and numerical simulations over New Delhi, India, Atmos. Meas. Tech., 12, 2595–2610, doi:10.5194/amt-12-2595-2019, 2019.

Ots, R., Heal, M. R., Young, D. E., Williams, L. R., Allan, J. D., Nemitz, E., Di Marco, C., Detournay, A., Xu, L., Ng, N. L., et al., Modelling carbonaceous aerosol from residential solid fuel burning with different assumptions for emissions, Atmos. Chem. Phys., 18, 4497-4518, doi:10.5194/acp-18-4497-2018, 2018.

Parkhi, N., Chate, D., Ghude, S. D., Peshin, S., Mahajan, A., Srinivas, R., Surendran, D., Ali, K., Singh, S., Trimbake, H., et al., Large inter annual variation in air quality during the annual festival 'Diwali' in an Indian megacity, J. Environ. Sci.-China, 43, 265-272, doi:10.1016/j.jes.2015.08.015, 2016.

Pathania, R., Phadke, P., Gupta, R. K., and Ramanathan, S.; Centre for Science and Environment, New Delhi, Off-Target Status of Thermal Power Stations in Delhi NCR, http://www.indiaenvironmentportal.org.in/files/file/Off-Target---Status-of-Power-Stations-Report.pdf, 2018.

Paulot, F., Paynter, D., Ginoux, P., Naik, V., Whitburn, S., Van Damme, M., Clarisse, L., Coheur, P. F., and Horowitz, L. W., Gas-aerosol partitioning of ammonia in biomass burning plumes: Implications for the interpretation of spaceborne observations of ammonia and the radiative forcing of ammonium nitrate, Geophys. Res. Lett., 44, 8084-8093, doi:10.1002/2017gl074215, 2017.

Petrenko, M., Ichoku, C., and Leptoukh, G., Multi-sensor Aerosol Products Sampling System (MAPSS), Atmos. Meas. Tech., 5, 913-926, doi:10.5194/amt-5-913-2012, 2012.

Pope, R. J., Arnold, S. R., Chipperfield, M. P., Latter, B. G., Siddans, R., and Kerridge, B. J., Widespread changes in UK air quality observed from space, Atmos. Sci. Lett., 19, doi:10.1002/asl.817, 2018.

Ramachandran, S., Kedia, S., and Srivastava, R., Aerosol optical depth trends over different regions of India, Atmos. Environ., 49, 338-347, doi:10.1016/j.atmosenv.2011.11.017, 2012.

Reed, C., Evans, M. J., Di Carlo, P., Lee, J. D., and Carpenter, L. J., Interferences in photolytic NO_2 measurements: explanation for an apparent missing oxidant?, Atmos. Chem. Phys., 16, 4707-4724, doi:10.5194/acp-16-4707-2016, 2016.

Remer, L. A., Kaufman, Y. J., Tanre, D., Mattoo, S., Chu, D. A., Martins, J. V., Li, R. R., Ichoku, C., Levy, R. C., Kleidman, R. G., et al., The MODIS aerosol algorithm, products, and validation, J. Atmos. Sci., 62, 947-973, doi:10.1175/Jas3385.1, 2005.

Remer, L. A., Mattoo, S., Levy, R. C., and Munchak, L. A., MODIS 3 km aerosol product: algorithm and global perspective, Atmos. Meas. Tech., 6, 1829-1844, doi:10.5194/amt-6-1829-2013, 2013.

Richmond, B., Misra, A., Brown, P., Karagianni, E., Murrells, T., Pang, Y., Passant, N., Pepler, A., Stewart, R., Thistlethwaite, G., et al.; Environment, R. E., United Kingdom, UK Informative Inventory Report (1990 to 2018), https://uk-air.defra.gov.uk/assets/documents/reports/cat07/2003131327_GB_IIR_2020_v1.0.pdf, 2020.

Richter, A., Nitrogen oxides in the troposphere - What have we learned from satellite measurements?, Erca: From the Human Dimensions of Global Environmental Change to the Observation of the Earth from Space, Vol 8, WOS:000268062600011, 2009.

Sahu, L. K., Yadav, R., and Pal, D., Source identification of VOCs at an urban site of western India: Effect of marathon events and anthropogenic emissions, J. Geophys. Res.-Atmos., 121, 2416-2433, doi:10.1002/2015jd024454, 2016.

Sathe, Y., Kulkarni, S., Gupta, P., Kaginalkar, A., Islam, S., and Gargava, P., Application of Moderate Resolution Imaging Spectroradiometer (MODIS) Aerosol Optical Depth (AOD) and Weather Research Forecasting (WRF) model meteorological data for assessment of fine particulate matter ($PM_{2.5}$) over India, Atmos. Pollut. Res., 10, 418-434, doi:10.1016/j.apr.2018.08.016, 2019.

Schaap, M., Apituley, A., Timmermans, R. M. A., Koelemeijer, R. B. A., and de Leeuw, G., Exploring the relation between aerosol optical depth and $PM_{2.5}$ at Cabauw, the Netherlands, Atmos. Chem. Phys., 9, 909-925, doi:10.5194/acp-9-909-2009, 2009.

Schneider, P., Lahoz, W. A., and van der A, R., Recent satellite-based trends of tropospheric nitrogen dioxide over large urban agglomerations worldwide, Atmos. Chem. Phys., 15, 1205-1220, doi:10.5194/acp-15-1205-2015, 2015.

Shaddick, G., Thomas, M. L., Amini, H., Broday, D., Cohen, A., Frostad, J., Green, A., Gumy, S., Liu, Y., Martin, R. V., et al., Data integration for the assessment of population exposure to ambient air pollution for Global Burden of Disease assessment, Environ. Sci. Technol., 52, 9069-9078, doi:10.1021/acs.est.8b02864, 2018.

Shah, V., Jacob, D. J., Li, K., Silvern, R. F., Zhai, S., Liu, M., Lin, J., and Zhang, Q., Effect of changing NO_x lifetime on the seasonality and long-term trends of satellite-observed tropospheric NO_2 columns over China, Atmos. Chem. Phys., 20, 1483-1495, doi:10.5194/acp-20-1483-2020, 2020.

Silvern, R. F., Jacob, D. J., Travis, K. R., Sherwen, T., Evans, M. J., Cohen, R. C., Laughner, J. L., Hall, S. R., Ullmann, K., Crounse, J. D., et al., Observed NO/NO_2 Ratios in the Upper Troposphere Imply Errors in $NO\text{-}NO_2\text{-}O_3$ Cycling Kinetics or an Unaccounted NO_x Reservoir, Geophys. Res. Lett., 45, 4466-4474, doi:10.1029/2018gl077728, 2018.

Silvern, R. F., Jacob, D. J., Mickley, L. J., Sulprizio, M. P., Travis, K. R., Marais, E. A., Cohen, R. C., Laughner, J. L., Choi, S., Joiner, J., et al., Using satellite observations of tropospheric NO_2 columns to infer long-term trends in US NO_x emissions: the importance of accounting for the free tropospheric NO_2 background, Atmos. Chem. Phys., 19, 8863-8878, doi:10.5194/acp-19-8863-2019, 2019.

Singh, R. B., and Grover, A., Sustainable Urban Environment in Delhi Mega City: Emerging Problems and Prospects for Innovative Solutions https://sustainabledevelopment.un.org/content/documents/6494108_Singh%20and%20Grover_Sustainable%20Urban%20Environment%20in%20Delhi.pdf 2015.

Singh, S., and Kulshrestha, U. C., Abundance and distribution of gaseous ammonia and particulate ammonium at Delhi, India, Biogeosciences, 9, 5023-5029, doi:10.5194/bg-9-5023-2012, 2012.

Snider, G., Weagle, C. L., Martin, R. V., van Donkelaar, A., Conrad, K., Cunningham, D., Gordon, C., Zwicker, M., Akoshile, C., Artaxo, P., et al., SPARTAN: a global network to evaluate and enhance satellite-based estimates of ground-level particulate matter for global health applications, Atmos. Meas. Tech., 8, 505-521, doi:10.5194/amt-8-505-2015, 2015.

Stieger, B., Spindler, G., Fahlbusch, B., Muller, K., Gruner, A., Poulain, L., Thoni, L., Seitler, E., Wallasch, M., and Herrmann, H., Measurements of PM_{10} ions and trace gases with the online system MARGA at the research station Melpitz in Germany - A five-year study, J. Atmos. Chem., 75, 33-70, doi:10.1007/s10874-017-9361-0, 2018.

Streets, D. G., Canty, T., Carmichael, G. R., de Foy, B., Dickerson, R. R., Duncan, B. N., Edwards, D. P., Haynes, J. A., Henze, D. K., Houyoux, M. R., et al., Emissions estimation from satellite retrievals: A review of current capability, Atmos. Environ., 77, 1011-1042, doi:10.1016/j.atmosenv.2013.05.051, 2013.

Sugathan, A., Bhangale, R., Kansal, V., and Hulke, U., How can Indian power plants cost-effectively meet the new sulfur emission standards? Policy evaluation using marginal abatement cost-curves, Energ. Policy, 121, 124-137, doi:10.1016/j.enpol.2018.06.008, 2018.

Surl, L., Palmer, P. I., and Abad, G. G., Which processes drive observed variations of HCHO columns over India?, Atmos. Chem. Phys., 18, 4549-4566, doi:10.5194/acp-18-4549-2018, 2018.

Tang, Y. S., Braban, C. F., Dragosits, U., Dore, A. J., Simmons, I., van Dijk, N., Poskitt, J., Pereira, G. D., Keenan, P. O., Conolly, C., et al., Drivers for spatial, temporal and long-term trends in atmospheric ammonia and ammonium in the UK, Atmos. Chem. Phys., 18, 705-733, doi:10.5194/acp-18-705-2018, 2018.

Theys, N., Hedelt, P., De Smedt, I., Lerot, C., Yu, H., Vlietinck, J., Pedergnana, M., Arellano, S., Galle, B., Fernandez, D., et al., Global monitoring of volcanic SO_2 degassing with unprecedented resolution from TROPOMI onboard Sentinel-5 Precursor, Sci. Rep.-Uk, 9, doi:10.1038/s41598-019-39279-y, 2019.

ul-Haq, Z., Tariq, S., and Ali, M., Tropospheric NO_2 Trends over South Asia during the Last Decade (2004-2014) Using OMI Data, Adv. Meteorol., doi:10.1155/2015/959284, 2015.

UN; Department of Economic and Social Affairs - Population Division, New York, World Urbanization Prospects: The 2018 Revision, https://population.un.org/wup/Publications/Files/WUP2018-Report.pdf, 2019.

Valach, A. C., Langford, B., Nemitz, E., MacKenzie, A. R., and Hewitt, C. N., Concentrations of selected volatile organic compounds at kerbside and background sites in central London, Atmos. Environ., 95, 456-467, doi:10.1016/j.atmosenv.2014.06.052, 2014.

Van Damme, M., Clarisse, L., Heald, C. L., Hurtmans, D., Ngadi, Y., Clerbaux, C., Dolman, A. J., Erisman, J. W., and Coheur, P. F., Global distributions, time series and error characterization of atmospheric ammonia (NH_3) from IASI satellite observations, Atmos. Chem. Phys., 14, 2905-2922, doi:10.5194/acp-14-2905-2014, 2014.

Van Damme, M., Clarisse, L., Dammers, E., Liu, X., Nowak, J. B., Clerbaux, C., Flechard, C. R., Galy-Lacaux, C., Xu, W., Neuman, J. A., et al., Towards validation of ammonia (NH_3) measurements from the IASI satellite, Atmos. Meas. Tech., 8, 1575-1591, doi:10.5194/amt-8-1575-2015, 2015.

Van Damme, M., Whitburn, S., Clarisse, L., Clerbaux, C., Hurtmans, D., and Coheur, P. F., Version 2 of the IASI NH_3 neural network retrieval algorithm: near-real-time and reanalysed datasets, Atmos. Meas. Tech., 10, 4905-4914, doi:10.5194/amt-10-4905-2017, 2017.

Van Damme, M., Clarisse, L., Whitburn, S., Hadji-Lazaro, J., Hurtmans, D., Clerbaux, C., and Coheur, P. F., Industrial and agricultural ammonia point sources exposed, Nature, 564, 99-110, doi:10.1038/s41586-018-0747-1, 2018.

Van Damme, M., Clarisse, L., Franco, B., Sutton, M. A., Erisman, J. W., Kruit, R. J. W., van Zanten, M., Whitburn, S., Hadji-Lazaro, J., Hurtmans, D., et al., Global, regional and national trends of atmospheric ammonia derived from a decadal (2008-2018) satellite record, Environ. Res. Lett., doi:10.1088/1748-9326/abd5e0, 2020.

van der A, R. J., Peters, D. H. M. U., Eskes, H., Boersma, K. F., Van Roozendael, M., De Smedt, I., and Kelder, H. M., Detection of the trend and seasonal variation in tropospheric NO_2 over China, J. Geophys. Res.-Atmos., 111, doi:10.1029/2005jd006594, 2006.

van der A, R. J., Eskes, H. J., Boersma, K. F., van Noije, T. P. C., Van Roozendael, M., De Smedt, I., Peters, D. H. M. U., and Meijer, E. W., Trends, seasonal variability and dominant NO_x source derived from a ten year record of NO_2 measured from space, J. Geophys. Res.-Atmos., 113, doi:10.1029/2007jd009021, 2008.

van Donkelaar, A., Martin, R. V., and Park, R. J., Estimating ground-level $PM_{2.5}$ using aerosol optical depth determined from satellite remote sensing, J. Geophys. Res.-Atmos., 111, doi:10.1029/2005jd006996, 2006.

van Donkelaar, A., Martin, R. V., Brauer, M., Kahn, R., Levy, R., Verduzco, C., and Villeneuve, P. J., Global Estimates of Ambient Fine Particulate Matter Concentrations from Satellite-Based Aerosol Optical Depth: Development and Application, Environ. Health Persp., 118, 847-855, doi:10.1289/ehp.0901623, 2010.

van Donkelaar, A., Martin, R. V., Brauer, M., Hsu, N. C., Kahn, R. A., Levy, R. C., Lyapustin, A., Sayer, A. M., and Winker, D. M., Global estimates of fine particulate matter using a combined geophysical-statistical method with information from satellites, models, and monitors, Environ. Sci. Technol., 50, 3762-3772, doi:10.1021/acs.est.5b05833, 2016.

Vasilkov, A., Krotkov, N., Yang, E.-S., Lamsal, L., Joiner, J., Castellanos, P., Fasnacht, Z., and Spurr, R., Explicit and consistent aerosol correction for visible wavelength satellite cloud and nitrogen dioxide retrievals based on optical properties from a global aerosol analysis, Atmos. Meas. Tech. Discuss., doi:10.5194/amt-2019-458, 2020.

Venkataraman, C., Brauer, M., Tibrewal, K., Sadavarte, P., Ma, Q., Cohen, A., Chaliyakunnel, S., Frostad, J., Klimont, Z., Martin, R. V., et al., Source influence on emission pathways and ambient $PM_{2.5}$ pollution over India (2015-2050), Atmos. Chem. Phys., 18, 8017-8039, doi:10.5194/acp-18-8017-2018, 2018.

Vieno, M., Heal, M. R., Hallsworth, S., Famulari, D., Doherty, R. M., Dore, A. J., Tang, Y. S., Braban, C. F., Leaver, D., Sutton, M. A., et al., The role of long-range transport and domestic emissions in determining atmospheric secondary inorganic particle concentrations across the UK, Atmos. Chem. Phys., 14, 8435–8447, doi:10.5194/acp-14-8435-2014, 2014.

Vieno, M., Heal, M. R., Williams, M. L., Carnell, E. J., Nemitz, E., Stedman, J. R., and Reis, S., The sensitivities of emissions reductions for the mitigation of UK $PM_{2.5}$, Atmos. Chem. Phys., 16, 265-276, doi:10.5194/acp-16-265-2016, 2016.

Vodonos, A., Abu Awad, Y., and Schwartz, J., The concentration-response between long-term $PM_{2.5}$ exposure and mortality; A meta-regression approach, Environmental Research, 166, 677-689, doi:10.1016/j.envres.2018.06.021, 2018.

Walker, H. L., Heal, M. R., Braban, C. F., Ritchie, S., Conolly, C., Sanocka, A., Dragosits, U., and Twigg, M. M., Changing supersites: assessing the impact of the southern UK EMEP supersite relocation on measured atmospheric composition, Environ. Res. Comm., 1, doi:10.1088/2515-7620/ab1a6f, 2019.

Wang, L., Slowik, J. G., Tripathi, N., Bhattu, D., Rai, P., Kumar, V., Vats, P., Satish, R., Baltensperger, U., Ganguly, D., et al., Source characterization of volatile organic compounds measured by PTR-ToF-MS in Delhi, India, Atmos. Chem. Phys., doi:10.5194/acp-2020-11, 2020.

Wang, T., Song, Y., Xu, Z., Liu, M., Xu, T., Liao, W., Yin, L., Cai, X., Kang, L., Zhang, H., et al., Why the Indo-Gangetic Plain is the region with the largest NH_3 column in the globe during summertime?, Atmos. Chem. Phys., doi:10.5194/acp-2019-1026, 2019.

Warner, J. X., Dickerson, R. R., Wei, Z., Strow, L. L., Wang, Y., and Liang, Q., Increased atmospheric ammonia over the world's major agricultural areas detected from space, Geophys. Res. Lett., 44, 2875-2884, doi:10.1002/2016gl072305, 2017.

Weagle, C. L., Snider, G., Li, C., van Donkelaar, A., Philip, S., Bissonnette, P., Burke, I., Jackson, J., Latimer, R., Stone, E., et al., Global Sources of Fine Particulate Matter: Interpretation of $PM_{2.5}$ Chemical Composition Observed by SPARTAN using a Global Chemical Transport Model, Environ. Sci. Technol., 52, 11670-11681, doi:10.1021/acs.est.8b01658, 2018.

Weatherhead, E. C., Reinsel, G. C., Tiao, G. C., Meng, X. L., Choi, D. S., Cheang, W. K., Keller, T., DeLuisi, J., Wuebbles, D. J., Kerr, J. B., et al., Factors affecting the detection of trends: Statistical considerations and applications to environmental data, J. Geophys. Res.-Atmos., 103, 17149-17161, doi:10.1029/98jd00995, 1998.

Wei, J., Sun, L., Peng, Y. R., Wang, L. C., Zhang, Z. Y., Bilal, M., and Ma, Y. C., An Improved High-Spatial-Resolution Aerosol Retrieval Algorithm for MODIS Images Over Land, J. Geophys. Res.-Atmos., 123, 12291-12307, doi:10.1029/2017jd027795, 2018.

Wei, J., Li, Z. Q., Peng, Y. R., and Sun, L., MODIS Collection 6.1 aerosol optical depth products over land and ocean: validation and comparison, Atmos. Environ., 201, 428-440, doi:10.1016/j.atmosenv.2018.12.004, 2019.

Wei, J., Li, Z. Q., Sun, L., Peng, Y. R., Liu, L., He, L. J., Qin, W. M., and Cribb, M., MODIS Collection 6.1 3 km resolution aerosol optical depth product: global evaluation and uncertainty analysis, Atmos. Environ., 240, doi:10.1016/j.atmosenv.2020.117768, 2020.

Whalley, L. K., Stone, D., Bandy, B., Dunmore, R., Hamilton, J. F., Hopkins, J., Lee, J. D., Lewis, A. C., and Heard, D. E., Atmospheric OH reactivity in central London: observations, model predictions and estimates of in situ ozone production, Atmos. Chem. Phys., 16, 2109-2122, doi:10.5194/acp-16-2109-2016, 2016.

Whalley, L. K., Stone, D., Dunmore, R., Hamilton, J., Hopkins, J. R., Lee, J. D., Lewis, A. C., Williams, P., Kleffmann, J., Laufs, S., et al., Understanding in situ ozone production in the summertime through radical observations and modelling studies during the Clean air for London project (ClearfLo), Atmos. Chem. Phys., 18, 2547–2571, doi:10.5194/acp-18-2547-2018, 2018.

Whitburn, S., Van Damme, M., Clarisse, L., Bauduin, S., Heald, C. L., Hadji-Lazaro, J., Hurtmans, D., Zondlo, M. A., Clerbaux, C., and Coheur, P. F., A flexible and robust neural network IASI-NH_3 retrieval algorithm, J. Geophys. Res.-Atmos., 121, 6581-6599, doi:10.1002/2016jd024828, 2016.

WHO; World Health Organization, WHO Global Urban Ambient Air Pollution Database, https://www.who.int/phe/health_topics/outdoorair/databases/cities/en/, 2018.

World Bank, Leveraging Spatial Development Options for Uttar Pradesh, http://documents1.worldbank.org/curated/en/751141468269412833/pdf/889670WP0URGEN00Box385254B00PUBLIC0.pdf 2014.

Yadav, R., Sahu, L. K., Beig, G., Tripathi, N., and Jaaffrey, S. N. A., Ambient particulate matter and carbon monoxide at an urban site of India: Influence of anthropogenic emissions and dust storms, Environ. Pollut., 225, 291-303, doi:10.1016/j.envpol.2017.01.038, 2017.

Zara, M., Boersma, K. F., De Smedt, I., Richter, A., Peters, E., van Geffen, J. H. G. M., Beirle, S., Wagner, T., Van Roozendael, M., Marchenko, S., et al., Improved slant column density retrieval of nitrogen dioxide and formaldehyde for OMI and GOME-2A from QA4ECV: intercomparison, uncertainty characterisation, and trends, Atmos. Meas. Tech., 11, 4033-4058, doi:10.5194/amt-11-4033-2018, 2018.

Zara, M., Boersma, F., Eskes, H., van der Gon, H. D., de Arellano, J. V.-G., Krol, M., van der Swaluw, E., Schuch, W., and Velders, G. J. M., Reductions in nitrogen oxides over the Netherlands between 2005 and 2018 observed from space and on the ground: Decreasing

emissions and increasing O_3 indicate changing NO_x chemistry, Atmos. Environ., doi:10.1016/j.aeaoa.2021.100104, 2021.

Zhu, L., Jacob, D. J., Mickley, L. J., Marais, E. A., Cohan, D. S., Yoshida, Y., Duncan, B. N., Abad, G. G., and Chance, K. V., Anthropogenic emissions of highly reactive volatile organic compounds in eastern Texas inferred from oversampling of satellite (OMI) measurements of HCHO columns, Environ. Res. Lett., 9, doi:10.1088/1748-9326/9/11/114004, 2014.

Zhu, L., Jacob, D. J., Kim, P. S., Fisher, J. A., Yu, K., Travis, K. R., Mickley, L. J., Yantosca, R. M., Sulprizio, M. P., De Smedt, I., et al., Observing atmospheric formaldehyde (HCHO) from space: validation and intercomparison of six retrievals from four satellites (OMI, GOME2A, GOME2B, OMPS) with SEAC^{4}RS aircraft observations over the southeast US, Atmos. Chem. Phys., 16, 13477–13490, doi:10.5194/acp-16-13477-2016, 2016.

Zoogman, P., Jacob, D. J., Chance, K., Zhang, L., Le Sager, P., Fiore, A. M., Eldering, A., Liu, X., Natraj, V., and Kulawik, S. S., Ozone air quality measurement requirements for a geostationary satellite mission, Atmos. Environ., 45, 7143-7150, doi:10.1016/j.atmosenv.2011.05.058, 2011.

CHAPTER 3

LARGE AND SIGNIFICANT INCREASES IN EXPOSURE TO AIR POLLUTION DETRIMENTAL TO HEALTH IN TROPICAL FUTURE MEGACITIES

Abstract

Tropical cities are experiencing unprecedented population growth in the absence of effective environmental regulation. This has the potential to drastically increase exposure to air pollutants detrimental to health. Here we conduct targeted sampling of atmospheric composition over 46 future and current megacities in the tropics to determine recent (2000s-2010s) changes in air pollution and population exposure leading to adverse health outcomes. We use satellite observations to estimate trends in nitrogen dioxide (NO_2), ammonia, volatile organic compounds, fine particles ($PM_{2.5}$), and ozone formation dependence on precursor emissions. We find that upward trends in air pollutants are overwhelmingly influenced by anthropogenic activity. In tropical cities in Asia and Southern Africa increases in urban air pollutants are 2-3 times steeper than reported regional trends, and opposite in Northern Africa to the reported decline in regional air pollution attributed to recedence in biomass burning. Most striking is annual increases in population exposure to $PM_{2.5}$ and NO_2 of up to 23 % due in large part to urbanization rates of 2-10 % a^{-1} in Africa and 1-8 % a^{-1} in Southeast Asia. Steep, significant increases in NO_2 also pose a challenge for mitigating already severe ozone pollution, as ozone formation in some cities should transition from strongly NO_x-sensitive to the difficult to regulate VOC-sensitive regime as early as 2025. The COVID-19 pandemic has demonstrated that healthcare systems in tropical countries are vulnerable to the looming health crisis supported by our exposure trends. We also now have advanced technology to develop without environmental destruction, but urgent action is needed.

3.1 Introduction

More than 40 % of the global population resides in the tropics (UN, 2018). Of those, less than half are in urban areas, though this is expected to exceed 50 % by 2050 due to steep rates of urbanization and unprecedented population growth (UN, 2018). By 2100, 51 of the 70 global megacities are projected to be in the tropics, mostly in Africa and Asia (Hoornweg and Pope, 2017). This has the potential for severe impacts on air quality and climate, as megacities represent an overwhelming contribution to carbon and air pollutant emissions (Duren and Miller, 2012; Krzyzanowski et al., 2014). Many countries in tropical Asia and Africa are yet to implement robust policies and necessary infrastructure to monitor and mitigate air pollution (Fang et al., 2020). Even where policies exist, such as in large cities in India, there is limited evidence of remediation (Vohra et al., 2021a). Knowledge of recent trends in precursors, abundance, and population exposure to air pollution in these rapidly growing cities is crucial for demonstrating the scale of air quality degradation to hasten adoption of sustainable mitigation measures and avoid repeating past air pollution health crises.

Ambient air pollution in much of the tropics is dominated by widespread, intense seasonal open burning of biomass (Aghedo et al., 2007; Yin et al., 2019). The contribution from anthropogenic activity varies regionally and is greatest in Asia, predominantly from residential combustion and industrial activity (Reddington et al., 2019; Yin et al., 2019). Air pollution in Africa is also influenced by natural sources (desert dust and biogenic emissions) and residential and commercial production and use of solid fuels (Marais and Wiedinmyer, 2016; Bauer et al., 2019; Bockarie et al., 2020). Combined rapid growth in anthropogenic activity and tropical

deep convective injection of pollutants and precursors to the free troposphere also has the potential to greatly influence global chemistry and climate (Thompson et al., 1997).

Exposure to ambient fine particulate pollution ($PM_{2.5}$) is already a leading environmental health risk in many countries in the tropics (Stanaway et al., 2018; Fang et al., 2020). More than 30 % of premature deaths in Asia are attributable to exposure to $PM_{2.5}$ from fossil fuel combustion alone (Vohra et al., 2021b) and 170,000 global premature infant deaths, mostly in South Asia and sub-Saharan Africa, have been attributed to exposure to ambient $PM_{2.5}$ (HEI, 2020). Annual mean population-weighted $PM_{2.5}$ for the tropics is almost 3 times the WHO guideline (World Bank, 2019), though this was determined with very few measurements; < 1 monitor per million people in many tropical countries (Martin et al., 2019). The density of monitors has improved with deployment of low-cost sensors and additional reference-grade instruments (Brauer et al., 2019; Sahu et al., 2021), but large data gaps and data quality and access issues persist. India, for example, has an extensive network of monitors operated and maintained by local and national authorities and research institutions, but use of these for informing policies is hindered by data quality issues for the national network (Brauer et al., 2019; Vohra et al., 2021a) and restricted access to data collected by research institutions.

Satellite observations provide long-term, consistent global observations of a range of chemical components of the atmosphere. These can be used to estimate long-term changes in abundance of surface air pollutants, in precursor emissions of short-lived pollutants (Duncan et al., 2016; Van Damme et al., 2020), and in sensitivity of ozone formation to source types for informing policy measures to regulate already severe ozone pollution in the tropics (Aghedo et al., 2007).

As we also demonstrate in this work, these can be directly combined with population data to determine trends in city population exposure to $PM_{2.5}$ and nitrogen dioxide (NO_2) that are both detrimental to health.

The 46 cities in tropical Africa, the Middle East and Asia that are projected to be megacities (population of at least 10 million) by 2100 are shown in Figure 3.1. Only 12 are megacities now, mostly in India. Forecast population growth rates from 2020 to 2100 range from 3-31 % a^{-1} in Africa, 1 % a^{-1} for Riyadh and 8 % a^{-1} for Sana'a in the Middle East, 0.8-3 % a^{-1} in South Asia, and 0.5-7 % a^{-1} in Southeast Asia. The largest cities, forecast to surpass 50 million inhabitants by 2100, include Lagos (80 million) in Nigeria, Dar es Salaam (62 million) in Tanzania, Kinshasa (60 million) in the Democratic Republic of the Congo, and Mumbai (58 million) in India. There are also 5 cities in Central and South America that are already megacities, but our focus is on the cluster of cities in Asia, Africa and the Middle East due to their much faster projected growth (Hoornweg and Pope, 2017).

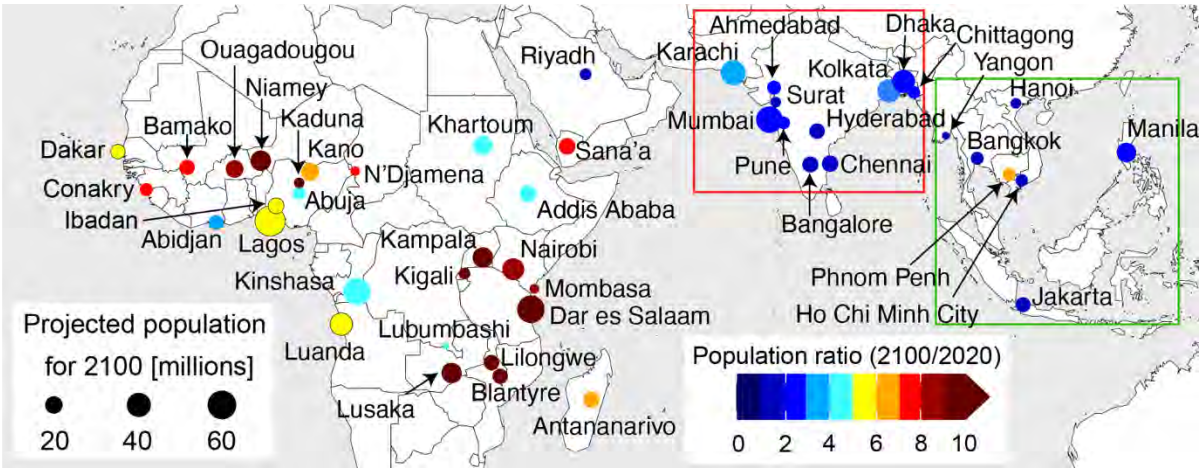

Figure 3.1 Projected population growth for cities in the tropics (25°S-25°N) anticipated to be megacities (population ≥ 10 million) by 2100. Circle sizes indicate 2100 population and colors 2100-to-2020 population ratios. Data for 2100 are from Hoornweg and Pope (2) and for 2020 from the UN (1). Boxes discern cities in South Asia (red) and Southeast Asia (green).

Here we use more than a decade of satellite observations of atmospheric composition to determine recent (2000s-2010s) trends in air pollution abundances and precursor emissions, and urban population exposure to $PM_{2.5}$ and NO_2 in fast-growing tropical cities in Africa, Asia and the Middle East to signal an emerging health and environmental crisis that demands urgent action.

3.2 Materials and Methods

3.2.1 Satellite Datasets, City Sampling and Trend Estimates

We use Earth observations of tropospheric column nitrogen dioxide (NO_2) and total column formaldehyde (HCHO) from the Ozone Monitoring Instrument (OMI), attenuation of light by aerosols throughout the atmospheric column or aerosol optical depth (AOD) from the Moderate Resolution Imaging Spectroradiometer (MODIS), and total column NH_3 from the Infrared Atmospheric Sounding Interferometer (IASI) to determine trends in air quality, precursor emissions, and population exposures over the rapidly growing tropical cities identified in Figure 3.1. The record of observations we use is for 2005-2018 from OMI and MODIS, and for 2008-2018 from IASI. Table 3.1 provides additional details of the instrument features, satellite data products, and data quality flags used to process the data. In our previous work, we demonstrated that space-based observations of tropospheric column NO_2 and total column NH_3 reproduce month-to-month variability in surface concentrations of these and that satellite observations of AOD reproduce long-term trends in surface observations of $PM_{2.5}$ (Vohra et al., 2021a). The same assessment of the skill of satellite observations of HCHO at reproducing changes in surface concentrations of reactive non-methane volatile organic compounds (NMVOCs) was

not possible, as measurements of reactive NMVOCs are sparse in space and time and routine measurements are limited to hydrocarbons.

Table 3.1 Satellite data products used to determine trends in NO_2, reactive NMVOCs, NH_3 and $PM_{2.5}$ for fast-growing cities in the tropics

Instrument	Launch platform	Launch date	Swath width	Measurement	Data product name	Pixel resolution[a]	Overpass time[b]	Global coverage[c]	Data retained
OMI[d]	Aura	October 2004	2600 km	NO_2	NASA SP v4.0[e]	13 km × 24 km	13h30 LST	Every 2 days[f]	cloud fraction < 50 %
									terrain reflectivity < 30 %
									solar zenith angle < 85°
				HCHO	QA4ECV v1.3[g]				processing error flag = 0
									processing quality flag = 0
									cloud fraction < 50 %
IASI[h]	Metop-A	October 2006	2130 km	NH_3	v3R[i]	12 km[j]	09h30 LST	Daily	cloud fraction < 10 %
MODIS[k]	Aqua	May 2002	2230 km	AOD	Merged SDS C6.1[l]	10 km × 10 km	13h30 LST	Near-daily	quality assurance flag = 3

[a] At nadir, [b] Local solar time (LST), [c] for relevant satellite overpass time, [d] Ozone Monitoring Instrument, [e] NASA Standard Product version 4.0 (https://doi.org/10.5067/Aura/OMI/DATA2017; last access 18 March 2021), [f] Global coverage degraded from daily in 2005-2009 to every 2 days thereafter due to the row anomaly, [g] Quality Assurance for Essential Climate Variables version 1.3 (https://doi.org/10.18758/71021031; last access 18 March 2021), [h] Infrared Atmospheric Sounding Interferometer, [i] Reanalysed IASI version 3.0.0 (https://iasi.aeris-data.fr/NH3R-ERA5_IASI_A_data/; last access 20 March 2021), [j] Circular pixels at nadir, [k] Moderate Resolution Imaging Spectroradiometer, [l] Merged Scientific Data Set Collection 6.1 (https://doi.org/10.5067/MODIS/MYD04_L2.061; last access 18 March 2021).

We calculate city-wide monthly means by sampling satellite pixel centers that fall within the city boundaries using shapefiles mostly from the Database of Global Administrative Areas (GADM) version 3.6 (https://gadm.org/; last accessed 12 March 2021). Satellite data coverage can be low for smaller cities, exacerbated by persistent clouds in the tropics. We address this by extending the sampling domain beyond the city boundaries relative to the instrument pixel size (6.5 km for OMI and MODIS, 10 km for IASI), as in Vohra et al. (2021a), for the 22 smallest tropical cities (indicated in Table S3.1). In our analysis, we only retain months with at least 5 pixels, as in Vohra et al. (2021a).

We isolate the contribution of local HCHO sources (direct emissions and oxidation by reactive NMVOCs) to total column HCHO by subtracting the background column component due to oxidation of methane and other long-lived VOCs (Marais et al., 2012; Vohra et al., 2021a). We do this by calculating monthly mean background columns over remote ocean domains closest to the cities of interest that extend over the same latitudinal range as the selected cities (Figure S3.1), where feasible. This ensures consistent seasonality between the background column and columns over the target cities. We then apply the non-linear fit described in van der A et al. (2006) that accounts for seasonality in the time series to the monthly mean background HCHO and subtract the fitted values from the city-wide monthly means, as in Marais et al. (2012) and Vohra et al. (2021a).

All atmospheric components of interest in this work exhibit a distinct seasonality in the tropics due to seasonality in photochemistry, planetary boundary layer dynamics, synoptic

meteorological events such as monsoons, and sources such as biomass burning (Shah et al., 2020; Van Damme et al., 2020; Vohra et al., 2021a). To account for this in the trend analysis, we fit the non-linear function from van der A et al. (2006) to the time series of city-wide monthly means. This is only applied to cities with > 30 % temporal coverage (> 50 months for OMI and MODIS, > 40 months for IASI). Trends are considered significant at the 95 % confidence interval (CI) (p-value < 0.05) if the CI range does not intersect zero.

3.2.2 Trends in Biomass Burning and Anthropogenic Activity

Intense regional open burning of biomass contributes to large seasonal enhancements in air pollution in the tropics. So, to determine whether biomass burning or anthropogenic activity influences trends in NO_2, NH_3 and reactive NMVOCs (Figure 3.2), we separate city-wide monthly means into months above and below the 75th percentile in each year. We find that months above 75th percentile values coincide with months known to be influenced by biomass burning in 22 of the cities in Figure 3.1 (indicated in Figure S3.2). These are December-March in Northern Africa and July-November in Southern Africa (Barbosa et al., 1999), and January-April in South Asia and Southeast Asia north of the Equator and August-October in Southeast Asia south of the Equator (Vadrevu et al., 2015; Bhardwaj et al., 2016). We remove from these biomass burning months the contribution of anthropogenic sources determined as the annual means of the monthly data that fall below the 75th percentile for the corresponding year. We refer to the resultant values as biomass burning months and the values below the 75th percentiles as non-biomass burning or anthropogenic activity months. We also assess consistency in trend directions between biomass burning months obtained with our statistical approach and biomass burning activity as indicated by satellite-derived burned fraction. The burned fraction product

we use is Global Fire Emissions Database (GFED) version 4.1 that includes improved detection of small fires (v4.1s, https://globalfiredata.org/pages/data/; last accessed 22 April 2021) (Giglio et al., 2013). This is provided at 0.25° × 0.25° for 2005-2016. We calculate annual burned fraction over the 22 target cities by sampling GFEDv4.1s grids that overlap with the same sampling extent as the satellite observations and apply the linear Theil-Sen median estimator (Theil, 1950; Sen, 1968) to biomass burning months, non-biomass burning (anthropogenic activity) months, and annual burned fraction to calculate trends in these.

3.2.3 Trends in Bottom-up Estimates of Anthropogenic Emissions

Satellite observations of the relatively short-lived pollutants NO_2 (lifetime of ~6 h against conversion to reservoir compounds), HCHO (lifetime of 2-3 h), and NH_3 (lifetime of 2-15 h) provide constraints on precursor emissions of NO_x, reactive NMVOCs and NH_3 (Marais et al., 2012; Duncan et al., 2016; Van Damme et al., 2018; Shah et al., 2020). We assess representation of these in bottom-up estimates of anthropogenic emissions and characterize possible anthropogenic sources contributing to the observed trends using the $CEDS_{GBD\text{-}MAPS}$ inventory (https://doi.org/10.5281/zenodo.3754964; last accessed 20 March 2021) developed for the US Health Effects Institute (HEI) Global Burden of Disease – Major Air Pollution Sources (GBD-MAPS) project. It extends the record of emissions of the original Community Emissions Data System (CEDS) inventory (Hoesly et al., 2018) from 1970-2014 to 1970-2017 and improves representation of regional emissions by updating activity data and emission factors with data from other global, regional and national inventories (McDuffie et al., 2020). Anthropogenic emissions in $CEDS_{GBD\text{-}MAPS}$ are provided as monthly gridded (0.5° × 0.5°) values for 11 broad source sectors (McDuffie et al., 2020). We sum 16 of the 23 NMVOCs classes with atmospheric

lifetimes < 2 days to represent reactive NMVOCs emissions. We isolate annual total city emissions from $CEDS_{GBD\text{-}MAPS}$ by sampling grids in the same way as we do GFEDv4.1s burned fraction and calculate trends using the same Theil-Sen median estimator (Theil, 1950; Sen, 1968). Emissions of NO_x and reactive NMVOCs are compared to trends in OMI NO_2 and the reactive NMVOCs component of OMI HCHO, respectively, for 2005-2017 and emissions of NH_3 are compared to trends from IASI NH_3 for 2008-2017.

3.2.4 Trends in Population Exposure to Toxic Air Pollutants

We determine trends in city population exposure to $PM_{2.5}$ and NO_2 by calculating annual city population pseudo-exposures to total column AOD and tropospheric column NO_2 using the standard population exposure (E_{pop}) formula:

$$E_{\text{pop}} = \sum_{i=1}^{N} C \qquad (3\text{-}1).$$

N is total population from the UN (UN, 2018) for the tropical cities in Figure 3.1 and C is the annual mean of the non-linear fit used to estimate trends in total column AOD as proxy for surface $PM_{2.5}$ (Figure S3.3a) and in tropospheric column NO_2 as proxy for surface NO_2 (Figure 3.2a). We calculate E_{pop} at the record start (2005) and end (2018) to estimate relative trends in exposure. This approach draws on our previous findings that trends in satellite observations of column values are consistent with trends in surface concentrations (AOD for surface $PM_{2.5}$, tropospheric column NO_2 for surface NO_2), even for cities where seasonality in AOD and $PM_{2.5}$ are decoupled (Vohra et al., 2021a).

3.3 Results and Discussion

3.3.1 Trends in Air Quality in Fast-Growing Tropical Cities

Figure 3.2 shows recent trends in the short-lived pollutants NO_2, ammonia (NH_3) and reactive NMVOCs over these cities obtained from a long-term, consistent record of satellite observations (Table 3.1, Section 3.2.1). NO_2 increases in almost all (41) cities, by 0.1-14.1 % a^{-1}, and the trends are significant for 34 of these 41 cities (Figure 3.2a). NO_2 triples over Chittagong (Bangladesh) and more than doubles over Antananarivo (Madagascar), Hanoi (Vietnam), Luanda (Angola) and Dhaka (Bangladesh). NO_2 declines in 5 cities, though the downward trend is only appreciable and significant for Jakarta (-2.0 % a^{-1}). This decline has already been identified using an earlier record of observations from the same satellite instrument (Lalitaporn et al., 2013; Duncan et al., 2016) and likely reflects emission controls imposed on vehicles since 2005 (Duncan et al., 2016; Kusumaningtyas et al., 2018). The record of NO_2 for cities in Africa starts at ~60 % lower values than Asian cities, due to prevalence across Africa of inefficient combustion sources with relatively low NO_x emissions (Marais and Wiedinmyer, 2016). In general, upward trends in NO_2 cover a similar range in Africa (0.3-8.2 % a^{-1}) and Asia (0.8-7.7 % a^{-1}, excluding 14.1 % a^{-1} for Chittagong). The directions of our NO_2 trends are consistent with previous studies that have focused on large cities around the world (Hilboll et al., 2013; Lelieveld et al., 2015; Schneider et al., 2015; Duncan et al., 2016; Georgoulias et al., 2019). This consistency includes trend reversals from positive to negative over Jakarta and Riyadh in 2011 and from negative to positive over Manila in 2009 (Lelieveld et al., 2015; Georgoulias et al., 2019). The significant increases in NO_2 in Northwest African cities, ranging from 0.3 % a^{-1} over Conakry to 4.4 % a^{-1} over Niamey and Lagos, are opposite to the large regional decline in NO_2 of 4.5 % a^{-1} reported by Hickman et al. (2021) for the same

instrument used here. They focused on the dry season (November-February) when there is intense and widespread open burning of biomass.

As with NO_2, NH_3 increases in almost all cities in Africa, the Middle East, and Southeast Asia (Figure 3.2b). Known dominant sources include agricultural activity, vehicles, and burning of waste and biomass in all regions, and large-scale industrial fertilizer production in Asia (Van Damme et al., 2018; Clarisse et al., 2019). The increase in NH_3 over Jakarta while NO_2 declines could reflect absence of air quality policies targeting agriculture and biomass burning (Van Damme et al., 2020). Decline in NH_3 in almost all South Asian cities coincides with increases in precursor (SO_2) emissions of acidic sulfate aerosols that promote partitioning of NH_3 to acidic aerosols to form $PM_{2.5}$ and contribute to significant increases in $PM_{2.5}$ of 2.5-7.8 % a^{-1} (Figure S3.3a). In India, SO_2 emissions, mostly from industry and coal-fired power plants, are estimated to have increased by 50 % from 2007 to 2016 (Li et al., 2017a). Aerosol partitioning of NH_3 would also be promoted by an increase in abundance of acidic nitrate aerosol due to an increase in precursor emissions of NO_x, supported by our positive trends in NO_2 (Figure 3.2a). An increase in abundance of chlorine from plastic waste fires would also promote aerosol uptake of NH_3 (Gunthe et al., 2021), but there are no routine measurements to quantify trends in chlorine abundance. Increases in waste generation and absence of effective waste management support an increase in chlorine emissions from this source (Hoornweg et al., 2013). Karachi is the lone city in South Asia with an increase in NH_3 of 2.9 % a^{-1}, due to an increase in fertilizer use (Xu et al., 2018; Van Damme et al., 2020). The positive trend for Karachi is consistent with a regional increase in NH_3 across the Indo-Gangetic Plain (IGP) caused by agricultural fires (Van Damme et al., 2020) and with reported increases in NH_3 over Indian cities also located in the IGP (Vohra et al., 2021a). NH_3 column densities at the start of

the record are similar for Asia and Africa, due to a combination of similar sources (Van Damme et al., 2018; Xu et al., 2018; Clarisse et al., 2019). Our positive city trends are generally 1.5-2.5 times steeper than the trends at regional and national scales reported by Van Damme et al. (2020). The steeper trends in cities could be due to greater abundance of urban sources of NH_3 (Clarisse et al., 2019; Sharma et al., 2020) and enhanced NH_3 volatilization due to the urban heat island effect (Kuttippurath et al., 2020).

Trends in reactive NMVOCs are estimated with the portion of the total formaldehyde (HCHO) column attributable to reactive NMVOCs (Section 3.2.1). The trends in these are not as homogenous or significant as trends in NO_2 and NH_3, apart from Jakarta and cities in South Asia. Significant decline in reactive NMVOCs in Jakarta of 1.7 % a^{-1} is similar to that for NO_2 (Figure 3.2a). This could be due to a decrease in vehicle exhaust emissions of unburned reactive hydrocarbons from enhanced efficiency of diesel vehicles due to greater use of biodiesel (Damanik et al., 2018). Biodiesel usage in Indonesia has increased 16-fold from 2010 to 2019 (Statista, 2021). Our upward trends in reactive NMVOCs for Lagos (1.5 % a^{-1}), Mumbai (1.7 % a^{-1}) and Kinshasa (2.0 % a^{-1}) support sustained increases in reactive NMVOCs identified for 1997-2009 using an earlier record of satellite observations (De Smedt et al., 2010). The greatest increase in reactive NMVOCs occurs over Sana'a (>10 % a^{-1}), though the HCHO column densities are close to instrument detection and very small (<1 × 10^{15} molecules cm^{-2}) at the beginning of the record, after removing the background contribution (Section 3.2.1). The population in Sana'a has increased by 4.7 % a^{-1}, but the country has also been embroiled in conflict and political instability and the other pollutants only increase by 0.07-1.15 % a^{-1} (Table S3.1).

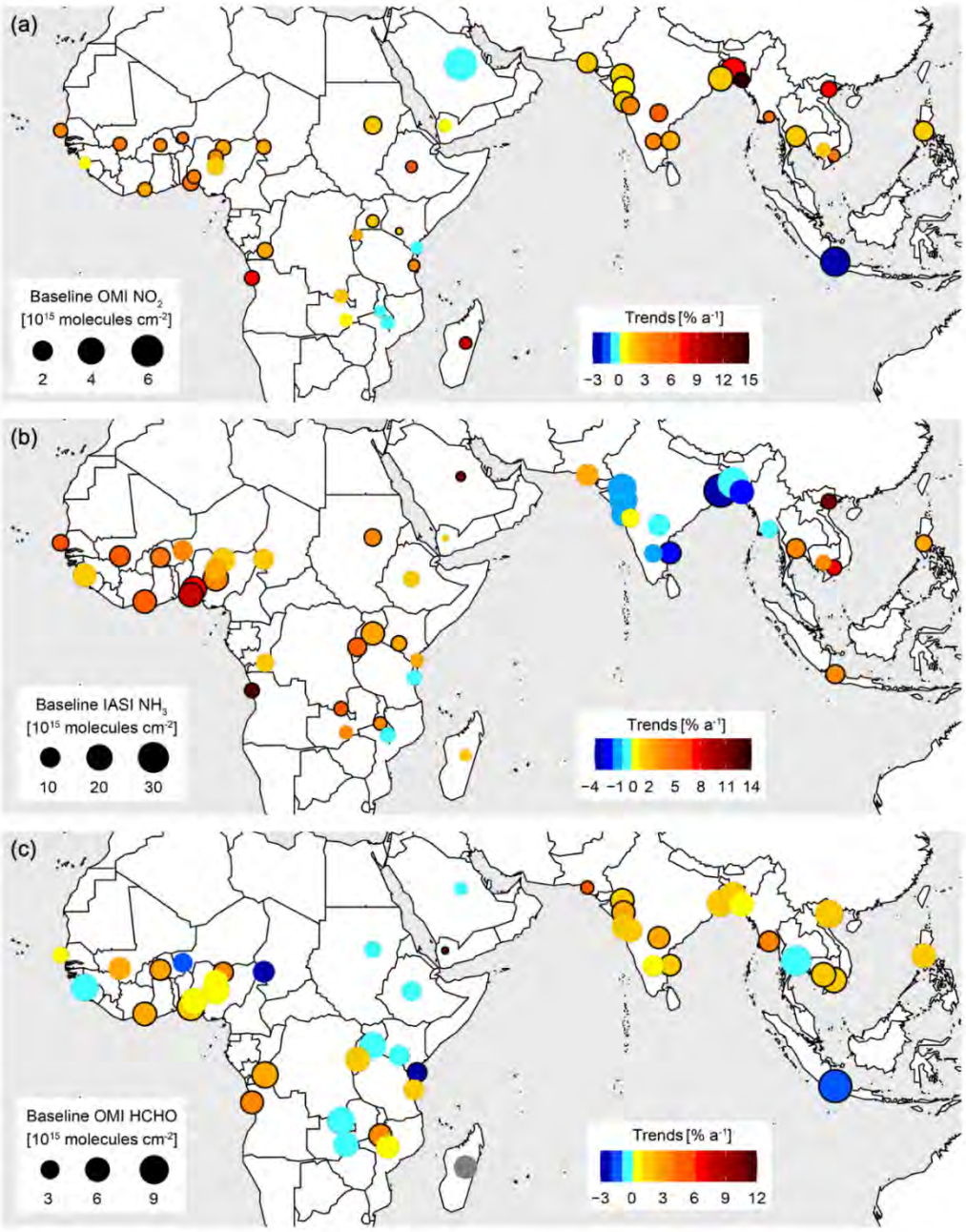

Figure 3.2 Trends in NO_2, NH_3 and reactive NMVOCs in rapidly growing cities in the tropics. Circle colors are relative trends and sizes are values at the start of the record (baseline). Outlines identify significant trends at the 95 % confidence interval (CI). Warm colors indicate positive trends, cool colors negative trends. Grey circles identify cities with low temporal coverage. Trend values are in Table S3.1.

Decline in reactive NMVOCs at the same time as NO_2 increases in 9 African cities (Conakry, Niamey, N'Djamena, Addis Ababa, Nairobi, Kampala, Khartoum, Lubumbashi and Lusaka) is consistent with a shift to more efficient combustion sources in these cities, as is suggested by

regional anthropogenic emission inventories (Marais and Wiedinmyer, 2016; Bockarie et al., 2020). Rates of increase in reactive NMVOCs in cities in South Asia of 0.6-4.3 % a^{-1} are less steep than trends in NO_2 (0.8-14.1 % a^{-1}). These differences in rates and directions of trends in NO_2 (and thus NO_x) and reactive NMVOCs has implications for surface ozone formed from photochemical oxidation of NMVOCs in the presence of NO_x. In much of the tropics, surface ozone is close to the WHO guideline (Sicard et al., 2017) and, at these levels, is harmful to staple crops prevalent in the tropics (Hayes et al., 2020). Ratios of total column HCHO (background + reactive NMVOCs) to tropospheric column NO_2 (HCHO/NO_2; Figure S3.3b) in 2005 exceed values of 2 in almost all cities (reaching 23 in Conakry and Nairobi), indicative of sensitivity of ozone formation to NO_x sources. During the record used here (2005-2018), most of these cities are transitioning to a regime in which ozone production is sensitive to NMVOCs sources, synonymous with many megacities in the US, Europe, and China. If the future mimics the past, the transition to sensitivity to NMVOCs that are very challenging to monitor and regulate (McDonald et al., 2018; Vohra et al., 2021a) could occur as soon as 2025 in Chittagong and Dhaka and 2030 in Addis Ababa, Hanoi and Luanda.

3.3.2 Factors Influencing Trends in Air Quality

To assess whether conventional biomass burning or emerging anthropogenic sources dominate tropical city trends in air quality, we compare trends in Figure 3.2 to those for biomass burning and non-biomass burning (anthropogenic activity) months in Figure 3.3. This analysis focuses on the 22 tropical cities we identify to be substantially influenced by biomass burning (Section 3.2.2). In general, there are fewer significant air pollutant trends in biomass burning months (Figure 3.3a-c) than there are in anthropogenic activity months (Figure 3.3d-f). The Figure 3.2

trends in reactive NMVOCs appear to be predominantly influenced by anthropogenic activity, supported by either the same or steeper trends in the anthropogenic activity months compared to all months (Figure 3.3f) and lack of consistency in trends for all but 1 city in the biomass burning months comparison (Figure 3.3c). The same conclusion can be drawn for NO_2 for most cities, though there are some cities that have similar positive trends in biomass burning and all months (shapes along the 1:1 line in Figure 3.3a). This suggests that for these cities, both biomass burning and anthropogenic activity influence trends in NO_2. Six African cities exhibit steep increases in anthropogenic activity NO_2 (points above the grey shading in Figure 3.3d). Three of these, all in West Africa (Abuja, Ibadan, Conakry), lie below the grey shading in Figure 3.3a, suggesting that increases in anthropogenic sources are ameliorated by negative or muted trends in biomass burning. This is consistent with findings from the regional study by Hickman et al. (2021) and supported by a decline in burned fraction for the 2 cities in Nigeria (Abuja and Ibadan; Figure S3.2). Regional bottom-up inventories also suggest that anthropogenic emissions of VOCs and other pollutants already or will soon rival those from biomass burning (Marais and Wiedinmyer, 2016; Bockarie et al., 2020).

The NH_3 trends (Figures 3.3b and 3.3e) exhibit a consistent compensating effect in many cities. Three cities (Lagos, Kaduna, Abidjan) with steep increases in biomass burning have much shallower trends in anthropogenic activity, and 6 cities with steep increases in anthropogenic activity of 1.0-31.6 % a^{-1} have negative trends in biomass burning. The 3 West African cities with very steep increases in biomass burning also exhibit positive trends in burned fraction, but the same steep increase is not apparent for trends in biomass burning NO_2 (Figure 3.3a) or reactive NMVOCs (Figure 3.3c). This may be due to a shift in the type of vegetation burned (Dwomoh and Wimberly, 2017), a transition to more anoxic fires favoring NH_3 over NO_x and

longer-lived hydrocarbons over reactive oxygenated VOCs, or due to greater prevalence in the dry season of anthropogenic NH_3 sources like waste burning. Evidence of these shifts requires further investigation.

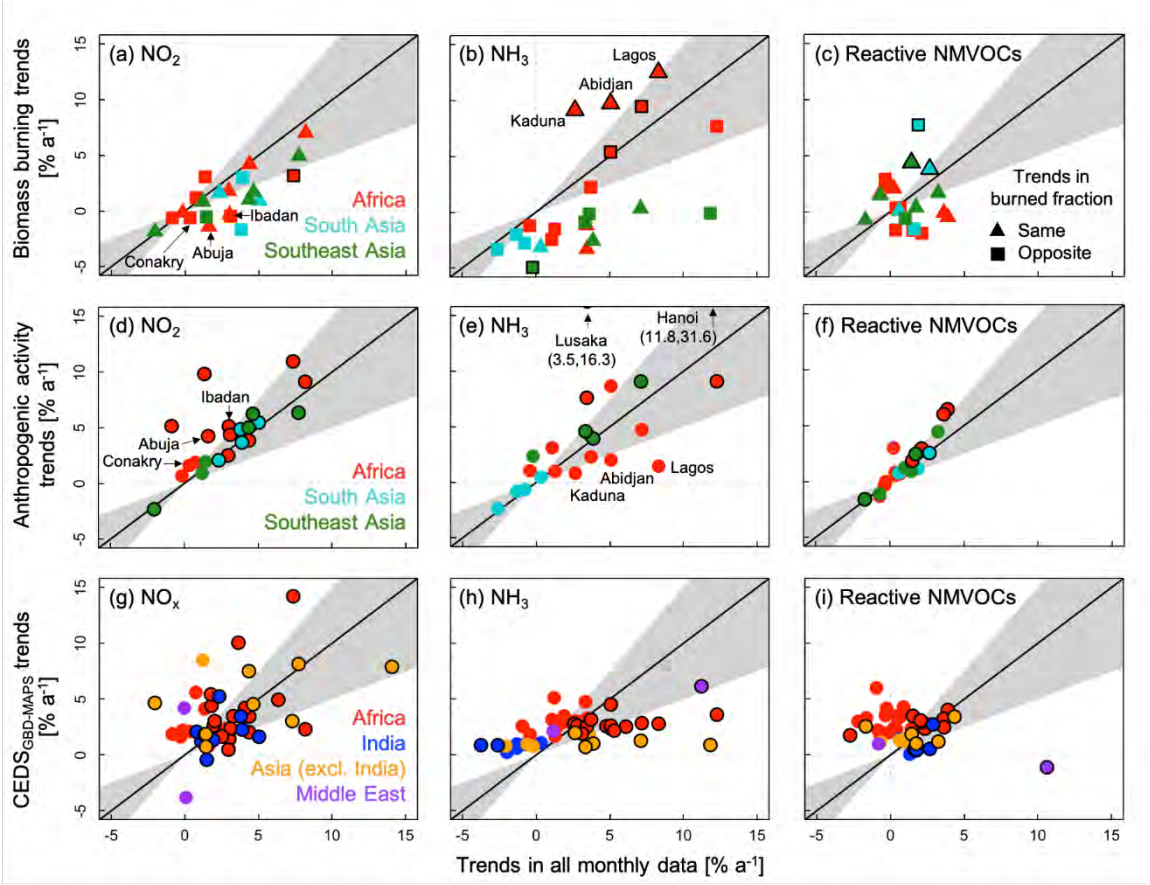

Figure 3.3 Constraints on factors influencing trends in short-lived air pollutants in rapidly growing cities in the tropics. Panels compare trends in all data (Figure 3.2) to trends in biomass burning (a-c) and anthropogenic activity (d-f) for 22 cities influenced by biomass burning (Figure S3.2; Section 3.2.2), and in bottom-up anthropogenic emissions (g-i) for all 46 cities. Shape colors distinguish regions and shape types in (a-c) indicate if burned fraction trend directions (Figure S3.2) are the same as (triangles) or opposite to (squares) those for biomass burning. Outlines identify significant trends at the 95 % CI for biomass burning (a-c), anthropogenic activity (d-f), and all data (g-i). Trends are significant for Lusaka and Hanoi in (e). Grey shading is the ±50 % spread around the black 1:1 line. Dotted lines discern positive and negative trends.

We also assess the skill of a contemporary anthropogenic emission inventory at reproducing trends in Figure 3.2 for all 46 cities (Figures 3.3g-i), as satellite observations provide constraints

on precursor emissions of short-lived pollutants (Marais et al., 2012; Duncan et al., 2016; Van Damme et al., 2018). We find that anthropogenic activity dominates trends in air quality in tropical cities. We employ the global $CEDS_{GBD\text{-}MAPS}$ inventory (Section 3.2.3) that has been used to estimate the global burden of disease due to exposure to air pollution from evolving anthropogenic source sectors (McDuffie et al., 2021). $CEDS_{GBD\text{-}MAPS}$ NO_x emission trends reproduce the direction of trends in satellite NO_2 for most cities (Figure 3.3g), though for many the discrepancy exceeds 50 %. $CEDS_{GBD\text{-}MAPS}$ does not capture the policy-driven decline in emissions in Jakarta (+4.7 % a^{-1} in $CEDS_{GBD\text{-}MAPS}$, -2.0 % a^{-1} in the observations) or the marginal, though non-significant, increase in NO_x in Sana'a (-3.8 % a^{-1} in $CEDS_{GBD\text{-}MAPS}$, +0.07 % a^{-1} in the observations). According to $CEDS_{GBD\text{-}MAPS}$, the steepest increases in NO_x emissions in African cities are from non-residential energy generation (4.6 % a^{-1}) and industry (4.2 % a^{-1}). These sources together account for 65-70 % of $CEDS_{GBD\text{-}MAPS}$ NO_x in Indian cities, but the steepest increases are for off-road transport (8.6 % a^{-1}) and a mix of non-traditional combustion sources (2.8 % a^{-1}). In Asian cities, excluding India, the largest growth in $CEDS_{GBD\text{-}MAPS}$ NO_x is from the dominant sectors energy generation (4.2 % a^{-1}), industry (5.3 % a^{-1}) and off-road transport (6.3 % a^{-1}).

Trends in $CEDS_{GBD\text{-}MAPS}$ NH_3 emissions are positive for all cities, but 2-5 times less than the trends in the observations (Figure 3.3h). Underestimates in $CEDS_{GBD\text{-}MAPS}$ are greatest for all but 2 of the cities that we identified to be strongly influenced by steep increases in anthropogenic sources (Figure 3.3e). Similarly large underestimates in emission inventory trends compared to those from satellite observations have been reported at the regional and national scale (Van Damme et al., 2020). Inventories may underestimate rapid changes in agricultural activity, such as increases in livestock numbers and use of synthetic nitrogen

fertilizers (Jayne and Sanchez, 2021; Zhang et al., 2021). Growth in agricultural productivity in general in sub-Saharan Africa is almost double the global average (Jayne and Sanchez, 2021). Waste burning emissions of NH_3 are also likely to increase rapidly. Across the tropics waste generation is projected to increase by 2-6 % a^{-1} and much of this will be burned in many countries in the tropics that lack effective waste management (Kaza et al., 2018). Divergence of NH_3 trends in Indian cities and nearby Asian cities is due to the increase in acidic aerosols already discussed. According to $CEDS_{GBD\text{-}MAPS}$, NH_3 emissions in Indian cities grew at a rate of 1 % a^{-1}, mostly due to a 2 % a^{-1} increase in agricultural emissions. Discrepancies in observed and $CEDS_{GBD\text{-}MAPS}$ NH_3 emissions in Riyadh and Sana'a are large, but emissions for these cities are small (3-10 kt a^{-1} during 2005-2017) compared to the other tropical cities (30-80 kt a^{-1} for the same time period) and mainly come from waste processing.

Trends in bottom-up and top-down reactive NMVOCs are generally similar for cities with significant increases in these and are dominated by increases in residential energy combustion in $CEDS_{GBD\text{-}MAPS}$. Trends diverge for Sana'a (-1.1 % a^{-1} for $CEDS_{GBD\text{-}MAPS}$, +10.6 % a^{-1} for the observations), but observed values are small and may be prone to error. As with NO_2, $CEDS_{GBD\text{-}MAPS}$ trends in reactive NMVOCs in Jakarta (+2.6 % a^{-1}) are opposite to the observations (-1.7 % a^{-1}). Significant decline in reactive NMVOCs over Mombasa in the observations (-2.7 % a^{-1}), and not in the inventory (+1.8 % a^{-1}), may be due to a shift toward combustion efficient sources due to substantial development of the Mombasa seaport to meet increasing demand for imported goods (Reuters, 2015), though this is not supported by the non-significant decline in NO_2 (0.3 % a^{-1}; Figure 3.2a).

3.3.3 Trends in Exposure to Air Pollutants Hazardous to Health

Urban population in the tropical cities in Figure 3.1 increased on average by 2-10 % a^{-1} in Africa, 4-5 % a^{-1} in the Middle East, 1-7 % a^{-1} in South Asia, and 1-8 % a^{-1} in Southeast Asia from 2005 to 2018. Rapid population growth combined with steep and significant increases in NO_2 in most of cities (Figure 3.2a) and in $PM_{2.5}$ in all cities in South Asia and many in Africa (Figure S3.3b), will substantially increase population exposure to hazardous pollutants. The effects of long-term exposure to ambient air pollution includes well-established health outcomes like respiratory and cardiovascular diseases (Burnett et al., 2018; Stieb et al., 2021) and recently identified health endpoints such as dementia, impaired cognition, and loss of fertility and eyesight (Cacciottolo et al., 2017; Zhang et al., 2018; Schraufnagel et al., 2019; Chua et al., 2021; Li et al., 2021). Premature mortality due to exposure to ambient $PM_{2.5}$ from anthropogenic sources is already substantial in Asia, but is relatively low in Africa, in particular in comparison to communicable diseases and exposure to indoor air pollution and ambient pollution from natural sources (Burnett et al., 2018; HEI, 2020; McDuffie et al., 2021; Vohra et al., 2021b). Hickman et al. (2021) suggest, using the same NO_2 observations as us, that regional air quality in Africa has improved due to decline in biomass burning activity. Their analysis focused on the burning season and did not account for rapid growth in urban population

leading to enhanced exposure to air pollution.

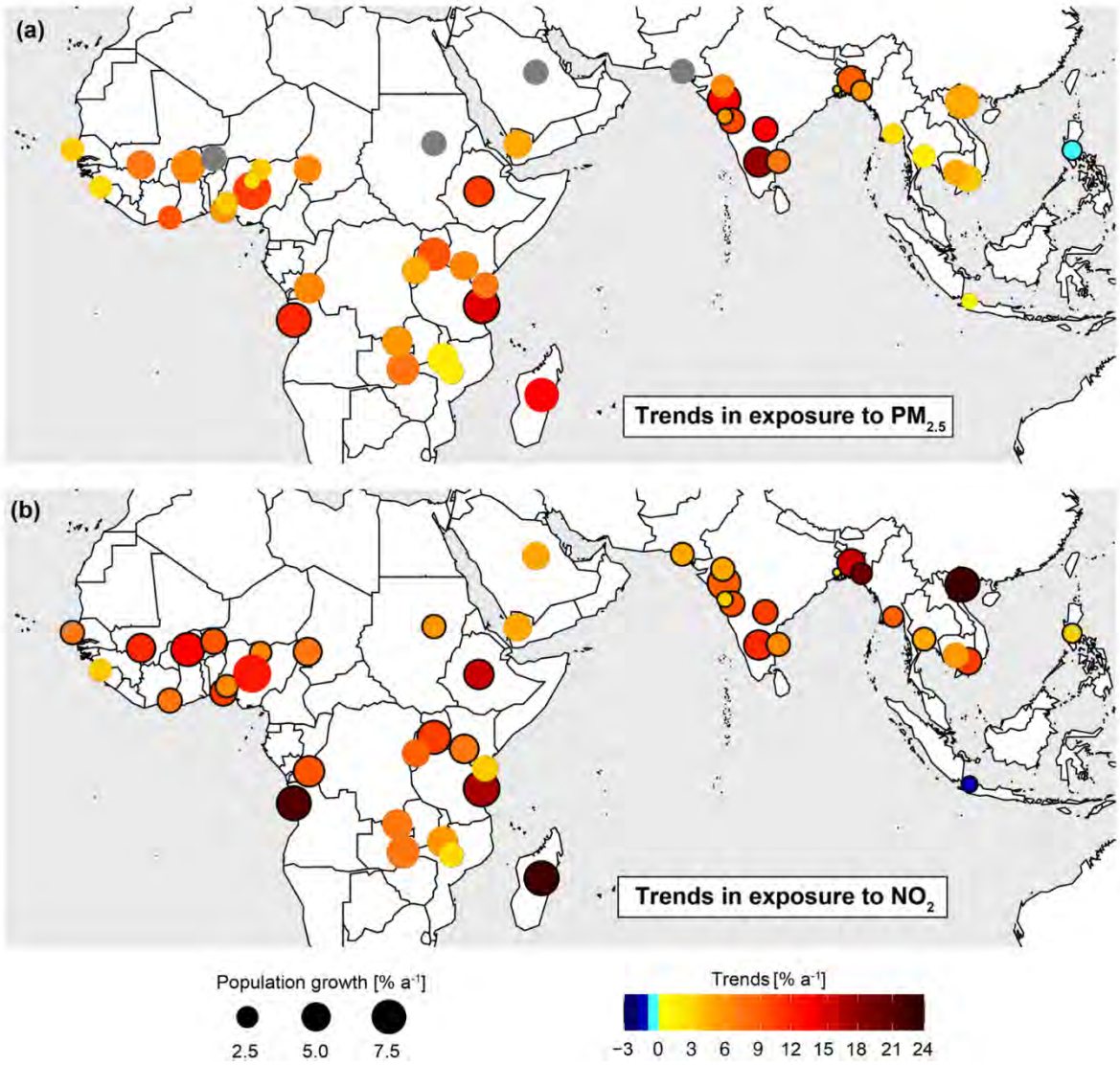

Figure 3.4 Trends in exposure to air pollutants hazardous to health in rapidly growing tropical cities. Circle colors are trends in exposure to $PM_{2.5}$ (a) and NO_2 (b). Circle sizes are annual average increases in urban population from 2005 to 2018. Outlines identify cities with significant trends in $PM_{2.5}$ (Figure S3.3a) and NO_2 (Figure 3.2a) at the 95 % CI. Cities with low temporal coverage in $PM_{2.5}$ are grey.

The trends in exposure to $PM_{2.5}$ and NO_2 that we obtain for the 46 tropical cities (Section 3.2.4) are shown in Figure 3.4. Population exposure to $PM_{2.5}$ increases in all cities except Manila (-0.8 % a^{-1}), as a 2.0 % a^{-1} decline in $PM_{2.5}$ (Figure S3.3a) counters an equivalent increase in

population. Exposure to NO_2 increases in all cities except Jakarta (-1.2 % a^{-1}), though the health gains due to decline in exposure to NO_2 in Jakarta will be more than offset by a 1.8 % a^{-1} increase in exposure to $PM_{2.5}$ due to a 1.3 % a^{-1} increase in population and a small, though not significant, increase in $PM_{2.5}$ (0.5 % a^{-1}; Figure S3.3a). In general, upward trends in exposure are 1.5-3 times steeper than the positive trends in $PM_{2.5}$ (Figure S3.3a) and NO_2 (Figure 3.2a) alone. Increases in population exposure to $PM_{2.5}$ are 3.1-17.9 % a^{-1} in South Asian cities and >10 % a^{-1} in Addis Ababa (10.6 % a^{-1}), Abuja (10.7 % a^{-1}), Antananarivo (13.0 % a^{-1}), Luanda (11.7 % a^{-1}) and Dar es Salam (14.8 % a^{-1}) in Africa. These same African cities also experience the steepest increases in NO_2 exposure of >12 % a^{-1}. Across Africa, the increase in exposure to NO_2 ranges from 2.0 % a^{-1} in Blantyre to 21.3 % a^{-1} in Luanda and 23.0 % a^{-1} in Antananarivo. Reliable surface observations are urgently needed in tropical cities to relate our dramatic relative increases in exposure to absolute values and quantify past and impending disease burdens to further compel action.

With our targeted sampling of satellite observations over densely populated fast-growing tropical cities, we find distressingly large increases in population exposure to air pollution. These will almost certainly be sustained in the future due to projected population growth (Figure 3.1) and absent effective air quality policies, as we find that degradation in air quality is mostly influenced by anthropogenic activity. The population forecasts we use predate the COVID-19 pandemic, but unemployment, inequitable healthcare access, and reduced fertility resulting from the pandemic (Aassve et al., 2020; Ullah et al., 2020) are only likely to delay rather than prevent the deleterious effects of exposure to air pollution that our findings suggest.

References

Aassve, A., Cavalli, N., Mencarini, L., Plach, S., and Bacci, M. L., The COVID-19 pandemic and human fertility, Science, 369, 370-371, doi:10.1126/science.abc9520, 2020.

Aghedo, A. M., Schultz, M. G., and Rast, S., The influence of African air pollution on regional and global tropospheric ozone, Atmos. Chem. Phys., 7, 1193-1212, doi:10.5194/acp-7-1193-2007, 2007.

Alpert, P., Shvainshtein, O., and Kishcha, P., AOD trends over megacities based on space monitoring using MODIS and MISR, Am. J. Clim. Change, 1, doi:10.4236/ajcc.2012.13010, 2012.

Barbosa, P. M., Stroppiana, D., Gregoire, J. M., and Pereira, J. M. C., An assessment of vegetation fire in Africa (1981-1991): Burned areas, burned biomass, and atmospheric emissions, Global Biogeochem. Cy., 13, 933-950, doi:10.1029/1999gb900042, 1999.

Bauer, S. E., Im, U., Mezuman, K., and Gao, C. Y., Desert dust, industrialization, and agricultural fires: Health impacts of outdoor air pollution in Africa, J. Geophys. Res.-Atmos., 124, 4104-4120, doi:10.1029/2018jd029336, 2019.

Bhardwaj, P., Naja, M., Kumar, R., and Chandola, H. C., Seasonal, interannual, and long-term variabilities in biomass burning activity over South Asia, Environ. Sci. Pollut. R., 23, 4397-4410, doi:10.1007/s11356-015-5629-6, 2016.

Bockarie, A. S., Marais, E. A., and MacKenzie, A. R., Air pollution and climate forcing of the charcoal industry in Africa, Environ. Sci. Technol., 54, 13429-13438, doi:10.1021/acs.est.0c03754, 2020.

Brauer, M., Guttikunda, S. K., Nishad, K., Dey, S., Tripathi, S. N., Weagle, C., and Martin, R. V., Examination of monitoring approaches for ambient air pollution: A case study for India, Atmos. Environ., 216, doi:10.1016/j.atmosenv.2019.116940, 2019.

Buchholz, R. R., Worden, H. M., Park, M., Francis, G., Deeter, M. N., Edwards, D. P., Emmons, L. K., Gaubert, B., Gille, J., Martinez-Alonso, S., et al., Air pollution trends measured from Terra: CO and AOD over industrial, fire-prone, and background regions, Remote Sens. Environ., 256, doi:10.1016/j.rse.2020.112275, 2021.

Burnett, R., Chen, H., Szyszkowicz, M., Fann, N., Hubbell, B., Pope, C. A., Apte, J. S., Brauer, M., Cohen, A., Weichenthal, S., et al., Global estimates of mortality associated with

long-term exposure to outdoor fine particulate matter, Proc. Natl. Acad. Sci. U.S.A., 115, 9592-9597, doi:10.1073/pnas.1803222115, 2018.

Cacciottolo, M., Wang, X., Driscoll, I., Woodward, N., Saffari, A., Reyes, J., Serre, M. L., Vizuete, W., Sioutas, C., Morgan, T. E., et al., Particulate air pollutants, APOE alleles and their contributions to cognitive impairment in older women and to amyloidogenesis in experimental models, Transl. Psychiat., 7, doi:10.1038/tp.2016.280, 2017.

Chua, S. Y. L., Warwick, A., Peto, T., Balaskas, K., Moore, A. T., Reisman, C., Desai, P., Lotery, A. J., Dhillon, B., Khaw, P. T., et al., Association of ambient air pollution with age-related macular degeneration and retinal thickness in UK Biobank, Br. J. Ophthalmol., doi:10.1136/bjophthalmol-2020-316218, 2021.

Clarisse, L., Van Damme, M., Clerbaux, C., and Coheur, P. F., Tracking down global NH_3 point sources with wind-adjusted superresolution, Atmos. Meas. Tech., 12, 5457-5473, doi:10.5194/amt-12-5457-2019, 2019.

Damanik, N., Ong, H. C., Tong, C. W., Mahlia, T. M. I., and Silitonga, A. S., A review on the engine performance and exhaust emission characteristics of diesel engines fueled with biodiesel blends, Environ. Sci. Pollut. R., 25, 15307-15325, doi:10.1007/s11356-018-2098-8, 2018.

De Smedt, I., Stavrakou, T., Muller, J. F., van der A, R. J., and Van Roozendael, M., Trend detection in satellite observations of formaldehyde tropospheric columns, Geophys. Res. Lett., 37, doi:10.1029/2010gl044245, 2010.

Duncan, B. N., Yoshida, Y., Olson, J. R., Sillman, S., Martin, R. V., Lamsal, L., Hu, Y. T., Pickering, K. E., Retscher, C., Allen, D. J., et al., Application of OMI observations to a space-based indicator of NO_x and VOC controls on surface ozone formation, Atmos. Environ., 44, 2213-2223, doi:10.1016/j.atmosenv.2010.03.010, 2010.

Duncan, B. N., Lamsal, L. N., Thompson, A. M., Yoshida, Y., Lu, Z. F., Streets, D. G., Hurwitz, M. M., and Pickering, K. E., A space-based, high-resolution view of notable changes in urban NO_x pollution around the world (2005-2014), J. Geophys. Res.-Atmos., 121, 976-996, doi:10.1002/2015jd024121, 2016.

Duren, R. M., and Miller, C. E., Measuring the carbon emissions of megacities, Nat. Clim. Change, 2, 560-562, doi:10.1038/nclimate1629, 2012.

Dwomoh, F. K., and Wimberly, M. C., Fire regimes and forest resilience: alternative vegetation states in the West African tropics, Landsc. Ecol., 32, 1849-1865, doi:10.1007/s10980-017-0553-4, 2017.

Fang, S. C., Rodrigues, E. G., and Christiani, D. C., Environmental health hazards in the tropics, in: Hunter's Tropical Medicine and Emerging Infectious Diseases, Tenth ed., edited by: Ryan, E. T., Hill, D. R., Solomon, T., Aronson, N. E., and Endy, T. P., Elsevier, 200-208, 2020.

Farahat, A., Comparative analysis of MODIS, MISR, and AERONET climatology over the Middle East and North Africa, Ann. Geophys.-Germany, 37, 49-64, doi:10.5194/angeo-37-49-2019, 2019.

Georgoulias, A. K., van der A, R. J., Stammes, P., Boersma, K. F., and Eskes, H. J., Trends and trend reversal detection in 2 decades of tropospheric NO_2 satellite observations, Atmos. Chem. Phys., 19, 6269-6294, doi:10.5194/acp-19-6269-2019, 2019.

Giglio, L., Randerson, J. T., and van der Werf, G. R., Analysis of daily, monthly, and annual burned area using the fourth-generation global fire emissions database (GFED4), J. Geophys. Res.-Biogeo., 118, 317-328, doi:10.1002/jgrg.20042, 2013.

Gunthe, S. S., Liu, P. F., Panda, U., Raj, S. S., Sharma, A., Darbyshire, E., Reyes-Villegas, E., Allan, J., Chen, Y., Wang, X., et al., Enhanced aerosol particle growth sustained by high continental chlorine emission in India, Nat. Geosci., 14, doi:10.1038/s41561-020-00677-x, 2021.

Gupta, P., Christopher, S. A., Wang, J., Gehrig, R., Lee, Y., and Kumar, N., Satellite remote sensing of particulate matter and air quality assessment over global cities, Atmos. Environ., 40, 5880-5892, doi:10.1016/j.atmosenv.2006.03.016, 2006.

Hammer, M. S., van Donkelaar, A., Li, C., Lyapustin, A., Sayer, A. M., Hsu, N. C., Levy, R. C., Garay, M. J., Kalashnikova, O. V., Kahn, R. A., et al., Global estimates and long-term trends of fine particulate matter concentrations (1998-2018), Environ. Sci. Technol., 54, 7879-7890, doi:10.1021/acs.est.0c01764, 2020.

Hayes, F., Harmens, H., Sharps, K., and Radbourne, A., Ozone dose-response relationships for tropical crops reveal potential threat to legume and wheat production, but not to millets, Sci. Afr., 9, doi:10.1016/j.sciaf.2020.e00482, 2020.

HEI, State of Global Air 2020. Special Report, Health Effects Institute, Boston, MA, 2020.

Hickman, J. E., Andela, N., Tsigaridis, K., Galy-Lacaux, C., Ossohou, M., and Bauer, S. E., Reductions in NO_2 burden over north equatorial Africa from decline in biomass burning in spite of growing fossil fuel use, 2005 to 2017, Proc. Natl. Acad. Sci. U.S.A., 118, doi:10.1073/pnas.2002579118, 2021.

Hilboll, A., Richter, A., and Burrows, J. P., Long-term changes of tropospheric NO_2 over megacities derived from multiple satellite instruments, Atmos. Chem. Phys., 13, 4145-4169, doi:10.5194/acp-13-4145-2013, 2013.

Hoesly, R. M., Smith, S. J., Feng, L. Y., Klimont, Z., Janssens-Maenhout, G., Pitkanen, T., Seibert, J. J., Vu, L., Andres, R. J., Bolt, R. M., et al., Historical (1750-2014) anthropogenic emissions of reactive gases and aerosols from the Community Emissions Data System (CEDS), Geosci. Model Dev., 11, 369-408, doi:10.5194/gmd-11-369-2018, 2018.

Hoornweg, D., Bhada-Tata, P., and Kennedy, C., Waste production must peak this century, Nature, 502, 615-617, doi:10.1038/502615a, 2013.

Hoornweg, D., and Pope, K., Population predictions for the world's largest cities in the 21st century, Environ. Urban., 29, 195-216, doi:10.1177/0956247816663557, 2017.

Hu, Z., Jin, Q., Ma, Y., Pu, B., Ji, Z., Wang, Y., and Dong, W., Temporal evolution of aerosols and their extreme events in polluted Asian regions during Terra's 20-year observations, Remote Sens. Environ., 263, 112541, doi:10.1016/j.rse.2021.112541, 2021.

Jayne, T. S., and Sanchez, P. A., Agricultural productivity must improve in sub-Saharan Africa, Science, 372, 1045-1047, doi:10.1126/science.abf5413, 2021.

Jin, X. M., Fiore, A. M., Murray, L. T., Valin, L. C., Lamsal, L. N., Duncan, B., Folkert Boersma, K., De Smedt, I., Abad, G. G., Chance, K., et al., Evaluating a Space-Based Indicator of Surface Ozone-NO_x-VOC Sensitivity Over Midlatitude Source Regions and Application to Decadal Trends, J. Geophys. Res.-Atmos., 122, 10231-10253, doi:10.1002/2017jd026720, 2017.

Kaza, S., Yao, L., Bhada-Tata, P., and Van Woerden, F., What a Waste 2.0: A Global Snapshot of Solid Waste Management to 2050, World Bank, Washington, DC, 2018.

Koplitz, S. N., Jacob, D. J., Sulprizio, M. P., Myllyvirta, L., and Reid, C., Burden of disease from rising coal-fired power plant emissions in Southeast Asia, Environ. Sci. Technol., 51, 1467-1476, doi:10.1021/acs.est.6b03731, 2017.

Krzyzanowski, M., Apte, J. S., Bonjour, S. P., Brauer, M., Cohen, A., and Prüss-Ustun, A. M., Air pollution in the mega-cities, Curr. Envir. Health Rpt., 185–191, doi:10.1007/s40572-014-0019-7, 2014.

Kusumaningtyas, S. D. A., Aldrian, E., Wati, T., Atmoko, D., and Sunaryo, The recent state of ambient air quality in Jakarta, Aerosol Air. Qual. Res., 18, 2343-2354, doi:10.4209/aaqr.2017.10.0391, 2018.

Kuttippurath, J., Singh, A., Dash, S. P., Mallick, N., Clerbaux, C., Van Damme, M., Clarisse, L., Coheur, P. F., Raj, S., Abbhishek, K., et al., Record high levels of atmospheric ammonia over India: Spatial and temporal analyses, Sci. Total Environ., 740, doi:ARTN 139986

10.1016/j.scitotenv.2020.139986, 2020.

Lalitaporn, P., Kurata, G., Matsuoka, Y., Thongboonchoo, N., and Surapipith, V., Long-term analysis of NO_2, CO, and AOD seasonal variability using satellite observations over Asia and intercomparison with emission inventories and model, Air Qual. Atmos. Health, 6, 655-672, doi:10.1007/s11869-013-0205-z, 2013.

Lelieveld, J., Beirle, S., Hormann, C., Stenchikov, G., and Wagner, T., Abrupt recent trend changes in atmospheric nitrogen dioxide over the Middle East, Sci. Adv., 1, doi:10.1126/sciadv.1500498, 2015.

Li, C., McLinden, C., Fioletov, V., Krotkov, N., Carn, S., Joiner, J., Streets, D., He, H., Ren, X. R., Li, Z. Q., et al., India Is overtaking China as the world's largest emitter of anthropogenic sulfur dioxide, Sci. Rep., 7, doi:10.1038/s41598-017-14639-8, 2017a.

Li, C., Martin, R. V., van Donkelaar, A., Boys, B. L., Hammer, M. S., Xu, J. W., Marais, E. A., Reff, A., Strum, M., Ridley, D. A., et al., Trends in chemical composition of global and regional population-weighted fine particulate matter estimated for 25 years, Environ. Sci. Technol., 51, 11185-11195, doi:10.1021/acs.est.7b02530, 2017b.

Li, Q., Zheng, D. N., Wang, Y. Y., Li, R., Wu, H. P., Xu, S. X., Kang, Y. F., Cao, Y. X., Chen, X. J., Zhu, Y. M., et al., Association between exposure to airborne particulate matter less than 2.5 μm and human fecundity in China, Environ. Int., 146, doi:10.1016/j.envint.2020.106231, 2021.

Marais, E. A., Jacob, D. J., Kurosu, T. P., Chance, K., Murphy, J. G., Reeves, C., Mills, G., Casadio, S., Millet, D. B., Barkley, M. P., et al., Isoprene emissions in Africa inferred from OMI observations of formaldehyde columns, Atmos. Chem. Phys., 12, 6219-6235, doi:10.5194/acp-12-6219-2012, 2012.

Marais, E. A., and Wiedinmyer, C., Air quality impact of Diffuse and Inefficient Combustion Emissions in Africa (DICE-Africa), Environ. Sci. Technol., 50, 10739-10745, doi:10.1021/acs.est.6b02602, 2016.

Martin, R. V., Fiore, A. M., and Van Donkelaar, A., Space-based diagnosis of surface ozone sensitivity to anthropogenic emissions, Geophys. Res. Lett., 31, doi:10.1029/2004gl019416, 2004.

Martin, R. V., Brauer, M., van Donkelaar, A., Shaddick, G., Narain, U., and Dey, S., No one knows which city has the highest concentration of fine particulate matter, Atmos. Environ.-X, 3, doi:10.1016/j.aeaoa.2019.100040, 2019.

McDonald, B. C., de Gouw, J. A., Gilman, J. B., Jathar, S. H., Akherati, A., Cappa, C. D., Jimenez, J. L., Lee-Taylor, J., Hayes, P. L., McKeen, S. A., et al., Volatile chemical products emerging as largest petrochemical source of urban organic emissions, Science, 359, 760-764, doi:10.1126/science.aaq0524, 2018.

McDuffie, E. E., Smith, S. J., O'Rourke, P., Tibrewal, K., Venkataraman, C., Marais, E. A., Zheng, B., Crippa, M., Brauer, M., and Martin, R. V., A global anthropogenic emission inventory of atmospheric pollutants from sector- and fuel-specific sources (1970-2017): an application of the Community Emissions Data System (CEDS), Earth Syst. Sci. Data, 12, 3413-3442, doi:10.5194/essd-12-3413-2020, 2020.

McDuffie, E. E., Martin, R. V., Spadaro, J. V., Burnett, R., Smith, S. J., O'Rourke, P., Hammer, M. S., van Donkelaar, A., Bindle, L., Shah, V., et al., Source sector and fuel contributions to ambient $PM_{2.5}$ and attributable mortality across multiple spatial scales, Nat. Commun., 12, 3594, doi:10.1038/s41467-021-23853-y, 2021.

Provencal, S., Kishcha, P., da Silva, A. M., Elhacham, E., and Alpert, P., AOD distributions and trends of major aerosol species over a selection of the world's most populated cities based on the 1st version of NASA's MERRA Aerosol Reanalysis, Urban. Clim., 20, 168-191, doi:10.1016/j.uclim.2017.04.001, 2017.

Reddington, C. L., Conibear, L., Knote, C., Silver, B., Li, Y. J., Chan, C. K., Arnold, S. R., and Spracklen, D. V., Exploring the impacts of anthropogenic emission sectors on $PM_{2.5}$ and human health in South and East Asia, Atmos. Chem. Phys., 19, 11887-11910, doi:10.5194/acp-19-11887-2019, 2019.

Kenya's Mombasa port shows growth, increased efficiency, https://www.reuters.com/article/ozabs-uk-kenya-ports-idAFKCN0QP0OQ20150820, Last accessed: 1 July 2021, 2015.

Sahu, R., Nagal, A., Dixit, K. K., Unnibhavi, H., Mantravadi, S., Nair, S., Simmhan, Y., Mishra, B., Zele, R., Sutaria, R., et al., Robust statistical calibration and characterization of portable low-cost air quality monitoring sensors to quantify real-time O_3 and NO_2

concentrations in diverse environments, Atmos. Meas. Tech., 14, 37-52, doi:10.5194/amt-14-37-2021, 2021.

Santoso, M., Lestiani, D. D., Damastuti, E., Kurniawati, S., Kusmartini, I., Atmodjo, D. P. D., Sari, D. K., Muhtarom, T., Permadi, D. A., and Hopke, P. K., Long term characteristics of atmospheric particulate matter and compositions in Jakarta, Indonesia, Atmos. Pollut. Res., 11, 2215-2225, doi:10.1016/j.apr.2020.09.006, 2020.

Schneider, P., Lahoz, W. A., and van der A, R., Recent satellite-based trends of tropospheric nitrogen dioxide over large urban agglomerations worldwide, Atmos. Chem. Phys., 15, 1205-1220, doi:10.5194/acp-15-1205-2015, 2015.

Schraufnagel, D. E., Balmes, J. R., Cowl, C. T., De Matteis, S., Jung, S. H., Mortimer, K., Perez-Padilla, R., Rice, M. B., Riojas-Rodriguez, H., Sood, A., et al., Air pollution and noncommunicable diseases A review by the Forum of International Respiratory Societies' Environmental Committee, Part 1: The damaging effects of air pollution, Chest, 155, 409-416, doi:10.1016/j.chest.2018.10.042, 2019.

Schroeder, J. R., Crawford, J. H., Fried, A., Walega, J., Weinheimer, A., Wisthaler, A., Muller, M., Mikoviny, T., Chen, G., Shook, M., et al., New insights into the column CH_2O/NO_2 ratio as an indicator of near-surface ozone sensitivity, J. Geophys. Res.-Atmos., 122, 8885-8907, doi:10.1002/2017jd026781, 2017.

Sen, P. K., Estimates of the regression coefficient based on Kendall's Tau, J. Am.Stat. Assoc., 63, 1379-1389, doi:10.2307/2285891, 1968.

Shaddick, G., Thomas, M. L., Amini, H., Broday, D., Cohen, A., Frostad, J., Green, A., Gumy, S., Liu, Y., Martin, R. V., et al., Data integration for the assessment of population exposure to ambient air pollution for Global Burden of Disease assessment, Environ. Sci. Technol., 52, 9069-9078, doi:10.1021/acs.est.8b02864, 2018.

Shah, V., Jacob, D. J., Li, K., Silvern, R. F., Zhai, S. X., Liu, M. Y., Lin, J. T., and Zhang, Q., Effect of changing NO_x lifetime on the seasonality and long-term trends of satellite-observed tropospheric NO_2 columns over China, Atmos. Chem. Phys., 20, 1483-1495, doi:10.5194/acp-20-1483-2020, 2020.

Sharma, S. K., Kotnala, G., and Mandal, T. K., Spatial variability and sources of atmospheric ammonia in India: A review, Aerosol Sci. Eng., 4, 1-8, doi:10.1007/s41810-019-00052-3, 2020.

Sicard, P., Anav, A., De Marco, A., and Paoletti, E., Projected global ground-level ozone impacts on vegetation under different emission and climate scenarios, Atmos. Chem. Phys., 17, 12177-12196, doi:10.5194/acp-17-12177-2017, 2017.

Souri, A. H., Choi, Y., Jeon, W., Woo, J. H., Zhang, Q., and Kurokawa, J., Remote sensing evidence of decadal changes in major tropospheric ozone precursors over East Asia, J. Geophys. Res.-Atmos., 122, 2474-2492, doi:10.1002/2016jd025663, 2017.

Souri, A. H., Nowlan, C. R., Wolfe, G. M., Lamsal, L. N., Miller, C. E. C., Abad, G. G., Janz, S. J., Fried, A., Blake, D. R., Weinheimer, A. J., et al., Revisiting the effectiveness of $HCHO/NO_2$ ratios for inferring ozone sensitivity to its precursors using high resolution airborne remote sensing observations in a high ozone episode during the KORUS-AQ campaign, Atmos. Environ., 224, doi:10.1016/j.atmosenv.2020.117341, 2020.

Stanaway, J. D., Afshin, A., Gakidou, E., Lim, S. S., Abate, D., Abate, K. H., Abbafati, C., Abbasi, N., Abbastabar, H., Abd-Allah, F., et al., Global, regional, and national comparative risk assessment of 84 behavioural, environmental and occupational, and metabolic risks or clusters of risks for 195 countries and territories, 1990-2017: a systematic analysis for the Global Burden of Disease Study 2017, Lancet, 392, 1923-1994, doi:10.1016/S0140-6736(18)32225-6, 2018.

Biodiesel consumption in Indonesia 2010-2020, https://www.statista.com/statistics/1055635/indonesia-biodiesel-consumption/, Last accessed: 25 June 2021, 2021.

Stieb, D. M., Berjawi, R., Emode, M., Zheng, C., Salama, D., Hocking, R., Lyrette, N., Matz, C., Lavigne, E., and Shin, H. H., Systematic review and meta-analysis of cohort studies of long term outdoor nitrogen dioxide exposure and mortality, Plos One, 16, doi:10.1371/journal.pone.0246451, 2021.

Theil, H., A rank-invariant method of linear and polynomial regression analysis, Proc. K. Ned. Akad. Wet., Series A, 53, 386-392, 1950.

Thompson, A. M., Tao, W. K., Pickering, K. E., Scala, J. R., and Simpson, J., Tropical deep convection and ozone formation, B. Am. Meteorol. Soc., 78, 1043-1054, doi:10.1175/1520-0477(1997)078<1043:TDCAOF>2.0.CO;2, 1997.

Ullah, M. A., Moin, A., Araf, Y., Bhuiyan, A. R., Griffiths, M. D., and Gozal, D., Potential effects of the COVID-19 pandemic on future birth rate, Front. Public Health, 8, doi:10.3389/fpubh.2020.578438, 2020.

World Urbanization Prospects: The 2018 revision, online edition., https://population.un.org/wup/Download/, Last accessed: 14 June 2021, 2018.

Vadrevu, K. P., Lasko, K., Giglio, L., and Justice, C., Vegetation fires, absorbing aerosols and smoke plume characteristics in diverse biomass burning regions of Asia, Environ. Res. Lett., 10, doi:10.1088/1748-9326/10/10/105003, 2015.

Van Damme, M., Clarisse, L., Whitburn, S., Hadji-Lazaro, J., Hurtmans, D., Clerbaux, C., and Coheur, P. F., Industrial and agricultural ammonia point sources exposed, Nature, 564, 99-103, doi:10.1038/s41586-018-0747-1, 2018.

Van Damme, M., Clarisse, L., Franco, B., Sutton, M. A., Erisman, J. W., Kruit, R. W., van Zanten, M., Whitburn, S., Hadji-Lazaro, J., Hurtmans, D., et al., Global, regional and national trends of atmospheric ammonia derived from a decadal (2008-2018) satellite record, Environ. Res. Lett., doi:10.1088/1748-9326/abd5e0, 2020.

van der A, R. J., Peters, D. H. M. U., Eskes, H., Boersma, K. F., Van Roozendael, M., De Smedt, I., and Kelder, H. M., Detection of the trend and seasonal variation in tropospheric NO_2 over China, J. Geophys. Res.-Atmos., 111, doi:10.1029/2005jd006594, 2006.

van Donkelaar, A., Martin, R. V., Brauer, M., and Boys, B. L., Use of satellite observations for long-term exposure assessment of global concentrations of fine particulate matter, Environ. Health Persp., 123, 135-143, doi:10.1289/ehp.1408646, 2015.

van Donkelaar, A., Martin, R. V., Brauer, M., Hsu, N. C., Kahn, R. A., Levy, R. C., Lyapustin, A., Sayer, A. M., and Winker, D. M., Global estimates of fine particulate matter using a combined geophysical-statistical method with information from satellites, models, and monitors, Environ. Sci. Technol., 50, 3762-3772, doi:10.1021/acs.est.5b05833, 2016.

Vohra, K., Marais, E. A., Suckra, S., Kramer, L., Bloss, W. J., Sahu, R., Gaur, A., Tripathi, S. N., Van Damme, M., Clarisse, L., et al., Long-term trends in air quality in major cities in the UK and India: a view from space, Atmos. Chem. Phys., 21, 6275-6296, doi:10.5194/acp-21-6275-2021, 2021a.

Vohra, K., Vodonos, A., Schwartz, J., Marais, E. A., Sulprizio, M. P., and Mickley, L. J., Global mortality from outdoor fine particle pollution generated by fossil fuel combustion: Results from GEOS-Chem, Environ. Res., 195, 110754, doi:10.1016/j.envres.2021.110754, 2021b.

World development indicators, https://databank.worldbank.org/source/world-development-indicators, Last accessed: 14 June 2021, 2019.

Xu, R. T., Pan, S. F., Chen, J., Chen, G. S., Yang, J., Dangal, S. R. S., Shepard, J. P., and Tian, H. Q., Half-century ammonia emissions from agricultural systems in Southern Asia: Magnitude, spatiotemporal patterns, and implications for human health, Geohealth, 2, 40-53, doi:10.1002/2017gh000098, 2018.

Yin, S., Wang, X. F., Zhang, X. R., Guo, M., Miura, M., and Xiao, Y., Influence of biomass burning on local air pollution in mainland Southeast Asia from 2001 to 2016, Environ. Pollut., 254, doi:10.1016/j.envpol.2019.07.117, 2019.

Zhang, X., Chen, X., and Zhang, X. B., The impact of exposure to air pollution on cognitive performance, Proc. Natl. Acad. Sci. U.S.A., 115, 9193-9197, doi:10.1073/pnas.1809474115, 2018.

Zhang, Y. Z., Jacob, D. J., Lu, X., Maasakkers, J. D., Scarpelli, T. R., Sheng, J. X., Shen, L., Qu, Z., Sulprizio, M. P., Chang, J. F., et al., Attribution of the accelerating increase in atmospheric methane during 2010-2018 by inverse analysis of GOSAT observations, Atmos. Chem. Phys., 21, 3643-3666, doi:10.5194/acp-21-3643-2021, 2021.

Zoogman, P., Jacob, D. J., Chance, K., Zhang, L., Le Sager, P., Fiore, A. M., Eldering, A., Liu, X., Natraj, V., and Kulawik, S. S., Ozone air quality measurement requirements for a geostationary satellite mission, Atmos. Environ., 45, 7143-7150, doi:10.1016/j.atmosenv.2011.05.058, 2011.

Supplementary Information

The following is supporting text for estimating trends in aerosol optical depth (AOD) from the Moderate Resolution Imaging Spectroradiometer (MODIS) and ratios of formaldehyde (HCHO) to nitrogen dioxide (NO_2) (HCHO/NO_2) from the Ozone Monitoring Instrument (OMI) in 46 future megacities in the tropics, as well as trends in burned fraction from the Global Fire Emissions Database version 4.1s (GFEDv4.1s) for a subset of these cities.

Trends in $PM_{2.5}$ Abundance and Ozone Production Regimes

Figure S3.3a shows trends in AOD that we interpret as trends in surface fine particles ($PM_{2.5}$) (Vohra et al., 2021a). The relationship between AOD and $PM_{2.5}$ is complicated by $PM_{2.5}$ composition, vertical distribution of aerosols, relative humidity, cloud cover, and seasonality in planetary boundary layer dynamics and synoptic-scale meteorology (Gupta et al., 2006; van Donkelaar et al., 2015; 2016; Shaddick et al., 2018). This causes inconsistencies in month-to-month variability in AOD and surface concentrations of $PM_{2.5}$, but not in the long-term trends (Vohra et al., 2021a). AOD at the start of the record is > 0.25 over cities in West Africa, the Middle East, South Asia and Southeast Asia due to a mix of large aerosol sources such as biomass burning in all these regions, desert dust in West Africa, the Middle East and South Asia, and additional contributions from anthropogenic emissions in Asia (Farahat, 2019; Hammer et al., 2020; Hu et al., 2021). $PM_{2.5}$ trends in South Asian cities are steep (2.3-7.8 % a^{-1}) and significant. $PM_{2.5}$ more than doubles in Bangalore (7.8 % a^{-1}) and Hyderabad (7.3 % a^{-1}). Earlier studies have reported similar positive trends for these cities (Alpert et al., 2012; Provencal et al., 2017), so our contemporary record supports sustained rapid growth in $PM_{2.5}$. The substantial increase in $PM_{2.5}$ in South Asia is due to increased formation of secondary inorganic aerosols due to increases in SO_2 emissions forming sulfate (Li et al., 2017b; Provencal et al., 2017), NO_x emissions forming nitrate (Figures 3.2a and 3.3g), and partitioning of

ammonia (NH_3) to these acidic aerosols that also leads to decline in NH_3 abundance (Figure 3.2b). The increase in reactive non-methane volatile organic compounds (NMVOCs) (Figure 3.2c) that should include precursors of secondary organic aerosol likely also contributes to the increase in $PM_{2.5}$. Trends in cities in other regions are not as consistent as for South Asia. In Southeast Asia there is only a significant decline in Manila (-2.0 % a^{-1}), and in Africa a significant increase in Luanda (2.3 % a^{-1}), Addis Ababa (3.3 % a^{-1}) and Dar es Salaam (3.3 % a^{-1}). $PM_{2.5}$ increases in Jakarta despite a significant decrease in precursor emissions of NO_x (Figure 3.2a) and reactive NMVOCs (Figure 3.2c). This may be due to an increase in sulfate in Jakarta from high sulfur fuel combustion and regional adoption of coal-fired power generation (Koplitz et al., 2017; Santoso et al., 2020) as well as lack of policies targeting biomass burning and agricultural sources. Our positive trends in $PM_{2.5}$ for most West African cities are opposite to a reported weak regional decline in AOD of 0.1 % a^{-1} (Buchholz et al., 2021).

Satellite observations of tropospheric column ozone have limited sensitivity to surface concentrations of ozone (Zoogman et al., 2011), but ratios of HCHO-to-NO_2 ($HCHO/NO_2$) can be used to diagnose sensitivity of surface ozone formation to precursor emissions of NO_x and NMVOCs (Martin et al., 2004; Duncan et al., 2010). The trends in these are in Figure S3.3b. The HCHO used is the total column without removal of the background to relate $HCHO/NO_2$ we obtain to values reported in the literature. Typically, $HCHO/NO_2 > \sim 2$ indicates that policies to mitigate ozone pollution should target NO_x sources, whereas $HCHO/NO_2 < 1$ supports targeting VOCs sources (Martin et al., 2004). The transition between these regimes occurs for $HCHO/NO_2$ of 1-2 (Duncan et al., 2010; Jin et al., 2017; Souri et al., 2017). The actual threshold value for the NO_x-sensitive regime varies geographically, due to dependence on the local oxidation regime (Duncan et al., 2010; Schroeder et al., 2017; Souri et al., 2020). Of the tropical

cities in Figure 3.1, only Riyadh is in a NO_x-saturated regime ($HCHO/NO_2$ = 0.9) at the beginning and throughout the record, as values of NO_2 are large (~6×10^{15} molecules cm^{-2}) and decline in NO_2 is slow and not significant (0.05 % a^{-1}; Figure 3.2a). All other cities are in a NO_x-sensitive regime throughout the record. $HCHO/NO_2$ increases in Jakarta and Sana'a by 1.5 % a^{-1} due a steep decline in NO_2 in Jakarta (Figure 3.2a) and a steep increase in HCHO in Sana'a (Figure 3.2c), so ozone formation in both cities remains NO_x-sensitive.

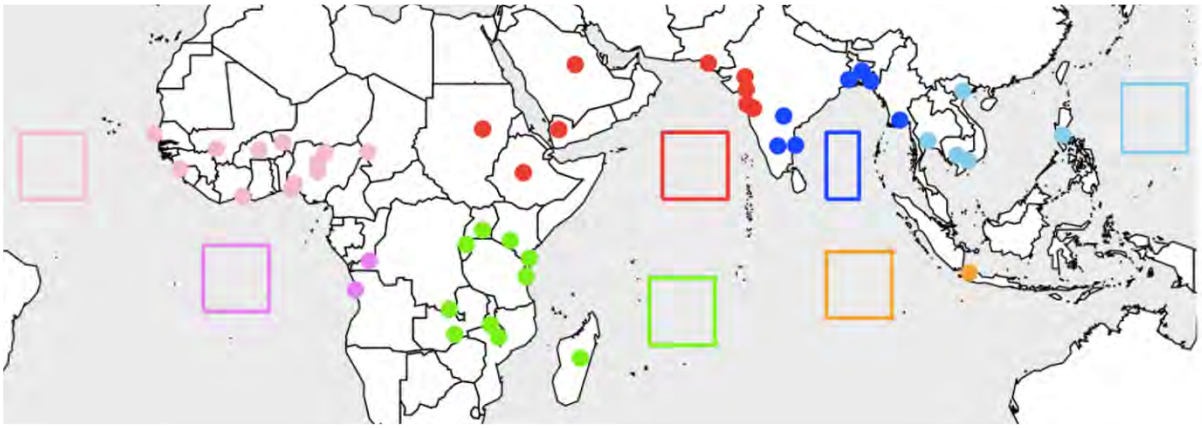

Figure S3.1 Domains over remote oceans selected to calculate background OMI HCHO. Box colors indicate ocean domains used to determine background total column HCHO for cities with the same color (circles).

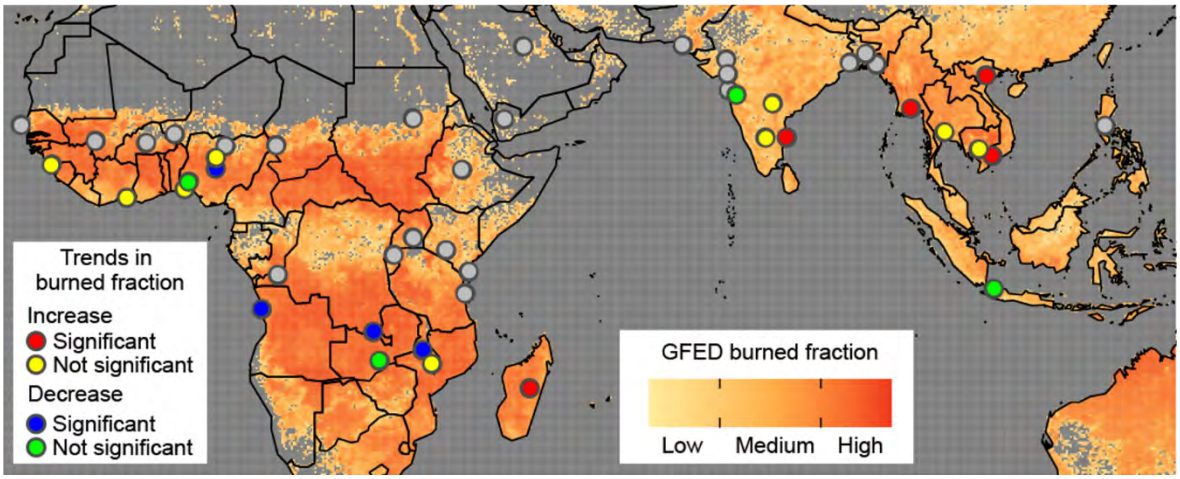

Figure S3.2 Spatial distribution and trends in burned fraction in rapidly growing cities in the tropics. Background map is the multiyear (2005-2016) mean GFEDv4.1s burned fraction at 0.25° × 0.25° for 2005-2016. The logarithmic scale distinguishes grids with low ($<10^{-7.5}$), medium ($10^{-7.5}$-$10^{-2.5}$), and high ($>10^{-2.5}$) burned fraction. Grey circles are cities with no

discernible influence from biomass burning in our statistical analysis of the satellite observations (Section 3.2.2).

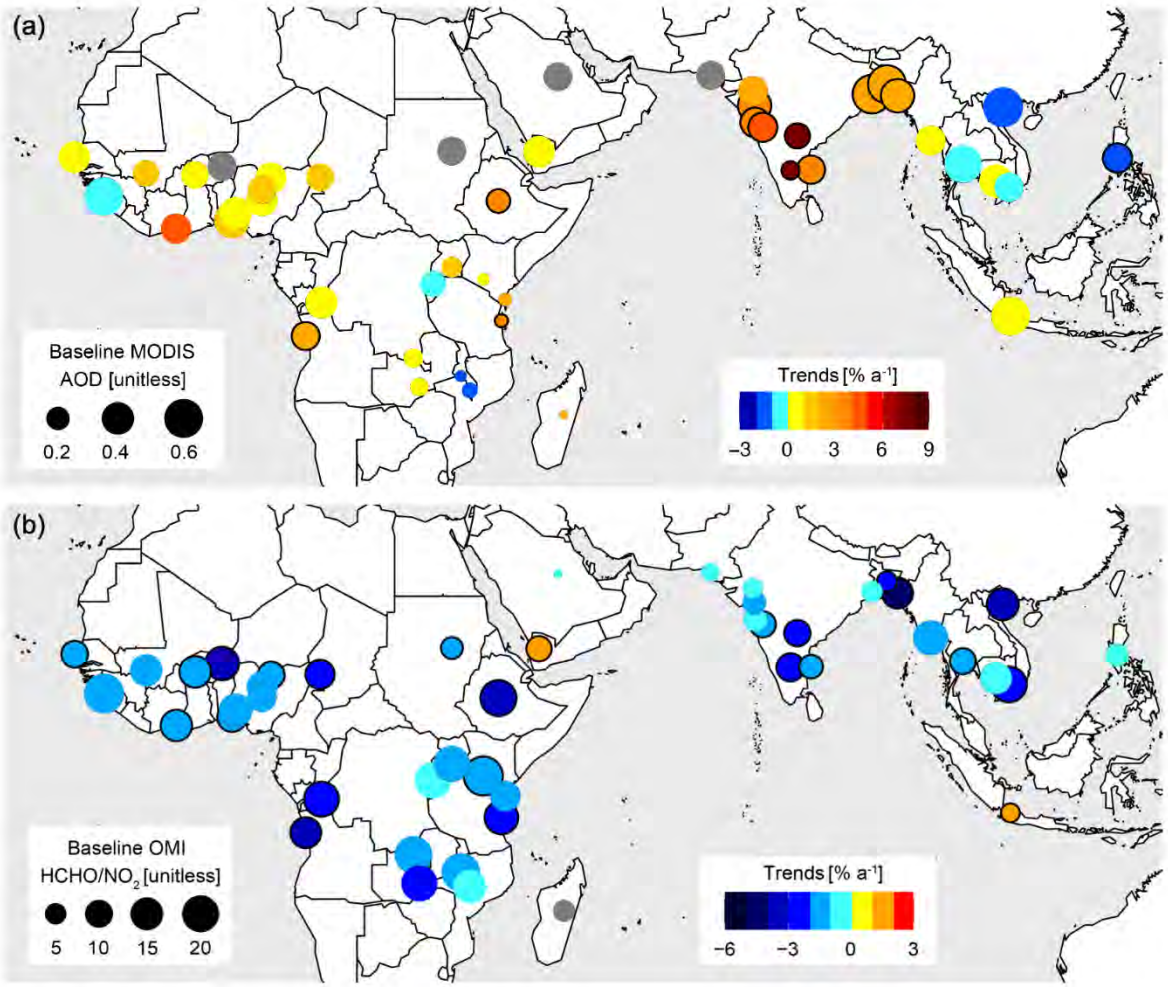

Figure S3.3 Trends in $PM_{2.5}$ abundance and ozone production regimes in rapidly growing cities in the tropics. Circle colors are relative trends in AOD (a) and $HCHO/NO_2$ (b) and sizes are values at the start of the record (baseline). Outlines identify significant trends at the 95 % CI. Warm colors indicate positive trends, cool colors negative trends. Cities with poor temporal coverage are grey. $PM_{2.5}$ trend values are in Table S3.1.

Table S3.1 Trends in air quality in the 51 fastest growing cities in the tropics.

City[a]	Long-term trends [% a^{-1}][b]			
	NO_2	NH_3	Reactive NMVOCs	$PM_{2.5}$
Africa				
Abidjan§	**2.96** [1.3,5.1]	**5.07** [1.2,11.2]	**2.14** [0.8,3.7]	4.35 [-1.2,33.1]
Abuja	1.61[-0.1,3.9]	**3.72** [0.6,8.6]	0.39 [-0.6,1.6]	0.63 [-1.3,3.5]
Addis Ababa§	**6.35** [3.3,10.7]	1.22 [-0.5,3.3]	-0.96 [-3.5,3.6]	**3.27** [1.3,5.9]
Antananarivo§	**8.18** [4,3,14.1]	1.08 [-2.8,8.8]	—	2.95 [-0.7,9.6]
Bamako§	**4.10** [2.1, 6.7]	**5.08** [1.8,10.0]	2.51 [-0.9,8.0]	1.39 [-0.1,3.4]
Blantyre§	-0.86 [-3.2, 3.0]	-0.42 [-2.7,2.8]	0.25 [-2.1,4.0]	-1.06 [-3.2,2.4]
Conakry§	0.33 [-1.3,2.6]	1.27 [-0.9,4.3]	-0.68 [-1.8,0.7]	-0.09 [-1.0,0.9]
Dakar§	**3.64** [2.1,5.6]	**6.09** [1.4,14.4]	0.88 [-2.3,6.8]	0.61 [-1.3,4.1]
Dar es Salaam	**3.93** [1.6,7.1]	-0.94 [-3.9,4.1]	1.42 [-0.5,4.1]	**3.26** [0.9,6.6]
Ibadan	**3.02** [0.7,6.4]	**7.17** [2.6,14.9]	0.67 [-0.3,1.8]	0.91 [-2.3,7.5]
Kaduna§	**3.09** [1.4,5.2]	2.65 [-0.5,7.7]	0.36 [-2.5,4.6]	1.37 [-0.7,4.4]
Kampala§	**1.95** [0.2,4.3]	**2.79** [0.9,5.2]	-0.17 [-1.6,1.6]	1.19 [-0.6,3.6]
Kano§	**2.98** [1.9,4.3]	1.44 [-0.8,4.5]	**3.60** [0.8,8.0]	0.92 [-1.6,6.1]
Khartoum§	**1.77** [1.0,2.6]	**3.11** [0.4,6.8]	-0.83 [-3.9,4.8]	—
Kigali§	2.73 [-0.01,6.9]	**5.29** [2.0,10.1]	1.56 [-0.5,4.4]	-0.07 [-1.8,2.3]
Kinshasa§	**2.51** [0.4,5.4]	1.89 [-2.2,9.6]	**2.03** [0.7,3.6]	0.36 [-1.0,2.1]
Lagos§	**4.37** [2.3,7.2]	**8.31** [3.5,16.6]	**1.52** [0.5,2.8]	1.15 [-1.0,4.5]
Lilongwe§	-0.16 [-2.2,3.0]	**3.43** [0.7,7.3]	**3.63** [0.6,8.3]	-2.12 [-4.2,1.3]
Luanda	**7.36** [4.8,10.7]	**12.26** [2.8,40.8]	**3.90** [2.3,5.9]	**2.34** [0.6,4.6]
Lubumbashi	1.36 [-1.3,5.5]	**5.06** [0.6,13.0]	-0.28 [-1.6,1.4]	0.14 [-1.8,3.0]
Lusaka	0.74 [-1.1,3.4]	3.46 [-0.1,9.2]	-0.34 [-1.8,1.5]	0.80 [-1.4,4.1]
Mombasa§	-0.30 [-2.0,2.0]	2.95 [-1.7,12.2]	**-2.74** [-4.5,-0.1]	2.44 [-0.9,8.4]
N'Djamena§	**2.02** [0.9,3.4]	1.88 [-0.6,5.3]	-2.20 [-3.8,0.1]	1.12 [-0.5,4.3]
Nairobi	**1.81** [0.8,3.0]	**2.57** [1.0,4.5]	-0.71 [-1.7,0.4]	0.78 [-1.2,3.6]
Niamey§	**4.37** [2.8,6.3]	3.34 [-0.1,9.0]	-1.64 [-4.6,3.8]	—
Ouagadougou	**3.28** [2.0,4.8]	**4.76** [1.7,9.0]	**2.34** [0.3,5.2]	0.01 [-1.4,1.9]
South Asia				
Ahmedabad	**1.48** [0.7,2.3]	-1.27 [-3.0,1.0]	**1.75** [0.1,3.9]	2.25 [-0.1,5.6]
Bangalore	**3.80** [2.6,5.2]	-1.32 [-3.1,1.0]	0.61 [-1.1,2.9]	**7.77** [4.2,13.4]
Chennai	**2.33** [1.5,3.3]	**-2.61** [-4.3,-0.4]	**1.62** [0.02,3.7]	**3.32** [1.8,5.2]
Chittagong§	**14.07** [9.7,20.5]	-2.06 [-4.6,2.2]	0.59 [-2.0,4.6]	**2.72** [1.3,4.5]
Dhaka	**7.30** [5.1,10.2]	-0.62 [-3.0,2.9]	1.05 [-0.2,2.6]	**2.69** [1.4,4.3]
Hyderabad	**5.04** [3.5,7.0]	-0.76 [-2.4,1.3]	**2.67** [1.1,4.7]	**7.28** [5.1,10.1]
Karachi	**1.35** [0.7,2.1]	2.90 [-0.9,9.4]	**4.34** [0.4,11.9]	—
Kolkata	**1.12** [0.3,2.0]	**-3.75** [-5.2,-1.8]	1.31 [-0.001,2.9]	**2.49** [1.3,3.9]

City[a]	Long-term trends [% a^{-1}][b]			
	NO_2	NH_3	Reactive NMVOCs	$PM_{2.5}$
Mumbai	**1.92** [1.1,2.9]	-1.32 [-2.8,0.5]	1.74 [-0.03,4.1]	**3.86** [2.5,5.5]
Pune	**3.90** [2.6,5.5]	0.33 [-1.8,3.2]	1.90 [-0.01,4.5]	**4.57** [2.4,7.5]
Surat	**0.80** [0.05,1.6]	-2.00 [-3.6,0.1]	**2.88** [1.2,5.0]	**3.73** [1.9,6.0]
Southeast Asia				
Bangkok	**1.44** [0.4,2.7]	**3.34** [1.0,6.5]	-0.67 [-1.3,0.1]	-0.75 [-1.6,0.2]
Hanoi	**7.73** [3.9,13.9]	**11.82** [5.0,25.4]	1.02 [-0.2,2.5]	-1.33 [-2.5,0.1]
Ho Chi Minh City	**4.35** [2.9,6.1]	**7.10** [4.4,10.6]	**1.74** [0.8,2.9]	-0.08 [-1.1,1.2]
Jakarta§	**-2.04** [-2.9,-1.1]	**3.87** [0.9,8.1]	**-1.68** [-2.4,-0.8]	0.49 [-0.7,2.0]
Manila§	**1.42** [0.2,2.9]	**2.64** [0.1,6.2]	1.23 [-0.9,4.4]	**-2.04** [-3.4.-0.3]
Phnom Penh§	1.21 [-0.2,3.0]	3.61 [-0.2,10.0]	**1.43** [0.05,3.2]	0.52 [-1.1,2.7]
Yangon	**4.64** [2.7,7.1]	-0.22 [-2.5,3.0]	**3.25** [1.1,6.1]	0.38 [-0.9,2.0]
Middle East				
Riyadh	-0.05 [-0.6,0.6]	**11.21** [1.6,44.4]	-0.81 [-4.1,6.6]	—
Sana'a	0.07 [-0.6,0.8]	1.15 [-3.0,9.3]	**10.62** [2.2,42.0]	0.19 [-1.1,1.7]
Central and South America				
Bogotá§	—	**7.28** [2.9,14.3]	2.92 [-2.3,19.8]	-0.32 [-3.1,5.4]
Lima	**4.44** [3.4,5.7]	**6.57** [4.5,9.2]	**1.35** [0.3,2.6]	—
Mexico City	0.43 [-0.4,1.3]	**2.00** [0.8,3.4]	**-1.39** [-2.1,-0.5]	0.28 [-0.9,1.8]
Rio De Janeiro	**1.26** [0.6,2.0]	0.28 [-1.9,3.4]	1.03 [-0.6,3.2]	0.02 [-1.6,2.2]
São Paulo	0.61 [-0.2,1.5]	**4.42** [1.0,9.6]	1.09 [-0.8,3.7]	-0.54 [-2.0,1.4]

[a] Current (2020) megacities are in bold. Small cities for which the satellite sampling domain is extended beyond the city boundary (Section 3.2.1) are marked with §; [b] Trends in NO_2, reactive NMVOCs (HCHO) and $PM_{2.5}$ (AOD) are for 2005-2018 and trends in NH_3 are for 2008-2018. Trend values significant at the 95 % CI (given in square brackets) are in bold. Missing trends denoted with "—" are due to too few monthly means (Section 3.2.1).

CHAPTER 4

GLOBAL MORTALITY FROM OUTDOOR FINE PARTICLE POLLUTION GENERATED BY FOSSIL FUEL COMBUSTION:

RESULTS FROM GEOS-CHEM

Abstract

The burning of fossil fuels – especially coal, petrol, and diesel – is a major source of airborne fine particulate matter ($PM_{2.5}$), and a key contributor to the global burden of mortality and disease. Previous risk assessments have examined the health response to total $PM_{2.5}$, not just $PM_{2.5}$ from fossil fuel combustion, and have used a concentration-response function with limited support from the literature and data at both high and low concentrations. This assessment examines mortality associated with $PM_{2.5}$ from only fossil fuel combustion, making use of a recent meta-analysis of newer studies with a wider range of exposure. We also estimated mortality due to lower respiratory infections (LRI) among children under the age of five in the Americas and Europe, regions for which we have reliable data on the relative risk of this health outcome from $PM_{2.5}$ exposure. We used the chemical transport model GEOS-Chem to estimate global exposure levels to fossil-fuel related $PM_{2.5}$ in 2012. Relative risks of mortality were modeled using functions that link long-term exposure to $PM_{2.5}$ and mortality, incorporating nonlinearity in the concentration response. We estimate a global total of 10.2 (95 % CI: -47.1 to 17.0) million premature deaths annually attributable to the fossil-fuel component of $PM_{2.5}$. The greatest mortality impact is estimated over regions with substantial fossil fuel related $PM_{2.5}$, notably China (3.9 million), India (2.5 million) and parts of eastern US, Europe and Southeast Asia. The estimate for China predates substantial decline in fossil fuel emissions and decreases to 2.4 million premature deaths due to 43.7 % reduction in fossil fuel $PM_{2.5}$ from 2012 to 2018 bringing the global total to 8.7 (95 % CI: -1.8 to 14.0) million premature deaths. We also estimated excess annual deaths due to LRI in children (0-4 years old) of 876 in North America, 747 in South America, and 605 in Europe. This study demonstrates that the fossil fuel component of $PM_{2.5}$ contributes a large mortality burden. The steeper concentration-response function slope at lower concentrations leads to larger estimates than previously found in Europe

and North America, and the slower drop-off in slope at higher concentrations results in larger estimates in Asia. Fossil fuel combustion can be more readily controlled than other sources and precursors of $PM_{2.5}$ such as dust or wildfire smoke, so this is a clear message to policymakers and stakeholders to further incentivize a shift to clean sources of energy.

4.1. Introduction

The burning of fossil fuels – especially coal, petrol, and diesel – is a major source of airborne particulate matter (PM) and ground-level ozone, which have both been implicated as key contributors to the global burden of mortality and disease (Lim et al., 2013; Dedoussi and Barrett, 2014; Apte et al., 2015). A series of studies have reported an association between exposure to air pollution and adverse health outcomes (Brook et al., 2010), even at low exposure levels (< 10 μg m^{-3}, the current World Health Organization, WHO, guideline) (Di et al., 2017). The Global Burden of Diseases, Injuries, and Risk Factors Study 2015 (GBD 2015) identified ambient air pollution as a leading cause of the global disease burden, especially in low-income and middle-income countries (Forouzanfar et al., 2016). Recent estimates of the global burden of disease suggest that exposure to $PM_{2.5}$ (particulate matter with an aerodynamic diameter < 2.5 μm) causes 4.2 million deaths and 103.1 million disability-adjusted life-years (DALYs) in 2015, representing 7.6 % of total global deaths and 4.2 % of global DALYs, with 59 % of these in east and south Asia (Cohen et al., 2017).

A series of newer studies conducted at lower concentrations and at higher concentrations have reported higher slopes than incorporated into the GBD using the integrated exposure–response (IER) curve (Burnett et al., 2014). These studies examined mortality due to exposure to $PM_{2.5}$ at concentrations below 10 μg m^{-3} in North America (Pinault et al., 2016; Di et al., 2017) and

above 40 μg m^{-3} in Asia (Katanoda et al., 2011; Ueda et al., 2012; Tseng et al., 2015; Wong et al., 2015; 2016; Yin et al., 2017). Here we have used a concentration-response curve from a recently published meta-analysis of long-term $PM_{2.5}$ mortality association among adult populations which incorporates those new findings at high and low $PM_{2.5}$ concentrations (Vodonos et al., 2018). We also focus our study on the health impacts of fossil-fuel derived $PM_{2.5}$. In contrast, GBD reports only the health impacts of total $PM_{2.5}$ and does not distinguish mortality from fossil-fuel derived $PM_{2.5}$ and that from other kinds of $PM_{2.5}$, including dust, wildfire smoke, and biogenically-sourced particles. We focus only on $PM_{2.5}$ since recent studies have provided mixed results on the link between ozone and mortality (Atkinson et al., 2016) and there does not exist a global coherent concentration-response function (CRF) for ozone.

The developing fetus and children younger than 5 years of age are more biologically and neurologically susceptible to the many adverse effects of air pollutants from fossil-fuel combustion than adults. This differential susceptibility to air pollution is due to their rapid growth, developing brain, and immature respiratory, detoxification, immune, and thermoregulatory systems (Bateson and Schwartz, 2008; Perera, 2018). Children also breathe more air per kilogram of body weight than adults, and are therefore more exposed to pollutants in air (WHO, 2006; Xu et al., 2012). The WHO estimated that in 2012, 169,000 global deaths among children under the age of 5 were attributable to ambient air pollution (WHO, 2016). Further estimation of the burden of mortality due to $PM_{2.5}$ (particularly from anthropogenic sources) among the young population would highlight the need for intervention aimed at reducing children's exposure.

Using the chemical transport model GEOS-Chem, we quantified the number of premature deaths attributable to ambient air pollution from fossil fuel combustion. Improved knowledge of this very immediate and direct consequence of fossil fuel use provides evidence of the benefits to current efforts to cut greenhouse gas emissions and invest in alternative sources of energy. It also helps quantify the magnitude of the health impacts of a category of $PM_{2.5}$ that can be more readily controlled than other kinds of $PM_{2.5}$ such as dust or wildfire smoke.

4.2. Materials and Methods

4.2.1. Calculation of Surface $PM_{2.5}$ Concentrations

Previous studies examining the global burden of disease from outdoor air pollution have combined satellite and surface observations with models to obtain improved estimates of global annual mean concentrations of $PM_{2.5}$ (Shaddick et al., 2018). However, the goal of such studies was to quantify the health response to $PM_{2.5}$ from all sources, both natural and anthropogenic (Brauer et al., 2016; Cohen et al., 2017). Here the focus of our study is on surface ambient $PM_{2.5}$ generated by fossil fuel combustion, and for that we rely solely on the chemical transport model GEOS-Chem since current satellite and surface measurements cannot readily distinguish between the sources of $PM_{2.5}$. Results from GEOS-Chem have been extensively validated against surface, aircraft, and space-based observations around the world, including simulation of surface pollution over the United States (Drury et al., 2010; Heald et al., 2012; Leibensperger et al., 2012; Zhang et al., 2012; Ford and Heald, 2013; Marais et al., 2016), Asia (Lin et al., 2014; Koplitz et al., 2016), Europe (Veefkind et al., 2011; Protonotariou et al., 2013), and Africa (Marais et al., 2014a; 2014b; 2016; Lacey et al., 2017; 2019). The model has also been applied to previous studies quantifying the global burden of disease from particulate matter from all sources (Brauer et al., 2016; Cohen et al., 2017).

In this analysis we used GEOS-Chem with fossil fuel emissions from multiple sectors (power generation, industry, ships, aircraft, ground transportation, backup generators, kerosene, oil/gas extraction), detailed oxidant-aerosol chemistry, and reanalysis meteorology from the NASA Global Modeling and Assimilation Office. Fossil fuel emissions are from regional inventories where these are available for the US, Europe, Asia, and Africa, and from global inventories everywhere else (such as Mexico, Australia, South America and Canada). More details of the specific fossil fuel inventories used in GEOS-Chem are in Table S4.1. Global-scale simulations in GEOS-Chem were carried out on a coarse spatial grid (2° × 2.5°, about 200 km × 250 km). Four regional simulations were also performed at fine spatial scale (0.5° × 0.67°, about 50 km × 60 km) for North America, Europe, Asia, and Africa using boundary conditions from the global model. The regional simulations allow for a better match with the spatial distribution of population, thus enhancing the accuracy of the estimates of health impacts. All simulations were set up to replicate 2012 pollution conditions. As described in the Supplemental Material, we find that globally, GEOS-Chem captures observed annual mean $PM_{2.5}$ concentrations with a spatial correlation of 0.70 and mean absolute error of 3.4 μg m^{-3}, values which compare well with those from other models (Xing et al., 2015; Shindell et al., 2018). We performed two sets of simulations: one set with fossil fuel emissions turned on and the other with such emissions turned off. We then assumed that the difference between the two sets of simulations represents the contribution of fossil fuel combustion to surface $PM_{2.5}$. More information on our choice of GEOS-Chem, the model setup, details of relevant anthropogenic emissions, and model validation is described in the Supplemental material.

4.2.2. Population and Health Data

We used population data from the Center for International Earth Science Information Network (CIESIN) (CIESIN, 2018). The Gridded Population of the World, Version 4 Revision 11 (GPWv4.11) is gridded with an output resolution of 30 arc-seconds (approximately 1 km at the equator). Since the population data are provided only at five-year intervals, we applied 2015 population statistics to the results of our 2012 GEOS-Chem simulation. CIESIN population data was then aggregated to the spatial scale of the model for the exposure estimates. Country/region level data on baseline mortality rates were from GBD data for 2015 (based on the 2017 iteration) (IHME, 2017). USA state-specific mortality rates were obtained from the CDC Wide-ranging Online Data for Epidemiologic Research (WONDER) compressed mortality files (WONDER). Canada death estimates by province were obtained from Statistics Canada, CANSIM (Canada, 2018).

4.2.3. $PM_{2.5}$ Mortality Concentration–Response Model

The risk of air pollution to health in a population is usually estimated by applying a concentration–response function (CRF), which is typically based on Relative Risk (RR) estimates derived from epidemiological studies. CRFs are necessary elements for the quantification of health impacts due to air pollution and require regular evaluation and update to incorporate new developments in the literature.

Global assessments of air pollution risk often use the Integrated Exposure-Response model (IER) (Burnett et al., 2014), which combined information on $PM_{2.5}$–mortality associations from non-outdoor $PM_{2.5}$ sources, including secondhand smoke, household air pollution from use of solid fuels, and active smoking. The IER used data from active smoking and passive smoking

to address the limited number of outdoor $PM_{2.5}$ epidemiologic studies at $PM_{2.5} > 40$ μg m^{-3} available at the time. The IER formed the basis of the estimates of disease burden attributable to $PM_{2.5}$ (e.g., 4 million deaths in 2015 in GBD 2015). This function was then updated in 2018 using the Global Exposure Mortality Model (GEMM). In GEMM, data from 41 epidemiological cohort studies were applied (Burnett et al., 2018). Independently conducted analyses were conducted on 15 of these cohorts to characterize the shapes of $PM_{2.5}$–mortality associations in each cohort, using a specified functional form of the CRF. For the remaining 26 cohorts, the concentration-response was examined with a linear concentration hazard ratio model. A recent meta-analysis of the association between long-term $PM_{2.5}$ and mortality (Vodonos et al., 2018) applied techniques involving flexible penalized spline CRF in a multivariate random effects and meta-regression model. This approach allows the data to specify the shape of the CRF. The meta-regression pooled 135 estimates from 53 studies examining long-term $PM_{2.5}$ and mortality of cohorts aged 15 years and older. The estimate of the confidence intervals about the CRF includes a random variance component. This meta-analysis provided evidence of a nonlinear association between $PM_{2.5}$ exposure and mortality in which the exposure-mortality slopes decreases at higher concentrations (Figure S4.5 in Supplemental Material). We have chosen to use the dose-response function from the meta-analysis rather than the GEMM function as the meta-regression approach is more flexible and does not constrain the CRF to a specific functional form, it incorporates a random variance component in estimating the uncertainty around that curve, it is derived with more studies than previous approaches, and its estimates at high and low exposures are closer to the estimates in cohorts restricted to only very high and very low exposures. To ensure consistency with the concentration-response curve, premature mortality rates for the portion of the population >14

years of age were determined using the population and baseline mortality rates for different age groups from GBD data for 2015.

4.2.4. Health Impact Calculations

We estimated the number of premature deaths attributable to fossil fuel $PM_{2.5}$ using: (1) GEOS-Chem $PM_{2.5}$ estimated with all emission sources and GEOS-Chem $PM_{2.5}$ estimated without fossil fuel emissions, as a comparison against the first simulation, (2) total population above the age of 14 gridded to the GEOS-Chem grid resolution, (3) baseline all-cause mortality rates for population above the age of 14 (per country or per state in the US and province in Canada), and (4) the meta-analysis CRF (Vodonos et al., 2018). All health impacts were calculated on a per-grid basis at the spatial resolution of the model. We applied the following health impact function to estimate premature mortality related to exposure to fossil fuel $PM_{2.5}$ in each GEOS-Chem grid cell:

$$\sum \Delta y = y_o * p * AF \quad (4.1)$$

$$AF = \frac{\exp^{(\bar{\beta}*\Delta x)}-1}{\exp^{(\bar{\beta}*\Delta x)}} \quad (4.2)$$

$$\bar{\beta}(PM_{2.5})=\int_{PM_{2.5}\ \text{no fossil fuel}}^{PM_{2.5}\ \text{all emissions}} \beta(PM_{2.5}) \quad (4.3)$$

where Δy is the change in the number of premature deaths due to exposure to fossil fuel $PM_{2.5}$, y_o is the country/state/province specific baseline (all-cause) mortality rate, p is to the total population above the age of 14, AF is the attributable fraction of deaths (the fraction of total deaths attributable to $PM_{2.5}$ exposure), $\bar{\beta}$ is the mean estimate for long-term $PM_{2.5}$ mortality

concentration-response over a range of concentrations from the penalized spline model in the recent meta-analysis, and Δx is the change in $PM_{2.5}$ concentration, calculated as the difference between GEOS-Chem $PM_{2.5}$ with all emissions and GEOS-Chem $PM_{2.5}$ without fossil fuel emissions.

For each country, we summed the change in premature deaths (Δy) in each grid cell over all grid cells in that country. To estimate the change in deaths between the two scenarios (with and without fossil fuel combustion), we computed the change in deaths in each grid cell, based on its population, baseline rate, and exposure under the two scenarios (Equation 4.1). The attributable fraction (AF), or proportion of deaths estimated as due to long-term exposure to $PM_{2.5}$ fossil fuel air pollution, was calculated using the concentration-response estimate, following the form shown in Equation 4.2 (Figure S4.5 in Supplemental material). Because these estimates of mortality concentration response (β) are a nonlinear function of concentration, we used the penalized spline model predictions from this meta-analysis to integrate the concentration-specific β in each grid cell from the low $PM_{2.5}$ scenario (without fossil fuel emissions) to the high $PM_{2.5}$ scenario (with all emissions, including fossil fuel). In this way, we could calculate a mean value of β for each grid cell. There exist insufficient epidemiological data to calculate a robust health response function specific to fossil-fuel $PM_{2.5}$. GEOS-Chem is a deterministic model. Therefore, our 95 % confidence intervals (CI) for our estimates reflect only the 95 % CI for the concentration response function.

4.2.5. Secondary Analysis Among Children <5 years old

Lower respiratory infections (LRI), including pneumonia and bronchiolitis of bacterial and viral origin, are the largest single cause of mortality among young children worldwide and thus account for a significant global burden of disease worldwide (Nair et al., 2010). As mentioned previously, young children are more susceptible to the adverse effects of particulate air pollution than adults. Mehta et al. (2013) estimated the overall impact of $PM_{2.5}$ concentration with Relative Risk (RR) of 1.12 for LRI mortality per 10 μg m^{-3} increase in annual average $PM_{2.5}$ concentration, as compared to RR of 1.04 for respiratory mortality among adults (Vodonos et al., 2018). We estimated the number of premature deaths attributable to $PM_{2.5}$ among children under the age of 5 years due to a range of LRI classifications (ICD-10, International Classification of Diseases codes: A48.1, A70, J09-J15.8, J16-J16.9, J20-J21.9, P23.0-P23.4). Baseline numbers of deaths due to LRI were obtained from the GBD for 2015 (IHME, 2017). We used the Relative Risk (RR) of 1.12 (1.03-1.30) for LRI occurrence per 10 μg m^{-3} increase in annual average $PM_{2.5}$ concentration (Mehta et al., 2013). Studies of longer-term exposure of $PM_{2.5}$ and LRI in that meta-analysis were conducted in only a few developed countries with relatively low levels of annual mean $PM_{2.5}$ (< 25 μg m^{-3}), specifically the Netherlands, Czech Republic, Germany, Canada and USA. We therefore calculated the number of premature LRI deaths attributable to $PM_{2.5}$ only in North America, South America, and Europe.

4.3. Results

4.3.1. Impact of Fossil Fuel Use on $PM_{2.5}$

Figure 4.1 shows the difference between global GEOS-Chem $PM_{2.5}$ with and without fossil fuel emissions, plotted as the annual mean for 2012. Results show large contributions of 50-100 μg

m^{-3} in $PM_{2.5}$ over China and India, with smaller increments of 10-50 μg m^{-3} over large swaths of the United States and Europe, industrialized countries in Africa (South Africa and Nigeria), and along the North African coastline due to European pollution.

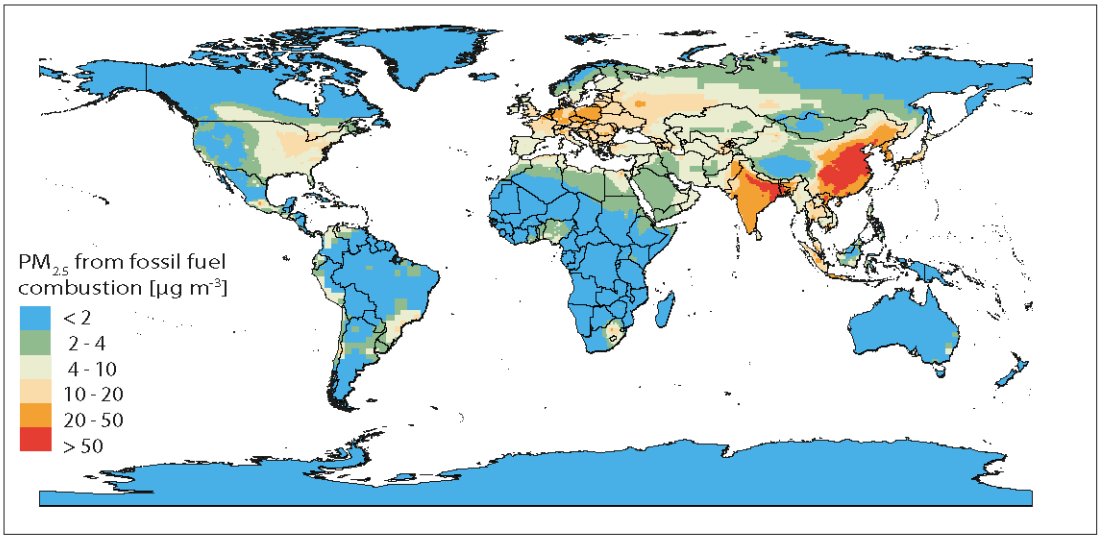

Figure 4.1 Contribution of fossil fuel combustion to surface $PM_{2.5}$, as calculated by the chemical transport model GEOS-Chem. The plot shows the difference in surface $PM_{2.5}$ concentrations from GEOS-Chem with and without fossil fuel emissions.

4.3.2. Global Assessment of Mortality Attributable to $PM_{2.5}$

Based on the annual $PM_{2.5}$ simulation with and without global fossil fuel emissions, we estimated the excess deaths and attributable fraction (AF %) for the population above 14 years old. Figure 4.2 shows the simulated annual global premature mortality due to exposure to ambient $PM_{2.5}$ from fossil fuel emissions. Greatest mortality is simulated over regions with substantial influence of fossil-fuel related $PM_{2.5}$, notably parts of Eastern North America, western Europe, and South-East Asia.

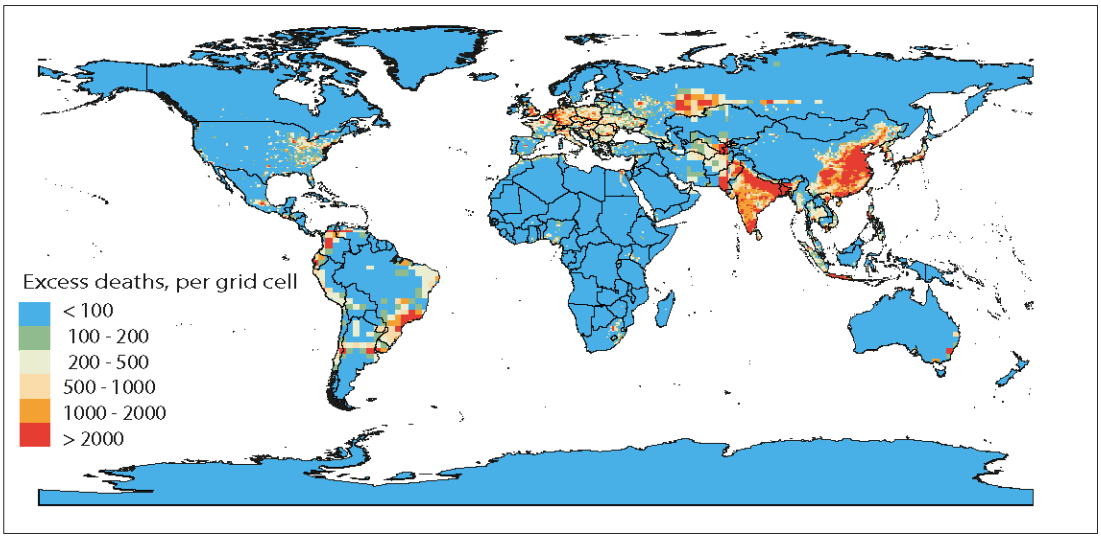

Figure 4.2 Estimated annual excess deaths due to exposure to ambient $PM_{2.5}$ generated by fossil fuel combustion.

We estimated a total global annual burden premature mortality due to fossil fuel combustion in 2012 of 10.2 million (95 % CI: -47.1 to 17.0 million). Table 4.1 reports the baseline number of deaths for people >14 years old, the annual $PM_{2.5}$ simulation with and without global fossil fuel emissions, the estimated excess deaths, and the attributable fraction for the populated continents. As shown in Table 4.1, we calculated 483,000 premature deaths in North America (95 % CI: 284,000-670,000), 187,000 deaths in South America (95 % CI: 107,000-263,000), 1,447,000 deaths in Europe (95 % CI: 896,000-1,952,000), 7,916,000 deaths in Asia (95 % CI: -48,106,000 to 13,622,000), and 194,000 deaths in Africa (95 % CI: -237,000 to 457,000). The wide confidence intervals in Asia and Africa are due to the lack of data for areas where the exposure remains outside the range of the concentration response curve ($PM_{2.5}$ > 50 μg m^{-3}; Figure S4.5). The population-weighted pollution concentrations presented in Table 4.1 are higher than the average $PM_{2.5}$ concentrations for each country, since fossil-fuel $PM_{2.5}$ is mainly emitted in populous areas. The two countries with the highest premature mortality are China

with 3.91 million and India with 2.46 million. Supplemental Table S4.2 provides extended data of the health impact calculations for each country. For comparison, Table 4.1 also reports the number of premature deaths attributable to fossil fuel $PM_{2.5}$ when the GEMM function is applied to the GEOS-Chem output. For most regions, the number of premature deaths calculated with GEMM is significantly lower than that calculated with the new function from Vodonos et al. (2018). Globally, the GEMM function yields 6.7 million deaths in 2012 due to fossil fuel combustion.

Table 4.1 Number of deaths attributable to exposure to fine particulate matter ($PM_{2.5}$) generated by fossil fuel combustion for the population >14 years old

GEOS-Chem spatial grid resolution[a]	Region[b]		Total deaths >14 years old, in thousands	Population-weighted annual mean $PM_{2.5}$ concentration, μg m^{-3}			Mean attributable fraction of deaths, % (95% CI)[d]	Deaths attributable to fossil-fuel related $PM_{2.5}$, in thousands (95% CI)[c]	GEMM function deaths attributable to fossil-fuel related $PM_{2.5}$, in thousands (95% CI)[e]
				$PM_{2.5}$ from all emission sources	$PM_{2.5}$ without fossil fuel	Estimated $PM_{2.5}$ from fossil fuel, %			
Fine	North America	Central America & the Caribbean	1,148	10.06	3.03	7.03 (69.9)	8.2 (4.5-11.6)	94 (52-133)	80 (62-98)
		USA	2,705	11.81	2.15	9.66 (81.8)	13.1 (7.8-18.1)	355 (212-490)	305 (233-375)
		Canada	250	12.01	1.76	10.25 (85.4)	13.6 (8.0-18.7)	34 (20-47)	28 (22-35)
Coarse	South America		2,389	8.66	3.02	5.65 (65.2)	7.8 (4.5-11.0)	187 (107-263)	159 (121-195)
Fine	Europe		8,626	19.22	4.68	14.54 (75.7)	16.8 (10.4-22.6)	1,447 (896-1,952)	1,033 (798-1,254)
Fine	Asia	Eastern Asia	25,468	51.72	8.68	43.05 (83.2)	30.7 (-189.1-52.9)	7,821 (-48,150-13,478)	4,945 (3,943-5,826)
Coarse		Western Asia & the Middle East	1,456	26.95	20.73	6.22 (23.1)	6.5 (3.0-9.9)	95 (44-144)	54 (43-65)
Fine	Africa		5,274	32.98	28.98	4.00 (12.1)	3.7 (-4.5-8.7)	194 (-237-457)	102 (81-121)
Coarse	Australia & Oceania		189	4.17	2.19	1.98 (47.4)	3.2 (1.6-4.8)	6.0 (2.9-9.0)	6.4 (4.8-7.9)
	Global		47,506	38.01	11.14	26.87 (70.7)	21.5 (-99.0-35.7)	10,235 (-47,054-16,972)	6,713 (5,308-7,976)

[a] Fine spatial scale is 0.5° × 0.67°, or about 50 km × 60 km. Coarse spatial scale is 2° × 2.5°, or about 200 km × 250 km

[b] List of countries for each region and subregion is provided in supplemental Table S4.2

[c] Annual number of deaths attributable to long-term exposure to $PM_{2.5}$ derived from fossil fuel combustion. CI is the confidence interval.

[d] Mean proportion of all deaths which can be attributed to long-term exposure to $PM_{2.5}$ generated by fossil fuel combustion, averaged over the country or region. CI; confidence interval.

[e] Attributable deaths calculated with the Global Exposure Mortality Model (GEMM) concentration-response function.

Table 4.2 Number of deaths due to lower respiratory infection (LRI) attributable to exposure to fine particulate matter ($PM_{2.5}$) from fossil fuel combustion for the population <5 years old

Region	Total deaths for children <5 years old due to LRI	LRI deaths attributable to fossil-fuel $PM_{2.5}$ (95% CI) [a]	Mean attributable fraction of deaths, % (95% CI) [b]
North America	**13,230**	**876 (-26-1,657)**	**6.6 (-0.2-12.5)**
Central America & the Caribbean	12,507	802 (-23-1,516)	6.4 (-0.2-12.1)
USA	672	69 (-2-131)	10.2 (-0.3-19.5)
Canada	50	5 (0-10)	10.8 (-0.3-20.5)
South America	**13,231**	**747 (-21-1,443)**	**5.7 (-0.2-10.9)**
Europe	**4,446**	**605 (-18-1,126)**	**13.6 (-0.4-25.3)**

[a] Annual number of deaths attributed to long-term exposure to $PM_{2.5}$ derived from fossil fuel combustion.

[b] Mean proportion of deaths due to long-term exposure to $PM_{2.5}$ generated by fossil fuel combustion. CI is the confidence interval.

4.3.3. Assessment of Children (under the age of 5) LRI Mortality Attributable to $PM_{2.5}$

We estimated the number of premature deaths attributable to $PM_{2.5}$ among children under the age of 5 due to LRI only for those countries or regions with levels of annual $PM_{2.5}$ concentrations below 25 μg m^{-3}. These include North America, South America, and Europe. Based on the annual $PM_{2.5}$ simulation with and without fossil fuel emissions, we calculated 876 excess deaths due to LRI in North and Central America, 747 in South America, and 605 in Europe (Table 4.2). Using the GBD estimate of total deaths due to LRI (Institute for Health Metrics and Evaluation), we estimate that $PM_{2.5}$ from fossil fuel combustion accounted on average for 7.2 % of LRI mortality among children under the age of 5 in these regions, with the largest proportion of 13.6 % in Europe (95 % CI -0.4 to 25.3 %) .

4.4. Discussion

We used the chemical transport model GEOS-Chem to quantify the global mortality attributed to $PM_{2.5}$ air pollution from fossil fuel combustion. Using the updated concentration response relationship between relative mortality and airborne $PM_{2.5}$, we estimated global premature mortality in 2012 of 10.2 million per year from fossil fuel combustion alone. China has the highest burden of 3.91 million per year, followed by India with 2.46 million per year. These estimates carry large uncertainty (e.g., 95 % CI of -47.1 to 17.0 million for the global estimate) from the concentration-response curve, as it is an improved function that provides a more realistic picture of the health consequences of $PM_{2.5}$ compared to previous studies.

Our estimate is for the year when fossil fuel emissions in China peaked and so predates large and dramatic reductions in fossil fuel emissions due to strict mitigation measures. These reductions led to a 30-50 % decline in annual mean $PM_{2.5}$ across the country from 2013 to 2018

(Zhai et al., 2019). If we apply a 43.7 % reduction in GEOS-Chem $PM_{2.5}$ concentrations from the simulation with all emission sources, premature mortality in China decreases from 3.91 million to 2.36 million. India has recently imposed controls on pollution sources, but there is not yet evidence of air quality improvements in densely populated cities like Delhi (Vohra et al., 2021). Consideration of the 2012-2018 decrease in $PM_{2.5}$ exposure in China reduces the total global premature mortality due to fossil fuel $PM_{2.5}$ from 10.2 million premature deaths each year to 8.7 (95 % CI: -1.8 to 14.0) million.

In 2012, the population-weighted $PM_{2.5}$ is 72.8 μg m^{-3} for China and 52.0 μg m^{-3} for India from all sources and 9.9 μg m^{-3} for China and 9.0 μg m^{-3} for India without fossil fuel emissions. The low value of non-fossil fuel $PM_{2.5}$ is reasonable for southern India (Dey et al., 2012) but may be an underestimate in the Indo-Gangetic Plain where crop residue burning contributes to high levels of $PM_{2.5}$ (100-200 μg m^{-3}) during the post-monsoon season (Ojha et al., 2020). An increase in the concentration of non-fossil-fuel $PM_{2.5}$ would decrease our estimate of the number of premature deaths due to fossil fuel $PM_{2.5}$ in India and China, as this would decrease the risk of premature mortality with a unit change in $PM_{2.5}$ (Figure S4.5).

4.4.1. Comparison with Previous Estimates of Global Mortality Attributable to Outdoor $PM_{2.5}$

Previous estimates of the GBD for 2015 suggest that exposure to total $PM_{2.5}$ causes 4.2 million deaths (Cohen et al., 2017), whereas here we estimate more than double (10.2 million) the number of premature deaths from fossil fuel combustion alone in 2012. Differences between the current study and the 2015 GBD lower estimates are related mainly to the choice of the

shape of the concentration-response function and the relative risk estimate. First, to provide information about exposure response at higher concentrations, the 2015 GBD study used the integrated exposure–response (IER) model in which active and second-hand smoking exposures were converted to estimated annual $PM_{2.5}$ exposure equivalents using inhaled doses of particle mass (Burnett et al., 2014). Recent cohort studies from Asia indicate that this substantially underestimates the CRF at high concentrations. In contrast, in the current study we applied a CRF that was directly estimated from $PM_{2.5}$ studies alone, as described in a recent meta-analysis that included estimates from studies in countries like China with higher $PM_{2.5}$ concentrations than our included in previous derivations of CRFs (Vodonos et al., 2018). The CRF from this recent meta-analysis flattens out at higher concentrations, as does the IER curve. However, this flattening is not as great as in the IER, as Asian cohort studies at high $PM_{2.5}$ concentrations report larger effects than would be expected from the IER. Hence estimates of the global attributable fraction of deaths due to air pollution using the function from the recent meta-analysis are higher than the estimates using the IER function. In addition, at much lower concentrations (< 10 μg m^{-3}), we applied higher slopes than assumed in the IER function. Recent studies at very low concentrations similarly show that the IER underestimated effects in this range (Pinault et al., 2016). Since GEOS-Chem estimated quite low concentrations in developed countries in Europe and North America, the number of premature deaths from $PM_{2.5}$ in these countries is greater than previous estimates.

Following an approach similar to the recent meta-analysis (Vodonos et al., 2018), Burnett et al. (2018) modeled the shape of the association between $PM_{2.5}$ and non-accidental mortality using data from 41 cohorts from 16 countries with GEMM. In that study, the uncertainty in a subset (15 cohorts) was characterized in the shape of the concentration-response parameter by

calculating the Shape-Constrained Health Impact Function, a prespecified functional form. These estimated shapes varied across the cohorts included in the function. GEMM predicted 8.9 million (95 % CI: 7.5–10.3) deaths in 2015 attributable to long-term exposure to $PM_{2.5}$ from all sources; 120 % higher excess deaths than previous estimates, but still lower than our estimate of mortality from exposure to fossil-fuel derived $PM_{2.5}$ for 2012. Lelieveld et al. (2019) estimated the global and regional mortality burden of fossil fuel attributable $PM_{2.5}$ by applying the GEMM CRF to a global chemistry-climate model that is overall coarser (~1.9° latitude and longitude) than the model used in this work. The authors reported 3.61 million deaths per year attributable to pollution from fossil fuel combustion and 5.55 million deaths per year due to pollution from all anthropogenic sources. The estimated deaths from fossil fuel combustion are much lower than those in the current study for several reasons. First, the meta-analysis function used in our work includes 135 coefficients of all-cause mortality for adults aged 14-64 years old, together with cause-specific mortality and all-cause mortality among adults aged 65 and older, thus incorporating many more studies in a meta-regression framework than the 41 cohorts and coefficients in the GEMM function. Second, the approach used to estimate the CRF in Vodonos et al. (2018) allows for additional flexibility in the shape of the function because of its use of penalized splines. In contrast, the GEMM pooled CRF integrates a set of 26 log-linear functions and 15 functions characterized by three parameters governing the shape of the function. Third, while Cohen et al. (2017), Lelieveld et al. (2019) and Burnett et al. (2018) accounted for mortality from five specific causes (ischemic heart disease, stroke, chronic obstructive pulmonary disease, lung cancer and acute respiratory infections), in the current analysis we estimated changes in deaths from all causes. Fourth, some of the difference in the mortality estimates may come from differences in the age range. Our approach considers a wider population age range of over 14 years old (Vodonos et al., 2018) compared to the other

studies, which considered a population age range of over 25 years (Cohen et al., 2017; Burnett et al., 2018; Lelieveld et al., 2019). Our approach has wider age range since the age range for the studies in the meta-analysis (Vodonos et al., 2018) included people younger than 25 years old (Hart et al., 2011; Pinault et al., 2016) . Finally, the finer spatial resolution that GEOS-Chem utilizes over much of the globe improves co-location of PM hotspots and population centers, yielding higher estimates of excess mortality compared to Lelieveld et al. (2019).

4.4.2. Limitations

There are a number of limitations that must be acknowledged. First, vulnerability to $PM_{2.5}$ exposure may vary by population characteristics such as ethnicity, socio-economic status (SES), risk behaviors such as smoking and underlying comorbidities (Krewski et al., 2000; Pope et al., 2004; Wang et al., 2017) and by different exposure characteristics. We were limited in our ability to undertake a comprehensive analysis of factors influencing the association between $PM_{2.5}$ and mortality since the global mortality data were not available by detailed age, ethnicity, SES, lifestyle, and underlying disease strata. In addition, the 95 % CI of our estimates reflect the lower and upper bound of the CRF, which flattens out at higher concentrations. Regions with very high concentrations (>50 μg m^{-3}) are beyond the data range in the meta-analysis; thus, the lower limit of the CI for those regions (China, West and North Africa; Table 4.1) are much less than zero. Second, for LRI in children, we have restricted our analysis to developed countries with annual $PM_{2.5}$ < 25 μg m^{-3}, in accordance with the geographical locations of the studies included in the meta-analysis by Mehta et al. (2013). Developing countries have much higher LRI mortality rates, and this restriction doubtless results in an underestimate. Finally, GEOS-Chem estimates of $PM_{2.5}$ concentrations almost certainly contains errors in estimates of emissions of pollution precursors, meteorological effects on air quality, and representation of the complex physical and chemical formation pathways. In the absence of systematic bias, such model error may not produce large aggregate errors in the mortality burden of $PM_{2.5}$, but bias may be present as well. In any event, it is challenging to estimate the true size of this error.

4.5. Conclusions

The effects of CO_2-driven climate change on human health and welfare are complex, ranging from greater incidence of extreme weather events, more frequent storm-surge flooding, and increased risk of crop failure (Duffy et al., 2019). One consequence of increasing reliance on fossil fuel as an energy source that has thus far received comparatively little attention is the potential health impact of the pollutants co-emitted with the greenhouse gas CO_2. Such pollutants include $PM_{2.5}$ and the gas-phase precursors of $PM_{2.5}$. This study demonstrates that the fossil fuel component of $PM_{2.5}$ contributes a large global mortality burden. By quantifying this sometimes overlooked health consequence of fossil fuel combustion, a clear message is sent to policymakers and stakeholders of the co-benefits of a transition to alternative energy sources.

References

Apte, J. S., Marshall, J. D., Cohen, A. J., and Brauer, M., Addressing Global Mortality from Ambient $PM_{2.5}$, Environ. Sci. Technol., 49, 8057-8066, doi:10.1021/acs.est.5b01236, 2015.

Atkinson, R. W., Butland, B. K., Dimitroulopoulou, C., Heal, M. R., Stedman, J. R., Carslaw, N., Jarvis, D., Heaviside, C., Vardoulakis, S., Walton, H., et al., Long-term exposure to ambient ozone and mortality: a quantitative systematic review and meta-analysis of evidence from cohort studies, Bmj Open, 6, doi:10.1136/bmjopen-2015-009493, 2016.

Aunan, K., Ma, Q., Lund, M. T., and Wang, S. X., Population-weighted exposure to $PM_{2.5}$ pollution in China: An integrated approach, Environ. Int., 120, 111-120, doi:10.1016/j.envint.2018.07.042, 2018.

Bateson, T. F., and Schwartz, J., Children's response to air pollutants, J. Toxicol. Env. Heal. A, 71, 238-243, doi:10.1080/15287390701598234, 2008.

Bond, T. C., Bhardwaj, E., Dong, R., Jogani, R., Jung, S. K., Roden, C., Streets, D. G., and Trautmann, N. M., Historical emissions of black and organic carbon aerosol from energy-related combustion, 1850-2000, Global Biogeochem. Cy., 21, doi:10.1029/2006gb002840, 2007.

Brauer, M., Freedman, G., Frostad, J., van Donkelaar, A., Martin, R. V., Dentener, F., van Dingenen, R., Estep, K., Amini, H., Apte, J. S., et al., Ambient Air Pollution Exposure Estimation for the Global Burden of Disease 2013, Environ. Sci. Technol., 50, 79-88, doi:10.1021/acs.est.5b03709, 2016.

Brook, R. D., Rajagopalan, S., Pope, C. A., Brook, J. R., Bhatnagar, A., Diez-Roux, A. V., Holguin, F., Hong, Y. L., Luepker, R. V., Mittleman, M. A., et al., Particulate Matter Air Pollution and Cardiovascular Disease An Update to the Scientific Statement From the American Heart Association, Circulation, 121, 2331-2378, doi:10.1161/CIR.0b013e3181dbece1, 2010.

Burnett, R., Pope, C. A., Ezzati, M., Olives, C., Lim, S. S., Mehta, S., Shin, H. H., Singh, G., Hubbell, B., Brauer, M., et al., An Integrated Risk Function for Estimating the Global Burden of Disease Attributable to Ambient Fine Particulate Matter Exposure, Environ. Health Persp., 122, 397-403, doi:10.1289/ehp.1307049, 2014.

Burnett, R., Chen, H., Szyszkowicz, M., Fann, N., Hubbell, B., Pope, C. A., Apte, J. S., Brauer, M., Cohen, A., Weichenthal, S., et al., Global estimates of mortality associated with long-term exposure to outdoor fine particulate matter, P. Natl. Acad. Sci. USA, 115, 9592-9597, doi:10.1073/pnas.1803222115, 2018.

Government of Canada, https://www150.statcan.gc.ca/n1/en/type/data, Last, 2018.

Chang, L. Y., Xu, J. M., Tie, X. X., and Wu, J. B., Impact of the 2015 El Nino event on winter air quality in China, Sci. Rep.-Uk, 6, doi:10.1038/srep34275, 2016.

CIESIN, Center for International Earth Science Information Network - Columbia University; Gridded Population of the World, Version 4 (GPWv4): Population Count Adjusted to Match 2015 Revision of UN WPP Country Totals, Revision 11, in, NASA Socioeconomic Data and Applications Center (SEDAC), Palisades, NY, 2018.

Cohen, A. J., Brauer, M., Burnett, R., Anderson, H. R., Frostad, J., Estep, K., Balakrishnan, K., Brunekreef, B., Dandona, L., Dandona, R., et al., Estimates and 25-year trends of the global burden of disease attributable to ambient air pollution: an analysis of data from the Global Burden of Diseases Study 2015, Lancet, 389, 1907-1918, doi:10.1016/S0140-6736(17)30505-6, 2017.

Cusworth, D. H., Mickley, L. J., Sulprizio, M. P., Liu, T. J., Marlier, M. E., DeFries, R. S., Guttikunda, S. K., and Gupta, P., Quantifying the influence of agricultural fires in northwest India on urban air pollution in Delhi, India, Environ. Res. Lett., 13, doi:10.1088/1748-9326/aab303, 2018.

Dedoussi, I. C., and Barrett, S. R. H., Air pollution and early deaths in the United States. Part II: Attribution of $PM_{2.5}$ exposure to emissions species, time, location and sector, Atmos. Environ., 99, 610-617, doi:10.1016/j.atmosenv.2014.10.033, 2014.

Dey, S., Di Girolamo, L., van Donkelaar, A., Tripathi, S. N., Gupta, T., and Mohan, M., Variability of outdoor fine particulate ($PM_{2.5}$) concentration in the Indian Subcontinent: A remote sensing approach, Remote Sens. Environ., 127, 153-161, doi:10.1016/j.rse.2012.08.021, 2012.

Di, Q., Koutrakis, P., and Schwartz, J., A hybrid prediction model for $PM_{2.5}$ mass and components using a chemical transport model and land use regression, Atmos. Environ., 131, 390-399, doi:10.1016/j.atmosenv.2016.02.002, 2016.

Di, Q., Wang, Y., Zanobetti, A., Wang, Y., Koutrakis, P., Choirat, C., Dominici, F., and Schwartz, J. D., Air Pollution and Mortality in the Medicare Population, N. Engl. J. Med., 376, 2513-2522, doi:10.1056/NEJMoa1702747, 2017.

Drury, E., Jacob, D. J., Spurr, R. J. D., Wang, J., Shinozuka, Y., Anderson, B. E., Clarke, A. D., Dibb, J., McNaughton, C., and Weber, R., Synthesis of satellite (MODIS), aircraft (ICARTT), and surface (IMPROVE, EPA-AQS, AERONET) aerosol observations over

eastern North America to improve MODIS aerosol retrievals and constrain surface aerosol concentrations and sources, J. Geophys. Res.-Atmos., 115, doi:10.1029/2009jd012629, 2010.

Duffy, P. B., Field, C. B., Diffenbaugh, N. S., Doney, S. C., Dutton, Z., Goodman, S., Heinzerling, L., Hsiang, S., Lobell, D. B., Mickley, L. J., et al., Strengthened scientific support for the Endangerment Finding for atmospheric greenhouse gases, Science, 363, 597-+, doi:10.1126/science.aat5982, 2019.

Eyring, V., Kohler, H. W., van Aardenne, J., and Lauer, A., Emissions from international shipping: 1. The last 50 years, J. Geophys. Res.-Atmos., 110, doi:10.1029/2004jd005619, 2005.

Fairlie, T. D., Jacob, D. J., and Park, R. J., The impact of transpacific transport of mineral dust in the United States, Atmos. Environ., 41, 1251-1266, doi:10.1016/j.atmosenv.2006.09.048, 2007.

Ford, B., and Heald, C. L., Aerosol loading in the Southeastern United States: reconciling surface and satellite observations, Atmos. Chem. Phys., 13, 9269-9283, doi:10.5194/acp-13-9269-2013, 2013.

Ford, B., and Heald, C. L., Exploring the uncertainty associated with satellite-based estimates of premature mortality due to exposure to fine particulate matter, Atmos. Chem. Phys., 16, 3499-3523, doi:10.5194/acp-16-3499-2016, 2016.

Forouzanfar, M. H., Afshin, A., Alexander, L. T., Anderson, H. R., Bhutta, Z. A., Biryukov, S., Brauer, M., Burnett, R., Cercy, K., Charlson, F. J., et al., Global, regional, and national comparative risk assessment of 79 behavioural, environmental and occupational, and metabolic risks or clusters of risks, 1990-2015: a systematic analysis for the Global Burden of Disease Study 2015, Lancet, 388, 1659-1724, doi:10.1016/S0140-6736(16)31679-8, 2016.

Fountoukis, C., and Nenes, A., ISORROPIA II: a computationally efficient thermodynamic equilibrium model for K^+-Ca^{2+}-Mg^{2+}-Nh_4^+-Na^+-SO_4^{2-}-NO_3^--Cl^--H_2O aerosols, Atmos. Chem. Phys., 7, 4639-4659, doi:10.5194/acp-7-4639-2007, 2007.

Giglio, L., Randerson, J. T., and van der Werf, G. R., Analysis of daily, monthly, and annual burned area using the fourth-generation global fire emissions database (GFED4), J. Geophys. Res.-Biogeo., 118, 317-328, doi:10.1002/jgrg.20042, 2013.

Guenther, A. B., Jiang, X., Heald, C. L., Sakulyanontvittaya, T., Duhl, T., Emmons, L. K., and Wang, X., The Model of Emissions of Gases and Aerosols from Nature version 2.1 (MEGAN2.1): an extended and updated framework for modeling biogenic emissions, Geosci. Model Dev., 5, 1471-1492, doi:10.5194/gmd-5-1471-2012, 2012.

Hart, J. E., Garshick, E., Dockery, D. W., Smith, T. J., Ryan, L., and Laden, F., Long-Term Ambient Multipollutant Exposures and Mortality, Am. J. Resp. Crit. Care, 183, 73-78, doi:10.1164/rccm.200912-1903OC, 2011.

Heald, C. L., Jacob, D. J., Turquety, S., Hudman, R. C., Weber, R. J., Sullivan, A. P., Peltier, R. E., Atlas, E. L., de Gouw, J. A., Warneke, C., et al., Concentrations and sources of organic carbon aerosols in the free troposphere over North America, J. Geophys. Res.-Atmos., 111, doi:10.1029/2006jd007705, 2006.

Heald, C. L., Coe, H., Jimenez, J. L., Weber, R. J., Bahreini, R., Middlebrook, A. M., Russell, L. M., Jolleys, M., Fu, T. M., Allan, J. D., et al., Exploring the vertical profile of atmospheric organic aerosol: comparing 17 aircraft field campaigns with a global model, Atmos. Chem. Phys., 11, 12673-12696, doi:10.5194/acp-11-12673-2011, 2011.

Heald, C. L., Collett, J. L., Lee, T., Benedict, K. B., Schwandner, F. M., Li, Y., Clarisse, L., Hurtmans, D. R., Van Damme, M., Clerbaux, C., et al., Atmospheric ammonia and particulate inorganic nitrogen over the United States, Atmos. Chem. Phys., 12, 10295-10312, doi:10.5194/acp-12-10295-2012, 2012.

Hudman, R. C., Moore, N. E., Mebust, A. K., Martin, R. V., Russell, A. R., Valin, L. C., and Cohen, R. C., Steps towards a mechanistic model of global soil nitric oxide emissions: implementation and space based-constraints, Atmos. Chem. Phys., 12, 7779-7795, doi:10.5194/acp-12-7779-2012, 2012.

IHME, Institute for Health Metrics and Evaluation, in, 21st June 2018, 2017.

Jaegle, L., Quinn, P. K., Bates, T. S., Alexander, B., and Lin, J. T., Global distribution of sea salt aerosols: new constraints from in situ and remote sensing observations, Atmos. Chem. Phys., 11, 3137-3157, doi:10.5194/acp-11-3137-2011, 2011.

Katanoda, K., Sobue, T., Satoh, H., Tajima, K., Suzuki, T., Nakatsuka, H., Takezaki, T., Nakayama, T., Nitta, H., Tanabe, K., et al., An Association Between Long-Term Exposure to Ambient Air Pollution and Mortality From Lung Cancer and Respiratory Diseases in Japan, J. Epidemiol., 21, 132-143, doi:10.2188/jea.JE20100098, 2011.

Keller, C. A., Long, M. S., Yantosca, R. M., Da Silva, A. M., Pawson, S., and Jacob, D. J., HEMCO v1.0: a versatile, ESMF-compliant component for calculating emissions in atmospheric models, Geosci. Model Dev., 7, 1409-1417, doi:10.5194/gmd-7-1409-2014, 2014.

Koplitz, S. N., Mickley, L. J., Marlier, M. E., Buonocore, J. J., Kim, P. S., Liu, T. J., Sulprizio, M. P., DeFries, R. S., Jacob, D. J., Schwartz, J., et al., Public health impacts of the severe haze in Equatorial Asia in September-October 2015: demonstration of a new framework for informing fire management strategies to reduce downwind smoke exposure, Environ. Res. Lett., 11, doi:10.1088/1748-9326/11/9/094023, 2016.

Krewski, D., Burnett, R. T., Goldberg, M. S., Hoover, K., and Siemiatycki, J., Special report reanalysis of the Harvard six cities study and the American Cancer Society Study of particulate air pollution and mortality part II: Sensitivity Analyses Appendix C. Flexible Modeling of the Effects of Fine Particles and Sulphate on Mortality, Health Effects Institute, 2000.

Lacey, F. G., Marais, E. A., Henze, D. K., Lee, C. J., van Donkelaar, A., Martin, R. V., Hannigan, M. P., and Wiedinmyer, C., Improving present day and future estimates of anthropogenic sectoral emissions and the resulting air quality impacts in Africa, Faraday Discuss., 200, 397-412, doi:10.1039/c7fd00011a, 2017.

Lee, H. M., Park, R. J., Henze, D. K., Lee, S., Shim, C., Shin, H. J., Moon, K. J., and Woo, J. H., $PM_{2.5}$ source attribution for Seoul in May from 2009 to 2013 using GEOS-Chem and its adjoint model, Environ. Pollut., 221, 377-384, doi:10.1016/j.envpol.2016.11.088, 2017.

Leibensperger, E. M., Mickley, L. J., Jacob, D. J., Chen, W. T., Seinfeld, J. H., Nenes, A., Adams, P. J., Streets, D. G., Kumar, N., and Rind, D., Climatic effects of 1950-2050 changes in US anthropogenic aerosols - Part 1: Aerosol trends and radiative forcing, Atmos. Chem. Phys., 12, 3333-3348, doi:10.5194/acp-12-3333-2012, 2012.

Lelieveld, J., Klingmuller, K., Pozzer, A., Burnett, R. T., Haines, A., and Ramanathan, V., Effects of fossil fuel and total anthropogenic emission removal on public health and climate, P. Natl. Acad. Sci. USA, 116, 7192-7197, doi:10.1073/pnas.1819989116, 2019.

Li, M., Zhang, Q., Kurokawa, J., Woo, J. H., He, K. B., Lu, Z. F., Ohara, T., Song, Y., Streets, D. G., Carmichael, G. R., et al., MIX: a mosaic Asian anthropogenic emission inventory under the international collaboration framework of the MICS-Asia and HTAP, Atmos. Chem. Phys., 17, 935-963, doi:10.5194/acp-17-935-2017, 2017.

Li, X., Wu, J. R., Elser, M., Feng, T., Cao, J. J., El-Haddad, I., Huang, R. J., Tie, X. X., Prevot, A. S. H., and Li, G. H., Contributions of residential coal combustion to the air quality in Beijing-Tianjin-Hebei (BTH), China: a case study, Atmos. Chem. Phys., 18, 10675-10691, doi:10.5194/acp-18-10675-2018, 2018.

Li, Y., Henze, D. K., Jack, D., and Kinney, P. L., The influence of air quality model resolution on health impact assessment for fine particulate matter and its components, Air Qual. Atmos. Health, 9, 51-68, doi:10.1007/s11869-015-0321-z, 2016.

Lim, S. S., Vos, T., Flaxman, A. D., AlMazroa, M. A., and Memish, Z. A., A comparative risk assessment of burden of disease and injury attributable to 67 risk factors and risk factor clusters in 21 regions, 1990-2010: a systematic analysis for the Global Burden of Disease Study 2010 (vol 380, pg 2224, 2012), Lancet, 381, 628-628, 2013.

Lin, J. T., van Donkelaar, A., Xin, J. Y., Che, H. Z., and Wang, Y. S., Clear-sky aerosol optical depth over East China estimated from visibility measurements and chemical transport modeling, Atmos. Environ., 95, 258-267, doi:10.1016/j.atmosenv.2014.06.044, 2014.

Liu, H. Y., Jacob, D. J., Bey, I., and Yantosca, R. M., Constraints from ^{210}Pb and ^{7}Be on wet deposition and transport in a global three-dimensional chemical tracer model driven by assimilated meteorological fields, J. Geophys. Res.-Atmos., 106, 12109-12128, doi:10.1029/2000jd900839, 2001.

Mao, J. Q., Paulot, F., Jacob, D. J., Cohen, R. C., Crounse, J. D., Wennberg, P. O., Keller, C. A., Hudman, R. C., Barkley, M. P., and Horowitz, L. W., Ozone and organic nitrates over the eastern United States: Sensitivity to isoprene chemistry, J. Geophys. Res.-Atmos., 118, 11256-11268, doi:10.1002/jgrd.50817, 2013.

Marais, E. A., Jacob, D. J., Guenther, A., Chance, K., Kurosu, T. P., Murphy, J. G., Reeves, C. E., and Pye, H. O. T., Improved model of isoprene emissions in Africa using Ozone Monitoring Instrument (OMI) satellite observations of formaldehyde: implications for oxidants and particulate matter, Atmos. Chem. Phys., 14, 7693-7703, doi:10.5194/acp-14-7693-2014, 2014a.

Marais, E. A., Jacob, D. J., Wecht, K., Lerot, C., Zhang, L., Yu, K., Kurosu, T. P., Chance, K., and Sauvage, B., Anthropogenic emissions in Nigeria and implications for atmospheric ozone pollution: A view from space, Atmos. Environ., 99, 32-40, doi:10.1016/j.atmosenv.2014.09.055, 2014b.

Marais, E. A., and Wiedinmyer, C., Air Quality Impact of Diffuse and Inefficient Combustion Emissions in Africa (DICE-Africa), Environ. Sci. Technol., 50, 10739-10745, doi:10.1021/acs.est.6b02602, 2016.

Marais, E. A., Jacob, D. J., Jimenez, J. L., Campuzano-Jost, P., Day, D. A., Hu, W., Krechmer, J., Zhu, L., Kim, P. S., Miller, C. C., et al., Aqueous-phase mechanism for secondary organic aerosol formation from isoprene: application to the southeast United States

and co-benefit of SO_2 emission controls, Atmos. Chem. Phys., 16, 1603-1618, doi:10.5194/acp-16-1603-2016, 2016.

Marais, E. A., Jacob, D. J., Turner, J. R., and Mickley, L. J., Evidence of 1991-2013 decrease of biogenic secondary organic aerosol in response to SO_2 emission controls, Environ. Res. Lett., 12, doi:10.1088/1748-9326/aa69c8, 2017.

Marais, E. A., Silvern, R. F., Vodonos, A., Dupin, E., Bockarie, A. S., Mickley, L. J., and Schwartz, J., Air Quality and Health Impact of Future Fossil Fuel Use for Electricity Generation and Transport in Africa, Environ. Sci. Technol., 53, 13524-13534, doi:10.1021/acs.est.9b04958, 2019.

Mehta, S., Shin, H., Burnett, R., North, T., and Cohen, A. J., Ambient particulate air pollution and acute lower respiratory infections: a systematic review and implications for estimating the global burden of disease, Air Qual. Atmos. Health, 6, 69-83, doi:10.1007/s11869-011-0146-3, 2013.

Murray, L. T., Jacob, D. J., Logan, J. A., Hudman, R. C., and Koshak, W. J., Optimized regional and interannual variability of lightning in a global chemical transport model constrained by LIS/OTD satellite data, J. Geophys. Res.-Atmos., 117, doi:10.1029/2012jd017934, 2012.

Nair, H., Nokes, D. J., Gessner, B. D., Dherani, M., Madhi, S. A., Singleton, R. J., O'Brien, K. L., Roca, A., Wright, P. F., Bruce, N., et al., Global burden of acute lower respiratory infections due to respiratory syncytial virus in young children: a systematic review and meta-analysis, Lancet, 375, 1545-1555, doi:10.1016/S0140-6736(10)60206-1, 2010.

Ojha, N., Sharma, A., Kumar, M., Girach, I., Ansari, T. U., Sharma, S. K., Singh, N., Pozzer, A., and Gunthe, S. S., On the widespread enhancement in fine particulate matter across the Indo-Gangetic Plain towards winter, Sci. Rep.-Uk, 10, doi:10.1038/s41598-020-62710-8, 2020.

Olivier, J. G. J., and Berdowski, J. J. M., Global emission sources and sinks, in: The Climate System, A.A. Balkema Publishers/Swets & Zeitlinger Publishers, Lisse, The Netherlands, 33-78, 2001.

Park, R. J., Jacob, D. J., Field, B. D., Yantosca, R. M., and Chin, M., Natural and transboundary pollution influences on sulfate-nitrate-ammonium aerosols in the United States: Implications for policy, J. Geophys. Res.-Atmos., 109, doi:10.1029/2003jd004473, 2004.

Perera, F., Pollution from Fossil-Fuel Combustion is the Leading Environmental Threat to Global Pediatric Health and Equity: Solutions Exist, Int. J. Env. Res. Pub. He., 15, doi:10.3390/ijerph15010016, 2018.

Pinault, L., Tjepkema, M., Crouse, D. L., Weichenthal, S., van Donkelaar, A., Martin, R. V., Brauer, M., Chen, H., and Burnett, R. T., Risk estimates of mortality attributed to low concentrations of ambient fine particulate matter in the Canadian community health survey cohort, Environ. Health-Glob., 15, doi:10.1186/s12940-016-0111-6, 2016.

Pope, C. A., Burnett, R. T., Thurston, G. D., Thun, M. J., Calle, E. E., Krewski, D., and Godleski, J. J., Cardiovascular mortality and long-term exposure to particulate air pollution - Epidemiological evidence of general pathophysiological pathways of disease, Circulation, 109, 71-77, doi:10.1161/01.Cir.0000108927.80044.7f, 2004.

Protonotariou, A. P., Bossioli, E., Tombrou, M., Mihalopoulos, N., Biskos, G., Kalogiros, J., Kouvarakis, G., and Amiridis, V., Air Pollution in Eastern Mediterranean: Nested-Grid GEOS-CHEM Model Results and Airborne Observations, in: Advances in Meteorology, Climatology and Atmospheric Physics, Springer Atmospheric Sciences, Springer, Berlin, Heidelberg, 1203-1209, 2013.

Pye, H. O. T., Liao, H., Wu, S., Mickley, L. J., Jacob, D. J., Henze, D. K., and Seinfeld, J. H., Effect of changes in climate and emissions on future sulfate-nitrate-ammonium aerosol levels in the United States, J. Geophys. Res.-Atmos., 114, doi:10.1029/2008jd010701, 2009.

Schultz, M. G., Backman, L., Balkanski, Y., Bjoerndalsaeter, S., Brand, R., Burrows, J. P., and S., D., REanalysis of the TROpospheric chemical composition over the past 40 years: Final report, in, 2007.

Shaddick, G., Thomas, M. L., Green, A., Brauer, M., van Donkelaar, A., Burnett, R., Chang, H. H., Cohen, A., Van Dingenen, R., Dora, C., et al., Data integration model for air quality: a hierarchical approach to the global estimation of exposures to ambient air pollution, J. R. Stat. Soc. C-Appl., 67, 231-253, doi:10.1111/rssc.12227, 2018.

Shen, L., and Mickley, L. J., Effects of El Nino on Summertime Ozone Air Quality in the Eastern United States, Geophys. Res. Lett., 44, 12543-12550, doi:10.1002/2017gl076150, 2017.

Shindell, D., Faluvegi, G., Seltzer, K., and Shindell, C., Quantified, localized health benefits of accelerated carbon dioxide emissions reductions, Nat. Clim. Change, 8, doi:10.1038/s41558-018-0108-y, 2018.

Silvern, R. F., Jacob, D. J., Kim, P. S., Marais, E. A., Turner, J. R., Campuzano-Jost, P., and Jimenez, J. L., Inconsistency of ammonium-sulfate aerosol ratios with thermodynamic models in the eastern US: a possible role of organic aerosol, Atmos. Chem. Phys., 17, 5107-5118, doi:10.5194/acp-17-5107-2017, 2017.

Stettler, M. E. J., Eastham, S., and Barrett, S. R. H., Air quality and public health impacts of UK airports. Part I: Emissions, Atmos. Environ., 45, 5415-5424, doi:10.1016/j.atmosenv.2011.07.012, 2011.

Travis, K. R., Jacob, D. J., Fisher, J. A., Kim, P. S., Marais, E. A., Zhu, L., Yu, K., Miller, C. C., Yantosca, R. M., Sulprizio, M. P., et al., Why do models overestimate surface ozone in the Southeast United States?, Atmos. Chem. Phys., 16, 13561-13577, doi:10.5194/acp-16-13561-2016, 2016.

Tseng, E., Ho, W. C., Lin, M. H., Cheng, T. J., Chen, P. C., and Lin, H. H., Chronic exposure to particulate matter and risk of cardiovascular mortality: cohort study from Taiwan, Bmc Public Health, 15, doi:10.1186/s12889-015-2272-6, 2015.

Ueda, K., Nagasawa, S., Nitta, H., Miura, K., Ueshima, H., and Grp, N. D. R., Exposure to Particulate Matter and Long-term Risk of Cardiovascular Mortality in Japan: NIPPON DATA80, J. Atheroscler. Thromb., 19, 246-254, doi:10.5551/jat.9506, 2012.

van Donkelaar, A., Martin, R. V., Leaitch, W. R., Macdonald, A. M., Walker, T. W., Streets, D. G., Zhang, Q., Dunlea, E. J., Jimenez, J. L., Dibb, J. E., et al., Analysis of aircraft and satellite measurements from the Intercontinental Chemical Transport Experiment (INTEX-B) to quantify long-range transport of East Asian sulfur to Canada, Atmos. Chem. Phys., 8, 2999-3014, doi:10.5194/acp-8-2999-2008, 2008.

van Donkelaar, A., Martin, R. V., Brauer, M., Hsu, N. C., Kahn, R. A., Levy, R. C., Lyapustin, A., Sayer, A. M., and Winker, D. M., Global Estimates of Fine Particulate Matter using a Combined Geophysical-Statistical Method with Information from Satellites, Models, and Monitors, Environ. Sci. Technol., 50, 3762-3772, doi:10.1021/acs.est.5b05833, 2016.

Veefkind, J. P., Boersma, K. F., Wang, J., Kurosu, T. P., Krotkov, N., Chance, K., and Levelt, P. F., Global satellite analysis of the relation between aerosols and short-lived trace gases, Atmos. Chem. Phys., 11, 1255-1267, doi:10.5194/acp-11-1255-2011, 2011.

Venkataraman, C., Brauer, M., Tibrewal, K., Sadavarte, P., Ma, Q., Cohen, A., Chaliyakunnel, S., Frostad, J., Klimont, Z., Martin, R. V., et al., Source influence on emission pathways and ambient $PM_{2.5}$ pollution over India (2015-2050), Atmos. Chem. Phys., 18, 8017-8039, doi:10.5194/acp-18-8017-2018, 2018.

Vinken, G. C. M., Boersma, K. F., Jacob, D. J., and Meijer, E. W., Accounting for non-linear chemistry of ship plumes in the GEOS-Chem global chemistry transport model, Atmos. Chem. Phys., 11, 11707-11722, doi:10.5194/acp-11-11707-2011, 2011.

Vodonos, A., Abu Awad, Y., and Schwartz, J., The concentration-response between long-term $PM_{2.5}$ exposure and mortality; A meta-regression approach, Environ. Res., 166, 677-689, doi:10.1016/j.envres.2018.06.021, 2018.

Vohra, K., Marais, E. A., Suckra, S., Kramer, L., Bloss, W. J., Sahu, R., Gaur, A., Tripathi, S. N., Van Damme, M., Clarisse, L., et al., Long-term trends in air quality in major cities in the UK and India: a view from space, Atmos. Chem. Phys., 21, 6275-6296, doi:10.5194/acp-21-6275-2021, 2021.

Wang, C., Corbett, J. J., and Firestone, J., Improving spatial representation of global ship emissions inventories, Environ. Sci. Technol., 42, 193-199, doi:10.1021/es0700799, 2008.

Wang, Q. Q., Jacob, D. J., Spackman, J. R., Perring, A. E., Schwarz, J. P., Moteki, N., Marais, E. A., Ge, C., Wang, J., and Barrett, S. R. H., Global budget and radiative forcing of black carbon aerosol: Constraints from pole-to-pole (HIPPO) observations across the Pacific, J. Geophys. Res.-Atmos., 119, 195-206, doi:10.1002/2013jd020824, 2014.

Wang, S. W., Zhang, Q., Streets, D. G., He, K. B., Martin, R. V., Lamsal, L. N., Chen, D., Lei, Y., and Lu, Z., Growth in NO_x emissions from power plants in China: bottom-up estimates and satellite observations, Atmos. Chem. Phys., 12, 4429-4447, doi:10.5194/acp-12-4429-2012, 2012.

Wang, Y., Shi, L. H., Lee, M., Liu, P. F., Di, Q., Zanobetti, A., and Schwartz, J. D., Long-term Exposure to $PM_{2.5}$ and Mortality Among Older Adults in the Southeastern US, Epidemiology, 28, 207-214, doi:10.1097/Ede.0000000000000614, 2017.

WHO, Ambient and household air pollution and health, in, World Health Organization.

WHO, World Health Organization; Principles for evaluating health risks in children associated with exposure to chemicals, in, 2006.

WHO, World Health Organization; Ambient air pollution: A global assessment of exposure and burden of disease, in, 2016.

Wiedinmyer, C., Yokelson, R. J., and Gullett, B. K., Global Emissions of Trace Gases, Particulate Matter, and Hazardous Air Pollutants from Open Burning of Domestic Waste, Environ. Sci. Technol., 48, 9523-9530, doi:10.1021/es502250z, 2014.

WONDER, C., Centers for Disease Control and Prevention Wide-ranging ONline Data for Epidemiologic Research in, 21st June 2018.

Wong, C. M., Lai, H. K., Tsang, H., Thach, T. Q., Thomas, G. N., Lam, K. B. H., Chan, K. P., Yang, L., Lau, A. K. H., Ayres, J. G., et al., Satellite-Based Estimates of Long-Term Exposure to Fine Particles and Association with Mortality in Elderly Hong Kong Residents, Environ. Health Persp., 123, 1167-1172, doi:10.1289/ehp.1408264, 2015.

Wong, C. M., Tsang, H., Lai, H. K., Thomas, G. N., Lam, K. B., Chan, K. P., Zheng, Q. S., Ayres, J. G., Lee, S. Y., Lam, T. H., et al., Cancer Mortality Risks from Long-term Exposure to Ambient Fine Particle, Cancer Epidem. Biomar., 25, 839-845, doi:10.1158/1055-9965.Epi-15-0626, 2016.

Xiao, Y. P., Logan, J. A., Jacob, D. J., Hudman, R. C., Yantosca, R., and Blake, D. R., Global budget of ethane and regional constraints on US sources, J. Geophys. Res.-Atmos., 113, doi:10.1029/2007jd009415, 2008.

Xing, J., Mathur, R., Pleim, J., Hogrefe, C., Gan, C. M., Wong, D. C., and Wei, C., Can a coupled meteorology-chemistry model reproduce the historical trend in aerosol direct radiative effects over the Northern Hemisphere?, Atmos. Chem. Phys., 15, 9997-10018, doi:10.5194/acp-15-9997-2015, 2015.

Xu, Z. W., Sheffield, P. E., Hu, W. B., Su, H., Yu, W. W., Qi, X., and Tong, S. L., Climate Change and Children's Health-A Call for Research on What Works to Protect Children, Int. J. Env. Res. Pub. He., 9, 3298-3316, doi:10.3390/ijerph9093298, 2012.

Yin, P., Brauer, M., Cohen, A., Burnett, R. T., Liu, J. M., Liu, Y. N., Liang, R. M., Wang, W. H., Qi, J. L., Wang, L. J., et al., Long-term Fine Particulate Matter Exposure and Nonaccidental and Cause-specific Mortality in a Large National Cohort of Chinese Men, Environ. Health Persp., 125, doi:10.1289/Ehp1673, 2017.

Zender, C. S., Bian, H. S., and Newman, D., Mineral Dust Entrainment and Deposition (DEAD) model: Description and 1990s dust climatology, J. Geophys. Res.-Atmos., 108, doi:10.1029/2002jd002775, 2003.

Zhai, S. X., Jacob, D. J., Wang, X., Shen, L., Li, K., Zhang, Y. Z., Gui, K., Zhao, T. L., and Liao, H., Fine particulate matter ($PM_{2.5}$) trends in China, 2013-2018: separating contributions from anthropogenic emissions and meteorology, Atmos. Chem. Phys., 19, 11031-11041, doi:10.5194/acp-19-11031-2019, 2019.

Zhang, L., Jacob, D. J., Knipping, E. M., Kumar, N., Munger, J. W., Carouge, C. C., van Donkelaar, A., Wang, Y. X., and Chen, D., Nitrogen deposition to the United States: distribution, sources, and processes, Atmos. Chem. Phys., 12, 4539-4554, doi:10.5194/acp-12-4539-2012, 2012.

Zhang, L. M., Gong, S. L., Padro, J., and Barrie, L., A size-segregated particle dry deposition scheme for an atmospheric aerosol module, Atmos. Environ., 35, 549-560, doi:10.1016/S1352-2310(00)00326-5, 2001.

Supplementary Information

Description of GEOS-Chem

GEOS-Chem is a three-dimensional chemical transport model that includes detailed oxidant-aerosol chemistry in the troposphere and is used by more than 80 groups worldwide (*www.geos-chem.org*). The model is widely cited in the peer-reviewed literature – e.g., more than 4000 times in the year 2017 alone (http://acmg.seas.harvard.edu/geos/geos_pub.html). The model has been frequently applied to interpret observed $PM_{2.5}$ in regions dominated by anthropogenic sources – e.g., China (Aunan et al., 2018), Korea (Lee et al., 2017), India (Venkataraman et al., 2018), and the US (Di et al., 2016; Silvern et al., 2017); and validation has been performed for specific source sectors – e.g., transportation (Travis et al., 2016), biogenic sources (Marais et al., 2017), and power plants (Wang et al., 2012). Here we use GEOS-Chem v10-01, driven by 2012 GEOS-5 meteorology (gmao.gsfc.nasa.gov/GEOS_systems/). The GEOS-5 data are produced at 0.5°×0.667° horizontal resolution and are re-gridded here to 2°×2.5° for the global simulation. We also perform four regional simulations – for Europe, North America, Africa, and Asia – and for these simulations we keep the native grid resolution. Boundary conditions at 2°×2.5° from the global simulation are applied to these regional simulations. Most fine-scale, regional models, such as the Community Multiscale Air Quality Model, rely on chemical boundary conditions from global models with different chemical schemes, but our approach permits application of a consistent scheme across the globe. The 0.5°×0.667° horizontal resolution in GEOS-Chem over key regions is, however, relatively coarse compared to that in some other regional models. Li et al. (2016) show that application of coarse resolution leads to an underestimate of health impacts of 8 %, implying that our mortality estimates are conservative. Our choice of 2012 as the simulation year is discussed below.

GEOS-Chem simulates the mass concentrations of key particle types including sulfate, nitrate, and ammonium (Park et al., 2004; Zhang et al., 2012), organic carbon (Heald et al., 2006; 2011) black carbon (Wang et al., 2014), dust (Fairlie et al., 2007), and sea salt (Jaegle et al., 2011). Particle chemistry is coupled to gas-phase chemistry as described by (Mao et al., 2013). Gas/particle partitioning of sulfate, nitrate and ammonium (SNA) particles is computed with the ISORROPIA II thermodynamic module (Fountoukis and Nenes, 2007; Pye et al., 2009). Wet and dry deposition of particles follow Liu et al. (2001) and Zhang et al. (2001), respectively.

Emissions in GEOS-Chem are computed by the Harvard-NASA Emission Component (HEMCO) (Keller et al., 2014), which combines and regrids ensembles of user-selected emission inventories. We apply global anthropogenic emissions but supersede these with regional emissions where the latter are more reliable (Table S4.1). Fossil fuel emissions in Africa include (1) industry and power plants from the global inventories and (2) diffuse and inefficient combustion sources (diesel and petrol generators, ad-hoc oil refining, gas flares, kerosene use, cars, and motorcycles) from the DICE-Africa inventory (Marais and Wiedinmyer, 2016). We scale all anthropogenic inventories to 2012, as described by van Donkelaar et al. (2008). Biogenic emissions are from MEGAN v2.1 for volatile organic compounds (Guenther et al., 2012) and from Hudman et al. (2012) for soil nitrogen oxides. Lightning emissions of nitrogen oxides are computed as a function of cloud top height as described by Murray et al. (2012). Dust entrainment and deposition follow the DEAD scheme of Zender et al. (2003) as implemented in GEOS-Chem by Fairlie et al. (2007). Biomass burning emissions are from the Global Fire Emissions Database version 4 (GFED4) (Giglio et al., 2013).

For this study, we first calculate the surface fine particle mass concentrations ($PM_{2.5}$), with all emissions sources turned on. For consistency with the $PM_{2.5}$ measurement protocol set by the U.S. Environmental Protection Agency, we assume 35 % relative humidity everywhere (except for Europe) and standard ambient conditions, with temperature of 298.15 K and surface pressure of 1013.25 hPa. In Europe, we assume 50 % relative humidity, as is the protocol there. We then perform the identical simulation with emissions arising from fossil fuel combustion turned off. The same meteorological fields are applied for both simulations – i.e., the simulation does not allow feedbacks from particles onto meteorology. In the no-fossil-fuel case, all fossil fuel sources are turned off in both the nested simulations and in the global simulation providing boundary conditions. The difference between the two simulations (with and without fossil fuel) represents the contribution of fossil-fuel combustion to surface $PM_{2.5}$. This approach assumes a linear response of surface $PM_{2.5}$ to changes in emissions.

Our choice of 2012 as the simulation year requires explanation. Air quality is influenced not just by emissions but also by meteorological variables such as surface temperature and wind speed, which can vary greatly on inter-annual timescales. Ideally, our analysis would involve multi-year simulations on both the coarse- and fine-scale grids, but such effort would be computationally expensive. We choose instead to do a one-year simulation for a year not influenced by El Niño conditions, which can worsen or ameliorate air pollution, depending on the region (e.g., Chang et al. (2016), Shen and Mickley (2017)). To gauge the error implied by our choice to simulate just one year rather than a span of years, we examine the inter-annual variation in total $PM_{2.5}$ concentrations at the surface estimated from the Dalhousie University archive (van Donkelaar et al., 2016). The $PM_{2.5}$ values in the Dalhousie archive are calculated by first combining satellite observations with GEOS-Chem estimates, and then calibrating the

resulting concentrations with available ground-based observations (mostly Europe, the US, India and China). We find that the global mean average of the relative standard deviation of total $PM_{2.5}$ in the Dalhousie archive over 2008 to 2016 is just 7 %. Averaged over large regions on the continental scale, the relative standard deviation ranges from 4 % over Australia to 11 % over the Asia nested grid domain (Figure S4.1). Inter-annual variability in this metric is greatest (> 60 %) for smaller regions influenced by wildfires or biomass burning – e.g., Indonesia and remote areas at high northern latitudes where few people live. To test our choice of 2012 as a representative year, we calculate the 2012 anomaly in the Dalhousie $PM_{2.5}$ time series (Figure S4.2). Again on a continental scale, we find that 2012 concentrations range from 0.7 μg m^{-3} less to 0.4 μg m^{-3} greater than the 2008-2016 average (Figure S4.2). Given the relatively small inter-annual variability in surface $PM_{2.5}$ in the Dalhousie archive over most populated regions, as well as the small anomalies in $PM_{2.5}$ in 2012 relative to the long-term mean, we conclude that the 2012 GEOS-Chem simulation provides a representative snapshot of global air quality.

To validate the 2012 $PM_{2.5}$ results from GEOS-Chem, we rely on archived $PM_{2.5}$ concentrations from the World Health Organization database (WHO). We find that GEOS-Chem captures the observed annual mean $PM_{2.5}$ concentrations with a correlation of 0.70, mean absolute error of 3.4 μg m^{-3}, and normalized mean bias of 27 % (Figure S4.3). Our high bias in the US (where most North American WHO data are located) is opposite to the low bias estimated by Ford and Heald (2016) in urban (-25 %) and rural (-6 %) areas; such biases may be due to differences in US emission inventories for both gas-phase aerosol precursors and primary particles (Xing et al., 2015). A caveat in our comparison is that most observations (95 %) in the WHO database

with at least 75 % temporal coverage in 2012 are in North America and Europe. We add to Figure S4.3 the 2012 observations from the US embassy in Shanghai (those for Beijing are already in the WHO dataset), and national monitoring sites embassies in Delhi (Cusworth et al., 2018), and the Highveld region in South Africa (South African Air Quality Information System; data obtained by request from the South African Weather Service in July 2018). Over the European domain in Figure S4.1, we find that GEOS-Chem yields a correlation of 0.60, mean absolute error of 5.2 μg m^{-3} and a normalized mean bias of 33 % in surface $PM_{2.5}$; over the North American domain in Figure S4.1, these values are 0.52, 1.8 μg m^{-3} and 20 % (Figure S4.4). Taken together, these validation statistics are similar to those reported by other studies examining surface $PM_{2.5}$ in global models (e.g., Shindell et al. (2018)) and regional models (e.g., Xing et al. (2015)) .

Table S4.1 GEOS-Chem anthropogenic emissions. All emissions are scaled to 2012 conditions.

Region	Inventory name	Species	Reference
Global	EDGAR v4.2[a,c]	NO, CO, SO_2, sulfate, ammonia	Olivier and Berdowski (2001)
Global	RETRO[a,c]	Non-methane VOCs	Schultz et al. (2007)
Global	---	Ethane	Xiao et al. (2008)
Global	GEIA	Biofuel ammonia	www.geiacenter.org
Global	BOND[a,c]	Carbonaceous particles	Bond et al. (2007)
Global	AEIC v2.0 aircraft	NO, CO, etc.	Stettler et al. (2011)
Global	ARTCAS ship	SO_2	Eyring et al. (2005)
Global	ICOADS ship	CO	Wang et al. (2008)
Global	PARANOX ship	NO	Vinken et al. (2011)
United States	NEI 2011[a,b,c]	Many species	US EPA, www3.epa.gov/airtrends
Europe	EMEP[b,c]	Many species	www.emep.int
Asia	MIX[c]	Many species	Li et al. (2017), Venkataraman et al. (2018), Li et al. (2018)
Africa	DICE[c,d]	Many species	Marais and Wiedinmyer (2016)
Africa	---	Open waste burning species	Wiedinmyer et al. (2014)

[a] Includes biofuel sources

[b] Includes ship emissions

[c] Includes land-based transport emissions

[d] Includes only diffuse and inefficient sources of anthropogenic emissions – residential fuelwood, diesel and petrol generators, ad-hoc oil refining, gas flares, kerosene use, charcoal production and use, road transport (including motorcycles). For emissions from formal industry and powerplants, we use the global inventories.

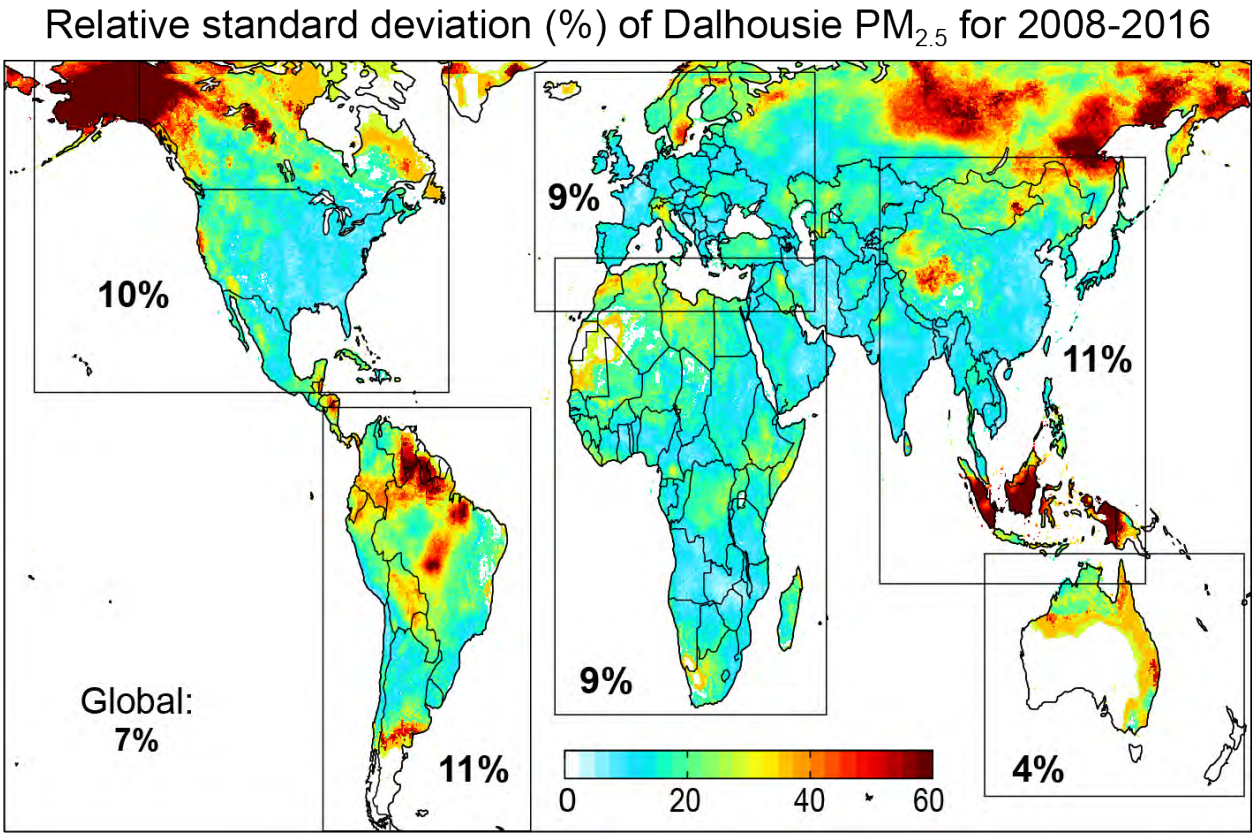

Figure S4.1 Uncertainty in 2012 $PM_{2.5}$ due to interannual variability. Interannual variability is estimated as the relative standard deviation of the Dalhousie satellite-derived $PM_{2.5}$ product (van Donkelaar et al., 2016) for 2008-2016 at 0.1°×0.1°. Values inset are the domain mean relative standard deviations for North America, South America, Western Europe (including portions of North Africa and the Middle East), Africa (including a portion of the Middle East), Southeast Asia, and Australia.

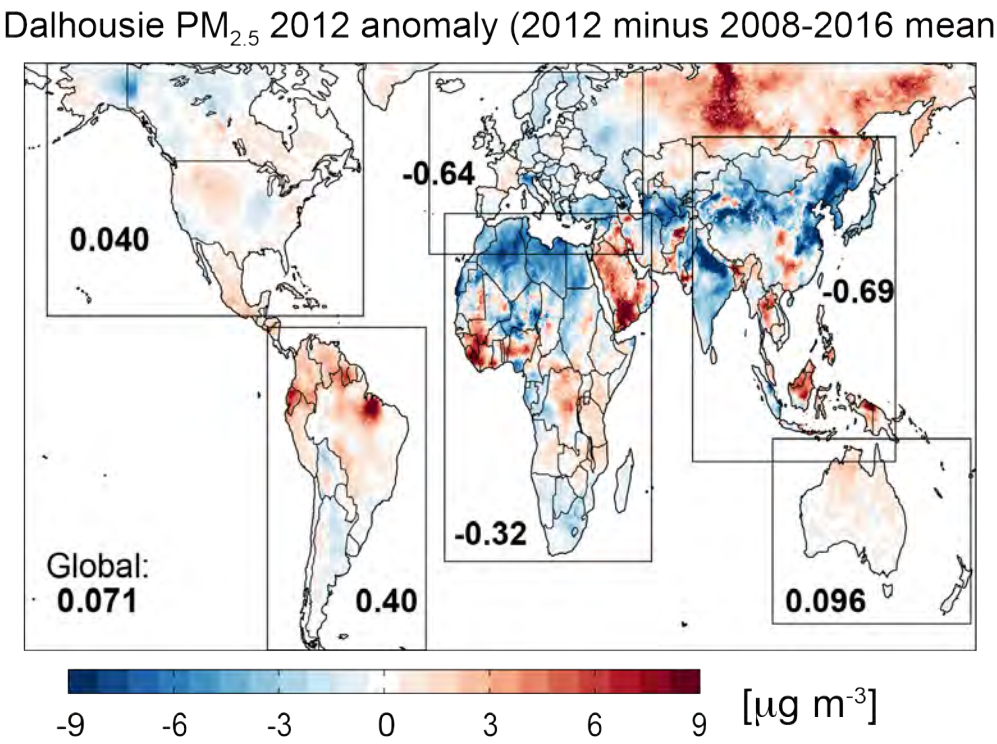

Figure S4.2 Representativeness of $PM_{2.5}$ in 2012, calculated as the absolute difference in 2012 and 2008-2016 mean $PM_{2.5}$ from Dalhousie (van Donkelaar et al., 2016) at 0.1°×0.1°. Values inset are domain mean anomalies for North America, South America, Western Europe (including portions of North Africa and the Middle East), Africa (including a portion of the Middle East), Southeast Asia, and Australia.

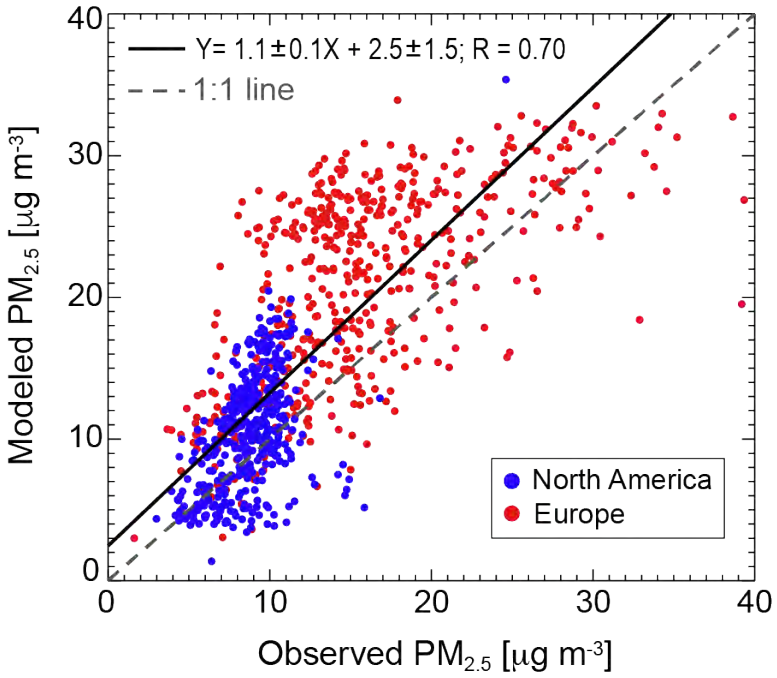

Figure S4.3 Evaluation of GEOS-Chem $PM_{2.5}$. Points are annual mean $PM_{2.5}$ for coincident 0.5° × 0.667° grid squares with at least 75 % temporal coverage in the observations. GEOS-Chem $PM_{2.5}$ is estimated at 50 % relative humidity (RH) in Europe and 35 % RH everywhere else, following standard protocols in measurements of $PM_{2.5}$. Reduced major axis (RMA) regression line (solid black line) and statistics, and the Pearson's correlation coefficient for all coincident grid squares are given inset. Points in red are in Europe and in blue are in North America. Only 7 out of 957 points exceed the range shown.

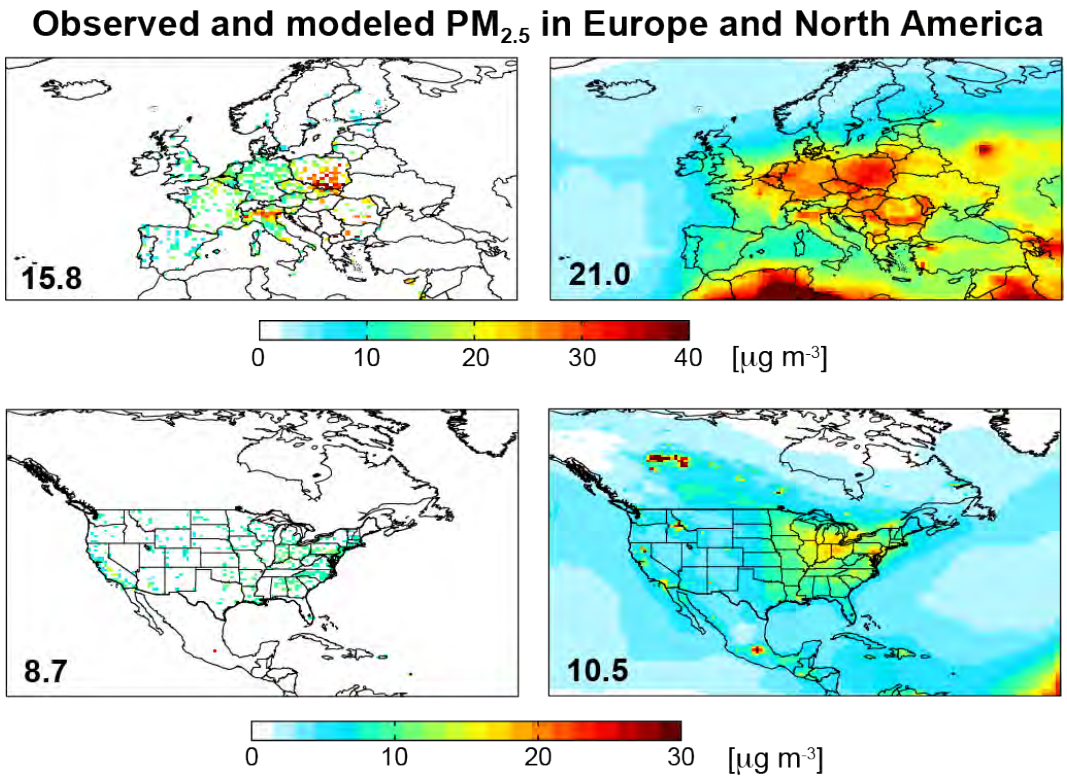

Figure S4.4 Comparison of the spatial distribution of observed and modeled $PM_{2.5}$ in Europe and North America. Data are on a uniform 0.5° × 0.667° grid. Only observations with at least 75 % temporal coverage are used. $PM_{2.5}$ are obtained at 50 % RH in Europe and 35 % RH in North America. Data for the two domains are plotted on different scales. Mean $PM_{2.5}$ for coincident grid squares is given inset.

$PM_{2.5}$ Mortality Concentration–Response Model

We estimated the number of premature deaths attributable to fossil-fuel related $PM_{2.5}$ using a health impact function. To estimate the excess number of deaths associated with $PM_{2.5}$ exposure one requires estimates of exposure, the size of the population exposed, the mortality rate for that population, and the fraction of total deaths attributable to that exposure (AF %).

Recent meta-analysis of the association between long-term $PM_{2.5}$ and mortality (Vodonos et al., 2018) applied a multivariate linear random effects meta-analysis and meta-regression models that polled 135 hazard ratio estimates derived from 53 studies examined long-term $PM_{2.5}$ and mortality. This meta-analysis provided an evidence of a nonlinear association where the exposure-mortality slopes decreased at higher concentrations (Figure S4.5). For example, each 1 $\mu g\ m^{-3}$ increase in $PM_{2.5}$ was associated with a 1.29 % increase in all-age all-cause mortality (95 % CI 1.09-1.50) at a mean exposure of 10 $\mu g\ m^{-3}$, which decreased to 0.94 % (95 % CI 0.76-1.12) at a mean exposure of 20 $\mu g\ m^{-3}$, to 0.81 % (95 % CI 0.52-1.12) at 30 $\mu g\ m^{-3}$ and to 0.79 % (95 % CI 0.40-1.13) at 40 $\mu g/m^{3.}$

Hence, for examining a reduction of $PM_{2.5}$ levels from 15 to 10 $\mu g/m^3$, we calculated the mean slope as area under the curve between 0.014 and 0.011= 0.0125. A reduction of $PM_{2.5}$ levels from 30 to 20 $\mu g/m^3$, the mean slope was calculated as area under the curve between 0.009 and 0.008 = 0.00814. Mean value of estimates of mortality ($\bar{\beta}$) for each grid cell was calculated as area under the curve for the concentration-specific β in each grid cell from the low $PM_{2.5}$ scenario (without fossil fuel emissions) to the high $PM_{2.5}$ scenario (with all emissions, including fossil fuel) following the form shown in Equation S4.1.

$$\bar{\beta}(PM_{2.5}) = \int_{PM_{2.5}\ \text{no fossil fuel}}^{PM_{2.5}\ \text{all emissions}} \beta(PM_{2.5}) \quad \text{(S4.1)}$$

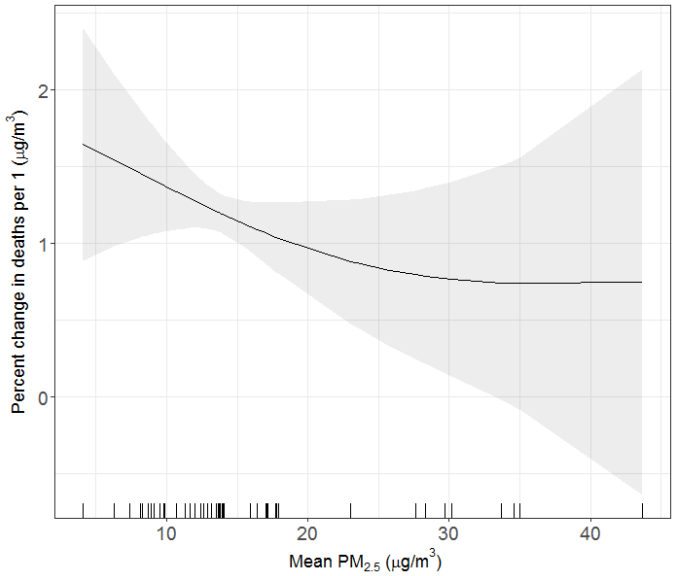

Figure S4.5 Estimates for long-term $PM_{2.5}$ mortality dose-response, drawn from the meta-analysis of long-term association between $PM_{2.5}$ and mortality (Vodonos et al., 2018).

Table S4.2 Global regions, number of deaths, attributable fraction (%) for the population above 14 years old attributable to fine particulate matter ($PM_{2.5}$) exposure in 2012

Country name	Total Deaths >14 years old	Mean population weighted annual $PM_{2.5}$ ($\mu g\ m^{-3}$)			Attributable deaths[a]	Mean attributable fraction (%)[b]
		With all emission sources	Without fossil fuel	Estimated fossil fuel $PM_{2.5}$		
North America						
Bermuda	488	3	1.9	1.1	9	1.8
Greenland	472	1.2	0.9	0.3	3	0.6
Central America & the Caribbean						
Antigua and Barbuda	538	4.4	4.1	0.3	2	0.4
Bahamas	2,347	4.1	2.8	1.4	53	2.3
Barbados	2,523	4.9	4.7	0.2	7	0.3
Belize	1,530	5	4	1.1	26	1.7
Costa Rica	38,094	5.4	2.9	2.6	1,557	4.1
Cuba	95,635	5.3	3.8	1.5	2,334	2.4
Dominica	668	4.9	4.7	0.2	2	0.3
Dominican Republic	60,949	11.2	5.3	6	4,925	8.1
El Salvador	44,036	9.7	3.4	6.3	4,029	9.1
Grenada	983	4.6	4.3	0.4	6	0.6
Guatemala	67,426	9.7	3.2	6.5	6,205	9.2

Haiti	70,013	8.2	4.9	3.3	3,409	4.9
Country name	Total Deaths >14 years old	Mean population weighted annual $PM_{2.5}$ ($\mu g\ m^{-3}$)			Attributable deaths[a]	Mean attributable fraction (%)[b]
		With all emission sources	Without fossil fuel	Estimated fossil fuel $PM_{2.5}$		
Honduras	40,564	7.9	3.5	4.4	2,620	6.5
Jamaica	18,511	9.1	4.7	4.4	1,183	6.4
Mexico	615,874	11.8	2.4	9.5	65,871	10.7
Nicaragua	20,467	5.4	3.5	1.9	614	3.0
Panama	16,364	4.7	2.5	2.2	594	3.6
Puerto Rico	28,717	5.5	4.6	0.9	409	1.4
Saint Lucia	1,191	5	4.8	0.2	4	0.3
Saint Vincent and the Grenadines	913	4.7	4.5	0.2	3	0.3
Trinidad and Tobago	19,561	5.4	4.5	0.9	277	1.4
United States Virgin Islands	1,202	4.6	4.2	0.4	7	0.6
South America						
Argentina	306,979	7.9	3.4	4.5	20,385	6.6
Bolivia	50,854	5.7	4.4	1.3	1,095	2.2
Brazil	1,161,922	8.9	2.9	6.1	94,216	8.1
Chile	108,995	10	2.4	7.6	11,202	10.3
Colombia	247,981	8.2	2.7	5.5	20,045	8.1
Ecuador	74,588	6.7	2.1	4.6	5,357	7.2
Guyana	4,830	8	6.6	1.4	96	2.0
Paraguay	29,665	9.2	6	3.2	1,374	4.6

Peru	120,778	7.3	1.8	5.5	10,209	8.5
Suriname	3,667	6.9	6.2	0.7	36	1.0
Country name	Total Deaths >14 years old	Mean population weighted annual $PM_{2.5}$ ($\mu g\ m^{-3}$)			Attributable deaths[a]	Mean attributable fraction (%)[b]
		With all emission sources	Without fossil fuel	Estimated fossil fuel $PM_{2.5}$		
Uruguay	30,980	6.5	2.4	4.1	1,967	6.3
Venezuela	247,407	10.6	4.3	6.2	21,185	8.6
Europe						
Albania	20,072	19.8	8.6	11.2	2,458	12.2
Andorra	654	13.4	5.8	7.6	65	9.9
Austria	79,627	21.4	4.3	17.1	15,018	18.9
Belarus	115,131	20.6	2.9	17.8	23,397	20.3
Belgium	108,113	25.5	2.8	22.7	25,633	23.7
Bosnia and Herzegovina	36,427	21	6.8	14.2	5,628	15.5
Bulgaria	106,938	20.2	7.2	13	15,346	14.4
Croatia	52,156	20.2	5.6	14.6	8,454	16.2
Cyprus	7,171	15.4	9.2	6.3	543	7.6
Czech Republic	109,205	26.2	3.4	22.8	25,467	23.3
Denmark	51,600	16.3	2.1	14.2	9,202	17.8
Estonia	14,761	12.6	1.6	11	2,227	15.1
Finland	50,553	8.6	1.3	7.3	5,506	10.9
France	562,481	18.1	3.4	14.7	97,242	17.3
Georgia	51,550	23.3	10.2	13.1	6,670	12.9

Germany	896,319	23.9	3.2	20.7	198,569	22.2
Greece	116,757	15.6	8.1	7.5	10,616	9.1
Hungary	128,981	24.7	4.7	20	26,863	20.8
Country name	Total Deaths >14 years old	Mean population weighted annual $PM_{2.5}$ ($\mu g\ m^{-3}$)			Attributable deaths[a]	Mean attributable fraction (%)[b]
		With all emission sources	Without fossil fuel	Estimated fossil fuel $PM_{2.5}$		
Iceland	1,891	2.6	1.6	1	31	1.6
Ireland	30,421	8.3	2	6.4	2,902	9.5
Italy	622,080	18.8	6	12.8	89,412	14.4
Kazakhstan	126,168	17.1	9.2	7.9	11,343	9.0
Latvia	31,672	16.2	2	14.3	5,719	18.1
Lithuania	40,380	21.4	2.3	19.1	8,729	21.6
Malta	3,593	16	11.4	4.6	193	5.4
Moldova	43,245	25.4	5.2	20.2	8,922	20.6
Montenegro	6,223	18	7.9	10.1	724	11.6
Netherlands	143,387	24.2	2.7	21.5	32,972	23.0
Norway	29,299	5.9	1.4	4.5	2,065	7.0
Poland	393,724	26.5	3.1	23.4	93,842	23.8
Portugal	104,738	8.9	3.7	5.2	8,032	7.7
Romania	269,933	23.9	6.2	17.7	49,583	18.4
Russia	1,833,839	19	4.9	14.1	289,922	15.8
Serbia	100,172	24.8	6.9	17.9	18,076	18.0
Slovakia	53,258	24.9	4.1	20.8	11,522	21.6
Slovenia	19,680	21.7	5.3	16.3	3,528	17.9

Spain	418,063	12.9	4.8	8.1	44,603	10.7
Sweden	88,058	10	1.6	8.5	10,548	12.0
Switzerland	62,993	20.3	4.6	15.8	11,196	17.8
Turkey	361,723	18.2	8.1	10.1	41,811	11.6
Country name	Total Deaths >14 years old	Mean population weighted annual $PM_{2.5}$ ($\mu g\ m^{-3}$)			Attributable deaths[a]	Mean attributable fraction (%)[b]
		With all emission sources	Without fossil fuel	Estimated fossil fuel $PM_{2.5}$		
Ukraine	731,672	19.4	5.1	14.3	120,217	16.4
United Kingdom	579,747	15.4	2	13.5	99,069	17.1
Africa						
Algeria	142,304	31.4	20.5	10.9	13,295	9.3
Angola	100,845	15.4	14.1	1.3	1,537	1.5
Benin	42,616	40.4	36.2	4.2	1,450	3.4
Botswana	12,721	8.2	6	2.1	397	3.1
Burkina Faso	84,040	55.9	54.6	1.3	855	1.0
Burundi	44,973	16.2	15.4	0.8	419	0.9
Cameroon	118,759	39.7	38.2	1.5	1,520	1.3
Cape Verde	2,545	66.9	66	0.9	18	0.7
Central African Republic	41,111	30.7	30.1	0.6	178	0.4
Chad	56,523	59.8	58.7	1	460	0.8
Comoros	3,878	1.6	1.4	0.1	9	0.2
Congo	21,705	20.6	19.3	1.3	287	1.3
Cote d'Ivoire	111,211	29.3	28.2	1.1	1,065	1.0

Democratic Republic of the Congo	419,021	21.3	20.7	0.6	2,261	0.5
Djibouti	4,509	21.2	17.5	3.8	164	3.6
Egypt	392,226	56.7	40.2	16.5	46,783	11.9
Equatorial Guinea	4,679	10	9.5	0.5	32	0.7
Eritrea	20,386	31.3	28.5	2.8	444	2.2
Country name	Total Deaths >14 years old	Mean population weighted annual $PM_{2.5}$ ($\mu g\ m^{-3}$)			Attributable deaths[a]	Mean attributable fraction (%)[b]
		With all emission sources	Without fossil fuel	Estimated fossil fuel $PM_{2.5}$		
Ethiopia	287,855	17	15.2	1.8	5,657	2.0
Gabon	13,783	11	10.5	0.5	90	0.7
Gambia	9,610	58	56	2	151	1.6
Ghana	149,177	31.5	28.9	2.6	3,361	2.3
Guinea	63,691	49.7	48.8	1	467	0.7
Guinea-Bissau	9,223	51.9	50.6	1.3	89	1.0
Kenya	219,806	8.3	6.4	2	6,035	2.7
Lesotho	25,223	12.6	7.5	5.1	1,689	6.7
Liberia	19,482	25.3	24.7	0.7	113	0.6
Libya	26,745	42.3	34.3	8	1,565	5.9
Madagascar	97,088	3.7	3.3	0.4	641	0.7
Malawi	83,919	9.9	9.4	0.6	681	0.8
Mali	69,737	60.3	59.3	1	555	0.8
Mauritania	13,520	98.7	97.4	1.3	159	1.2
Mauritius	9,564	1.6	1.3	0.3	43	0.4
Morocco	186,609	23.8	16.9	6.9	12,436	6.7

Mozambique	163,474	6.8	6.3	0.5	1,309	0.8
Namibia	12,923	11.1	10.2	0.9	159	1.2
Niger	63,052	73.3	71.6	1.7	844	1.3
Nigeria	689,902	59.7	54.9	4.8	25,282	3.7
Rwanda	43,547	16.4	15.2	1.2	557	1.3
Sao Tome and Principe	821	5.5	5.4	0.1	2	0.2
Country name	Total Deaths >14 years old	Mean population weighted annual $PM_{2.5}$ ($\mu g\ m^{-3}$)			Attributable deaths[a]	Mean attributable fraction (%)[b]
		With all emission sources	Without fossil fuel	Estimated fossil fuel $PM_{2.5}$		
Senegal	61,877	71.2	69.3	1.8	916	1.5
Seychelles	702	1.5	1.2	0.3	4	0.6
Sierra Leone	33,549	42	41	0.9	230	0.7
Somalia	47,288	9.5	8.3	1.3	789	1.7
South Africa	487,500	21.9	11.7	10.2	45,134	9.3
Sudan[c]	165,624	35.3	33.6	1.7	2,197	1.3
Swaziland	9,954	10.6	6.7	3.9	534	5.4
Tanzania	202,713	6.9	6.4	0.5	1,660	0.8
Togo	34,797	36.6	34.4	2.1	617	1.8
Tunisia	59,521	25.5	17.1	8.3	4,711	7.9
Uganda	127,825	13.1	11.8	1.3	2,018	1.6
Zambia	71,697	12.7	12.2	0.6	511	0.7
Zimbabwe	88,229	10.5	9	1.6	1,797	2.0
Western Asia & the Middle East						

Afghanistan	148,817	20.9	13.9	7	11,153	7.5
Armenia	25,420	22.6	11.9	10.7	2,721	10.7
Azerbaijan	85,764	29.8	17.6	12.2	8,733	10.2
Bahrain	3,315	33.1	30.2	2.9	73	2.2
Iran	330,324	28.5	23.8	4.7	13,168	4.0
Iraq	95,874	30.1	26.4	3.7	2,942	3.1
Israel	40,291	21.2	14.4	6.9	2,776	6.9
Country name	Total Deaths >14 years old	Mean population weighted annual $PM_{2.5}$ ($\mu g\ m^{-3}$)			Attributable deaths[a]	Mean attributable fraction (%)[b]
		With all emission sources	Without fossil fuel	Estimated fossil fuel $PM_{2.5}$		
Jordan	13,031	22.9	16.6	6.2	766	5.9
Kuwait	5,120	37.4	34.4	3	110	2.1
Kyrgyzstan	29,441	17.3	8.4	8.9	3,041	10.3
Lebanon	27,756	18	11.7	6.3	1,931	7.0
Oman	7,482	46.5	40.6	5.8	321	4.3
Palestine	12,562	22.7	15.6	7.1	853	6.8
Qatar	4,252	35.2	31.7	3.5	109	2.6
Saudi Arabia	82,403	32.6	29.6	3	1,893	2.3
Syria	140,751	19.4	12.7	6.7	10,159	7.2
Tajikistan	38,948	21.7	9.6	12.1	4,914	12.6
Turkmenistan	51,096	31.7	26.4	5.3	2,124	4.2
United Arab Emirates	16,636	54	45.8	8.1	1,000	6.0
Uzbekistan	205,829	24.8	12.8	12	23,912	11.6
Yemen	90,616	23	19.9	3.1	2,520	2.8

Eastern Asia						
Bangladesh	692,081	58.9	6.7	52.3	252,927	36.5
Bhutan	2,909	23.6	5.7	17.9	516	17.7
Brunei	1,684	6.1	3.3	2.8	72	4.3
Cambodia	85,803	20.9	11.6	9.2	8,445	9.8
China	9,720,397	72.8	9.9	62.9	3,910,916	40.2
China (2018)[d]	9,720,397	41	9.7	31.2	2,355,579	24.2
Country name	Total Deaths >14 years old	Mean population weighted annual $PM_{2.5}$ ($\mu g\ m^{-3}$)			Attributable deaths[a]	Mean attributable fraction (%)[b]
		With all emission sources	Without fossil fuel	Estimated fossil fuel $PM_{2.5}$		
India	8,009,357	52	9	42.9	2,458,384	30.7
Indonesia	1,495,066	20.9	5.7	15.3	230,097	15.4
Japan	1,284,769	22.6	4.6	18	242,561	18.9
Laos	33,822	19.6	8	11.6	4,404	13.0
Malaysia	154,090	18.9	5.3	13.6	22,228	14.4
Maldives	865	5.9	2.3	3.7	50	5.8
Mongolia	12,013	8.4	4.8	3.5	628	5.2
Myanmar	340,623	16.4	7.4	9	36,978	10.9
Nepal	168,690	38.8	9.5	29.3	39,066	23.2
North Korea	201,841	35.8	5.3	30.5	52,942	26.2
Pakistan	1,115,784	36.7	15.1	21.7	188,406	16.9
Papua New Guinea	63,224	3.1	2.9	0.2	168	0.3
Philippines	559,792	8.7	2.1	6.7	51,203	9.1

Singapore	14,100	21.9	4.9	16.9	2,616	18.6
South Korea	265,641	44	5.3	38.8	80,962	30.5
Sri Lanka	116,032	13.4	3.5	9.9	14,998	12.9
Taiwan	164,488	14.5	3.2	11.3	23,711	14.4
Thailand	418,824	20.6	4.7	15.9	71,184	17.0
Timor-Leste	5,381	6.4	5	1.4	115	2.1
Vietnam	541,064	31.7	4.4	27.4	127,614	23.6

Country name	Total Deaths >14 years old	Mean population weighted annual $PM_{2.5}$ ($\mu g\ m^{-3}$)			Attributable deaths[a]	Mean attributable fraction (%)[b]
		With all emission sources	Without fossil fuel	Estimated fossil fuel $PM_{2.5}$		
Australia & Oceania						
American Samoa	301	0.7	0.7	0	0	0.0
Australia	142,935	4.9	2.4	2.5	5,686	4.0
Federated States of Micronesia	679	0.7	0.7	0	1	0.1
Fiji	5,538	1.3	1.2	0.1	9	0.2
Guam	1,112	1.2	1	0.2	4	0.4
Kiribati	852	0.8	0.8	0	0	0.0
Marshall Islands	336	1.1	1.1	0	0	0.0
New Zealand	29,923	2.2	1.5	0.6	320	1.1
Northern Mariana Islands	249	1.3	1.1	0.3	1	0.4
Samoa	960	0.7	0.7	0	0	0.0

Solomon Islands	3,286	1.2	1.2	0	2	0.1
Tonga	657	1.2	1.1	0.1	1	0.2
Vanuatu	1,791	2.2	2.2	0.1	2	0.1

USA						
State name	Total Deaths >14 years old	Mean population weighted annual $PM_{2.5}$ ($\mu g\ m^{-3}$)			Attributable deaths[a]	Mean attributable fraction (%)[b]
		With all emission sources	Without fossil fuel	Estimated fossil fuel $PM_{2.5}$		
Alabama	50,411	9.4	2.6	6.9	5,067	10.1
Alaska	3,384	2.2	1.4	0.9	51	1.5
Arizona	56,565	7.9	4	3.9	3,263	5.8
Arkansas	26,345	10.3	2.6	7.6	2,887	11.0
California	259,363	12.2	2.4	9.8	34,081	13.1
Colorado	36,885	6.8	3	3.8	2,140	5.8
Connecticut	32,639	12.1	1.7	10.5	4,749	14.6
Delaware	4,436	13.2	1.7	11.5	694	15.6
Florida	191,646	6.6	2.4	4.2	12,483	6.5

Georgia	75,518	11.3	2.5	8.8	9,290	12.3
Hawaii	11,032	2.6	2.1	0.4	83	0.8
Idaho	13,006	6.2	3.3	2.8	581	4.5
Illinois	102,593	16.6	1.9	14.7	18,952	18.5
Indiana	66,979	17	1.9	15.1	12,637	18.9
Iowa	33,378	11.9	2.1	9.8	4,562	13.7
Kansas	33,671	10.4	1.9	8.5	4,094	12.2
Kentucky	52,325	14.3	2	12.4	8,500	16.2
Louisiana	42,176	10.4	2.8	7.5	4,505	10.7
Maine	14,555	7.7	1.6	6.1	1,350	9.3
Maryland	40,784	15.8	1.8	14.1	7,336	18.0
State name	Total Deaths >14 years old	Mean population weighted annual $PM_{2.5}$ ($\mu g\ m^{-3}$)			Attributable deaths[a]	Mean attributable fraction (%)[b]
		With all emission sources	Without fossil fuel	Estimated fossil fuel $PM_{2.5}$		
Massachusetts	53,851	11.8	1.6	10.2	7,654	14.2
Michigan	93,585	16.7	1.8	14.9	17,438	18.6
Minnesota	39,674	13.3	2.2	11.1	5,877	14.8
Mississippi	40,360	10	2.6	7.3	4,263	10.6
Missouri	48,205	11.2	2.1	9.1	6,161	12.8
Montana	9,520	5.1	3.4	1.7	266	2.8
Nebraska	13,881	9	2.1	7	1,432	10.3
Nevada	23,541	6.7	3.4	3.3	1,192	5.1
New Hampshire	12,314	10	1.6	8.3	1,495	12.1
New Jersey	97,747	15.7	1.6	14.1	17,646	18.1

New Mexico	21,308	4.9	2.2	2.7	938	4.4
New York	129,489	14.6	1.6	13	21,931	16.9
North Carolina	95,239	12.5	2.2	10.3	13,357	14.0
North Dakota	4,070	6.9	2	4.9	309	7.6
Ohio	115,955	16.8	1.7	15	21,818	18.8
Oklahoma	40,908	8.7	1.9	6.8	4,190	10.2
Oregon	38,128	8.1	2.4	5.6	3,152	8.3
Pennsylvania	133,771	17.1	1.7	15.4	25,382	19.0
Rhode Island	4,910	10	1.6	8.3	597	12.2
South Carolina	51,014	10.9	2.5	8.4	6,048	11.9
South Dakota	7,036	7.4	2.1	5.4	574	8.2
Tennessee	67,804	11.4	2.1	9.3	8,844	13.0
State name	Total Deaths >14 years old	Mean population weighted annual $PM_{2.5}$ ($\mu g\ m^{-3}$)			Attributable deaths[a]	Mean attributable fraction (%)[b]
		With all emission sources	Without fossil fuel	Estimated fossil fuel $PM_{2.5}$		
Texas	183,885	8.4	1.9	6.4	17,663	9.6
Utah	16,534	6.5	2.7	3.8	981	5.9
Vermont	6,415	9.8	1.6	8.2	770	12.0
Virginia	71,555	13.9	2	11.9	11,206	15.7
Washington	50,955	7.7	2.3	5.4	4,138	8.1
West Virginia	22,500	11	1.9	9.1	2,900	12.9
Wisconsin	59,470	14.7	2	12.7	9,842	16.5
Wyoming	3,642	4.7	2.8	1.9	114	3.1

Canada						
Province name	Total Deaths >14 years old	Mean population weighted annual $PM_{2.5}$ ($\mu g\ m^{-3}$)			Attributable deaths[a]	Mean attributable fraction (%)[b]
		With all emission sources	Without fossil fuel	Estimated fossil fuel $PM_{2.5}$		
Alberta	21,535	8	2	6	1,958	9.1
British Columbia	33,403	8.7	1.9	6.8	3,237	9.7
Manitoba	9,868	7.9	2.7	5.2	778	7.9
New Brunswick	7,095	4.8	1.5	3.4	391	5.5
Newfoundland & Labrador	1,588	2.4	1.4	1	27	1.7
Northwest Territories	172	3.2	2.8	0.4	1	0.6

Nova Scotia	9,158	4.9	1.6	3.3	497	5.4
Nunavut	129	1.2	0.8	0.4	1	0.8
Ontario	90,996	15	1.6	13.4	15,728	17.3
Prince Edward Island	1,269	4.3	1.4	2.9	61	4.8
Quebec	66,494	13.9	1.6	12.3	10,645	16.0
Saskatchewan	8,515	7.5	2.4	5.2	678	8.0
Yukon Territory	193	1.1	0.9	0.3	1	0.5

[a] Annual number of deaths attributed to long term exposure to $PM_{2.5}$ generated by fossil fuel combustion.

[b] Mean proportion of deaths attributed to long term exposure to fossil-fuel related $PM_{2.5}$.

[c] Includes South Sudan

[d] Estimates derived after applying a 43.7 % reduction to $PM_{2.5}$ from all sources for China

CHAPTER 5

SYNTHESIS

5.1 **Summary and Conclusions**

The main research objective of this thesis was the application of a dynamic range of tools and datasets such as Earth observations (EO), ground-based measurements and chemical transport models (1) to determine long-term changes in air quality that provide insight into the impact of rapid economic and population development on air pollution and the efficacy of air quality policies, and (2) to estimate the health burden at different scales ranging from cities to the globe and identify the areas of greatest health burden that can aid policymakers and stakeholders in making informed decisions.

This thesis focused on three research areas, addressing critical research gaps identified in Chapter 1:

- The evaluation of EO of atmospheric composition to assess the skill of these at reproducing temporal variability in surface air pollution for the development of a methodology to determine long-term trends in air quality in cities
- Quantifying long-term trends of the abundance of air pollutants and precursor emissions of short-lived pollutants in emerging megacities in the tropics, statistical determination of the relative contribution of open burning of biomass and anthropogenic activity to these trends, and examining the combined effect of population increase and air pollution on the trends in urban population exposure to these hazardous pollutants
- The application of a chemical transport model and an updated health risk assessment model to determine global premature mortality as a result of exposure to fine particle air pollution from fossil fuel combustion

This thesis uses wide-ranging datasets from in-situ measurements, EO, emission inventories, a chemical transport model, and health risk assessment models. Here, the key research findings in each chapter are summarised along with opportunities for future research.

Chapter 2 evaluated the skill of EO of atmospheric composition in reproducing the monthly variability in surface air pollution in major cities in the UK (London and Birmingham) and India (Delhi and Kanpur). Monthly means of quality assured EO of nitrogen dioxide (NO_2), ammonia (NH_3), formaldehyde (HCHO), and aerosol optical depth (AOD) were sampled for each target city and validated against available reliable surface observations in the UK and India, following careful screening of the surface observations for spurious values. Temporal consistency ($R \geq 0.5$) between tropospheric column and surface NO_2 occurred for all 4 cities and between total column and surface NH_3 occurred at 2 out of 3 rural sites in the UK. Measurements of AOD have poor temporal correlation ($R < 0.4$) with surface fine particulate matter ($PM_{2.5}$), but reproduce the long-term trends in surface $PM_{2.5}$ in both London and Birmingham. This provided the confidence to use satellite observations to determine recent long-term trends in NO_2, NH_3, HCHO as a marker for reactive non-methane volatile organic compounds (NMVOCs) and AOD for $PM_{2.5}$ for the four target cities. Trends in all pollutants (except NH_3 in Kanpur) are positive in the Indian cities suggesting no improvements in air quality despite recent pollution control measures. Trends in all pollutants (with the exception of reactive NMVOCs in London) declined in cities in the UK likely due to successful control on vehicular emissions. Reactive NMVOCs increased by more than 65 % in London during 2012-2018 possibly due to increases in oxygenated VOCs from household products, the food and beverage industry and residential combustion. This is likely to have implications for surface ozone formation which is sensitive to emissions of VOCs in NO_x-saturated London.

This work has demonstrated that EO provide constraints on long-term trends in variability of surface air pollution to determine the efficacy of air quality policies or the effects of rapid unabated development on air quality across an entire city that can't be achieved with the surface monitoring network alone. Our validation results have also been used to interpret the weak temporal consistency between space-based and surface NO_2 in the UK cities during winter (Potts et al., 2021) and our trend results for AOD have been used to interpret the increase in aerosol layer height in India and decrease in Europe (Brakhasi et al., 2021).

Chapter 2 demonstrated the use of EO in regions with extensive surface monitoring networks and in regions with limited surface monitoring capabilities, so that in Chapter 3 these validated EO were used to determine long-term trends in air quality in fast-growing cities in the tropics which are projected to be megacities by 2100 that are in countries yet to implement regulations and setup necessary infrastructure to mitigate air pollution. As in Chapter 2, EO observations of NO_2, NH_3, HCHO and AOD were sampled over the 46 fastest growing cities in the tropics. Most pollutants in almost all tropical cities increase at rates 2-3 times faster than or opposite in direction to reported national and regional trends (Van Damme et al., 2020; Buchholz et al., 2021; Hickman et al., 2021). Crucially, this work identified that emerging anthropogenic sources rather than traditional biomass burning are the cause for the long-term trends. This involved innovative application of statistical techniques to city-wide monthly means for each city and findings were supported by trends in fire activity from a widely used satellite-derived burned area data product. The city-wide trends in emissions of NO_x, NH_3 and reactive NMVOCs are then used to evaluate a contemporary anthropogenic emission inventory (McDuffie et al., 2020). Our results show that trends in emissions from the emission inventory

are generally within 50 % of the satellite observation trends for NO_x, but substantially underestimate observed NH_3 trends by a factor of 2-5. The ozone formation regime in the emerging megacities is also determined, using the standard method of ratios of EO of HCHO and NO_2, to be on a trajectory to transition from being NO_x-sensitive to NO_x-saturated, making it even more difficult to mitigate surface ozone pollution. This is caused by the steep increase in NO_x emissions and muted increase in reactive NMVOCs emissions. The combined effect of rapid increase in population and anthropogenic air pollution is estimated using population data, and annual mean AOD and NO_2 derived using our trends for each city in 2005 and 2018. Increases in absolute population exposure to $PM_{2.5}$ and NO_2 for these cities of up to 23 % a^{-1} for NO_2 and 18 % a^{-1} for $PM_{2.5}$ were obtained and attributed to the combined increase in anthropogenic air pollution and population, suggesting an impending health crisis.

Chapter 4 examined the global mortality associated with $PM_{2.5}$ arising from fossil-fuel combustion using $PM_{2.5}$ simulated with the state-of-the-art chemical transport model GEOS-Chem and the relationship between exposure and premature mortality from a recent meta-analysis of cohort studies (Vodonos et al., 2018). This meta-analysis includes more cohort studies from Asia compared to previous studies, covers a wider range in exposure and age-group, and accounts for more health endpoints than previous studies (Burnett et al., 2014; 2018). This recent meta-analysis estimates higher relative risks than previous models at both very high and very low $PM_{2.5}$ exposures (Vodonos et al., 2018). The meta-analysis was used to calculate the fraction of all-cause premature deaths (population > 14 years old) attributable to $PM_{2.5}$ exposure using the GEOS-Chem $PM_{2.5}$ for 2012. The number of adult premature deaths was estimated using this attributable fraction, country-level age-specific baseline mortality rates and population in each country older than 14 years old, and world population data gridded

at the GEOS-Chem resolution. Fossil-fuel related $PM_{2.5}$ pollution was responsible for 10.2 million adult premature deaths in 2012 with more than 60 % of these deaths in China and India. Substantial reduction in fossil fuel use in China from 2012 to 2018 led to a 38 % decline in premature deaths from 3.9 million in 2012 to 2.4 million in 2018. Our premature mortality estimates are higher than previous studies (Cohen et al., 2017; Burnett et al., 2018; Lelieveld et al., 2019) because we use an updated health risk assessment model and a finer spatial resolution chemical transport model. Relative risk from a previous study (Mehta et al., 2013) was used to estimate that more than 2000 children were affected by lower respiratory infections as a result of exposure to $PM_{2.5}$ from combustion of fossil fuels. This analysis was restricted to North America, South America and Europe, as health risk data was limited to regions with $PM_{2.5} < 25\ \mu g\ m^{-3}$. The results showed that $PM_{2.5}$ from fossil-fuel combustion contributes significantly to the premature mortality burden. $PM_{2.5}$ from fossil-fuel combustion can be readily controlled compared to other sources of $PM_{2.5}$ such as dust or wildfire smoke, as evidenced by the substantial decline in deaths in China.

This work has shown that the greatest premature mortality burden is in areas with substantial fossil fuel related $PM_{2.5}$ and successful pollution control measures can be effective in mitigating these premature deaths. Our premature mortality estimates are more than double those from the Global Burden of Disease (Cohen et al., 2017) emphasizing the urgency to shift to cleaner sources of energy and the need to reliably account for the range of air pollution concentrations and the growing list of health outcomes attributable to air pollution. This work has been used to evidence the global mortality burden related to combustion of fossil fuels (Mendoza et al., 2021; Schmitz et al., 2021) and to stress the health benefits that can be achieved from successful policies (Fears et al., 2021).

5.2 **Opportunities for Future Research**

The TROPOspheric Monitoring Instrument (TROPOMI) was launched in October 2017 and has much higher spatial resolution than its predecessors providing at least 12-20 times more data than the Ozone Monitoring Instrument (OMI). Methods like the oversampling technique (Zhu et al., 2014; 2017) can be used to further enhance the spatial resolution, though with loss in temporal variability, to determine intra-city variability and obtain data for small cities without extending the sampling domain beyond the administrative boundary, as was required in Chapters 2 and 3.

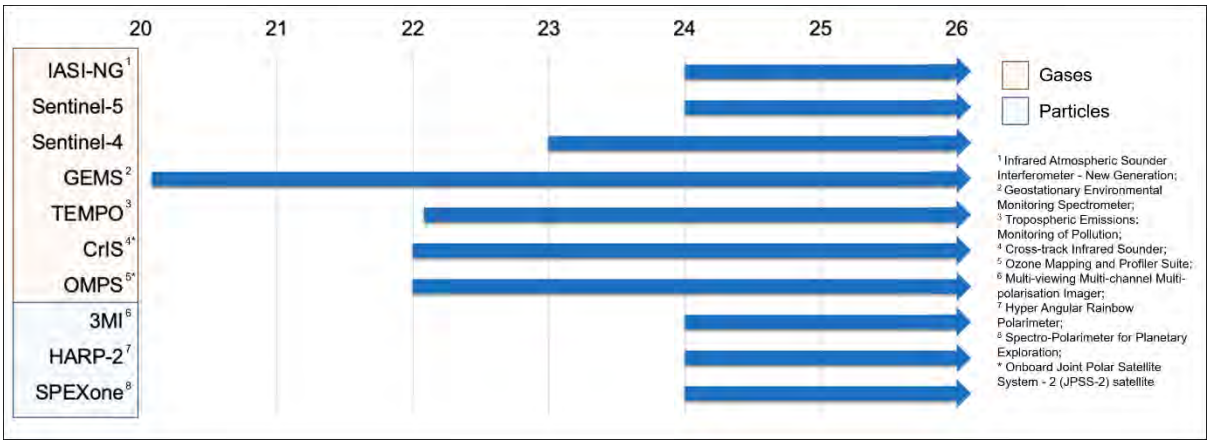

Figure 5.1 Timeline of proposed launch dates of LEO and GEO instruments which will measure trace gases and particles in the future. GEMS launched in 2020.

Figure 5.1 shows the proposed launch dates of upcoming satellite instruments. Future EO missions will sustain the record of low-Earth orbiting (LEO) satellites with operational missions

like Sentinel-5 at relatively fine spatial resolution of 7 km × 7 km (Guhne et al., 2017). This thesis focused on EO from LEO satellites but there will also be observations from satellites in geostationary orbit (GEO). These will monitor a limited domain, but will be able to provide much more temporal information than LEO satellites about the variability of surface air pollution within that domain (Kim et al., 2020). The Geostationary Environment Monitoring Spectrometer (GEMS) was launched in February 2020 and provides observations over East Asia (Kim et al., 2020). GEMS offers data up to every hour during sunlight hours as shown by the wider sampling period of GEMS in Figure 5.2 than the instruments OMI and TROPOMI that pass overhead in the middle of the day only. Future GEO missions include Sentinel-4 over Europe (Courreges-Lacoste et al., 2017) and Tropospheric Emissions: Monitoring of Pollution (TEMPO) over North America (Zoogman et al., 2017) which present an excellent opportunity to extend this assessment of variability in air pollutants, though limited to the northern hemisphere.

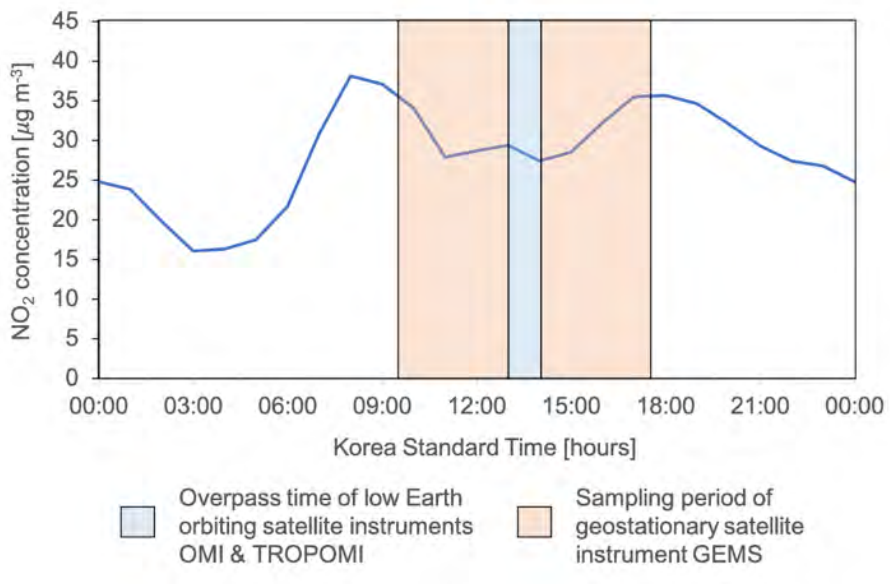

Figure 5.2 Diurnal profile (solid blue line) of NO_2 near Earth's surface and shaded regions denote sampling periods of GEMS (orange) and overpass time of OMI and TROPOMI (blue).

There are also uncertainties inherent in the other EO products used as additional constraints. The burned area product we use in Chapter 3, for example, underestimates the contribution from small fires. The underestimate for Africa is a factor of 8-9 (Ramo et al., 2021). This is likely to affect the size of trend in burned area but not the direction. This is because the trend in burned area is in general consistent with trends in atmospheric composition during the months of biomass burning (Hickman et al., 2021). Currently this new burned area product that better captures the contribution from small fires (Ramo et al., 2021) is only available for 2016 and is limited by the launch date (June 2015) of the high-resolution sensor and so can only provide us with recent short-term variability in burned area.

The meta-analysis used to provide a relationship between long-term exposure to $PM_{2.5}$ and premature mortality in Chapter 4 highlights the dearth of cohort studies at high $PM_{2.5}$ concentrations (>50 μg m^{-3}). More cohort studies at such high concentrations of $PM_{2.5}$ would reduce the uncertainty in the meta-analysis and also the premature mortality estimates. It would also be helpful to have more cohort studies for young children suffering from lower respiratory infections (LRIs) in developing countries, though there are clear logistical and ethical challenges in conducting these studies. This can then be used to obtain a global estimate of LRI cases in young children from combustion of fossil-fuels. The approach to estimate $PM_{2.5}$ concentrations from fossil-fuel combustion and its health impact can also be extended to determine the relative contribution of the individual source sectors that use fossil fuel, such as transport, energy generation and industrial processes. Also relevant is the upstream and downstream processing of fossil fuels prior to combustion.

Future research on improving bottom-up emission inventories using the top-down emission estimates from EO are crucial for better representing these in regions where changes are dramatic due to rapid development or strict regulations. This also has the substantial benefit of improving the emissions in chemical transport models used to better understand atmospheric chemistry and inform policies.

References

Brakhasi, F., Hajeb, M., Mielonen, T., Matkan, A., and Verbesselt, J., Investigating aerosol vertical distribution using CALIPSO time series over the Middle East and North Africa (MENA), Europe, and India: A BFAST-based gradual and abrupt change detection, Remote Sens. Environ., 264, 112619, doi:https://doi.org/10.1016/j.rse.2021.112619, 2021.

Buchholz, R. R., Worden, H. M., Park, M., Francis, G., Deeter, M. N., Edwards, D. P., Emmons, L. K., Gaubert, B., Gille, J., Martinez-Alonso, S., et al., Air pollution trends measured from Terra: CO and AOD over industrial, fire-prone, and background regions, Remote Sens. Environ., 256, doi:10.1016/j.rse.2020.112275, 2021.

Burnett, R., Pope, C. A., Ezzati, M., Olives, C., Lim, S. S., Mehta, S., Shin, H. H., Singh, G., Hubbell, B., Brauer, M., et al., An Integrated Risk Function for Estimating the Global Burden of Disease Attributable to Ambient Fine Particulate Matter Exposure, Environ. Health Persp., 122, 397-403, doi:10.1289/ehp.1307049, 2014.

Burnett, R., Chen, H., Szyszkowicz, M., Fann, N., Hubbell, B., Pope, C. A., Apte, J. S., Brauer, M., Cohen, A., Weichenthal, S., et al., Global estimates of mortality associated with long-term exposure to outdoor fine particulate matter, P. Natl. Acad. Sci. USA, 115, 9592-9597, doi:10.1073/pnas.1803222115, 2018.

Cohen, A. J., Brauer, M., Burnett, R., Anderson, H. R., Frostad, J., Estep, K., Balakrishnan, K., Brunekreef, B., Dandona, L., Dandona, R., et al., Estimates and 25-year trends of the global burden of disease attributable to ambient air pollution: an analysis of data from the Global Burden of Diseases Study 2015, Lancet, 389, 1907-1918, doi:10.1016/S0140-6736(17)30505-6, 2017.

Courreges-Lacoste, G. B., Sallusti, M., Bulsa, G., Bagnasco, G., Veihelmann, B., Riedl, S., Smith, D. J., and Maurer, R., The Copernicus Sentinel 4 mission - A Geostationary Imaging UVN Spectrometer for Air Quality Monitoring, Sensors, Systems, and Next-Generation Satellites Xxi, 10423, doi:10.1117/12.2282158, 2017.

Fears, R., Abdullah, K. A. B., Canales-Holzeis, C., Caussy, D., Haines, A., Harper, S. L., McNeil, J. N., Mogwitz, J., and ter Meulen, V., Evidence-informed policy for tackling adverse climate change effects on health: Linking regional and global assessments of science to catalyse action, Plos Med, 18, doi:ARTN e1003719 10.1371/journal.pmed.1003719, 2021.

Guhne, T., Keim, C., Bartsch, P., Weiss, S., Melf, M., and Seefelder, W., Sentinel-5 Instrument: Status of Design, Performance and Development, Sensors, Systems, and Next-Generation Satellites Xxi, 10423, doi:10.1117/12.2278564, 2017.

Hickman, J. E., Andela, N., Tsigaridis, K., Galy-Lacaux, C., Ossohou, M., and Bauer, S. E., Reductions in NO_2 burden over north equatorial Africa from decline in biomass burning in spite of growing fossil fuel use, 2005 to 2017, Proc. Natl. Acad. Sci. U.S.A., 118, doi:10.1073/pnas.2002579118, 2021.

Kim, J., Jeong, U., Ahn, M. H., Kim, J. H., Park, R. J., Lee, H., Song, C. H., Choi, Y. S., Lee, K. H., Yoo, J. M., et al., New Era of Air Quality Monitoring from Space: Geostationary Environment Monitoring Spectrometer (GEMS), B. Am. Meteorol. Soc., 101, E1-E22, doi:10.1175/Bams-D-18-0013.1, 2020.

Lelieveld, J., Klingmuller, K., Pozzer, A., Burnett, R. T., Haines, A., and Ramanathan, V., Effects of fossil fuel and total anthropogenic emission removal on public health and climate, P. Natl. Acad. Sci. USA, 116, 7192-7197, doi:10.1073/pnas.1819989116, 2019.

McDuffie, E. E., Smith, S. J., O'Rourke, P., Tibrewal, K., Venkataraman, C., Marais, E. A., Zheng, B., Crippa, M., Brauer, M., and Martin, R. V., A global anthropogenic emission inventory of atmospheric pollutants from sector- and fuel-specific sources (1970-2017): an application of the Community Emissions Data System (CEDS), Earth Syst. Sci. Data, 12, 3413-3442, doi:10.5194/essd-12-3413-2020, 2020.

Mehta, S., Shin, H., Burnett, R., North, T., and Cohen, A. J., Ambient particulate air pollution and acute lower respiratory infections: a systematic review and implications for estimating the global burden of disease, Air Qual. Atmos. Health, 6, 69-83, doi:10.1007/s11869-011-0146-3, 2013.

Mendoza, D. L., Benney, T. M., Bares, R., and Crosman, E. T., Intra-city variability of fine particulate matter during COVID-19 lockdown: A case study from Park City, Utah, Environmental Research, 201, 111471, doi:https://doi.org/10.1016/j.envres.2021.111471, 2021.

Potts, D. A., Marais, E. A., Boesch, H., Pope, R. J., Lee, J., Drysdale, W., Chipperfield, M. P., Kerridge, B., Siddans, R., Moore, D. P., et al., Diagnosing air quality changes in the UK during the COVID-19 lockdown using TROPOMI and GEOS-Chem, Environ. Res. Lett., 16, doi:10.1088/1748-9326/abde5d, 2021.

Ramo, R., Roteta, E., Bistinas, I., van Wees, D., Bastarrika, A., Chuvieco, E., and van der Werf, G. R., African burned area and fire carbon emissions are strongly impacted by small fires undetected by coarse resolution satellite data, Proc. Natl. Acad. Sci. U.S.A., 118, doi:10.1073/pnas.2011160118, 2021.

Schmitz, S., Caseiro, A., Kerschbaumer, A., and von Schneidemesser, E., Do new bike lanes impact air pollution exposure for cyclists?-a case study from Berlin, Environ. Res. Lett., 16, doi:ARTN 084031
10.1088/1748-9326/ac1379, 2021.

Van Damme, M., Clarisse, L., Franco, B., Sutton, M. A., Erisman, J. W., Kruit, R. W., van Zanten, M., Whitburn, S., Hadji-Lazaro, J., Hurtmans, D., et al., Global, regional and national trends of atmospheric ammonia derived from a decadal (2008-2018) satellite record, Environ. Res. Lett., doi:10.1088/1748-9326/abd5e0, 2020.

Vodonos, A., Abu Awad, Y., and Schwartz, J., The concentration-response between long-term $PM_{2.5}$ exposure and mortality; A meta-regression approach, Environ. Res., 166, 677-689, doi:10.1016/j.envres.2018.06.021, 2018.

Zhu, L., Jacob, D. J., Mickley, L. J., Marais, E. A., Cohan, D. S., Yoshida, Y., Duncan, B. N., Abad, G. G., and Chance, K. V., Anthropogenic emissions of highly reactive volatile organic compounds in eastern Texas inferred from oversampling of satellite (OMI) measurements of HCHO columns, Environ. Res. Lett., 9, doi:Artn 114004 10.1088/1748-9326/9/11/114004, 2014.

Zhu, L., Jacob, D. J., Keutsch, F. N., Mickley, L. J., Scheffe, R., Strum, M., Abad, G. G., Chance, K., Yang, K., Rappengluck, B., et al., Formaldehyde (HCHO) As a Hazardous Air Pollutant: Mapping Surface Air Concentrations from Satellite and Inferring Cancer Risks in the United States, Environ. Sci. Technol., 51, 5650-5657, doi:10.1021/acs.est.7b01356, 2017.

Zoogman, P., Liu, X., Suleiman, R. M., Pennington, W. F., Flittner, D. E., Al-Saadi, J. A., Hilton, B. B., Nicks, D. K., Newchurch, M. J., Carr, J. L., et al., Tropospheric emissions: Monitoring of pollution (TEMPO), J Quant Spectrosc Ra, 186, 17-39, doi:10.1016/j.jqsrt.2016.05.008, 2017.

APPENDIX:

PEER-REVIEWED ARTICLES

ACCEPTED FOR PUBLICATION

Atmos. Chem. Phys., 21, 6275–6296, 2021
https://doi.org/10.5194/acp-21-6275-2021

Atmospheric Chemistry and Physics
Open Access
EGU

Long-term trends in air quality in major cities in the UK and India: a view from space

Karn Vohra[1], Eloise A. Marais[2,a], Shannen Suckra[1,b], Louisa Kramer[1,c], William J. Bloss[1], Ravi Sahu[3], Abhishek Gaur[3], Sachchida N. Tripathi[3], Martin Van Damme[4], Lieven Clarisse[4], and Pierre-F. Coheur[4]

[1]School of Geography, Earth and Environmental Sciences, University of Birmingham, Birmingham, UK
[2]School of Physics and Astronomy, University of Leicester, Leicester, UK
[3]Department of Civil Engineering, Indian Institute of Technology Kanpur, Kanpur, India
[4]Université libre de Bruxelles (ULB), Spectroscopy, Quantum Chemistry and Atmospheric Remote Sensing (SQUARES), Brussels, Belgium
[a]now at: Department of Geography, University of College London, London, UK
[b]now at: National Environment & Planning Agency, Kingston, Jamaica
[c]now at: Ricardo Energy & Environment, Harwell, UK

Correspondence: Eloise A. Marais (e.marais@ucl.ac.uk)

Received: 8 April 2020 – Discussion started: 26 August 2020
Revised: 11 March 2021 – Accepted: 12 March 2021 – Published: 29 April 2021

Abstract. Air quality networks in cities can be costly and inconsistent and typically monitor a few pollutants. Space-based instruments provide global coverage spanning more than a decade to determine trends in air quality, augmenting surface networks. Here we target cities in the UK (London and Birmingham) and India (Delhi and Kanpur) and use observations of nitrogen dioxide (NO_2) from the Ozone Monitoring Instrument (OMI), ammonia (NH_3) from the Infrared Atmospheric Sounding Interferometer (IASI), formaldehyde (HCHO) from OMI as a proxy for non-methane volatile organic compounds (NMVOCs), and aerosol optical depth (AOD) from the Moderate Resolution Imaging Spectroradiometer (MODIS) for $PM_{2.5}$. We assess the skill of these products at reproducing monthly variability in surface concentrations of air pollutants where available. We find temporal consistency between column and surface NO_2 in cities in the UK and India ($R = 0.5$–0.7) and NH_3 at two of three rural sites in the UK ($R = 0.5$–0.7) but not between AOD and surface $PM_{2.5}$ ($R < 0.4$). MODIS AOD is consistent with AERONET at sites in the UK and India ($R \geq 0.8$) and reproduces a significant decline in surface $PM_{2.5}$ in London ($2.7\,\%\,a^{-1}$) and Birmingham ($3.7\,\%\,a^{-1}$) since 2009. We derive long-term trends in the four cities for 2005–2018 from OMI and MODIS and for 2008–2018 from IASI. Trends of all pollutants are positive in Delhi, suggesting no air quality improvements there, despite the roll-out of controls on industrial and transport sectors. Kanpur, identified by the WHO as the most polluted city in the world in 2018, experiences a significant and substantial ($3.1\,\%\,a^{-1}$) increase in $PM_{2.5}$. The decline of NO_2, NH_3, and $PM_{2.5}$ in London and Birmingham is likely due in large part to emissions controls on vehicles. Trends are significant only for NO_2 and $PM_{2.5}$. Reactive NMVOCs decline in Birmingham, but the trend is not significant. There is a recent (2012–2018) steep ($> 9\,\%\,a^{-1}$) increase in reactive NMVOCs in London. The cause for this rapid increase is uncertain but may reflect the increased contribution of oxygenated volatile organic compounds (VOCs) from household products, the food and beverage industry, and domestic wood burning, with implications for the formation of ozone in a VOC-limited city.

1 Introduction

More than 55 % of people live in urban areas, and this is projected to increase to 68 % by 2050 (UN, 2019). Air pollution in cities routinely exceeds levels safe for human health (Landrigan et al., 2018). Regulatory air quality monitoring networks, such as those employed in cities in the UK and India, provide detailed data concerning individual species and spe-

cific locations but are labour-intensive to operate and maintain, with potential gaps in spatial coverage and discontinuities hindering longer term trend discovery. Here we assess the ability to use the long record of satellite observations of atmospheric composition to monitor long-term trends in surface air quality in cities in the UK (London, Birmingham) and India (Delhi, Kanpur) of variable size, at a range of development stages, and with air pollutant concentrations that pose a greater risk to health than previously thought (Vodonos et al., 2018; Vohra et al., 2021).

Our study focuses on two large cities in the UK (London and Birmingham) and two in India (Delhi and Kanpur). Each is at a different stage of development: London is well developed, Birmingham is undergoing urban renewal, Delhi is experiencing rapid development (Singh and Grover, 2015), and Kanpur is a rapidly industrialising city (World Bank, 2014). Air quality policy is well established in the UK, and the rapid decline in regulated air pollutants and their precursors has been monitored since 1970. According to the National Atmospheric Emission Inventory (NAEI), precursor emissions of fine particles with aerodynamic diameter $< 2.5\,\mu m$ ($PM_{2.5}$) decreased in 1970–2017 by $1.5\,\%\,a^{-1}$ for nitrogen oxides ($NO_x \equiv NO + NO_2$), $2.0\,\%\,a^{-1}$ for sulfur dioxide (SO_2), and $1.4\,\%\,a^{-1}$ for non-methane volatile organic compounds (NMVOCs). Primary $PM_{2.5}$ emissions decreased by $1.6\,\%\,a^{-1}$ over the same time period compared to a decline of just $0.2\,\%\,a^{-1}$ for ammonia (NH_3) emissions during 1980–2017 (Defra, 2019a). In UK cities, vehicles make a large contribution to air pollution year-round, with seasonal contributions from residential fuelwood burning, agricultural activity, and construction and sporadic contributions from the long-range transport of Saharan dust (Fuller et al., 2014; Crilley et al., 2015; 2017; Harrison et al., 2018; Ots et al., 2018; Carnell et al., 2019). Despite the decline in emissions, many areas in the UK still exceed the legal annual mean limit of NO_2 of $40\,\mu g\,m^{-3}$ (Barnes et al., 2018), a threshold that may not adequately protect against the health effects of long-term exposure to NO_2 (Lyons et al., 2020). Many areas will also exceed the annual mean $PM_{2.5}$ standard, if updated from 25 to $10\,\mu g\,m^{-3}$, according to the WHO guideline (Defra, 2019b). Reported annual mean $PM_{2.5}$ in 2016, obtained as the surface monitoring network average, is $12\,\mu g\,m^{-3}$ for London and $10\,\mu g\,m^{-3}$ for Birmingham (WHO, 2018). There is increasing concern over emissions of the important $PM_{2.5}$ precursor, NH_3, as there are no direct controls on the agricultural sector, the dominant NH_3 source (Carnell et al., 2019). There has even been a recent increase in NH_3 emissions of $1.9\,\%\,a^{-1}$ in 2013–2017 (Defra, 2019a), attributed to agriculture (Carnell et al., 2019).

Air quality policy in India is in its infancy compared to the UK. The first air pollution act was passed in 1981, 30 years after the equivalent in the UK. There has been a steady roll-out of European-style (Euro VI) vehicle emission standards, starting with Delhi in 2018 and scaling up to the whole country by 2020 (Govt. of India, 2016). Strict controls on coal-fired power plants have been in place since December 2015, but most power plants are non-compliant (Sugathan et al., 2018). National $PM_{2.5}$ concentration targets have been set at 20 %–30 % reductions by 2024 relative to 2017 levels (Govt. of India, 2019), but in 2016, measured annual mean $PM_{2.5}$ in Delhi and Kanpur exceeded the national standard ($40\,\mu g\,m^{-3}$) by about a factor of 4 : $143\,\mu g\,m^{-3}$ for Delhi and $173\,\mu g\,m^{-3}$ for Kanpur (WHO, 2018). In Delhi and Kanpur, year-round emissions are dominated by vehicles, construction, and household biofuel use in the city and industrial activity and coal combustion nearby (Guttikunda and Jawahar, 2014; Venkataraman et al., 2018). Seasonal enhancements come from intense agricultural fires along the Indo-Gangetic Plain (IGP) north of Delhi, frequent firework festivals, and dust storms originating from the Thar Desert and Arabian Peninsula (Ghosh et al., 2014; Parkhi et al., 2016; Yadav et al., 2017; Cusworth et al., 2018; Liu et al., 2018). Like the UK, the agricultural sector is not directly regulated, and intense agricultural activity in the IGP contributes to the largest global NH_3 hotspot (Warner et al., 2017; Van Damme et al., 2018; T. Wang et al., 2020).

Surface monitoring networks in cities in the UK and India needed to evaluate citywide trends in air pollutant concentrations and precursor emissions can be exceedingly sparse and are often short-term. To illustrate this, we show in Fig. 1 the coverage of surface sites in the four cities that continuously monitor NO_2, the most widely monitored air pollutant in both countries. There are also diffusion tubes and emerging technologies that measure NO_2 at low cost, but these are susceptible to biases (Heal et al., 1999; Castell et al., 2017) and so are excluded. The points in Fig. 1 show sites established and maintained by national agencies, local city councils, and academic institutions. These are coloured by multi-year mean NO_2 around the satellite midday overpass (12:00–15:00 local time or LT) for our period of interest (2005–2018). London has the most extensive surface coverage. There can be more than 100 sites operating simultaneously, but many of these are short-term. Most long-term sites are in central London, and southeast London is devoid of stations. Birmingham has eight monitoring stations, but only two operated for the majority of 2005–2018. There are recently established comprehensive air quality monitoring sites in London and Birmingham, but these started operating in late 2018. More than 40 % of the NO_2 monitoring stations in Delhi were established in 2018, and there are concerns over data access and quality (Cusworth et al., 2018). Fewer stations in the four cities monitor $PM_{2.5}$ than NO_2, and measurements of NMVOCs are limited to a few short-term intensive campaigns and long-term sites that only measure light (short-chain) non-methane hydrocarbons. Long-term continuous monitoring of NH_3 in the UK is limited to hourly measurements at rural European Monitoring and Evaluation Programme (EMEP) sites (Fig. 1) and monthly measurements at UK Eutrophying and Acidifying Pollutants (UKEAP) network sites.

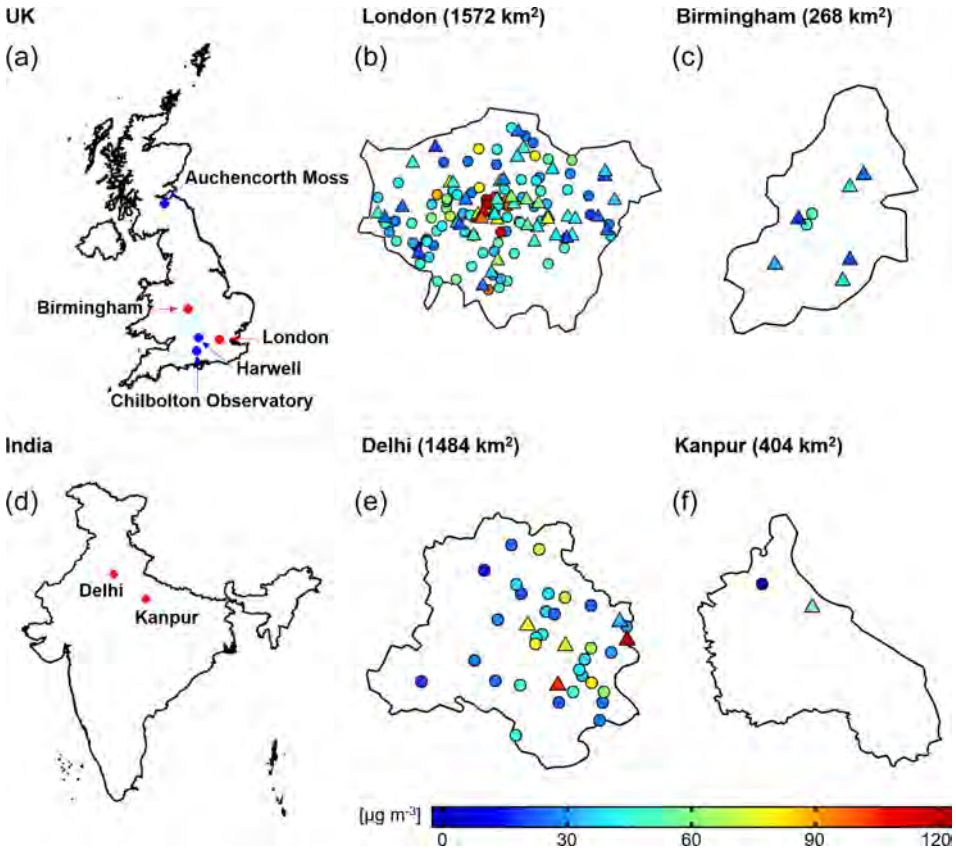

Figure 1. Spatial extent of surface NO_2 monitoring stations in London **(b)**, Birmingham **(c)**, Delhi **(e)**, and Kanpur **(f)**. Panels **(a)** and **(d)** show the location of the target cities (red) and UK sites that are part of the European Monitoring and Evaluation Programme (EMEP) (blue). Panels **(b)**, **(c)**, **(e)**, and **(f)** show the locations of local authority regulatory NO_2 monitoring stations within the administrative boundaries of each city, coloured by mean midday NO_2 for 2005–2018 and separated into sites used (triangles) and not used (circles) to assess satellite observations of NO_2 (see text for details). The surface area of each city is indicated. Country and city boundaries are from GADM version 3.6 (GADM, 2018) and DataMeet (DataMeet, 2018).

Satellite observations of atmospheric composition (Earth observations) provide consistent, long records (> 10 years) and global coverage of multiple air pollutants, complementing surface monitoring networks with limited spatial coverage and temporal records (Streets et al., 2013; Duncan et al., 2014). These have been used extensively as constraints on temporal changes in surface concentrations of air pollutants and precursor emissions (Kim et al., 2006; Lamsal et al., 2011; Zhu et al., 2014) but typically just targeting one–two pollutants. In this work, we consider Earth observations of NO_2, formaldehyde (HCHO), NH_3, and aerosol optical depth (AOD). HCHO is a prompt, high-yield, ubiquitous oxidation product of NMVOCs used as a constraint on NMVOCs emissions (Miller et al., 2008; De Smedt et al., 2010; Marais et al., 2012, 2014a, b). AOD has been used to derive surface concentrations of $PM_{2.5}$ for the global assessment of the impact of air pollution on health (van Donkelaar et al., 2006, 2010, Brauer et al., 2016; Anenberg et al., 2019).

Here we conduct a systematic evaluation of the ability of satellite observations of NO_2, NH_3, HCHO, and AOD to reproduce the temporal variability of surface air pollution in the UK and India before going on to apply these satellite observations to estimate long-term changes in air pollution to assess the efficacy of air quality policies in the four cities of interest.

2 Space-based and surface air quality observations

Earth observations of NO_2 and HCHO are from the Ozone Monitoring Instrument (OMI), NH_3 from the Infrared Atmospheric Sounding Interferometer (IASI), and AOD from the Moderate Resolution Imaging Spectroradiometer (MODIS). There are also observations of SO_2 and the secondary pollutant ozone from OMI, but SO_2 is below or close to the detection limit year-round for all cities, except in some months in Delhi, and UV measurements of tropospheric column ozone have limited sensitivity to ozone in the boundary layer (Zoogman et al., 2011). TROPOspheric Monitoring Instrument (TROPOMI) sensitivity to SO_2 is 4-fold bet-

ter than OMI, but the observation record is short (October 2017 launch) (Theys et al., 2019). We use hourly observations of NO_2 and $PM_{2.5}$ from the network of surface sites in the four target cities and NH_3 from the rural EMEP sites in the UK, to assess whether satellite observations of NO_2, AOD, and NH_3 reproduce temporal variability of surface air quality. There are no direct reliable measurements of HCHO in the UK, and measurements of NMVOCs are limited to a few sites that only measure light ($\leq$ C9) hydrocarbons.

Figure 1 shows locations of EMEP sites in Harwell, England, south of Oxford (51.57° N, 1.32° W), Chilbolton Observatory, England, 65 km south of Harwell (51.15° N, 1.44° W), and Auchencorth Moss, Scotland, south of Edinburgh (55.79° N, 3.24° W) (Malley et al., 2015, 2016; Walker et al., 2019). Instruments at the Harwell site were relocated to Chilbolton Observatory in 2016, providing the opportunity to assess the satellite data at sites with distinct agricultural activity and anthropogenic influence (Walker et al., 2019). There are also passive NH_3 samplers in the UK, but these have coarse temporal (monthly) resolution (Tang et al., 2018) and no temporal correlation ($R < 0.1$) with a previous version of the IASI NH_3 product (Van Damme et al., 2015).

2.1 Surface monitoring networks in the UK and India

Surface sites in the UK with continuous (hourly) observations of air pollutants typically use chemiluminescence instruments for NO_2, ion chromatography instruments for NH_3 (Stieger et al., 2018), and a range of reference instruments for PM_{10} and $PM_{2.5}$. Sites used here in London and Birmingham are from the national Department for Environment, Food and Rural Affairs (Defra) Automatic Urban and Rural Network (AURN) (https://uk-air.defra.gov.uk/data/data_selector; last access: 28 January 2020) with additional sites in London from the King's College London Air Quality Network (LAQN) (https://www.londonair.org.uk/london/asp/datadownload.asp; last access: 9 March 2019) and in Birmingham from Ricardo Energy & Environment (https://www.airqualityengland.co.uk/local-authority/data?la_id=407; last access: 24 January 2020) and Birmingham City Council. Observations at the UK EMEP sites are from the EMEP Chemical Coordinating Centre (http://ebas.nilu.no/; last access: 9 March 2019). Measurements in India are limited to NO_2, PM_{10}, and $PM_{2.5}$ monitoring sites maintained in Delhi by the Central Pollution Control Board (CPCB), India Meteorological Department (IMD), and Delhi Pollution Control Committee (DPCC) and in Kanpur by the Uttar Pradesh Pollution Control Board (UPPCB) and the Indian Institute of Technology (IIT) Kanpur (Gaur et al., 2014). $PM_{2.5}$ measurements at IIT Kanpur form part of the international Surface Particulate Matter Network (SPARTAN) (Snider et al., 2015; Weagle et al., 2018). Data from CPCB, IMD, DPCC, and UPPCB were downloaded from the CPCB site (https://app.cpcbccr.com/ccr/#/caaqm-dashboard/caaqm-landing; last access: 5 February 2020). NASA AErosol RObotic NETwork (AERONET) sun photometer AOD measurements (version 3.0, Level 2.0; https://aeronet.gsfc.nasa.gov/; last access: 5 February 2020) are used to validate MODIS AOD at Chilbolton (UK) and Kanpur (India) (Holben et al., 1998; Giles et al., 2019).

2.2 Earth observations of air pollution

OMI on board the NASA Aura satellite, launched in October 2004, has a nadir spatial resolution of 13 km × 24 km and a swath width of 2600 km and passes overhead twice each day. OMI is a UV–visible spectrometer and so only provides daytime observations (13:30 LT). Global coverage was daily in 2005–2009 and is every 2 d thereafter due to the row anomaly (http://omi.fmi.fi/anomaly.html, last access: 8 March 2020). We use the operational NASA OMI Level 2 product of tropospheric column NO_2 for 2005–2018 (version 3.0; https://doi.org/10.5067/Aura/OMI/DATA2017; last access: 29 February 2020) (Krotkov et al., 2017). Total columns of HCHO are from the Quality Assurance for Essential Climate Variables (QA4ECV) OMI Level 2 product for 2005–2018 (version 1.1; https://doi.org/10.18758/71021031; last access: 15 February 2020) (De Smedt et al., 2018). We remove OMI NO_2 scenes with cloud radiance fraction $\geq$ 50 %, terrain reflectivity $\geq$ 30 %, and solar zenith angle (SZA) $\geq$ 85° (Lamsal et al., 2010) and OMI HCHO scenes with processing errors and processing quality flags not equal to zero (De Smedt et al., 2017). This removes scenes with cloud radiance fraction $>$ 60 % and SZA $>$ 80°. We apply additional filtering to remove scenes with cloud radiance fraction $\geq$ 50 % to be consistent with the threshold applied to OMI NO_2. This additional filtering removes 16 % of the data for London, 19 % for Birmingham, 7 % for Delhi, and 8 % for Kanpur.

IASI on the polar sun-synchronous Metop-A satellite, launched in October 2006, is an infrared instrument with a morning (09:30 LT) and nighttime (21:30 LT) overpass. It provides global coverage twice a day with circular 12 km diameter pixels at nadir and a swath width of 2200 km. We use observations for the morning only, when the thermal contrast and sensitivity to the boundary layer are greatest (Clarisse et al., 2010; Van Damme et al., 2014). We use the Level 2 reanalysis product of total column NH_3 (version 3R) obtained with consistent meteorology (ERA5) for clear-sky conditions (cloud fraction $<$ 10 %) (Van Damme et al., 2020). The earlier IASI NH_3 product version (version 2R) was shown to be consistent with ground-based measurements of total column NH_3 at nine global sites (Dammers et al., 2016).

The MODIS sensor on board NASA's Aqua satellite, launched in May 2002, has a swath width of 2330 km, crosses the Equator at 13:30 LT, and provides near-daily global coverage. We use the Level 2 Collection 6.1 Dark Target daily AOD product at 550 nm and 3 km resolution (Remer et al., 2013; Wei et al., 2019) (https://ladsweb.modaps.eosdis.nasa.gov/; last access: 29 February 2020). We use only the highest

quality AOD data (quality assurance flag of 3) (Munchak et al., 2013; Remer et al., 2013; Gupta et al., 2018).

3 Consistency between Earth observations and surface air pollution

Earth observation products retrieve column densities of pollutants throughout the atmospheric column (total for HCHO, AOD and NH_3; troposphere for NO_2) and are compared in what follows to surface concentrations from the surface monitoring network sites. This is to evaluate whether monthly variability in the column reproduces variability in surface concentrations before going on to use the satellite observations to quantify long-term trends in air pollution in the four cities. The majority of the enhancement in the column, with the exception of events like long-range transport, is near the surface (Fishman et al., 2008; Duncan et al., 2014). Sources of errors in retrieval of HCHO and NO_2 column densities include uncertainties in simulated vertical profiles and the presence of clouds and aerosols (Boersma et al., 2004; Lin et al., 2015; Zhu et al., 2016; Silvern et al., 2018). Retrieval of NH_3 column densities from IASI relies on thermal contrast between the Earth's surface and atmosphere and a sufficiently large training dataset (Whitburn et al., 2016; Van Damme et al., 2017). Errors in retrieval of AOD include uncertainties in aerosol properties and atmospheric conditions in matching simulated and observed top-of-atmosphere radiances from single viewing angle instruments like MODIS (Remer et al., 2005; Levy et al., 2007, 2013). To the extent that errors are random, these are reduced with temporal and spatial averaging.

In what follows, city-average OMI NO_2 and MODIS AOD are compared to representative city-average surface concentrations of NO_2 in all four cities and $PM_{2.5}$ in London and Birmingham. IASI NH_3 is compared to coincident surface observations of NH_3 at UK EMEP sites (Fig. 1).

3.1 Assessment of OMI NO_2

Data for NO_2 in the UK include 152 monitoring sites in London, 8 in Birmingham, 37 in Delhi, and 2 in Kanpur (Fig. 1). The data we use for London and Birmingham have been independently ratified, but we still find and remove spurious NO_2 observations. These include persistent (> 24 h) low ($< 1\,\mu g\,m^{-3}$) values that do not exhibit diurnal variability. This occurs at fewer than 10 % of the sites and accounts for at most 1 % of the data at these sites. We identified that NO_2 data from DPCC and CPCB (Delhi) and from UPPCB (Kanpur) networks are inconsistently reported in either parts per billion by volume (ppbv) or micrograms per cubic metre ($\mu g\,m^{-3}$). As information on the units of the individual data is not provided, we determine whether NO_2 is reported in ppbv or $\mu g\,m^{-3}$ by regressing total NO_x (reported throughout in ppbv, following the CPCB protocol; CPCB, 2015) against the sum of the reported NO and NO_2. We identify that NO_2 reported in ppbv (29 % of DPCC, 10 % of CPCB and 74 % of UPPCB data) populates along the 1:1 line, and so we convert these data to $\mu g\,m^{-3}$ using $1.88\,\mu g\,m^{-3}$ ppbv^{-1}. The same unit inconsistency does not exist for the IMD NO_2 data. These are reported throughout in ppbv and so are converted to $\mu g\,m^{-3}$.

We only consider surface observations coincident with the OMI record (2005–2018), around the satellite overpass (12:00–15:00 LT). We find that NO_2 declines at most sites in London (ranging from $-0.8\,\%\,a^{-1}$ to $-3.6\,\%\,a^{-1}$) and Birmingham ($-1.1\,\%\,a^{-1}$ to $-3.8\,\%\,a^{-1}$), with the exception of a few sites influenced by local sources. These include Marylebone Road in central London and Moor Street in Birmingham city centre. Both are impacted by dense traffic and development projects (Carslaw et al., 2016; Harrison and Beddows, 2017). We find that NO_2 increases in Moor Street by $6.8\,\%\,a^{-1}$ from 2013 to 2017. There are too few long-term sites in Delhi and Kanpur to determine trends at individual sites. We do not filter out sites based on site classification, as this information is not readily available for sites in India. Instead, we remove sites influenced by local effects and not consistent with month-to-month variability representative of the city. This we do by detrending surface NO_2 at each site, cross-correlating the detrended data for each site and selecting sites with consistent month-to-month variability ($R > 0.5$) in the detrended data. The original surface NO_2 (including the trend) at the selected sites is then used to obtain city-average monthly mean NO_2 for comparison to OMI NO_2.

The selected sites are shown as triangles in Fig. 1. Filtering for spurious data and selection of consistent sites leads to 14 years of data at 46 sites in London, 5.5 years of data at 6 sites in Birmingham, and 8 years of data at 5 sites in Delhi. There are only 2 sites in Kanpur, but these are not consistent for the brief period of overlap ($R < 0.5$ for 2011–2012), so we choose the site with the longest record (2011–2018). For the period of overlap for London and Birmingham (2011–2016), mean city-average midday NO_2 is $42.8\,\mu g\,m^{-3}$ for London and $26.5\,\mu g\,m^{-3}$ for Birmingham. For Delhi and Kanpur (2011–2018 overlap), mean city-average midday NO_2 is $91.9\,\mu g\,m^{-3}$ for Delhi and $48.4\,\mu g\,m^{-3}$ for Kanpur.

We sample satellite observations within the administrative boundaries of the four cities (Fig. 1) to capture the domain that policymakers would target and assess. This is extended a few kilometres beyond the administrative boundary for Birmingham, as otherwise there are too few observations due to frequent clouds and small city size ($\sim 300\,km^2$). Error-weighted OMI NO_2 monthly means are estimated for individual pixels centred within the administrative boundaries (including 6.5 km beyond for Birmingham). Months with $<$ five observations are removed. The number of months retained is 77 % for Birmingham, > 90 % for London, and > 95 % for Delhi and Kanpur.

Figure 2 compares OMI and surface NO_2. The comparison for London and Birmingham is divided into months excluding winter (December–February) and winter months only. Factors that contribute to seasonality in the relationship between tropospheric column and surface NO_2 in locations with large seasonal shifts in temperature and solar insolation include reduced photolysis rates, leading to longer NO_x lifetime in winter than summer (Boersma et al., 2009; Kenagy et al., 2018; Shah et al., 2020) and a lower mixed layer height in winter than summer contributing to accumulation of pollution. Maximum mixed layer height for London is 900 m in winter compared to 1500 m in summer (Kotthaus and Grimmond, 2018). The slope for Birmingham in winter (0.43×10^{15} molecules cm^{-2} $(\mu g\, m^{-3})^{-1}$) is steeper than that for non-winter months (0.27×10^{15} molecules cm^{-2} $(\mu g\, m^{-3})^{-1}$), but the difference is not significant. The surface NO_2 measurements are also susceptible to interferences (positive biases) from thermal decomposition of NO_x reservoir compounds, such as peroxyacetyl nitrates in chemiluminescence instruments that use heated molybdenum catalysts (Dunlea et al., 2007; Reed et al., 2016). The effect is worse in winter than summer in London and Birmingham due to the abundance of NO_x reservoir compounds in winter (Lamsal et al., 2010). OMI and surface NO_2 monthly variability is consistent ($R = 0.51$–0.71), except for London in winter ($R = 0.33$). The correlation degrades ($R = 0.40$ for London, $R = 0.54$ for Birmingham) if all months are considered. The seasonal dependence of the relationship between satellite and surface NO_2 affects the ability to use OMI NO_2 to infer seasonality in the underlying NO_x emissions. The same consistency in monthly mean OMI and surface NO_2 in non-winter months ($R \geq 0.6$) has also been found over the UK city of Leicester (surface area 73 km^2) (Kramer et al., 2008). Data for all months are used for Delhi and Kanpur, as there is less variability in mixed layer height in India than the UK. Seasonal mean maximum planetary boundary layer height in Delhi varies from 1200 m in winter to 1400 m during monsoon months (Nakoudi et al., 2019). Month-to-month variability in tropospheric column and surface NO_2 (Fig. 2) is consistent in Delhi ($R = 0.55$) and Kanpur ($R = 0.52$). OMI NO_2 exhibits much greater variability for an increment change in surface NO_2 in the UK than in India, resulting in order-of-magnitude lower slopes for Delhi and Kanpur (0.033 and 0.039×10^{15} molecules cm^{-2} $(\mu g\, m^{-3})^{-1}$) than for London and Birmingham (0.35 and 0.27×10^{15} molecules cm^{-2} $(\mu g\, m^{-3})^{-1}$) (Fig. 2). This difference is likely due to a combination of representativeness of surface sites and systematic biases in the OMI NO_2 retrieval. In Delhi, the proportion of sites used in Fig. 2 that measure the relatively lower concentration range of NO_2 (annual mean $NO_2 < 50\, \mu g\, m^{-3}$) is just 20 % compared to 74 % for London, leading to a positive bias in city-average surface NO_2 in Delhi. In Kanpur, we use only one site located 600 m from a national motorway. Aerosols are not explicitly accounted for in the OMI NO_2 retrieval (Krotkov et al., 2017). For very polluted cities like Delhi and Kanpur, this can lead to an ~ 20 % underestimate in OMI NO_2 (Choi et al., 2020; Vasilkov et al., 2020).

3.2 Assessment of IASI NH_3

Figure 3 compares monthly mean IASI and surface NH_3 at the three UK EMEP sites. IASI is sampled up to 20 km around the surface site following the approach of Dammers et al. (2016), and surface observations are sampled around the IASI morning overpass (08:00–11:00 LT) on days with coincident IASI observations. As with NO_2, only months with more than five observations are used. A total of 38 % of months are retained for Auchencorth Moss, 62 % for Harwell, and 61 % for Chilbolton Observatory. For the months retained, average NH_3 is 1.6 µg nitrogen (N) m^{-3} for Auchencorth Moss, 2.5 µg N m^{-3} for Harwell and 6.1 µg N m^{-3} for Chilbolton Observatory. Chilbolton is southwest of mixed farmland, contributing to levels of NH_3 about 3 times higher than at Harwell (Walker et al., 2019). Harwell has a more dynamic range in NH_3 and stronger correlation ($R = 0.69$) than the other two sites ($R = 0.37$ for Auchencorth Moss; $R = 0.50$ for Chilbolton Observatory). Weak correlation at Auchencorth Moss may be because surface NH_3 concentrations are near the instrument detection limit (monthly mean $NH_3 < 2.0\, \mu g\, N\, m^{-3}$) and also because of low thermal contrast between the surface and overlying atmosphere (Van Damme et al., 2015; Dammers et al., 2016). The slope for Auchencorth Moss (4.02×10^{15} molecules cm^{-2} $(\mu g\, N\, m^{-3})^{-1}$) is steeper than the slopes observed at sites with greater surface concentrations of NH_3 (Harwell = 2.23×10^{15} molecules cm^{-2} $(\mu g\, N\, m^{-3})^{-1}$ and Chilbolton = 2.07×10^{15} molecules cm^{-2} $(\mu g\, N\, m^{-3})^{-1}$). Steeper slopes for sites with relatively low NH_3 concentrations are consistent with the assessment of earlier IASI NH_3 product versions (Van Damme et al., 2015; Dammers et al., 2016).

3.3 Assessment of MODIS AOD

Figure 4 compares city-average monthly means of MODIS AOD and $PM_{2.5}$ for London in 2009–2018 and for Birmingham in 2009–2017. We use $PM_{2.5}$ data from 24 sites in London and 8 sites in Birmingham. We add 2 more Birmingham sites by deriving $PM_{2.5}$ from PM_{10} at 2 sites with only PM_{10} measurements. We use a conversion factor of 0.85 ($PM_{2.5} = 0.85 \times PM_{10}$) that we obtain from the slope of SMA regression of hourly $PM_{2.5}$ and PM_{10} at 6 sites in Birmingham with both measurements. We use a similar approach as applied to NO_2 to assess AOD. Only surface observations around the satellite overpass (12:00–15:00 LT) and with consistent detrended month-to-month variability ($R > 0.5$) are retained to obtain citywide monthly mean $PM_{2.5}$. This results in 20 sites in London for 2009–2018 and 5 sites in Birmingham for 2009–2017. Mean midday city-average $PM_{2.5}$ for the period of overlap (2009–2017) is 13.7 µg m^{-3} in Lon-

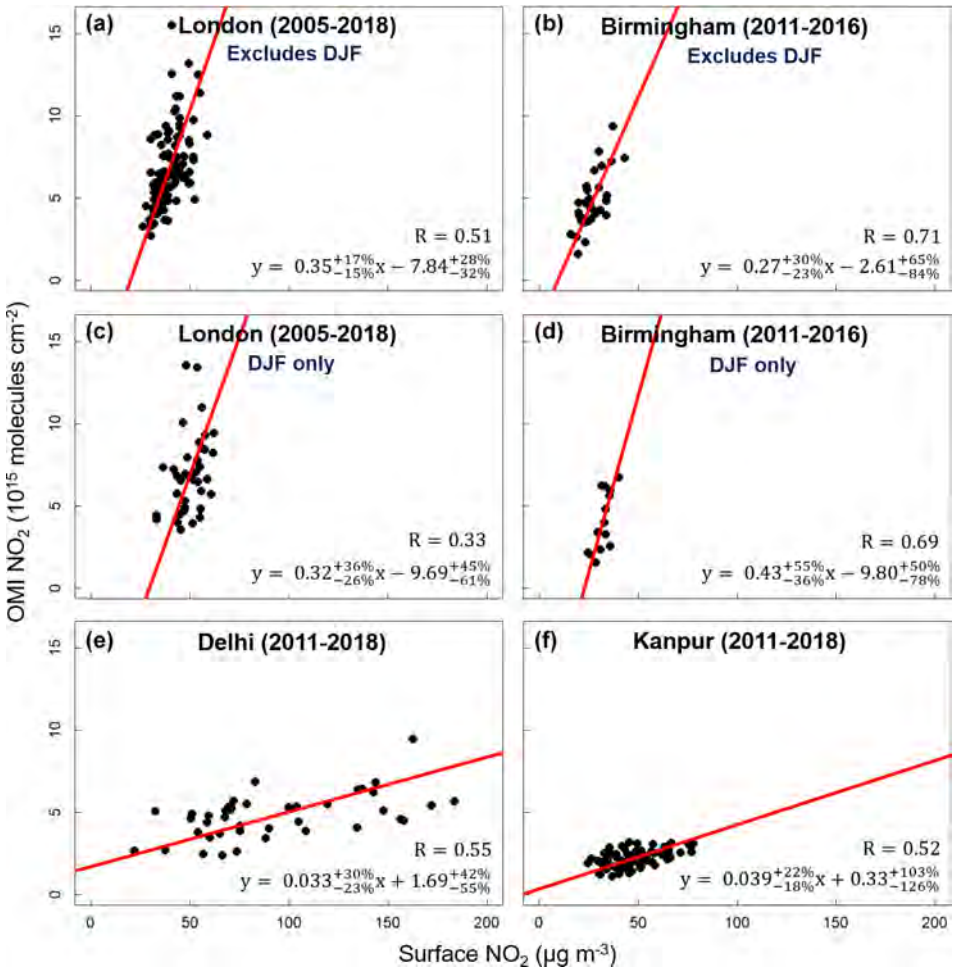

Figure 2. Assessment of OMI NO_2 with ground-based NO_2. Points are monthly means of city-average NO_2 from OMI and the surface networks for London **(a, c)**, Birmingham **(b, d)**, Delhi **(e)**, and Kanpur **(f)**. UK cities include panels with all months except December–February (DJF) **(a, b)** and DJF only **(c, d)**. Data for all months are given for cities in India. The red line is the standard major axis (SMA) regression. Values inset are Pearson's correlation coefficients and regression statistics. Relative errors on the slopes and intercepts are the 95 % confidence interval (CI).

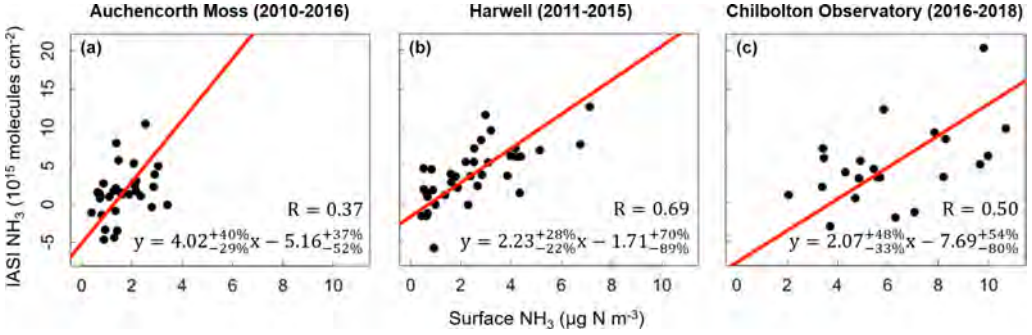

Figure 3. Assessment of IASI NH_3 with ground-based NH_3 at UK EMEP sites. Points are monthly means from IASI and the surface sites Auchencorth Moss **(a)**, Harwell **(b)**, and Chilbolton Observatory **(c)**. The red line is the SMA regression. Values inset are Pearson's correlation coefficients and regression statistics. Relative errors on the slope and intercept are the 95 % CI. Locations of UK EMEP sites are indicated in Fig. 1.

don and 11.3 $\mu g\,m^{-3}$ in Birmingham. MODIS AOD monthly means are estimated for London by averaging the pixels centred within its administrative boundary and for Birmingham within and 6.5 km beyond the administrative boundary, as with OMI NO_2 (Sect. 3.1). We remove months with < 160 observations, equivalent in spatial coverage to 5 OMI pixels at nadir (the threshold used for OMI). After filtering, 53 % of months are removed for London and 72 % for Birmingham, mostly in winter. Fewer months than OMI are retained, as MODIS uses stricter cloud filtering. The correlations in Fig. 4 are weak ($R = 0.34$ for London, $R = 0.23$ for Birmingham) and do not improve if we apply a less strict threshold for the number of observations required to calculate monthly means. The poor correlation may be due to environmental factors that complicate the relationship between AOD and surface $PM_{2.5}$, such as variability in meteorological conditions, aerosol composition, enhancements in aerosols above the boundary layer, and the aerosol radiative properties (Schaap et al., 2009; van Donkelaar et al., 2016; Shaddick et al., 2018; Sathe et al., 2019). We find that the same assessment is not feasible for Delhi or Kanpur as the record of surface $PM_{2.5}$ and PM_{10} in these cities is too short.

Figure 5 compares time series of monthly mean city-average MODIS AOD and surface $PM_{2.5}$ in London (2009–2018) and Birmingham (2009–2017) to assess whether the weak correlation in Fig. 4 affects agreement in trends of the two quantities. $PM_{2.5}$ is longer lived than NO_2, so trends in $PM_{2.5}$ (lifetime order weeks) for the limited number of sites mostly located in central London should be more representative of variability across the city than the surface sites of NO_2 (lifetime order hours against conversion to temporary reservoirs). The steeper decline in surface $PM_{2.5}$ in Birmingham (3.7 % a^{-1}) than in London (2.7 % a^{-1}) is reproduced in the AOD record (3.7 % a^{-1} in Birmingham; 2.5 % a^{-1} in London), although the AOD trends are not significant. In the two UK cities, surface $PM_{2.5}$ peaks in spring, whereas AOD peaks in the summer, determined from multi-year monthly means (not shown). There are too few $PM_{2.5}$ measurements in Delhi and Kanpur to compare long-term trends.

We compare the MODIS AOD product against ground-truth AOD from AERONET at long-term sites in Kanpur and Chilbolton to assess whether errors in satellite retrieval of AOD contribute to the weak temporal correlation between MODIS AOD and surface $PM_{2.5}$. Daily AERONET AOD at 550 nm is estimated by interpolation using the second-order polynomial relationship between the logarithmic AOD and logarithmic wavelengths at 440, 500, 675, and 870 nm (Kaufman, 1993; Eck et al., 1999; Levy et al., 2010; Li et al., 2012; Georgoulias et al., 2016). AERONET is sampled 30 min around the MODIS overpass, and MODIS is sampled 27.5 km around the AERONET site (Levy et al., 2010; Petrenko et al., 2012; Georgoulias et al., 2016; McPhetres and Aggarwal, 2018). Months with fewer than 160 MODIS observations are removed.

Figure 6 compares coincident AOD monthly means from MODIS and AERONET for Kanpur and Chilbolton. Monthly variability in MODIS and AERONET AOD is consistent at both sites ($R \geq 0.8$). MODIS exhibits no appreciable bias at Kanpur. There is positive variance (slope = 1.4) at Chilbolton that may result from sensitivity to errors in surface reflectivity at low AOD (Remer et al., 2013; Bilal et al., 2018) and residual cloud contamination (Wei et al., 2018, 2020). Mhawish et al. (2017) obtained similarly strong correlation ($R = 0.8$), but positive bias (26 %), of MODIS AOD at Kanpur from an earlier 3 km MODIS AOD product (Collection 6).

4 Air quality trends in London, Birmingham, Delhi, and Kanpur

The consistency we find between satellite and ground-based monthly mean city-average NO_2 (Fig. 2) and rural NH_3 (Fig. 3) and trends in city-average $PM_{2.5}$ (Fig. 5) supports the use of the satellite record to constrain surface air quality. Variability in NO_2, HCHO, and NH_3 columns can also be related to precursor emissions of NO_x, NMVOCs, and NH_3 (Martin et al., 2003; Lamsal et al., 2011; Marais et al., 2012; Zhu et al., 2014; Dammers et al., 2019), as their lifetimes against conversion to temporary or permanent sinks are relatively short, varying from 1–12 h depending on photochemical activity, abundance of pre-existing acidic aerosols, and proximity to large sources (Jones et al., 2009; Richter, 2009; Paulot et al., 2017; Van Damme et al., 2018). We adopt the same sampling approach as used to evaluate OMI NO_2. That is, we sample the satellite observations within the city administrative boundaries for London, Delhi, and Kanpur and extend the sampling domain for Birmingham beyond the administrative boundary by 6.5 km for OMI and MODIS and 10 km for IASI.

We apply the Theil–Sen single median estimator to the time series and also test the effect of fitting a non-linear function (Weatherhead et al., 1998; van der A et al., 2006; Pope et al., 2018) to account explicitly for seasonality:

$$Y_m = A + BX_m + C\sin(\omega X_m + \varnothing)\ . \quad (1)$$

Y_m is city-average satellite observations for month m, X_m is the number of months from the start month (January 2005 for OMI and MODIS, and January 2008 for IASI), and A, B, C, and $\varnothing$ are fit parameters. A is the city-average satellite observations in the start month, B is the linear trend, and $[C\sin(\omega X_m + \varnothing)]$ is the seasonal component that includes the amplitude C, frequency ω (fixed to 12 months), and phase shift $\varnothing$. We only show the fit in Eq. (1) if the trend B is different to that obtained with the Theil–Sen approach. The confidence intervals (CIs) for the Theil–Sen trends are estimated using bootstrap resampling, and trends are considered significant for p value < 0.05, that is, if the 95 % CI range does not intersect zero.

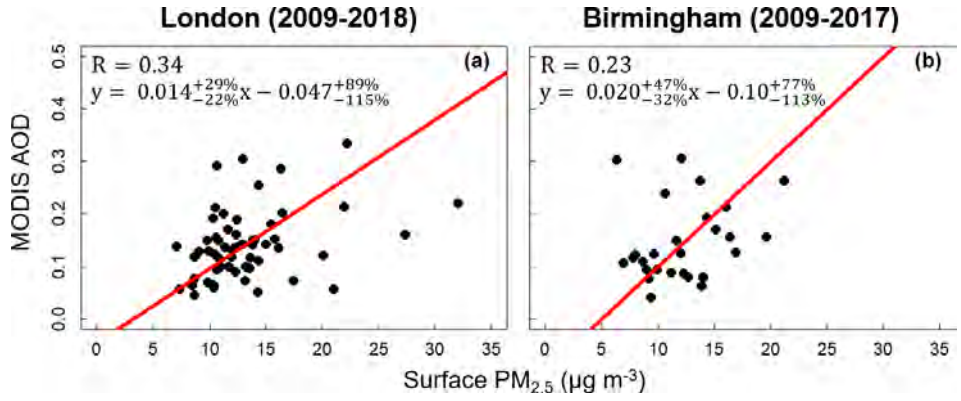

Figure 4. Assessment of MODIS AOD with surface $PM_{2.5}$ in London **(a)** and Birmingham **(b)**. Points are monthly means of city-average AOD from MODIS and $PM_{2.5}$ from surface networks for London and Birmingham. The red line is the SMA regression. Values inset are Pearson's correlation coefficients and regression statistics. Relative errors on the slopes and intercepts are the 95 % CI.

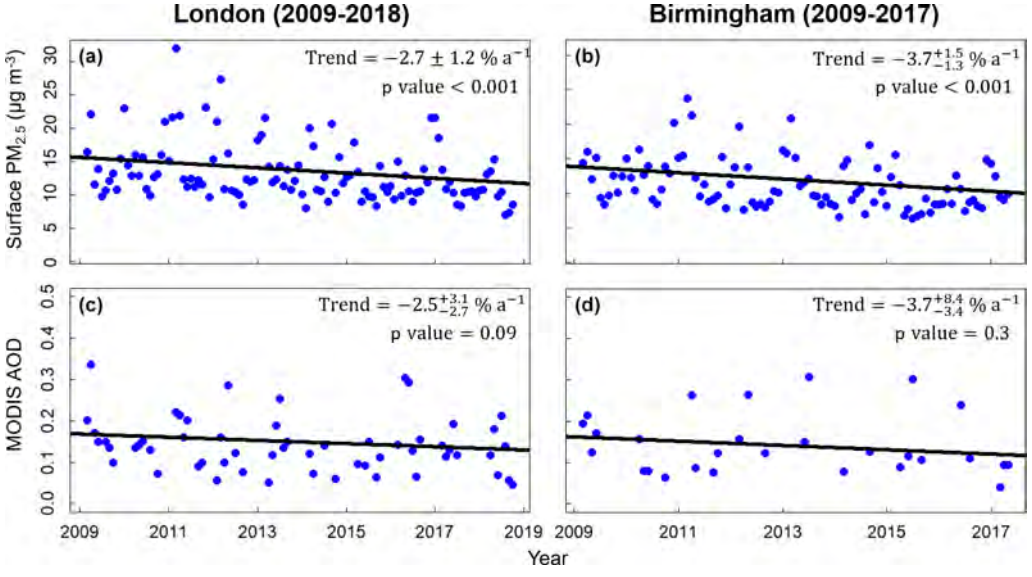

Figure 5. Time series of surface $PM_{2.5}$ and MODIS AOD in 2009–2018 for London **(a, c)** and 2009–2017 for Birmingham **(b, d)**. Points are city-average monthly means of $PM_{2.5}$ from the surface network **(a, b)** and AOD from MODIS **(c, d)**. Black lines are trends obtained with the Theil–Sen single median estimator. Values inset are annual trends and p values. Absolute errors on the trends are the 95 % CI. Trends are considered significant at the 95 % CI (p value < 0.05).

Figure 7 shows the time series of monthly means of city-average OMI NO_2 in the four cities for 2005–2018. Decline in OMI NO_2 in both London and Birmingham is 2.5 % a^{-1} and is significant. In Delhi, the OMI NO_2 increase is 2.0 % a^{-1} and is significant (p value $= 0.003$), whereas the increase in Kanpur of 0.9 % a^{-1} is not (p value $= 0.06$). The relationship between tropospheric column and surface NO_2 in London and Birmingham exhibits seasonality (Fig. 2). This is in part due to seasonality in mixing depth. We find that excluding the winter months in the time series has only a small effect on the trend. NO_2 should exhibit seasonality in all cities due to seasonal variability in its lifetime and sources (van der A et al., 2008). The fit in Eq. (1) yields significant seasonality for all cities (p value < 0.05 for the amplitude of the seasonality, C), but the linear trends are similar to those in Fig. 7: -2.4 % a^{-1} for London and Birmingham; unchanged for Delhi and Kanpur.

Comparison of the OMI NO_2 trends in Fig. 7 to surface observations is only possible for London, where there are 46 sites with consistent month-to-month variability representative of the city that operated continuously from 2005 to 2018. The trend obtained for OMI NO_2 in London (-2.5 % a^{-1}) is steeper than we estimate with the surface monitoring sites shown as triangles in Fig. 1 (1.8 % a^{-1} for 2005–2018). Most sites are in central London, and NO_2 trends in outer London are 1.6 times steeper than in central London (Carslaw et al.,

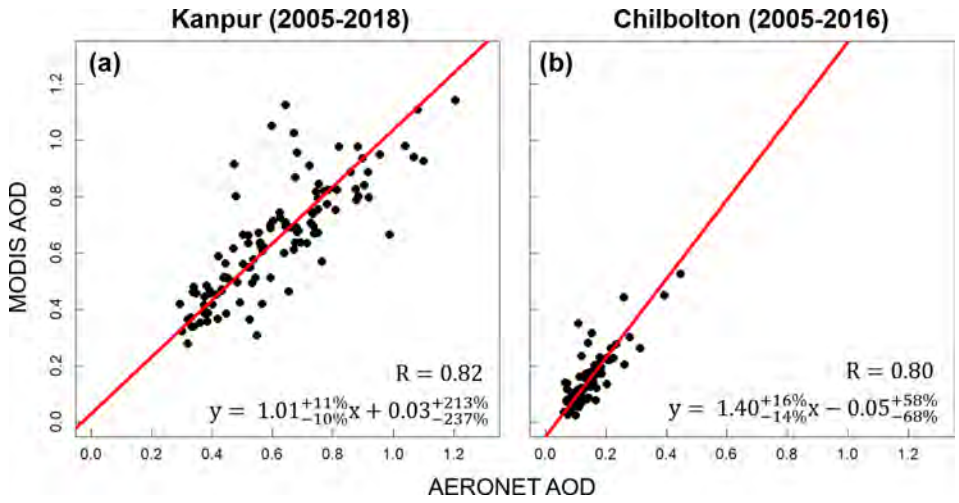

Figure 6. Validation of MODIS AOD with AERONET AOD in Kanpur and Chilbolton. Points are monthly means of MODIS and AERONET AOD for Kanpur **(a)** and Chilbolton **(b)**. The red line is the SMA regression. Values inset are Pearson's correlation coefficients and regression statistics. Relative errors on the slopes and intercepts are the 95 % CI.

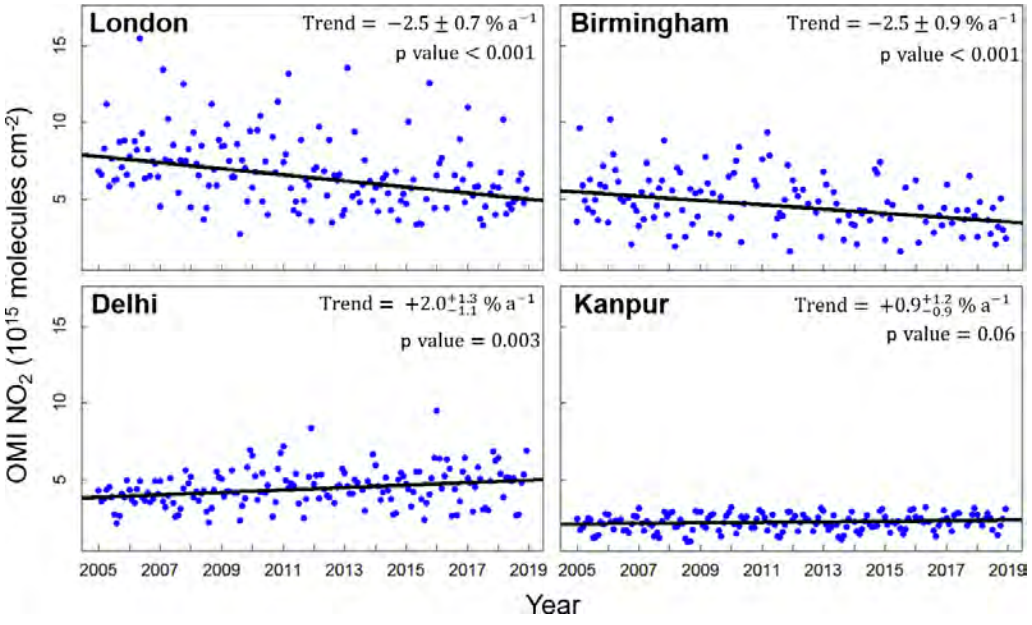

Figure 7. Time series of OMI NO_2 in 2005–2018 for London, Birmingham, Delhi, and Kanpur. Points are city-average monthly means. Black lines are trends obtained with the Theil–Sen single median estimator. Values inset are annual trends and p values. Absolute errors on the trends are the 95 % CI.

2011). The decline in NO_2 in the two UK cities is less than the rate of decline in national NO_x emissions (3.8 % a^{-1}) for 2005–2017 from the national bottom-up emission inventory (Defra, 2019a). This may reflect a combination of factors. There is less steep decline in NO_x emissions in London compared to the national total that may in part be due to discrepancies between real-world and reported diesel NO_x emissions (Fontaras et al., 2014), sustained heavy traffic in central London, and an increase in NO_2-to-NO_x emission ratios dampening decline in NO_2 (Grange et al., 2017). There is also weakened sensitivity of the tropospheric column to changes in surface NO_2 due to a gradual increase in the relative contribution of the free tropospheric background to the tropospheric column (Silvern et al., 2019). This weakening of the trend in the tropospheric column will likely be less in London than in Birmingham, due to greater local surface emissions in large cities such as London (Zara et al., 2021). The positive trends in Delhi and Kanpur likely reflect a 2-fold increase in vehicle ownership in Delhi (Govt. of Delhi, 2019), rapid industrialisation in Kanpur (Nagar et al., 2019),

and the limited effect of air quality policies on pollution sources. This is corroborated by NO_x emissions compliance failures at more than 50 % of coal-fired power plants in Delhi and the surrounding area (Pathania et al., 2018). The lack of trend reversal in Delhi, despite implementation of air quality policies, is consistent with the lack of trend reversal reported by Georgoulias et al. (2019). They used a 21-year record (1996–2017) of multiple space-based sensors to estimate a significant and sustained increase in NO_2 of $3.1\,\%\,a^{-1}$ in Delhi. By the end of 2018, tropospheric column NO_2 is similar in London and Delhi (5.7×10^{15} molecules cm^{-2}; Fig. 7), but OMI NO_2 over India may be biased low, due to the presence of optically thick aerosols (AOD > 0.4; Fig. 6) that are not explicitly accounted for in the retrieval (Sect. 3.1).

The direction of the trends for all four cities is consistent with other trend studies, with differences in the absolute size of the trend due to differences in instruments, time periods, and sampling domains. Pope et al. (2018) observed declines in OMI NO_2 for 2005–2015 of $2.3 \pm 0.5 \times 10^{14}$ molecules $cm^{-2}\,a^{-1}$ for London and $1.1 \pm 0.5 \times 10^{14}$ molecules $cm^{-2}\,a^{-1}$ for Birmingham. We obtain a similar trend for Birmingham but a steeper decline for London of 2.6×10^{14} molecules $cm^{-2}\,a^{-1}$ using our sampling domain for 2005–2015, though the difference is not significant. Schneider et al. (2015) obtained less steep and non-significant changes in NO_2 in London ($-1.7 \pm 1.2\,\%\,a^{-1}$) and Delhi ($1.4 \pm 1.2\,\%\,a^{-1}$) from the SCanning Imaging Absorption spectroMeter for Atmospheric CHartographY (SCIAMACHY) for 2002–2013. Trends in OMI NO_2 for 2005–2014 from ul-Haq et al. (2015) are similar to ours for Delhi ($2.0\,\%\,a^{-1}$) but lower for Kanpur ($0.2\,\%\,a^{-1}$). Studies have also combined multiple instruments to derive trends since the mid-1990s. These find decreases in NO_2 over London of $0.7\,\%\,a^{-1}$ for 1996–2006 (van der A et al., 2008) and $1.7\,\%\,a^{-1}$ for a longer observing period (1996–2011) (Hilboll et al., 2013) and a consistent increase for Delhi of $7.4\,\%\,a^{-1}$ in 1996–2006 (van der A et al., 2008) and 1996–2011 (Hilboll et al., 2013), much steeper than ours in Fig. 7.

Figure 8 shows time series of monthly means of city-average IASI NH_3 in the four cities for 2008–2018. Mean IASI NH_3 is 15–20 times more in Delhi and Kanpur than in London and Birmingham due to larger emissions of NH_3 in the IGP, higher ambient temperatures promoting volatilisation of NH_3, and greater sensitivity of IASI to NH_3 due to greater thermal contrast between the surface and the atmosphere over India (Van Damme et al., 2015; Dammers et al., 2016; T. Wang et al., 2020). IASI NH_3 decreases by $0.1\,\%\,a^{-1}$ in Kanpur, $0.6\,\%\,a^{-1}$ in Birmingham, and $2.4\,\%\,a^{-1}$ in London and increases by $0.5\,\%\,a^{-1}$ in Delhi. None of the trends are significant. Measurements of surface NH_3 from continuous monitors deployed in Delhi in April 2010 to July 2011 exhibit the same seasonality as IASI NH_3, peaking in the monsoon season (July–September) (Singh and Kulshrestha, 2012). We investigated the effect of NH_3 seasonality on the trend using Eq. (1) (solid grey lines in Fig. 8). Similar to NO_2, all four cities show significant seasonality (p value < 0.05 for the amplitude of the seasonality, C). The linear trends (dashed grey lines in Fig. 8) are more positive than those obtained with Theil–Sen for all four cities but are still not significant. This leads to a trend reversal in Kanpur ($+1.0\,\%\,a^{-1}$) and Birmingham ($+2.1\,\%\,a^{-1}$), steeper increase in Delhi ($+3.7\,\%\,a^{-1}$), and a less negative trend in London ($-0.6\,\%\,a^{-1}$).

Relating trends in NH_3 columns to trends in NH_3 emissions is complicated by partitioning of NH_3 to aerosols to form ammonium and dependence of this process on pre-existing aerosols that have declined in abundance across the UK due largely to controls on precursor emissions of SO_2 (Vieno et al., 2014). Harwell and Auchencorth Moss include measurements of gas-phase NH_3 and aerosol-phase ammonium in $PM_{2.5}$. These exhibit large and distinct seasonality, so we use Eq. (1) to estimate changes of $-0.096\,\mu g\,N\,m^{-3}\,a^{-1}$ for ammonium and $+0.031\,\mu g\,N\,m^{-3}\,a^{-1}$ for NH_3 at Auchencorth Moss in 2008–2012 and similar changes at Harwell in 2012–2015 of $-0.10\,\mu g\,N\,m^{-3}\,a^{-1}$ for ammonium and $+0.035\,\mu g\,N\,m^{-3}\,a^{-1}$ for NH_3. Only the decline in ammonium at Auchencorth Moss is significant. This suggests the increase in rural NH_3 includes contributions from unregulated agricultural emissions and reduced partitioning of NH_3 to pre-existing aerosols. The opposite trend (decline) in NH_3 in London obtained with Theil–Sen and Eq. (1) (Fig. 8) may be because decline in local vehicular emissions of NH_3 with a shift in catalytic converter technology (Richmond et al., 2020) outweighs the increase in NH_3 from waste and domestic combustion (Defra, 2019a), and nearby agriculture (Vieno et al., 2016) and offsets reduced partitioning of NH_3 to acidic aerosols with decline in sulfate. The opposite effect would be expected in Delhi due to nationwide increases in SO_2 emissions and sulfate abundance (Klimont et al., 2013; Aas et al., 2019). That is, the increase in NH_3 emissions may be steeper than the increase in NH_3 columns in Fig. 8 due to a corresponding increase in partitioning of NH_3 to pre-existing aerosols as these become more abundant.

Figure 9 shows the time series of city-average monthly mean OMI HCHO for the four cities for 2005–2018 after removing the background contribution from oxidation of methane and other long-lived volatile organic compounds (VOCs) to isolate variability in the column due to reactive NMVOCs (Zhu et al., 2016). A representative background is obtained as monthly mean OMI HCHO over the remote Atlantic Ocean (25–35° N, 35–45° W) for the UK and the remote Indian Ocean (10–20° S, 70–80° E) for India. The non-linear function in Eq. (1) is fit to these background HCHO values and used to subtract the background contribution, as in Marais et al. (2012), from the city-average monthly means. OMI HCHO columns from oxidation of reactive NMVOCs in Delhi and Kanpur are almost twice those in London and Birmingham due to a combination of unregulated sources (Venkataraman et al., 2018) and high temper-

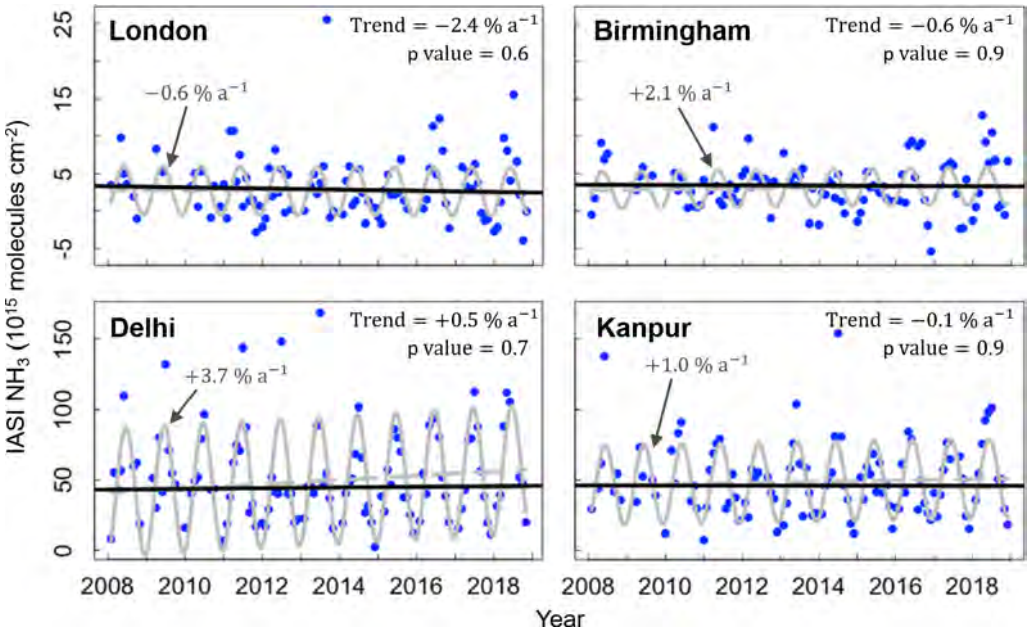

Figure 8. Time series of IASI NH_3 in 2008–2018 for London, Birmingham, Delhi, and Kanpur. Points are city-average monthly means. Black lines are trends obtained with the Theil–Sen single median estimator. The grey lines are the fit (solid) and trend component (B) (dashed) obtained with Eq. (1). Values inset are annual trends and p values for the Theil–Sen fit (in black) and annual trends obtained with Eq. (1) (grey). Trend errors (not shown) exceed ±150 % in all cities.

atures enhancing emissions of isoprene, a dominant HCHO precursor in India (Surl et al., 2018; Chalilyakunnel et al., 2019). The trends suggest reactive NMVOCs emissions have decreased in Birmingham (1.6 % a^{-1}) and increased in London (0.5 % a^{-1}), Delhi (1.9 % a^{-1}), and Kanpur (1.0 % a^{-1}). Only Delhi has a significant trend. The spread in values increases for Delhi and Kanpur from 19 %–24 % relative to the trend line in 2005 to 31 %–40 % in 2018. The change in the spread of values does not appear to be due to loss of data resulting from the row anomaly, as the change in the spread of HCHO over time is similar if we remove all pixels affected by the row anomaly for the entire data record (2005–2018). OMI HCHO slant columns (HCHO along the instrument viewing path) remain relatively stable throughout the OMI record (Zara et al., 2018), so the increase in variability may reflect more extreme emissions from seasonal sources like open fires in the IGP (Jethva et al., 2019). The trends from satellite observations of HCHO in megacities obtained by De Smedt et al. (2010) using multiple instruments for 1997–2009 are consistent with ours for Delhi (1.6 ± 0.7 % a^{-1}) but opposite for London (-0.4 ± 2.1 % a^{-1}). There is a shift in the magnitude of the HCHO trend for London around 2011 (Fig. 9) from an increase of 0.3 % a^{-1} (p value = 0.9) in 2005–2011 to a rapid increase of 9.3 % a^{-1} (95 % CI: 0 % a^{-1}–26 % a^{-1}) in 2012–2018. Visually the data suggest a decline in OMI HCHO in 2005–2011, as in De Smedt et al. (2010), but our trend estimate for 2005–2011 is affected by a limited analysis period and large interannual variability.

According to the UK bottom-up emission inventory, national NMVOCs emissions decreased by 2.4 % a^{-1} from 2005 to 2017 (Defra, 2019a). This is supported by decline in short-chain hydrocarbons measured at Harwell from 2–3 µg m^{-3} in 2008 to 0.8–0.9 µg m^{-3} in 2015. These include hydrocarbons from vegetation (isoprene and monoterpenes) and vehicles (light alkanes and aromatics) but exclude oxygenated VOCs (OVOCs) that in the UK include increasing contributions from domestic combustion, the food and beverage industry, and household products (Defra, 2019a). OVOCs have relatively high HCHO yields (Millet et al., 2006), and VOC concentrations measured during field campaigns in London and cities in India, including Delhi, are dominated by OVOCs (> 60 % in London) (Valach et al., 2014; Sahu et al., 2016; L. Wang et al., 2020). In London, OVOCs also dominate inferred fluxes of VOCs (Langford et al., 2010) and reactivity of VOCs with the main atmospheric oxidant, OH (Whalley et al., 2016). The rapid increase in HCHO also has implications for ozone air pollution and the radical budget in London, as ozone formation is VOC-limited, and HCHO photolysis is the second largest source of hydrogen oxide radicals ($HO_x \equiv OH + HO_2$) in London (Whalley et al., 2018).

Figure 10 shows the time series of city-average MODIS AOD monthly means in the four cities for 2005–2018. Trends in AOD are significant in all four cities and range from a decline of 4.2 % a^{-1} in Birmingham to an increase of 3.1 % a^{-1} in Kanpur. Mean AOD in Delhi and Kanpur is on average 5–

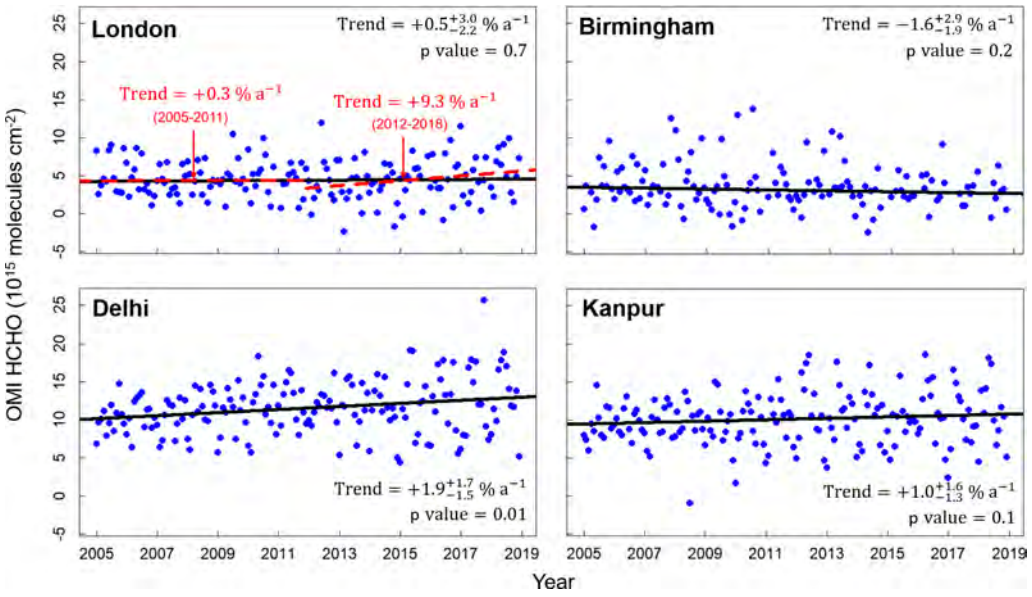

Figure 9. Time series of OMI HCHO for London, Birmingham, Delhi, and Kanpur. Points are city-average monthly means of OMI HCHO after removing the background contribution (see text for details). Solid black lines are trends for 2005–2018 obtained with the Theil–Sen single median estimator. Values inset are annual trends and p values. Absolute errors on the trends are the 95 % CI. Dashed red lines show trend lines for London in 2005–2011 and 2012–2018, and red text shows corresponding annual trends.

6 times more than in London and Birmingham, due to large local anthropogenic emissions, nearby agricultural emissions of $PM_{2.5}$ and its precursors in the IGP, and long-range transport of desert dust (David et al., 2018). Our results, as absolute AOD trends for London ($-0.004\,a^{-1}$) and Birmingham ($-0.007\,a^{-1}$) for 2005–2018, are similar to trends obtained by Pope et al. (2018) for 2005–2015 ($-0.006\,a^{-1}$ for London; $-0.005\,a^{-1}$ for Birmingham). Our trends for both cities in India are less steep than the increase for Delhi (4.9 % a^{-1}) obtained for 2000–2010 with the MODIS 10 km AOD product (Ramachandran et al., 2012) and for Kanpur (10.3 % a^{-1}) obtained for 2001–2010 with AERONET AOD at the Kanpur AERONET site (Kaskaoutis et al., 2012). This may reflect a recent dampening of the trend or differences in data products and sampling domain/period. Sulfate from coal-fired power plants in India makes a large contribution to $PM_{2.5}$ (Weagle et al., 2018), and emissions from these nearly doubled from 2004 to 2015 (Fioletov et al., 2016).

5 Conclusions

Satellite observations of atmospheric composition provide long-term and consistent global coverage of air pollutants. We assessed the ability of satellite observations of nitrogen dioxide (NO_2) and formaldehyde (HCHO) from OMI for 2005–2018, ammonia (NH_3) from IASI for 2008–2018, and aerosol optical depth (AOD) from MODIS for 2005–2018 to provide constraints on long-term changes in city-average NO_2, reactive NMVOCs, NH_3, and $PM_{2.5}$, respectively in four cities: two in the UK (London and Birmingham) and two in India (Delhi and Kanpur).

Assessment of satellite observations against ground-based measurements followed careful screening of the in situ measurements for poor-quality data, correcting NO_2 data reported in inconsistent units at monitoring sites in Delhi and Kanpur and removing sites influenced by local sources. OMI NO_2 reproduces monthly variability in surface concentrations of NO_2 in cities, whereas satellite AOD reproduces trends, but not monthly variability, in $PM_{2.5}$ in cities. MODIS and AERONET AOD are consistent at long-term monitoring sites in Kanpur and a UK EMEP site in southern England. IASI NH_3 is consistent with monthly variability in surface NH_3 concentrations at two of three rural UK EMEP sites. There were no appropriate measurements of reactive NMVOCs to compare to OMI HCHO.

According to the long-term record from Earth observations, NO_2, $PM_{2.5}$, and NMVOCs increased in Delhi and Kanpur. There is no reversal in the increase in NO_2 or $PM_{2.5}$ in Delhi or Kanpur, as would be expected from successful implementation of air pollution mitigation measures. In all four cities, the magnitude and direction of trends in NH_3 are sensitive to treatment of NH_3 seasonality, and none of the NH_3 trends are significant. In London and Birmingham, NO_2 and $PM_{2.5}$ decrease, and HCHO, a proxy for reactive NMVOCs emissions, decreases in Birmingham but exhibits a recent (2012–2018) sharp (> 9 % a^{-1}) increase in London. This may reflect increased emissions of oxygenated VOCs and long-chain hydrocarbons from household products, the food and beverage industry, and residential fuelwood burn-

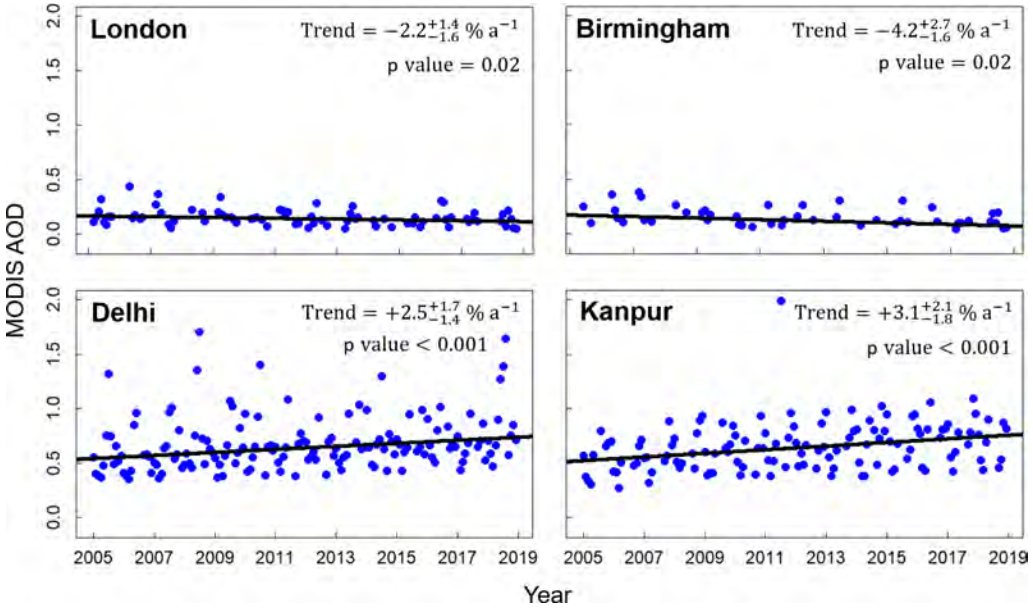

Figure 10. Time series of MODIS AOD for London, Birmingham, Delhi, and Kanpur. Points are city-average monthly means. Black lines are trends obtained with the Theil–Sen single median estimator. Values inset are annual trends and p values. Absolute errors on the trends are the 95 % CI.

ing. This would have implications for formation of secondary organic aerosols (SOAs) contributing to $PM_{2.5}$, the radical (HO_x) budget that includes a large contribution from HCHO photolysis, and formation of surface ozone that is VOC-limited in London.

Data availability. Corrected hourly NO_2 data for Delhi and Kanpur are available at https://github.com/karnvoh/India-NO2-data (last access: 6 April 2020) and https://doi.org/10.5281/zenodo.4696252 (Vohra, 2021). Data from IIT Kanpur can be obtained by contacting Sachchida N. Tripathi (snt@iitk.ac.in). Data for Birmingham not publicly available can be obtained by request from the Birmingham City Council. IASI NH_3 data were provided by Martin Van Damme, Lieven Clarisse, and Pierre-F. Coheur and are now available at https://iasi.aeris-data.fr/nh3/ (ULB, 2021).

Author contributions. KV analysed and interpreted the data and prepared the manuscript, and EAM assisted in the writing and provided supervisory guidance, with co-supervision from WJB. LK provided data analysis and usage guidance. ShS derived the relationship between hourly PM_{10} and $PM_{2.5}$ for Birmingham. Observations are from RS, AG, and SNT for the surface site in Kanpur and from MVD, LC, and PFC for IASI NH_3.

Competing interests. The authors declare that they have no conflict of interest.

Acknowledgements. We thank the NERC Field Spectroscopy Facility, principal investigators, and their staff for establishing and maintaining the AERONET sites at Kanpur and Chilbolton and Peter Porter from Birmingham City Council for providing the surface network data for Birmingham. URLs and DOIs (if available) of the data used in this study are given in Sect. 2.

Financial support. This work was funded by a University of Birmingham Global Challenges Studentship awarded to Karn Vohra, a NERC/EPSRC grant (EP/R513465/1) awarded to Eloise A. Marais, a Chevening Scholarship from the Foreign and Commonwealth Office and partner organisations awarded to Shannen Suckra, and a DBT grant (BT/IN/UK/APHH/41/KB/2016-17) and CPCB grant (AQM/Source apportionment_EPC Project/2017) awarded to Sachchida N. Tripathi. ULB research by Martin Van Damme, Lieven Clarisse, and Pierre-F. Coheur was supported by the Belgian State Federal Office for Scientific, Technical and Cultural Affairs (Prodex arrangement IASI.FLOW).

Review statement. This paper was edited by Michel Van Roozendael and reviewed by Richard Pope and two anonymous referees.

References

Aas, W., Mortier, A., Bowersox, V., Cherian, R., Faluvegi, G., Fagerli, H., Hand, J., Klimont, Z., Galy-Lacaux, C., Lehmann, C. M. B., Myhre, C. L., Myhre, G., Olivie, D., Sato, K., Quaas, J., Rao, P. S. P., Schulz, M., Shindell, D., Skeie, R. B., Stein, A., Takemura, T., Tsyro, S., Vet, R., and Xu, X. B.: Global

and regional trends of atmospheric sulfur, Sci. Rep.-UK, 9, 953, https://doi.org/10.1038/s41598-018-37304-0, 2019.

Anenberg, S. C., Achakulwisut, P., Brauer, M., Moran, D., Apte, J. S., and Henze, D. K.: Particulate matter-attributable mortality and relationships with carbon dioxide in 250 urban areas worldwide, Sci. Rep.-UK, 9, 11552, https://doi.org/10.1038/s41598-019-48057-9, 2019.

Barnes, J. H., Hayes, E. T., Chatterton, T. J., and Longhurst, J. W. S.: Policy disconnect: A critical review of UK air quality policy in relation to EU and LAQM responsibilities over the last 20 years, Environ. Sci. Policy, 85, 28–39, https://doi.org/10.1016/j.envsci.2018.03.024, 2018.

Bilal, M., Qiu, Z. F., Campbell, J. R., Spak, S. N., Shen, X. J., and Nazeer, M.: A New MODIS C6 Dark Target and Deep Blue Merged Aerosol Product on a 3 km Spatial Grid, Remote Sens.-Basel, 10, 463, https://doi.org/10.3390/rs10030463, 2018.

Boersma, K. F., Eskes, H. J., and Brinksma, E. J.: Error analysis for tropospheric NO_2 retrieval from space, J. Geophys. Res.-Atmos., 109, D04311, https://doi.org/10.1029/2003jd003962, 2004.

Boersma, K. F., Jacob, D. J., Trainic, M., Rudich, Y., DeSmedt, I., Dirksen, R., and Eskes, H. J.: Validation of urban NO_2 concentrations and their diurnal and seasonal variations observed from the SCIAMACHY and OMI sensors using in situ surface measurements in Israeli cities, Atmos. Chem. Phys., 9, 3867–3879, https://doi.org/10.5194/acp-9-3867-2009, 2009.

Brauer, M., Freedman, G., Frostad, J., van Donkelaar, A., Martin, R. V., Dentener, F., van Dingenen, R., Estep, K., Amini, H., Apte, J. S., Balakrishnan, K., Barregard, L., Broday, D., Feigin, V., Ghosh, S., Hopke, P. K., Knibbs, L. D., Kokubo, Y., Liu, Y., Ma, S. F., Morawska, L., Sangrador, J. L. T., Shaddick, G., Anderson, H. R., Vos, T., Forouzanfar, M. H., Burnett, R. T., and Cohen, A.: Ambient Air Pollution Exposure Estimation for the Global Burden of Disease 2013, Environ. Sci. Technol., 50, 79–88, https://doi.org/10.1021/acs.est.5b03709, 2016.

Carnell, E., Vieno, M., Vardoulakis, S., Beck, R., Heaviside, C., Tomlinson, S., Dragosits, U., Heal, M. R., and Reis, S.: Modelling public health improvements as a result of air pollution control policies in the UK over four decades – 1970 to 2010, Environ. Res. Lett., 14, 074001, https://doi.org/10.1088/1748-9326/ab1542, 2019.

Carslaw, D. C., Beevers, S. D., Westmoreland, E., Williams, M. L., Tate, J. E., Murrells, T., Stedman, J., Li, Y., Grice, S., Kent, A., and Tsagatakis, I.: Trends in NO_x and NO_2 emissions and ambient measurements in the UK, available at: https://uk-air.defra.gov.uk/assets/documents/reports/cat05/1108251149_110718_AQ0724_Final_report.pdf (last access: 16 January 2020) 2011.

Carslaw, D. C., Murrells, T. P., Andersson, J., and Keenan, M.: Have vehicle emissions of primary NO_2 peaked?, Faraday Discuss., 189, 439–454, https://doi.org/10.1039/c5fd00162e, 2016.

Castell, N., Dauge, F. R., Schneider, P., Vogt, M., Lerner, U., Fishbain, B., Broday, D., and Bartonova, A.: Can commercial low-cost sensor platforms contribute to air quality monitoring and exposure estimates?, Environ. Int., 99, 293–302, https://doi.org/10.1016/j.envint.2016.12.007, 2017.

Chalilyakunnel, S., Millet, D. B., and Chen, X.: Constraining emissions of volatile organic compounds over the Indian subcontinent using spacebased formaldehyde measurements, J. Geophys. Res., 124, 10525–10545, https://doi.org/10.1029/2019JD031262, 2019.

Choi, S., Lamsal, L. N., Follette-Cook, M., Joiner, J., Krotkov, N. A., Swartz, W. H., Pickering, K. E., Loughner, C. P., Appel, W., Pfister, G., Saide, P. E., Cohen, R. C., Weinheimer, A. J., and Herman, J. R.: Assessment of NO_2 observations during DISCOVER-AQ and KORUS-AQ field campaigns, Atmos. Meas. Tech., 13, 2523–2546, https://doi.org/10.5194/amt-13-2523-2020, 2020.

Clarisse, L., Shephard, M. W., Dentener, F., Hurtmans, D., Cady-Pereira, K., Karagulian, F., Van Damme, M., Clerbaux, C., and Coheur, P. F.: Satellite monitoring of ammonia: A case study of the San Joaquin Valley, J. Geophys. Res.-Atmos., 115, D13302, https://doi.org/10.1029/2009jd013291, 2010.

CPCB: Central Pollution Control Board, India, Protocol for Data Transmission from CAAQM Stations Existing as on Date, available at: https://app.cpcbccr.com/ccr_docs/Protocol_CAAQM.pdf (last access: 8 March 2020), 2015.

Crilley, L. R., Bloss, W. J., Yin, J., Beddows, D. C. S., Harrison, R. M., Allan, J. D., Young, D. E., Flynn, M., Williams, P., Zotter, P., Prevot, A. S. H., Heal, M. R., Barlow, J. F., Halios, C. H., Lee, J. D., Szidat, S., and Mohr, C.: Sources and contributions of wood smoke during winter in London: assessing local and regional influences, Atmos. Chem. Phys., 15, 3149–3171, https://doi.org/10.5194/acp-15-3149-2015, 2015.

Crilley, L. R., Lucarelli, F., Bloss, W. J., Harrison, R. M., Beddows, D. C., Calzolai, G., Nava, S., Valli, G., Bernardoni, V., and Vecchi, R.: Source apportionment of fine and coarse particles at a roadside and urban background site in London during the 2012 summer ClearfLo campaign, Environ. Pollut., 220, 766–778, https://doi.org/10.1016/j.envpol.2016.06.002, 2017.

Cusworth, D. H., Mickley, L. J., Sulprizio, M. P., Liu, T. J., Marlier, M. E., DeFries, R. S., Guttikunda, S. K., and Gupta, P.: Quantifying the influence of agricultural fires in northwest India on urban air pollution in Delhi, India, Environ. Res. Lett., 13, 044018, https://doi.org/10.1088/1748-9326/aab303, 2018.

Dammers, E., Palm, M., Van Damme, M., Vigouroux, C., Smale, D., Conway, S., Toon, G. C., Jones, N., Nussbaumer, E., Warneke, T., Petri, C., Clarisse, L., Clerbaux, C., Hermans, C., Lutsch, E., Strong, K., Hannigan, J. W., Nakajima, H., Morino, I., Herrera, B., Stremme, W., Grutter, M., Schaap, M., Wichink Kruit, R. J., Notholt, J., Coheur, P.-F., and Erisman, J. W.: An evaluation of IASI-NH3 with ground-based Fourier transform infrared spectroscopy measurements, Atmos. Chem. Phys., 16, 10351–10368, https://doi.org/10.5194/acp-16-10351-2016, 2016.

Dammers, E., McLinden, C. A., Griffin, D., Shephard, M. W., Van Der Graaf, S., Lutsch, E., Schaap, M., Gainairu-Matz, Y., Fioletov, V., Van Damme, M., Whitburn, S., Clarisse, L., Cady-Pereira, K., Clerbaux, C., Coheur, P. F., and Erisman, J. W.: NH_3 emissions from large point sources derived from CrIS and IASI satellite observations, Atmos. Chem. Phys., 19, 12261–12293, https://doi.org/10.5194/acp-19-12261-2019, 2019.

Datameet India: Community data, available at: https://github.com/datameet/maps/tree/master/Country (last access: 12 March 2021), 2018.

David, L. M., Ravishankara, A. R., Kodros, J. K., Venkataraman, C., Sadavarte, P., Pierce, J. R., Chaliyakunnel, S., and Millet, D. B.: Aerosol Optical Depth Over India, J. Geophys. Res.-Atmos., 123, 3688–3703, https://doi.org/10.1002/2017jd027719, 2018.

De Smedt, I., Stavrakou, T., Muller, J. F., van der A, R. J., and Van Roozendael, M.: Trend detection in satellite observations of formaldehyde tropospheric columns, Geophys. Res. Lett., 37, L18808, https://doi.org/10.1029/2010gl044245, 2010.

De Smedt, I., van Geffen, J., Richter, A., Beirle, S., Yu, H., Vlietinck, J., Roozendael, M. V., van der A, R., Lorente, A., Scanlon, T., Compernolle, S., Wagner, T., Eskes, H., and Boersma, F.: Product User Guide for HCHO (Version 1.0), https://doi.org/10.18758/71021031, 2017.

De Smedt, I., Theys, N., Yu, H., Danckaert, T., Lerot, C., Compernolle, S., Van Roozendael, M., Richter, A., Hilboll, A., Peters, E., Pedergnana, M., Loyola, D., Beirle, S., Wagner, T., Eskes, H., van Geffen, J., Boersma, K. F., and Veefkind, P.: Algorithm theoretical baseline for formaldehyde retrievals from S5P TROPOMI and from the QA4ECV project, Atmos. Meas. Tech., 11, 2395–2426, https://doi.org/10.5194/amt-11-2395-2018, 2018.

Defra: Department for Environment Food & Rural Affairs, United Kingdom, Emissions of air pollutants in the UK, 1970 to 2017, available at: https://assets.publishing.service.gov.uk/government/uploads/system/uploads/attachment_data/file/778483/Emissions_of_air_pollutants_1990_2017.pdf, last access: 20 December 2019a.

Defra: Department for Environment Food & Rural Affairs, United Kingdom, Clean Air Strategy, available at: https://assets.publishing.service.gov.uk/government/uploads/system/uploads/attachment_data/file/770715/clean-air-strategy-2019.pdf (last access: 8 March 2020), 2019b.

Duncan, B. N., Prados, A. I., Lamsal, L. N., Liu, Y., Streets, D. G., Gupta, P., Hilsenrath, E., Kahn, R. A., Nielsen, J. E., Beyersdorf, A. J., Burton, S. P., Fiore, A. M., Fishman, J., Henze, D. K., Hostetler, C. A., Krotkov, N. A., Lee, P., Lin, M. Y., Pawson, S., Pfister, G., Pickering, K. E., Pierce, R. B., Yoshida, Y., and Ziemba, L. D.: Satellite data of atmospheric pollution for US air quality applications: Examples of applications, summary of data end-user resources, answers to FAQs, and common mistakes to avoid, Atmos. Environ., 94, 647–662, https://doi.org/10.1016/j.atmosenv.2014.05.061, 2014.

Dunlea, E. J., Herndon, S. C., Nelson, D. D., Volkamer, R. M., San Martini, F., Sheehy, P. M., Zahniser, M. S., Shorter, J. H., Wormhoudt, J. C., Lamb, B. K., Allwine, E. J., Gaffney, J. S., Marley, N. A., Grutter, M., Marquez, C., Blanco, S., Cardenas, B., Retama, A., Ramos Villegas, C. R., Kolb, C. E., Molina, L. T., and Molina, M. J.: Evaluation of nitrogen dioxide chemiluminescence monitors in a polluted urban environment, Atmos. Chem. Phys., 7, 2691–2704, https://doi.org/10.5194/acp-7-2691-2007, 2007.

Eck, T. F., Holben, B. N., Reid, J. S., Dubovik, O., Smirnov, A., O'Neill, N. T., Slutsker, I., and Kinne, S.: Wavelength dependence of the optical depth of biomass burning, urban, and desert dust aerosols, J. Geophys. Res.-Atmos., 104, 31333–31349, https://doi.org/10.1029/1999jd900923, 1999.

Fioletov, V. E., McLinden, C. A., Krotkov, N., Li, C., Joiner, J., Theys, N., Carn, S., and Moran, M. D.: A global catalogue of large SO2 sources and emissions derived from the Ozone Monitoring Instrument, Atmos. Chem. Phys., 16, 11497–11519, https://doi.org/10.5194/acp-16-11497-2016, 2016.

Fishman, J., Bowman, K. W., Burrows, J. P., Richter, A., Chance, K. V., Edwards, D. P., Martin, R. V., Morris, G. A., Pierce, R. B., Ziemke, J. R., Al-Saadi, J. A., Creilson, J. K., Schaack, T. K., and Thompson, A. M.: Remote sensing of tropospheric pollution from space, B. Am. Meteorol. Soc., 89, 805–821, https://doi.org/10.1175/2008bams2526.1, 2008.

Fontaras, G., Franco, V., Dilara, P., Martini, G., and Manfredi, U.: Development and review of Euro 5 passenger car emission factors based on experimental results over various driving cycles, Sci. Total Environ., 468, 1034–1042, https://doi.org/10.1016/j.scitotenv.2013.09.043, 2014.

Fuller, G. W., Tremper, A. H., Baker, T. D., Yttri, K. E., and Butterfield, D.: Contribution of wood burning to PM_{10} in London, Atmos. Environ., 87, 87–94, https://doi.org/10.1016/j.atmosenv.2013.12.037, 2014.

GADM Data: available atL https://gadm.org/ (last access: 12 March 2021), 2018.

Gaur, A., Tripathi, S. N., Kanawade, V. P., Tare, V., and Shukla, S. P.: Four-year measurements of trace gases (SO_2, NO_x, CO, and O_3) at an urban location, Kanpur, in Northern India, J. Atmos. Chem., 71, 283–301, https://doi.org/10.1007/s10874-014-9295-8, 2014.

Georgoulias, A. K., Alexandri, G., Kourtidis, K. A., Lelieveld, J., Zanis, P., Pöschl, U., Levy, R., Amiridis, V., Marinou, E., and Tsikerdekis, A.: Spatiotemporal variability and contribution of different aerosol types to the aerosol optical depth over the Eastern Mediterranean, Atmos. Chem. Phys., 16, 13853–13884, https://doi.org/10.5194/acp-16-13853-2016, 2016.

Georgoulias, A. K., van der A, R. J., Stammes, P., Boersma, K. F., and Eskes, H. J.: Trends and trend reversal detection in 2 decades of tropospheric NO_2 satellite observations, Atmos. Chem. Phys., 19, 6269–6294, https://doi.org/10.5194/acp-19-6269-2019, 2019.

Ghosh, S., Gupta, T., Rastogi, N., Gaur, A., Misra, A., Tripathi, S. N., Paul, D., Tare, V., Prakash, O., Bhattu, D., Dwivedi, A. K., Kaul, D. S., Dalai, R., and Mishra, S. K.: Chemical Characterization of Summertime Dust Events at Kanpur: Insight into the Sources and Level of Mixing with Anthropogenic Emissions, Aerosol Air Qual. Res., 14, 879–891, https://doi.org/10.4209/aaqr.2013.07.0240, 2014.

Giles, D. M., Sinyuk, A., Sorokin, M. G., Schafer, J. S., Smirnov, A., Slutsker, I., Eck, T. F., Holben, B. N., Lewis, J. R., Campbell, J. R., Welton, E. J., Korkin, S. V., and Lyapustin, A. I.: Advancements in the Aerosol Robotic Network (AERONET) Version 3 database – automated near-real-time quality control algorithm with improved cloud screening for Sun photometer aerosol optical depth (AOD) measurements, Atmos. Meas. Tech., 12, 169–209, https://doi.org/10.5194/amt-12-169-2019, 2019.

Govt. of Delhi: Planning Department, Delhi, Economic Survey of Delhi, 2018–2019, 2019.

Govt. of India: Ministry of Road Transport and Highways, India, Notification, available at: http://egazette.nic.in/WriteReadData/2016/168300.pdf (last access: 16 January 2020), 2016.

Govt. of India: Ministry of Environment Forest & Climate Change, India, National Clean Air Program, 2019.

Grange, S. K., Lewis, A. C., Moller, S. J., and Carslaw, D. C.: Lower vehicular primary emissions of NO_2 in Europe than assumed in policy projections, Nat. Geosci., 10, 914–918, https://doi.org/10.1038/s41561-017-0009-0, 2017.

Gupta, P., Remer, L. A., Levy, R. C., and Mattoo, S.: Validation of MODIS 3 km land aerosol optical depth from NASA's EOS

Terra and Aqua missions, Atmos. Meas. Tech., 11, 3145–3159, https://doi.org/10.5194/amt-11-3145-2018, 2018.

Guttikunda, S. K. and Jawahar, P.: Atmospheric emissions and pollution from the coal-fired thermal power plants in India, Atmos. Environ., 92, 449–460, https://doi.org/10.1016/j.atmosenv.2014.04.057, 2014.

Harrison, R. G., Nicoll, K. A., Marlton, G. J., Ryder, C. L., and Bennett, A. J., Saharan dust plume charging observed over the UK, Environ. Res. Lett., 13, https://doi.org/10.1088/1748-9326/aabcd9, 2018.

Harrison, R. M. and Beddows, D. C.: Efficacy of Recent Emissions Controls on Road Vehicles in Europe and Implications for Public Health, Sci. Rep.-UK, 7, 1152, https://doi.org/10.1038/s41598-017-01135-2, 2017.

Heal, M. R., O'Donoghue, M. A., and Cape, J. N.: Overestimation of urban nitrogen dioxide by passive diffusion tubes: a comparative exposure and model study, Atmos. Environ., 33, 513–524, https://doi.org/10.1016/S1352-2310(98)00290-8, 1999.

Hilboll, A., Richter, A., and Burrows, J. P., Long-term changes of tropospheric NO_2 over megacities derived from multiple satellite instruments, Atmos. Chem. Phys., 13, 4145-4169, https://doi.org/10.5194/acp-13-4145-2013, 2013.

Holben, B. N., Eck, T. F., Slutsker, I., Tanre, D., Buis, J. P., Setzer, A., Vermote, E., Reagan, J. A., Kaufman, Y. J., Nakajima, T., Lavenu, F., Jankowiak, I., and Smirnov, A.: AERONET – A federated instrument network and data archive for aerosol characterization, Remote Sens. Environ., 66, 1–16, https://doi.org/10.1016/S0034-4257(98)00031-5, 1998.

Jethva, H., Torres, O., Field, R. D., Lyapustin, A., Gautam, R., and Kayetha, V., Connecting Crop Productivity, Residue Fires, and Air Quality over Northern India, Sci. Rep.-UK, 9, 16594, https://doi.org/10.1038/s41598-019-52799-x, 2019.

Jones, N. B., Riedel, K., Allan, W., Wood, S., Palmer, P. I., Chance, K., and Notholt, J.: Long-term tropospheric formaldehyde concentrations deduced from ground-based fourier transform solar infrared measurements, Atmos. Chem. Phys., 9, 7131–7142, https://doi.org/10.5194/acp-9-7131-2009, 2009.

Kaskaoutis, D. G., Singh, R. P., Gautam, R., Sharma, M., Kosmopoulos, P. G., and Tripathi, S. N.: Variability and trends of aerosol properties over Kanpur, northern India using AERONET data (2001-10), Environ. Res. Lett., 7, 024003, https://doi.org/10.1088/1748-9326/7/2/024003, 2012.

Kaufman, Y. J.: Aerosol Optical-Thickness and Atmospheric Path Radiance, J. Geophys. Res.-Atmos., 98, 2677–2692, https://doi.org/10.1029/92jd02427, 1993.

Kenagy, H. S., Sparks, T. L., Ebben, C. J., Wooldrige, P. J., Lopez-Hilfiker, F. D., Lee, B. H., Thornton, J. A., McDuffie, E. E., Fibiger, D. L., Brown, S. S., Montzka, D. D., Weinheimer, A. J., Schroder, J. C., Campuzano-Jost, P., Day, D. A., Jimenez, J. L., Dibb, J. E., Campos, T., Shah, V., Jaegle, L., and Cohen, R. C.: NO_x Lifetime and NO_y Partitioning During WINTER, J. Geophys. Res.-Atmos., 123, 9813–9827, https://doi.org/10.1029/2018jd028736, 2018.

Kim, S. W., Heckel, A., McKeen, S. A., Frost, G. J., Hsie, E. Y., Trainer, M. K., Richter, A., Burrows, J. P., Peckham, S. E., and Grell, G. A.: Satellite-observed US power plant NO_x emission reductions and their impact on air quality, Geophys. Res. Lett., 33, L22812, https://doi.org/10.1029/2006gl027749, 2006.

Klimont, Z., Smith, S. J., and Cofala, J.: The last decade of global anthropogenic sulfur dioxide: 2000–2011 emissions, Environ. Res. Lett., 8, 014003, https://doi.org/10.1088/1748-9326/8/1/014003, 2013.

Kotthaus, S. and Grimmond, C. S. B.: Atmospheric boundary-layer characteristics from ceilometer measurements. Part 2: Application to London's urban boundary layer, Q. J. Roy. Meteor. Soc., 144, 1511–1524, https://doi.org/10.1002/qj.3298, 2018.

Kramer, L. J., Leigh, R. J., Remedios, J. J., and Monks, P. S.: Comparison of OMI and ground-based in situ and MAX-DOAS measurements of tropospheric nitrogen dioxide in an urban area, J. Geophys. Res.-Atmos., 113, D16S39, https://doi.org/10.1029/2007jd009168, 2008.

Krotkov, N. A., Lamsal, L. N., Celarier, E. A., Swartz, W. H., Marchenko, S. V., Bucsela, E. J., Chan, K. L., Wenig, M., and Zara, M.: The version 3 OMI NO2 standard product, Atmos. Meas. Tech., 10, 3133–3149, https://doi.org/10.5194/amt-10-3133-2017, 2017.

Lamsal, L. N., Martin, R. V., van Donkelaar, A., Celarier, E. A., Bucsela, E. J., Boersma, K. F., Dirksen, R., Luo, C., and Wang, Y.: Indirect validation of tropospheric nitrogen dioxide retrieved from the OMI satellite instrument: Insight into the seasonal variation of nitrogen oxides at northern midlatitudes, J. Geophys. Res.-Atmos., 115, D05302, https://doi.org/10.1029/2009jd013351, 2010.

Lamsal, L. N., Martin, R. V., Padmanabhan, A., van Donkelaar, A., Zhang, Q., Sioris, C. E., Chance, K., Kurosu, T. P., and Newchurch, M. J.: Application of satellite observations for timely updates to global anthropogenic NO_x emission inventories, Geophys. Res. Lett., 38, L05810, https://doi.org/10.1029/2010gl046476, 2011.

Landrigan, P. J., Fuller, R., Acosta, N. J. R., Adeyi, O., Arnold, R., Basu, N., Balde, A. B., Bertollini, R., Bose-O'Reilly, S., Boufford, J. I., Breysse, P. N., Chiles, T., Mahidol, C., Coll-Seck, A. M., Cropper, M. L., Fobil, J., Fuster, V., Greenstone, M., Haines, A., Hanrahan, D., Hunter, D., Khare, M., Krupnick, A., Lanphear, B., Lohani, B., Martin, K., Mathiasen, K. V., McTeer, M. A., Murray, C. J. L., Ndahimananjara, J. D., Perera, F., Potocnik, J., Preker, A. S., Ramesh, J., Rockstrom, J., Salinas, C., Samson, L. D., Sandilya, K., Sly, P. D., Smith, K. R., Steiner, A., Stewart, R. B., Suk, W. A., van Schayck, O. C. P., Yadama, G. N., Yumkella, K., and Zhong, M.: The Lancet Commission on pollution and health, Lancet, 391, 462–512, https://doi.org/10.1016/S0140-6736(17)32345-0, 2018.

Langford, B., Nemitz, E., House, E., Phillips, G. J., Famulari, D., Davison, B., Hopkins, J. R., Lewis, A. C., and Hewitt, C. N.: Fluxes and concentrations of volatile organic compounds above central London, UK, Atmos. Chem. Phys., 10, 627–645, https://doi.org/10.5194/acp-10-627-2010, 2010.

Levy, R. C., Remer, L. A., and Dubovik, O.: Global aerosol optical properties and application to Moderate Resolution Imaging Spectroradiometer aerosol retrieval over land, J. Geophys. Res.-Atmos., 112, D13210, https://doi.org/10.1029/2006jd007815, 2007.

Levy, R. C., Remer, L. A., Kleidman, R. G., Mattoo, S., Ichoku, C., Kahn, R., and Eck, T. F.: Global evaluation of the Collection 5 MODIS dark-target aerosol products over land, Atmos. Chem. Phys., 10, 10399–10420, https://doi.org/10.5194/acp-10-10399-2010, 2010.

Levy, R. C., Mattoo, S., Munchak, L. A., Remer, L. A., Sayer, A. M., Patadia, F., and Hsu, N. C.: The Collection 6 MODIS aerosol products over land and ocean, Atmos. Meas. Tech., 6, 2989–3034, https://doi.org/10.5194/amt-6-2989-2013, 2013.

Li, Q., Li, C. C., and Mao, J. T.: Evaluation of Atmospheric Aerosol Optical Depth Products at Ultraviolet Bands Derived from MODIS Products, Aerosol Sci. Tech., 46, 1025–1034, https://doi.org/10.1080/02786826.2012.687475, 2012.

Lin, J.-T., Liu, M.-Y., Xin, J.-Y., Boersma, K. F., Spurr, R., Martin, R., and Zhang, Q.: Influence of aerosols and surface reflectance on satellite NO_2 retrieval: seasonal and spatial characteristics and implications for NO_x emission constraints, Atmos. Chem. Phys., 15, 11217–11241, https://doi.org/10.5194/acp-15-11217-2015, 2015.

Liu, T. J., Marlier, M. E., DeFries, R. S., Westervelt, D. M., Xia, K. R., Fiore, A. M., Mickley, L. J., Cusworth, D. H., and Milly, G.: Seasonal impact of regional outdoor biomass burning on air pollution in three Indian cities: Delhi, Bengaluru, and Pune, Atmos. Environ., 172, 83–92, https://doi.org/10.1016/j.atmosenv.2017.10.024, 2018.

Lyons, R., Doherty, R., Reay, D., and Shackley, S.: Legal but lethal: Lessons from NO_2 related mortality in a city compliant with EU limit value, Atmos. Pollut. Res., 11, 43–50, https://doi.org/10.1016/j.apr.2020.02.016, 2020.

Malley, C. S., Braban, C. F., Dumitrean, P., Cape, J. N., and Heal, M. R.: The impact of speciated VOCs on regional ozone increment derived from measurements at the UK EMEP supersites between 1999 and 2012, Atmos. Chem. Phys., 15, 8361–8380, https://doi.org/10.5194/acp-15-8361-2015, 2015.

Malley, C. S., Heal, M. R., Braban, C. F., Kentisbeer, J., Leeson, S. R., Malcolm, H., Lingard, J. J. N., Ritchie, S., Maggs, R., Beccaceci, S., Quincey, P., Brown, R. J. C., and Twigg, M. M.: The contributions to long-term health-relevant particulate matter at the UK EMEP supersites between 2010 and 2013: Quantifying the mitigation challenge, Environ. Int., 95, 98–111, https://doi.org/10.1016/j.envint.2016.08.005, 2016.

Marais, E. A., Jacob, D. J., Kurosu, T. P., Chance, K., Murphy, J. G., Reeves, C., Mills, G., Casadio, S., Millet, D. B., Barkley, M. P., Paulot, F., and Mao, J.: Isoprene emissions in Africa inferred from OMI observations of formaldehyde columns, Atmos. Chem. Phys., 12, 6219–6235, https://doi.org/10.5194/acp-12-6219-2012, 2012.

Marais, E. A., Jacob, D. J., Wecht, K., Lerot, C., Zhang, L., Yu, K., Kurosu, T. P., Chance, K., and Sauvage, B.: Anthropogenic emissions in Nigeria and implications for atmospheric ozone pollution: A view from space, Atmos. Environ., 99, 32–40, https://doi.org/10.1016/j.atmosenv.2014.09.055, 2014a.

Marais, E. A., Jacob, D. J., Guenther, A., Chance, K., Kurosu, T. P., Murphy, J. G., Reeves, C. E., and Pye, H. O. T.: Improved model of isoprene emissions in Africa using Ozone Monitoring Instrument (OMI) satellite observations of formaldehyde: implications for oxidants and particulate matter, Atmos. Chem. Phys., 14, 7693–7703, https://doi.org/10.5194/acp-14-7693-2014, 2014b.

Martin, R. V., Jacob, D. J., Chance, K., Kurosu, T. P., Palmer, P. I., and Evans, M. J.: Global inventory of nitrogen oxide emissions constrained by space-based observations of NO_2 columns, J. Geophys. Res.-Atmos., 108, 4537, https://doi.org/10.1029/2003jd003453, 2003.

McPhetres, A. and Aggarwal, S.: An Evaluation of MODIS-Retrieved Aerosol Optical Depth over AERONET Sites in Alaska, Remote Sens.-Basel, 10, 1384, https://doi.org/10.3390/rs10091384, 2018.

Mhawish, A., Banerjee, T., Broday, D. M., Misra, A., and Tripathi, S. N.: Evaluation of MODIS Collection 6 aerosol retrieval algorithms over Indo-Gangetic Plain: Implications of aerosols types and mass loading, Remote Sens. Environ., 201, 297–313, https://doi.org/10.1016/j.rse.2017.09.016, 2017.

Miller, S. M., Matross, D. M., Andrews, A. E., Millet, D. B., Longo, M., Gottlieb, E. W., Hirsch, A. I., Gerbig, C., Lin, J. C., Daube, B. C., Hudman, R. C., Dias, P. L. S., Chow, V. Y., and Wofsy, S. C.: Sources of carbon monoxide and formaldehyde in North America determined from high-resolution atmospheric data, Atmos. Chem. Phys., 8, 7673–7696, https://doi.org/10.5194/acp-8-7673-2008, 2008.

Millet, D. B., Jacob, D. J., Turquety, S., Hudman, R. C., Wu, S. L., Fried, A., Walega, J., Heikes, B. G., Blake, D. R., Singh, H. B., Anderson, B. E., and Clarke, A. D.: Formaldehyde distribution over North America: Implications for satellite retrievals of formaldehyde columns and isoprene emission, J. Geophys. Res.-Atmos., 111, D24S02, https://doi.org/10.1029/2005jd006853, 2006.

Munchak, L. A., Levy, R. C., Mattoo, S., Remer, L. A., Holben, B. N., Schafer, J. S., Hostetler, C. A., and Ferrare, R. A.: MODIS 3 km aerosol product: applications over land in an urban/suburban region, Atmos. Meas. Tech., 6, 1747–1759, https://doi.org/10.5194/amt-6-1747-2013, 2013.

Nagar, P. K., Sharma, M., and Das, D.: A new method for trend analyses in PM_{10} and impact of crop residue burning in Delhi, Kanpur and Jaipur, India, Urban Clim., 27, 193–203, https://doi.org/10.1016/j.uclim.2018.12.003, 2019.

Nakoudi, K., Giannakaki, E., Dandou, A., Tombrou, M., and Komppula, M.: Planetary boundary layer height by means of lidar and numerical simulations over New Delhi, India, Atmos. Meas. Tech., 12, 2595–2610, https://doi.org/10.5194/amt-12-2595-2019, 2019.

Ots, R., Heal, M. R., Young, D. E., Williams, L. R., Allan, J. D., Nemitz, E., Di Marco, C., Detournay, A., Xu, L., Ng, N. L., Coe, H., Herndon, S. C., Mackenzie, I. A., Green, D. C., Kuenen, J. J. P., Reis, S., and Vieno, M.: Modelling carbonaceous aerosol from residential solid fuel burning with different assumptions for emissions, Atmos. Chem. Phys., 18, 4497–4518, https://doi.org/10.5194/acp-18-4497-2018, 2018.

Parkhi, N., Chate, D., Ghude, S. D., Peshin, S., Mahajan, A., Srinivas, R., Surendran, D., Ali, K., Singh, S., Trimbake, H., and Beig, G.: Large inter annual variation in air quality during the annual festival "Diwali" in an Indian megacity, J. Environ. Sci.-China, 43, 265–272, https://doi.org/10.1016/j.jes.2015.08.015, 2016.

Pathania, R., Phadke, P., Gupta, R. K., and Ramanathan, S.: Centre for Science and Environment, New Delhi, Off-Target Status of Thermal Power Stations in Delhi NCR, available at: http://www.indiaenvironmentportal.org.in/files/file/Off-Target---Status-of-Power-Stations-Report.pdf (last access: 16 January 2020), 2018.

Paulot, F., Paynter, D., Ginoux, P., Naik, V., Whitburn, S., Van Damme, M., Clarisse, L., Coheur, P. F., and Horowitz, L. W.: Gas-aerosol partitioning of ammonia in biomass burning plumes: Implications for the interpretation of space-

borne observations of ammonia and the radiative forcing of ammonium nitrate, Geophys. Res. Lett., 44, 8084–8093, https://doi.org/10.1002/2017gl074215, 2017.

Petrenko, M., Ichoku, C., and Leptoukh, G.: Multi-sensor Aerosol Products Sampling System (MAPSS), Atmos. Meas. Tech., 5, 913–926, https://doi.org/10.5194/amt-5-913-2012, 2012.

Pope, R. J., Arnold, S. R., Chipperfield, M. P., Latter, B. G., Siddans, R., and Kerridge, B. J.: Widespread changes in UK air quality observed from space, Atmos. Sci. Lett., 19, e817, https://doi.org/10.1002/asl.817, 2018.

Ramachandran, S., Kedia, S., and Srivastava, R.: Aerosol optical depth trends over different regions of India, Atmos. Environ., 49, 338–347, https://doi.org/10.1016/j.atmosenv.2011.11.017, 2012.

Reed, C., Evans, M. J., Di Carlo, P., Lee, J. D., and Carpenter, L. J.: Interferences in photolytic NO2 measurements: explanation for an apparent missing oxidant?, Atmos. Chem. Phys., 16, 4707–4724, https://doi.org/10.5194/acp-16-4707-2016, 2016.

Remer, L. A., Kaufman, Y. J., Tanre, D., Mattoo, S., Chu, D. A., Martins, J. V., Li, R. R., Ichoku, C., Levy, R. C., Kleidman, R. G., Eck, T. F., Vermote, E., and Holben, B. N.: The MODIS aerosol algorithm, products, and validation, J. Atmos. Sci., 62, 947–973, https://doi.org/10.1175/Jas3385.1, 2005.

Remer, L. A., Mattoo, S., Levy, R. C., and Munchak, L. A.: MODIS 3 km aerosol product: algorithm and global perspective, Atmos. Meas. Tech., 6, 1829–1844, https://doi.org/10.5194/amt-6-1829-2013, 2013.

Richmond, B., Misra, A., Brown, P., Karagianni, E., Murrells, T., Pang, Y., Passant, N., Pepler, A., Stewart, R., Thistlethwaite, G., Turtle, L., Wakeling, D., Walker, C., Wiltshire, J., Hobson, M., Gibbs, M., Misselbrook, T., Dragosit, U., and Tomlinson, S.: Environment, United Kingdom, UK Informative Inventory Report (1990 to 2018), available at: https://uk-air.defra.gov.uk/assets/documents/reports/cat07/2003131327_GB_IIR_2020_v1.0.pdf (last access: 20 December 2019), 2020.

Richter, A.: Nitrogen oxides in the troposphere – What have we learned from satellite measurements?, Erca: From the Human Dimensions of Global Environmental Change to the Observation of the Earth from Space, Vol 8, WOS:000268062600011, 2009.

Sahu, L. K., Yadav, R., and Pal, D.: Source identification of VOCs at an urban site of western India: Effect of marathon events and anthropogenic emissions, J. Geophys. Res.-Atmos., 121, 2416–2433, https://doi.org/10.1002/2015jd024454, 2016.

Sathe, Y., Kulkarni, S., Gupta, P., Kaginalkar, A., Islam, S., and Gargava, P.: Application of Moderate Resolution Imaging Spectroradiometer (MODIS) Aerosol Optical Depth (AOD) and Weather Research Forecasting (WRF) model meteorological data for assessment of fine particulate matter ($PM_{2.5}$) over India, Atmos. Pollut. Res., 10, 418–434, https://doi.org/10.1016/j.apr.2018.08.016, 2019.

Schaap, M., Apituley, A., Timmermans, R. M. A., Koelemeijer, R. B. A., and de Leeuw, G.: Exploring the relation between aerosol optical depth and $PM_{2.5}$ at Cabauw, the Netherlands, Atmos. Chem. Phys., 9, 909–925, https://doi.org/10.5194/acp-9-909-2009, 2009.

Schneider, P., Lahoz, W. A., and van der A, R.: Recent satellite-based trends of tropospheric nitrogen dioxide over large urban agglomerations worldwide, Atmos. Chem. Phys., 15, 1205–1220, https://doi.org/10.5194/acp-15-1205-2015, 2015.

Shaddick, G., Thomas, M. L., Amini, H., Broday, D., Cohen, A., Frostad, J., Green, A., Gumy, S., Liu, Y., Martin, R. V., Pruss-Ustun, A., Simpson, D., van Donkelaar, A., and Brauer, M.: Data Integration for the Assessment of Population Exposure to Ambient Air Pollution for Global Burden of Disease Assessment, Environ. Sci. Technol., 52, 9069–9078, https://doi.org/10.1021/acs.est.8b02864, 2018.

Shah, V., Jacob, D. J., Li, K., Silvern, R. F., Zhai, S., Liu, M., Lin, J., and Zhang, Q.: Effect of changing NOx lifetime on the seasonality and long-term trends of satellite-observed tropospheric NO_2 columns over China, Atmos. Chem. Phys., 20, 1483–1495, https://doi.org/10.5194/acp-20-1483-2020, 2020.

Silvern, R. F., Jacob, D. J., Travis, K. R., Sherwen, T., Evans, M. J., Cohen, R. C., Laughner, J. L., Hall, S. R., Ullmann, K., Crounse, J. D., Wennberg, P. O., Peischl, J., and Pollack, I. B.: Observed NO/NO_2 Ratios in the Upper Troposphere Imply Errors in $NO\text{-}NO_2\text{-}O_3$ Cycling Kinetics or an Unaccounted NO_x Reservoir, Geophys. Res. Lett., 45, 4466–4474, https://doi.org/10.1029/2018gl077728, 2018.

Silvern, R. F., Jacob, D. J., Mickley, L. J., Sulprizio, M. P., Travis, K. R., Marais, E. A., Cohen, R. C., Laughner, J. L., Choi, S., Joiner, J., and Lamsal, L. N.: Using satellite observations of tropospheric NO2 columns to infer long-term trends in US NOx emissions: the importance of accounting for the free tropospheric NO2 background, Atmos. Chem. Phys., 19, 8863–8878, https://doi.org/10.5194/acp-19-8863-2019, 2019.

Singh, R. B. and Grover, A.: Sustainable Urban Environment in Delhi Mega City: Emerging Problems and Prospects for Innovative Solutions, available at: https://sustainabledevelopment.un.org/content/documents/6494108_Singh\,%20and\,%20Grover_Sustainable\,%20Urban\,%20Environment\,%20in\,%20Delhi.pdf (last access: 10 February 2021), 2015.

Singh, S. and Kulshrestha, U. C.: Abundance and distribution of gaseous ammonia and particulate ammonium at Delhi, India, Biogeosciences, 9, 5023–5029, https://doi.org/10.5194/bg-9-5023-2012, 2012.

Snider, G., Weagle, C. L., Martin, R. V., van Donkelaar, A., Conrad, K., Cunningham, D., Gordon, C., Zwicker, M., Akoshile, C., Artaxo, P., Anh, N. X., Brook, J., Dong, J., Garland, R. M., Greenwald, R., Griffith, D., He, K., Holben, B. N., Kahn, R., Koren, I., Lagrosas, N., Lestari, P., Ma, Z., Vanderlei Martins, J., Quel, E. J., Rudich, Y., Salam, A., Tripathi, S. N., Yu, C., Zhang, Q., Zhang, Y., Brauer, M., Cohen, A., Gibson, M. D., and Liu, Y.: SPARTAN: a global network to evaluate and enhance satellite-based estimates of ground-level particulate matter for global health applications, Atmos. Meas. Tech., 8, 505–521, https://doi.org/10.5194/amt-8-505-2015, 2015.

Stieger, B., Spindler, G., Fahlbusch, B., Muller, K., Gruner, A., Poulain, L., Thoni, L., Seitler, E., Wallasch, M., and Herrmann, H.: Measurements of PM_{10} ions and trace gases with the online system MARGA at the research station Melpitz in Germany – A five-year study, J. Atmos. Chem., 75, 33–70, https://doi.org/10.1007/s10874-017-9361-0, 2018.

Streets, D. G., Canty, T., Carmichael, G. R., de Foy, B., Dickerson, R. R., Duncan, B. N., Edwards, D. P., Haynes, J. A., Henze, D. K., Houyoux, M. R., Jacobi, D. J., Krotkov, N. A., Lamsal, L. N., Liu, Y., Lu, Z. F., Martini, R. V., Pfister, G. G., Pinder, R. W., Salawitch, R. J., and Wechti,

K. J.: Emissions estimation from satellite retrievals: A review of current capability, Atmos. Environ., 77, 1011–1042, https://doi.org/10.1016/j.atmosenv.2013.05.051, 2013.

Sugathan, A., Bhangale, R., Kansal, V., and Hulke, U.: How can Indian power plants cost-effectively meet the new sulfur emission standards? Policy evaluation using marginal abatement cost-curves, Energ. Policy, 121, 124–137, https://doi.org/10.1016/j.enpol.2018.06.008, 2018.

Surl, L., Palmer, P. I., and González Abad, G.: Which processes drive observed variations of HCHO columns over India?, Atmos. Chem. Phys., 18, 4549–4566, https://doi.org/10.5194/acp-18-4549-2018, 2018.

Tang, Y. S., Braban, C. F., Dragosits, U., Dore, A. J., Simmons, I., van Dijk, N., Poskitt, J., Dos Santos Pereira, G., Keenan, P. O., Conolly, C., Vincent, K., Smith, R. I., Heal, M. R., and Sutton, M. A.: Drivers for spatial, temporal and long-term trends in atmospheric ammonia and ammonium in the UK, Atmos. Chem. Phys., 18, 705–733, https://doi.org/10.5194/acp-18-705-2018, 2018.

Theys, N., Hedelt, P., De Smedt, I., Lerot, C., Yu, H., Vlietinck, J., Pedergnana, M., Arellano, S., Galle, B., Fernandez, D., Carlito, C. J. M., Barrington, C., Taisne, B., Delgado-Granados, H., Loyola, D., and Van Roozendael, M.: Global monitoring of volcanic SO_2 degassing with unprecedented resolution from TROPOMI onboard Sentinel-5 Precursor, Sci. Rep.-UK, 9, 2643, https://doi.org/10.1038/s41598-019-39279-y, 2019.

ul-Haq, Z., Tariq, S., and Ali, M.: Tropospheric NO_2 Trends over South Asia during the Last Decade (2004–2014) Using OMI Data, Adv. Meteorol., https://doi.org/10.1155/2015/959284, 2015.

UN: Department of Economic and Social Affairs – Population Division, New York, World Urbanization Prospects: The 2018 Revision, available at: https://population.un.org/wup/Publications/Files/WUP2018-Report.pdf (last access: 8 February 2021), 2019.

Université libre de Bruxelles (ULB): IASI NH3 data, available at: https://iasi.aeris-data.fr/nh3/, last access: 8 March 2021.

Valach, A. C., Langford, B., Nemitz, E., MacKenzie, A. R., and Hewitt, C. N., Concentrations of selected volatile organic compounds at kerbside and background sites in central London, Atmos. Environ., 95, 456–467, https://doi.org/10.1016/j.atmosenv.2014.06.052, 2014.

Van Damme, M., Clarisse, L., Heald, C. L., Hurtmans, D., Ngadi, Y., Clerbaux, C., Dolman, A. J., Erisman, J. W., and Coheur, P. F.: Global distributions, time series and error characterization of atmospheric ammonia (NH3) from IASI satellite observations, Atmos. Chem. Phys., 14, 2905–2922, https://doi.org/10.5194/acp-14-2905-2014, 2014.

Van Damme, M., Clarisse, L., Dammers, E., Liu, X., Nowak, J. B., Clerbaux, C., Flechard, C. R., Galy-Lacaux, C., Xu, W., Neuman, J. A., Tang, Y. S., Sutton, M. A., Erisman, J. W., and Coheur, P. F.: Towards validation of ammonia (NH3) measurements from the IASI satellite, Atmos. Meas. Tech., 8, 1575–1591, https://doi.org/10.5194/amt-8-1575-2015, 2015.

Van Damme, M., Whitburn, S., Clarisse, L., Clerbaux, C., Hurtmans, D., and Coheur, P.-F.: Version 2 of the IASI NH_3 neural network retrieval algorithm: near-real-time and reanalysed datasets, Atmos. Meas. Tech., 10, 4905–4914, https://doi.org/10.5194/amt-10-4905-2017, 2017.

Van Damme, M., Clarisse, L., Whitburn, S., Hadji-Lazaro, J., Hurtmans, D., Clerbaux, C., and Coheur, P. F.: Industrial and agricultural ammonia point sources exposed, Nature, 564, 99-110, https://doi.org/10.1038/s41586-018-0747-1, 2018.

Van Damme, M., Clarisse, L., Franco, B., Sutton, M. A., Erisman, J. W., Kruit, R. J. W., van Zanten, M., Whitburn, S., Hadji-Lazaro, J., Hurtmans, D., Clerbaux, C., and Coheur, P. F.: Global, regional and national trends of atmospheric ammonia derived from a decadal (2008–2018) satellite record, Environ. Res. Lett., https://doi.org/10.1088/1748-9326/abd5e0, in press, 2020.

van der A, R. J., Peters, D. H. M. U., Eskes, H., Boersma, K. F., Van Roozendael, M., De Smedt, I., and Kelder, H. M.: Detection of the trend and seasonal variation in tropospheric NO_2 over China, J. Geophys. Res.-Atmos., 111, D12317, https://doi.org/10.1029/2005jd006594, 2006.

van der A, R. J., Eskes, H. J., Boersma, K. F., van Noije, T. P. C., Van Roozendael, M., De Smedt, I., Peters, D. H. M. U., and Meijer, E. W.: Trends, seasonal variability and dominant NO_x source derived from a ten year record of NO_2 measured from space, J. Geophys. Res.-Atmos., 113, D04302, https://doi.org/10.1029/2007jd009021, 2008.

van Donkelaar, A., Martin, R. V., and Park, R. J.: Estimating ground-level $PM_{2.5}$ using aerosol optical depth determined from satellite remote sensing, J. Geophys. Res.-Atmos., 111, D21201, https://doi.org/10.1029/2005jd006996, 2006.

van Donkelaar, A., Martin, R. V., Brauer, M., Kahn, R., Levy, R., Verduzco, C., and Villeneuve, P. J.: Global Estimates of Ambient Fine Particulate Matter Concentrations from Satellite-Based Aerosol Optical Depth: Development and Application, Environ. Health Persp., 118, 847–855, https://doi.org/10.1289/ehp.0901623, 2010.

van Donkelaar, A., Martin, R. V., Brauer, M., Hsu, N. C., Kahn, R. A., Levy, R. C., Lyapustin, A., Sayer, A. M., and Winker, D. M.: Global Estimates of Fine Particulate Matter using a Combined Geophysical-Statistical Method with Information from Satellites, Models, and Monitors, Environ. Sci. Technol., 50, 3762–3772, https://doi.org/10.1021/acs.est.5b05833, 2016.

Vasilkov, A., Krotkov, N., Yang, E.-S., Lamsal, L., Joiner, J., Castellanos, P., Fasnacht, Z., and Spurr, R.: Explicit and consistent aerosol correction for visible wavelength satellite cloud and nitrogen dioxide retrievals based on optical properties from a global aerosol analysis, Atmos. Meas. Tech. Discuss. [preprint], https://doi.org/10.5194/amt-2019-458, in review, 2020.

Venkataraman, C., Brauer, M., Tibrewal, K., Sadavarte, P., Ma, Q., Cohen, A., Chaliyakunnel, S., Frostad, J., Klimont, Z., Martin, R. V., Millet, D. B., Philip, S., Walker, K., and Wang, S.: Source influence on emission pathways and ambient $PM_{2.5}$ pollution over India (2015–2050), Atmos. Chem. Phys., 18, 8017–8039, https://doi.org/10.5194/acp-18-8017-2018, 2018.

Vieno, M., Heal, M. R., Hallsworth, S., Famulari, D., Doherty, R. M., Dore, A. J., Tang, Y. S., Braban, C. F., Leaver, D., Sutton, M. A., and Reis, S.: The role of long-range transport and domestic emissions in determining atmospheric secondary inorganic particle concentrations across the UK, Atmos. Chem. Phys., 14, 8435–8447, https://doi.org/10.5194/acp-14-8435-2014, 2014.

Vieno, M., Heal, M. R., Williams, M. L., Carnell, E. J., Nemitz, E., Stedman, J. R., and Reis, S.: The sensitivities of emissions reductions for the mitigation of UK $PM_{2.5}$, Atmos. Chem. Phys., 16, 265–276, https://doi.org/10.5194/acp-16-265-2016, 2016.

Vodonos, A., Abu Awad, Y., and Schwartz, J.: The concentration-response between long-term $PM_{2.5}$ exposure and mortality; A meta-regression approach, Environ. Res., 166, 677–689, https://doi.org/10.1016/j.envres.2018.06.021, 2018.

Vohra, K.: India NO2 data, Zenodo [Data set], https://doi.org/10.5281/zenodo.4696252, 2021.

Vohra, K., Vodonos, A., Schwartz, J., Marais, E. A., Sulprizio, M. P., and Mickley, L. J.: Global mortality from outdoor fine particle pollution generated by fossil fuel combustion: Results from GEOS-Chem, Environ. Res., 195, 110754, https://doi.org/10.1016/j.envres.2021.110754, 2021.

Walker, H. L., Heal, M. R., Braban, C. F., Ritchie, S., Conolly, C., Sanocka, A., Dragosits, U., and Twigg, M. M.: Changing supersites: assessing the impact of the southern UK EMEP supersite relocation on measured atmospheric composition, Environ. Res. Comm., 1, 041001, https://doi.org/10.1088/2515-7620/ab1a6f, 2019.

Wang, L., Slowik, J. G., Tripathi, N., Bhattu, D., Rai, P., Kumar, V., Vats, P., Satish, R., Baltensperger, U., Ganguly, D., Rastogi, N., Sahu, L. K., Tripathi, S. N., and Prévôt, A. S. H.: Source characterization of volatile organic compounds measured by proton-transfer-reaction time-of-flight mass spectrometers in Delhi, India, Atmos. Chem. Phys., 20, 9753–9770, https://doi.org/10.5194/acp-20-9753-2020, 2020.

Wang, T., Song, Y., Xu, Z., Liu, M., Xu, T., Liao, W., Yin, L., Cai, X., Kang, L., Zhang, H., and Zhu, T.: Why is the Indo-Gangetic Plain the region with the largest NH_3 column in the globe during pre-monsoon and monsoon seasons?, Atmos. Chem. Phys., 20, 8727–8736, https://doi.org/10.5194/acp-20-8727-2020, 2020.

Warner, J. X., Dickerson, R. R., Wei, Z., Strow, L. L., Wang, Y., and Liang, Q.: Increased atmospheric ammonia over the world's major agricultural areas detected from space, Geophys. Res. Lett., 44, 2875–2884, https://doi.org/10.1002/2016gl072305, 2017.

Weagle, C. L., Snider, G., Li, C., van Donkelaar, A., Philip, S., Bissonnette, P., Burke, I., Jackson, J., Latimer, R., Stone, E., Abboud, I., Akoshile, C., Anh, N. X., Brook, J. R., Cohen, A., Dong, J. L., Gibson, M. D., Griffith, D., He, K. B., Holben, B. N., Kahn, R., Keller, C. A., Kim, J. S., Lagrosas, N., Lestari, P., Khian, Y. L., Liu, Y., Marais, E. A., Martins, J. V., Misra, A., Muliane, U., Pratiwi, R., Quel, E. J., Salam, A., Segey, L., Tripathi, S. N., Wang, C., Zhang, Q., Brauer, M., Rudich, Y., and Martin, R. V.: Global Sources of Fine Particulate Matter: Interpretation of $PM_{2.5}$ Chemical Composition Observed by SPARTAN using a Global Chemical Transport Model, Environ. Sci. Technol., 52, 11670–11681, https://doi.org/10.1021/acs.est.8b01658, 2018.

Weatherhead, E. C., Reinsel, G. C., Tiao, G. C., Meng, X. L., Choi, D. S., Cheang, W. K., Keller, T., DeLuisi, J., Wuebbles, D. J., Kerr, J. B., Miller, A. J., Oltmans, S. J., and Frederick, J. E.: Factors affecting the detection of trends: Statistical considerations and applications to environmental data, J. Geophys. Res.-Atmos., 103, 17149–17161, https://doi.org/10.1029/98jd00995, 1998.

Wei, J., Sun, L., Peng, Y. R., Wang, L. C., Zhang, Z. Y., Bilal, M., and Ma, Y. C.: An Improved High-Spatial-Resolution Aerosol Retrieval Algorithm for MODIS Images Over Land, J. Geophys. Res.-Atmos., 123, 12291–12307, https://doi.org/10.1029/2017jd027795, 2018.

Wei, J., Li, Z. Q., Peng, Y. R., and Sun, L.: MODIS Collection 6.1 aerosol optical depth products over land and ocean: validation and comparison, Atmos. Environ., 201, 428–440, https://doi.org/10.1016/j.atmosenv.2018.12.004, 2019.

Wei, J., Li, Z. Q., Sun, L., Peng, Y. R., Liu, L., He, L. J., Qin, W. M., and Cribb, M.: MODIS Collection 6.1 3 km resolution aerosol optical depth product: global evaluation and uncertainty analysis, Atmos. Environ., 240, 117768, 10.1016/j.atmosenv.2020.117768, 2020.

Whalley, L. K., Stone, D., Bandy, B., Dunmore, R., Hamilton, J. F., Hopkins, J., Lee, J. D., Lewis, A. C., and Heard, D. E.: Atmospheric OH reactivity in central London: observations, model predictions and estimates of in situ ozone production, Atmos. Chem. Phys., 16, 2109–2122, https://doi.org/10.5194/acp-16-2109-2016, 2016.

Whalley, L. K., Stone, D., Dunmore, R., Hamilton, J., Hopkins, J. R., Lee, J. D., Lewis, A. C., Williams, P., Kleffmann, J., Laufs, S., Woodward-Massey, R., and Heard, D. E.: Understanding in situ ozone production in the summertime through radical observations and modelling studies during the Clean air for London project (ClearfLo), Atmos. Chem. Phys., 18, 2547–2571, https://doi.org/10.5194/acp-18-2547-2018, 2018.

Whitburn, S., Van Damme, M., Clarisse, L., Bauduin, S., Heald, C. L., Hadji-Lazaro, J., Hurtmans, D., Zondlo, M. A., Clerbaux, C., and Coheur, P. F.: A flexible and robust neural network IASI-NH_3 retrieval algorithm, J. Geophys. Res.-Atmos., 121, 6581–6599, https://doi.org/10.1002/2016jd024828, 2016.

WHO; World Health Organization, WHO Global Urban Ambient Air Pollution Database, available at: https://www.who.int/phe/health_topics/outdoorair/databases/cities/en/ (last access: 16 January 2020), 2018.

World Bank, Leveraging Spatial Development Options for Uttar Pradesh, available at: http://documents1.worldbank.org/curated/en/751141468269412833/pdf/889670WP0URGEN00Box385254B00PUBLIC0.pdf (last access: 8 March 2021), 2014.

Yadav, R., Sahu, L. K., Beig, G., Tripathi, N., and Jaaffrey, S. N. A.: Ambient particulate matter and carbon monoxide at an urban site of India: Influence of anthropogenic emissions and dust storms, Environ. Pollut., 225, 291–303, https://doi.org/10.1016/j.envpol.2017.01.038, 2017.

Zara, M., Boersma, K. F., De Smedt, I., Richter, A., Peters, E., van Geffen, J. H. G. M., Beirle, S., Wagner, T., Van Roozendael, M., Marchenko, S., Lamsal, L. N., and Eskes, H. J.: Improved slant column density retrieval of nitrogen dioxide and formaldehyde for OMI and GOME-2A from QA4ECV: intercomparison, uncertainty characterisation, and trends, Atmos. Meas. Tech., 11, 4033–4058, https://doi.org/10.5194/amt-11-4033-2018, 2018.

Zara, M., Boersma, F., Eskes, H., van der Gon, H. D., de Arellano, J. V.-G., Krol, M., van der Swaluw, E., Schuch, W., and Velders, G. J. M.: Reductions in nitrogen oxides over the Netherlands between 2005 and 2018 observed from space and on the ground: Decreasing emissions and increasing O_3 indicate changing NO_x chemistry, Atmos. Environ., 9, 100104, https://doi.org/10.1016/j.aeaoa.2021.100104, 2021.

Zhu, L., Jacob, D. J., Mickley, L. J., Marais, E. A., Cohan, D. S., Yoshida, Y., Duncan, B. N., Abad, G. G., and Chance, K. V.: Anthropogenic emissions of highly reactive volatile organic compounds in eastern Texas inferred from oversampling of satellite (OMI) measurements of HCHO columns, Environ. Res. Lett., 9, 114004, https://doi.org/10.1088/1748-9326/9/11/114004, 2014.

Zhu, L., Jacob, D. J., Kim, P. S., Fisher, J. A., Yu, K., Travis, K. R., Mickley, L. J., Yantosca, R. M., Sulprizio, M. P., De Smedt, I., González Abad, G., Chance, K., Li, C., Ferrare, R., Fried, A., Hair, J. W., Hanisco, T. F., Richter, D., Jo Scarino, A., Walega, J., Weibring, P., and Wolfe, G. M.: Observing atmospheric formaldehyde (HCHO) from space: validation and intercomparison of six retrievals from four satellites (OMI, GOME2A, GOME2B, OMPS) with SEAC^{4}RS aircraft observations over the southeast US, Atmos. Chem. Phys., 16, 13477–13490, https://doi.org/10.5194/acp-16-13477-2016, 2016.

Zoogman, P., Jacob, D. J., Chance, K., Zhang, L., Le Sager, P., Fiore, A. M., Eldering, A., Liu, X., Natraj, V., and Kulawik, S. S.: Ozone air quality measurement requirements for a geostationary satellite mission, Atmos. Environ., 45, 7143–7150, https://doi.org/10.1016/j.atmosenv.2011.05.058, 2011.

Environmental Research 195 (2021) 110754

Contents lists available at ScienceDirect

Environmental Research

journal homepage: www.elsevier.com/locate/envres

Global mortality from outdoor fine particle pollution generated by fossil fuel combustion: Results from GEOS-Chem

Karn Vohra [a,*], Alina Vodonos [b], Joel Schwartz [b], Eloise A. Marais [c,1], Melissa P. Sulprizio [d], Loretta J. Mickley [d]

[a] School of Geography, Earth and Environmental Sciences, University of Birmingham, Birmingham, UK
[b] Harvard T.H. Chan School of Public Health, Department of Environmental Health, Harvard University, Boston, MA, USA
[c] Department of Physics and Astronomy, University of Leicester, Leicester, UK
[d] John A. Paulson School of Engineering and Applied Sciences, Harvard University, Cambridge, MA, USA

ARTICLE INFO

Keywords:
Particulate matter
Fossil fuel
Mortality
Health impact assessment

ABSTRACT

The burning of fossil fuels – especially coal, petrol, and diesel – is a major source of airborne fine particulate matter ($PM_{2.5}$), and a key contributor to the global burden of mortality and disease. Previous risk assessments have examined the health response to total $PM_{2.5}$, not just $PM_{2.5}$ from fossil fuel combustion, and have used a concentration-response function with limited support from the literature and data at both high and low concentrations. This assessment examines mortality associated with $PM_{2.5}$ from only fossil fuel combustion, making use of a recent meta-analysis of newer studies with a wider range of exposure. We also estimated mortality due to lower respiratory infections (LRI) among children under the age of five in the Americas and Europe, regions for which we have reliable data on the relative risk of this health outcome from $PM_{2.5}$ exposure. We used the chemical transport model GEOS-Chem to estimate global exposure levels to fossil-fuel related $PM_{2.5}$ in 2012. Relative risks of mortality were modeled using functions that link long-term exposure to $PM_{2.5}$ and mortality, incorporating nonlinearity in the concentration response. We estimate a global total of 10.2 (95% CI: −47.1 to 17.0) million premature deaths annually attributable to the fossil-fuel component of $PM_{2.5}$. The greatest mortality impact is estimated over regions with substantial fossil fuel related $PM_{2.5}$, notably China (3.9 million), India (2.5 million) and parts of eastern US, Europe and Southeast Asia. The estimate for China predates substantial decline in fossil fuel emissions and decreases to 2.4 million premature deaths due to 43.7% reduction in fossil fuel $PM_{2.5}$ from 2012 to 2018 bringing the global total to 8.7 (95% CI: −1.8 to 14.0) million premature deaths. We also estimated excess annual deaths due to LRI in children (0–4 years old) of 876 in North America, 747 in South America, and 605 in Europe. This study demonstrates that the fossil fuel component of $PM_{2.5}$ contributes a large mortality burden. The steeper concentration-response function slope at lower concentrations leads to larger estimates than previously found in Europe and North America, and the slower drop-off in slope at higher concentrations results in larger estimates in Asia. Fossil fuel combustion can be more readily controlled than other sources and precursors of $PM_{2.5}$ such as dust or wildfire smoke, so this is a clear message to policymakers and stakeholders to further incentivize a shift to clean sources of energy.

1. Introduction

The burning of fossil fuels – especially coal, petrol, and diesel – is a major source of airborne particulate matter (PM) and ground-level ozone, which have both been implicated as key contributors to the global burden of mortality and disease (Apte et al., 2015; Dedoussi and Barrett, 2014; Lim et al., 2012). A series of studies have reported an association between exposure to air pollution and adverse health outcomes (Brook et al., 2010), even at low exposure levels (<10 μg m^{-3}, the current World Health Organization, WHO, guideline) (Di et al., 2017). The Global Burden of Diseases, Injuries, and Risk Factors Study 2015 (GBD, 2015) identified ambient air pollution as a leading cause of the global disease burden, especially in low-income and middle-income countries (Forouzanfar et al., 2016). Recent estimates of the global

* Corresponding author.
E-mail address: karnvohra@gmail.com (K. Vohra).
[1] Now at: Department of Geography, University College London, London, UK.

https://doi.org/10.1016/j.envres.2021.110754
Received 29 July 2019; Received in revised form 12 January 2021; Accepted 14 January 2021
Available online 9 February 2021
0013-9351/

burden of disease suggest that exposure to $PM_{2.5}$ (particulate matter with an aerodynamic diameter < 2.5 μm) causes 4.2 million deaths and 103.1 million disability-adjusted life-years (DALYs) in 2015, representing 7.6% of total global deaths and 4.2% of global DALYs, with 59% of these in east and south Asia Cohen et al. (2017).

A series of newer studies conducted at lower concentrations and at higher concentrations have reported higher slopes than incorporated into the GBD using the integrated exposure–response (IER) curve (Burnett et al., 2014). These studies examined mortality due to exposure to $PM_{2.5}$ at concentrations below 10 μg m^{-3} in North America (Di et al., 2017; Pinault et al., 2016) and above 40 μg m^{-3} in Asia (Katanoda et al., 2011; Tseng et al., 2015; Ueda et al., 2012; Wong et al., 2015, 2016; Yin et al., 2017). Here we have used a concentration-response curve from a recently published meta-analysis of long-term $PM_{2.5}$ mortality association among adult populations which incorporates those new findings at high and low $PM_{2.5}$ concentrations (Vodonos et al., 2018). We also focus our study on the health impacts of fossil-fuel derived $PM_{2.5}$. In contrast, GBD reports only the health impacts of total $PM_{2.5}$ and does not distinguish mortality from fossil-fuel derived $PM_{2.5}$ and that from other kinds of $PM_{2.5}$, including dust, wildfire smoke, and biogenically-sourced particles. We focus only on $PM_{2.5}$ since recent studies have provided mixed results on the link between ozone and mortality (Atkinson et al., 2016) and there does not exist a global coherent concentration-response function (CRF) for ozone.

The developing fetus and children younger than 5 years of age are more biologically and neurologically susceptible to the many adverse effects of air pollutants from fossil-fuel combustion than adults. This differential susceptibility to air pollution is due to their rapid growth, developing brain, and immature respiratory, detoxification, immune, and thermoregulatory systems (Bateson and Schwartz, 2008; Perera, 2018). Children also breathe more air per kilogram of body weight than adults, and are therefore more exposed to pollutants in air (WHO, 2006; Xu et al., 2012). The WHO estimated that in 2012, 169,000 global deaths among children under the age of 5 were attributable to ambient air pollution (WHO, 2016). Further estimation of the burden of mortality due to $PM_{2.5}$ (particularly from anthropogenic sources) among the young population would highlight the need for intervention aimed at reducing children's exposure.

Using the chemical transport model GEOS-Chem, we quantified the number of premature deaths attributable to ambient air pollution from fossil fuel combustion. Improved knowledge of this very immediate and direct consequence of fossil fuel use provides evidence of the benefits to current efforts to cut greenhouse gas emissions and invest in alternative sources of energy. It also helps quantify the magnitude of the health impacts of a category of $PM_{2.5}$ that can be more readily controlled than other kinds of $PM_{2.5}$ such as dust or wildfire smoke.

2. Materials and methods

2.1. Calculation of surface $PM_{2.5}$ concentrations

Previous studies examining the global burden of disease from outdoor air pollution have combined satellite and surface observations with models to obtain improved estimates of global annual mean concentrations of $PM_{2.5}$ (Shaddick et al., 2018). However, the goal of such studies was to quantify the health response to $PM_{2.5}$ from all sources, both natural and anthropogenic (Brauer et al., 2016; Cohen et al., 2017). Here the focus of our study is on surface ambient $PM_{2.5}$ generated by fossil fuel combustion, and for that we rely solely on the chemical transport model GEOS-Chem since current satellite and surface measurements cannot readily distinguish between the sources of $PM_{2.5}$. Results from GEOS-Chem have been extensively validated against surface, aircraft, and space-based observations around the world, including simulation of surface pollution over the United States (Drury et al., 2010; Ford and Heald, 2013; Heald et al., 2012; Leibensperger et al., 2012; Marais et al., 2016; Zhang et al., 2012), Asia (Koplitz et al., 2016; Lin et al., 2014), Europe (Protonotariou et al., 2013; Veefkind et al., 2011), and Africa (Lacey et al., 2017; Marais et al., 2014a, 2014b, 2019; Marais and Wiedinmyer, 2016). The model has also been applied to previous studies quantifying the global burden of disease from particulate matter from all sources (Brauer et al., 2016; Cohen et al., 2017).

In this analysis we used GEOS-Chem with fossil fuel emissions from multiple sectors (power generation, industry, ships, aircraft, ground transportation, backup generators, kerosene, oil/gas extraction), detailed oxidant-aerosol chemistry, and reanalysis meteorology from the NASA Global Modeling and Assimilation Office. Fossil fuel emissions are from regional inventories where these are available for the US, Europe, Asia, and Africa, and from global inventories everywhere else (such as Mexico, Australia, South America and Canada). More details of the specific fossil fuel inventories used in GEOS-Chem are in Table S1. Global-scale simulations in GEOS-Chem were carried out on a coarse spatial grid (2 ° × 2.5 °, about 200 km × 250 km). Four regional simulations were also performed at fine spatial scale (0.5 ° × 0.67 °, about 50 km × 60 km) for North America, Europe, Asia, and Africa using boundary conditions from the global model. The regional simulations allow for a better match with the spatial distribution of population, thus enhancing the accuracy of the estimates of health impacts. All simulations were set up to replicate 2012 pollution conditions. As described in the Supplemental Material, we find that globally, GEOS-Chem captures observed annual mean $PM_{2.5}$ concentrations with a spatial correlation of 0.70 and mean absolute error of 3.4 μg m^{-3}, values which compare well with those from other models (Shindell et al., 2018; Xing et al., 2015). We performed two sets of simulations: one set with fossil fuel emissions turned on and the other with such emissions turned off. We then assumed that the difference between the two sets of simulations represents the contribution of fossil fuel combustion to surface $PM_{2.5}$. More information on our choice of GEOS-Chem, the model setup, details of relevant anthropogenic emissions, and model validation is described in the Supplemental material.

2.2. Population and health data

We used population data from the Center for International Earth Science Information Network (CIESIN) (CIESIN, 2018). The Gridded Population of the World, Version 4 Revision 11 (GPWv4.11) is gridded with an output resolution of 30 arc-seconds (approximately 1 km at the equator). Since the population data are provided only at five-year intervals, we applied 2015 population statistics to the results of our 2012 GEOS-Chem simulation. CIESIN population data was then aggregated to the spatial scale of the model for the exposure estimates. Country/region level data on baseline mortality rates were from GBD data for 2015 (based on the 2017 iteration) (IHME, 2017). USA state-specific mortality rates were obtained from the CDC Wide-ranging Online Data for Epidemiologic Research (WONDER) compressed mortality files (CDC, 2016). Canada death estimates by province were obtained from Statistics Canada, CANSIM (Canada, 2018).

2.3. $PM_{2.5}$ mortality concentration –response model

The risk of air pollution to health in a population is usually estimated by applying a concentration–response function (CRF), which is typically based on Relative Risk (RR) estimates derived from epidemiological studies. CRFs are necessary elements for the quantification of health impacts due to air pollution and require regular evaluation and update to incorporate new developments in the literature.

Global assessments of air pollution risk often use the Integrated Exposure-Response model (IER) (Burnett et al., 2014), which combined information on $PM_{2.5}$–mortality associations from non-outdoor $PM_{2.5}$ sources, including secondhand smoke, household air pollution from use of solid fuels, and active smoking. The IER used data from active smoking and passive smoking to address the limited number of outdoor $PM_{2.5}$ epidemiologic studies at $PM_{2.5}$ > 40 μg m^{-3} available at the time.

The IER formed the basis of the estimates of disease burden attributable to $PM_{2.5}$ (e.g., 4 million deaths in 2015 in GBD, 2015). This function was then updated in 2018 using the Global Exposure Mortality Model (GEMM). In GEMM, data from 41 epidemiological cohort studies were applied (Burnett et al., 2018). Independently conducted analyses were conducted on 15 of these cohorts to characterize the shapes of $PM_{2.5}$–mortality associations in each cohort, using a specified functional form of the CRF. For the remaining 26 cohorts, the concentration-response was examined with a linear concentration hazard ratio model. A recent meta-analysis of the association between long-term $PM_{2.5}$ and mortality (Vodonos et al., 2018) applied techniques involving flexible penalized spline CRF in a multivariate random effects and meta-regression model. This approach allows the data to specify the shape of the CRF. The meta-regression pooled 135 estimates from 53 studies examining long-term $PM_{2.5}$ and mortality of cohorts aged 15 years and older. The estimate of the confidence intervals about the CRF includes a random variance component. This meta-analysis provided evidence of a nonlinear association between $PM_{2.5}$ exposure and mortality in which the exposure-mortality slopes decreases at higher concentrations (Figure S5 in Supplemental Material). We have chosen to use the dose-response function from the meta-analysis rather than the GEMM function as the meta-regression approach is more flexible and does not constrain the CRF to a specific functional form, it incorporates a random variance component in estimating the uncertainty around that curve, it is derived with more studies than previous approaches, and its estimates at high and low exposures are closer to the estimates in cohorts restricted to only very high and very low exposures. To ensure consistency with the concentration-response curve, premature mortality rates for the portion of the population >14 years of age were determined using the population and baseline mortality rates for different age groups from GBD data for 2015.

2.4. Health impact calculations

We estimated the number of premature deaths attributable to fossil fuel $PM_{2.5}$ using: (1) GEOS-Chem $PM_{2.5}$ estimated with all emission sources and GEOS-Chem $PM_{2.5}$ estimated without fossil fuel emissions, as a comparison against the first simulation, (2) total population above the age of 14 gridded to the GEOS-Chem grid resolution, (3) baseline all-cause mortality rates for population above the age of 14 (per country or per state in the US and province in Canada), and (4) the meta-analysis CRF (Vodonos et al., 2018). All health impacts were calculated on a per-grid basis at the spatial resolution of the model. We applied the following health impact function to estimate premature mortality related to exposure to fossil fuel $PM_{2.5}$ in each GEOS-Chem grid cell:

$$\sum \Delta y = y_o * p * AF \tag{1}$$

$$AF = \frac{\exp^{(\bar{\beta}*\Delta x)} - 1}{\exp^{(\bar{\beta}*\Delta x)}} \tag{2}$$

$$\bar{\beta}(PM_{2.5}) = \int_{PM_{2.5}\,no\ \ fossil\ \ fuel}^{PM_{2.5}\,all\ \ emissions} \beta(PM_{2.5}) \tag{3}$$

where Δy is the change in the number of premature deaths due to exposure to fossil fuel $PM_{2.5}$, y_o is the country/state/province specific baseline (all-cause) mortality rate, p is the total population above the age of 14, AF is the attributable fraction of deaths (the fraction of total deaths attributable to $PM_{2.5}$ exposure), $\bar{\beta}$ is the mean estimate for long-term $PM_{2.5}$ mortality concentration-response over a range of concentrations from the penalized spline model in the recent meta-analysis, and Δx is the change in $PM_{2.5}$ concentration, calculated as the difference between GEOS-Chem $PM_{2.5}$ with all emissions and GEOS-Chem $PM_{2.5}$ without fossil fuel emissions.

For each country, we summed the change in premature deaths (Δy) in each grid cell over all grid cells in that country. To estimate the change in deaths between the two scenarios (with and without fossil fuel combustion), we computed the change in deaths in each grid cell, based on its population, baseline rate, and exposure under the two scenarios (Equation (1)). The attributable fraction (AF), or proportion of deaths estimated as due to long-term exposure to $PM_{2.5}$ fossil fuel air pollution, was calculated using the concentration-response estimate, following the form shown in Equation (2) (Figure S5 in Supplemental material). Because these estimates of mortality concentration response (β) are a nonlinear function of concentration, we used the penalized spline model predictions from this meta-analysis to integrate the concentration-specific β in each grid cell from the low $PM_{2.5}$ scenario (without fossil fuel emissions) to the high $PM_{2.5}$ scenario (with all emissions, including fossil fuel). In this way, we could calculate a mean value of β for each grid cell. There exist insufficient epidemiological data to calculate a robust health response function specific to fossil-fuel $PM_{2.5}$. GEOS-Chem is a deterministic model. Therefore, our 95% confidence intervals (CI) for our estimates reflect only the 95% CI for the concentration response function.

2.5. Secondary analysis among children <5 years old

Lower respiratory infections (LRI), including pneumonia and bronchiolitis of bacterial and viral origin, are the largest single cause of mortality among young children worldwide and thus account for a significant global burden of disease worldwide (Nair et al., 2010). As mentioned previously, young children are more susceptible to the adverse effects of particulate air pollution than adults. Mehta et al. (2013) estimated the overall impact of $PM_{2.5}$ concentration with Relative Risk (RR) of 1.12 for LRI mortality per 10 $\mu g\ m^{-3}$ increase in annual average $PM_{2.5}$ concentration, as compared to RR of 1.04 for respiratory mortality among adults (Vodonos et al., 2018). We estimated the number of premature deaths attributable to $PM_{2.5}$ among children under the age of 5 years due to a range of LRI classifications (ICD-10, International Classification of Diseases codes: A48.1, A70, J09-J15.8, J16-J16.9, J20-J21.9, P23.0-P23.4). Baseline numbers of deaths due to LRI were obtained from the GBD for 2015 (IHME, 2017). We used the Relative Risk (RR) of 1.12 (1.03–1.30) for LRI occurrence per 10 $\mu g\ m^{-3}$ increase in annual average $PM_{2.5}$ concentration (Mehta et al., 2013). Studies of longer-term exposure of $PM_{2.5}$ and LRI in that meta-analysis were conducted in only a few developed countries with relatively low levels of annual mean $PM_{2.5}$ (<25 $\mu g\ m^{-3}$), specifically the Netherlands, Czech Republic, Germany, Canada and USA. We therefore calculated the number of premature LRI deaths attributable to $PM_{2.5}$ only in North America, South America, and Europe.

3. Results

3.1. Impact of fossil fuel use on $PM_{2.5}$

Fig. 1 shows the difference between global GEOS-Chem $PM_{2.5}$ with and without fossil fuel emissions, plotted as the annual mean for 2012. Results show large contributions of 50–100 $\mu g\ m^{-3}$ in $PM_{2.5}$ over China and India, with smaller increments of 10–50 $\mu g\ m^{-3}$ over large swaths of the United States and Europe, industrialized countries in Africa (South Africa and Nigeria), and along the North African coastline due to European pollution.

3.2. Global assessment of mortality attributable to $PM_{2.5}$

Based on the annual $PM_{2.5}$ simulation with and without global fossil fuel emissions, we estimated the excess deaths and attributable fraction (AF %) for the population above 14 years old. Fig. 2 shows the simulated annual global premature mortality due to exposure to ambient $PM_{2.5}$ from fossil fuel emissions. Greatest mortality is simulated over regions with substantial influence of fossil-fuel related $PM_{2.5}$, notably parts of

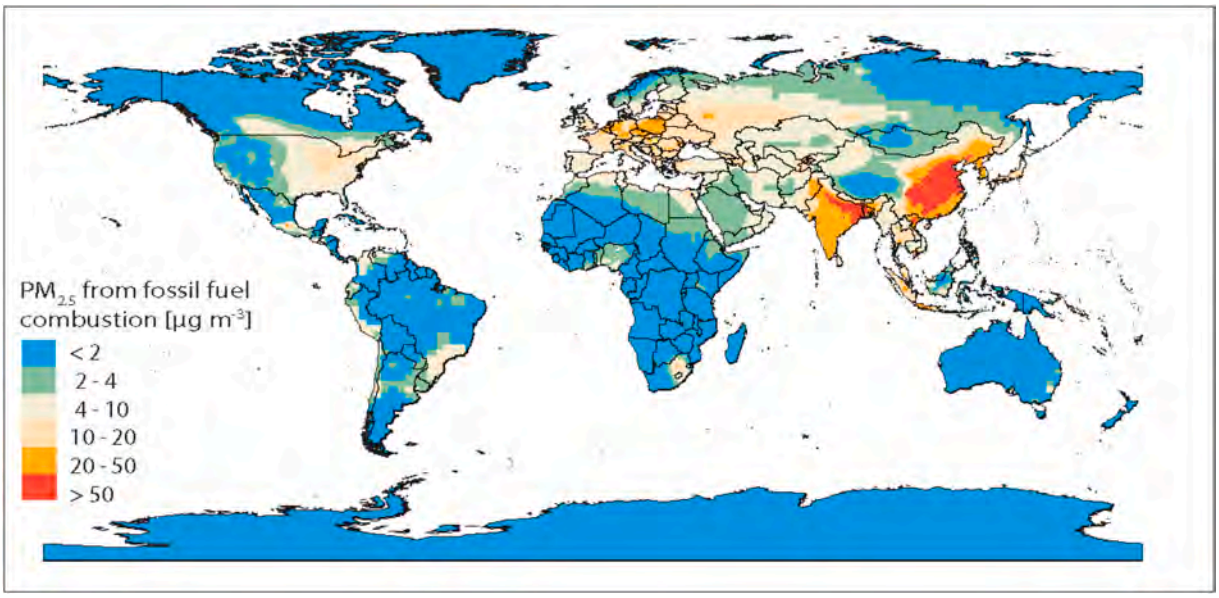

Fig. 1. Contribution of fossil fuel combustion to surface $PM_{2.5}$, as calculated by the chemical transport model GEOS-Chem. The plot shows the difference in surface $PM_{2.5}$ concentrations from GEOS-Chem with and without fossil fuel emissions.

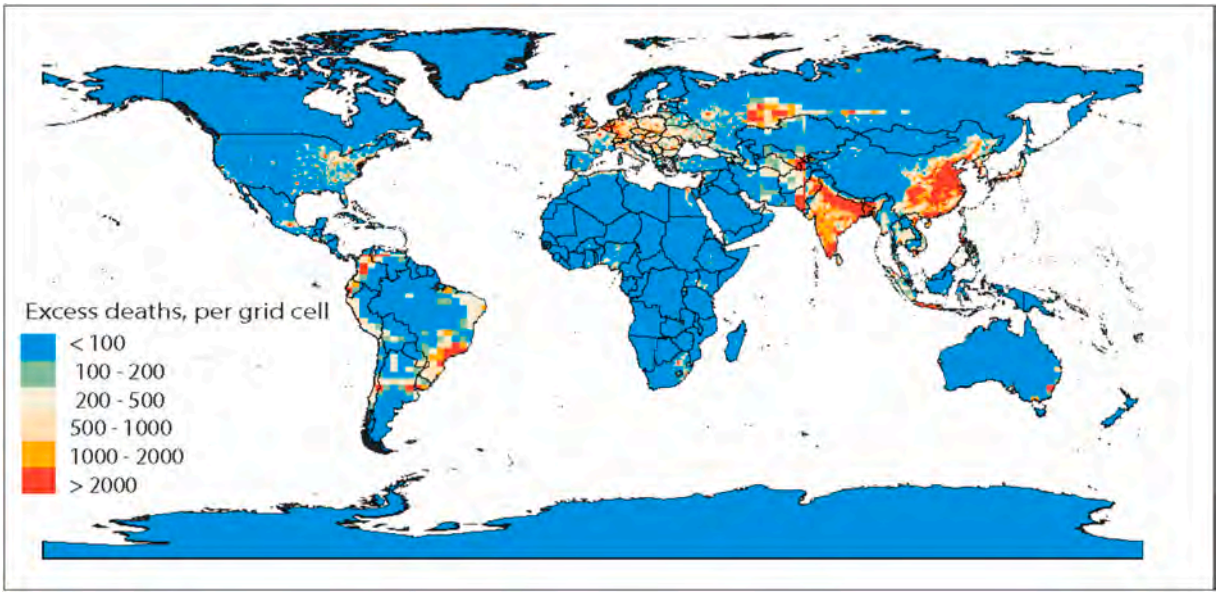

Fig. 2. Estimated annual excess deaths due to exposure to ambient $PM_{2.5}$ generated by fossil fuel combustion.

Eastern North America, western Europe, and South-East Asia.

We estimated a total global annual burden premature mortality due to fossil fuel combustion in 2012 of 10.2 million (95% CI: −47.1 to 17.0 million). Table 1 reports the baseline number of deaths for people >14 years old, the annual $PM_{2.5}$ simulation with and without global fossil fuel emissions, the estimated excess deaths, and the attributable fraction for the populated continents. As shown in Table 1, we calculated 483,000 premature deaths in North America (95% CI: 284,000–670,000), 187,000 deaths in South America (95% CI: 107,000–263,000), 1,447,000 deaths in Europe (95% CI: 896,000–1,952,000), 7,916,000 deaths in Asia (95% CI: −48,106,000 to 13,622,000), and 194,000 deaths in Africa (95% CI: −237,000 to 457,000). The wide confidence intervals in Asia and Africa are due to the lack of data for areas where the exposure remains outside the range of the concentration response curve ($PM_{2.5}$ > 50 μg m^{-3}; Figure S5). The population-weighted pollution concentrations presented in Table 1 are higher than the average $PM_{2.5}$ concentrations for each country, since fossil-fuel $PM_{2.5}$ is mainly emitted in populous areas. The two countries with the highest premature mortality are China with 3.91 million and India with 2.46 million. Supplemental Table S2 provides extended data of the health impact calculations for each country. For comparison, Table 1 also reports the number of premature deaths attributable to fossil fuel $PM_{2.5}$ when the GEMM function is applied to the GEOS-Chem output. For most regions, the number of premature deaths calculated with GEMM is significantly lower than that calculated with the new function from Vodonos et al. (2018). Globally, the GEMM function yields 6.7 million deaths in 2012 due to fossil fuel combustion.

3.3. Assessment of children (under the age of 5) LRI mortality attributable to $PM_{2.5}$

We estimated the number of premature deaths attributable to $PM_{2.5}$

Table 1
Number of deaths attributable to exposure to fine particulate matter ($PM_{2.5}$) generated by fossil fuel combustion for the population >14 years old.

GEOS-Chem spatial grid resolution[a]	Region[b]		Total deaths >14 years old, in thousands	Population-weighted annual mean $PM_{2.5}$ concentration, μg m^{-3}			Mean attributable fraction of deaths, % (95% CI)[d]	Deaths attributable to fossil-fuel related $PM_{2.5}$, in thousands (95% CI)[c]	GEMM function deaths attributable to fossil-fuel related $PM_{2.5}$, in thousands (95% CI)[e]
				$PM_{2.5}$ from all emission sources	$PM_{2.5}$ without fossil fuel	Estimated $PM_{2.5}$ from fossil fuel, %			
Fine	North America	Central America & the Caribbean	1148	10.06	3.03	7.03 (69.9)	8.2 (4.5–11.6)	94 (52–133)	80 (62–98)
		USA	2705	11.81	2.15	9.66 (81.8)	13.1 (7.8–18.1)	355 (212–490)	305 (233–375)
		Canada	250	12.01	1.76	10.25 (85.4)	13.6 (8.0–18.7)	34 (20–47)	28 (22–35)
Coarse	South America		2389	8.66	3.02	5.65 (65.2)	7.8 (4.5–11.0)	187 (107–263)	159 (121–195)
Fine	Europe		8626	19.22	4.68	14.54 (75.7)	16.8 (10.4–22.6)	1447 (896–1952)	1033 (798–1254)
Fine	Asia	Eastern Asia	25,468	51.72	8.68	43.05 (83.2)	30.7 (−189.1-52.9)	7821 (−48,150–13,478)	4945 (3943–5826)
Coarse		Western Asia & the Middle East	1456	26.95	20.73	6.22 (23.1)	6.5 (3.0–9.9)	95 (44–144)	54 (43–65)
Fine	Africa		5274	32.98	28.98	4.00 (12.1)	3.7 (−4.5-8.7)	194 (-237-457)	102 (81–121)
Coarse	Australia & Oceania		189	4.17	2.19	1.98 (47.4)	3.2 (1.6–4.8)	6.0 (2.9–9.0)	6.4 (4.8–7.9)
	Global		47,506	38.01	11.14	26.87 (70.7)	21.5 (−99.0-35.7)	10,235 (−47,054–16,972)	6713 (5308–7976)

[a] Fine spatial scale is 0.5 ° × 0.67 °, or about 50 km × 60 km. Coarse spatial scale is 2 ° × 2.5 °, or about 200 km × 250 km.
[b] List of countries for each region and subregion is provided in supplemental Table S2.
[c] Annual number of deaths attributable to long-term exposure to $PM_{2.5}$ derived from fossil fuel combustion. CI is the confidence interval.
[d] Mean proportion of all deaths which can be attributed to long-term exposure to $PM_{2.5}$ generated by fossil fuel combustion, averaged over the country or region. CI; confidence interval.
[e] Attributable deaths calculated with the Global Exposure Mortality Model (GEMM) concentration-response function.[44].

among children under the age of 5 due to LRI only for those countries or regions with levels of annual $PM_{2.5}$ concentrations below 25 μg m^{-3}. These include North America, South America, and Europe. Based on the annual $PM_{2.5}$ simulation with and without fossil fuel emissions, we calculated 876 excess deaths due to LRI in North and Central America, 747 in South America, and 605 in Europe (Table 2). Using the GBD estimate of total deaths due to LRI (Institute for Health Metrics and Evaluation), we estimate that $PM_{2.5}$ from fossil fuel combustion accounted on average for 7.2% of LRI mortality among children under the age of 5 in these regions, with the largest proportion of 13.6% in Europe (95% CI -0.4 to 25.3%).

Table 2
Number of deaths due to lower respiratory infection (LRI) attributable to exposure to fine particulate matter ($PM_{2.5}$) from fossil fuel combustion for the population <5 years old.

Region	Total deaths for children <5 years old due to LRI	LRI deaths attributable to fossil-fuel $PM_{2.5}$ (95% CI)[a]	Mean attributable fraction of deaths, % (95% CI)[b]
North America	**13,230**	**876 (-26-1657)**	**6.6 (−0.2-12.5)**
Central America & the Caribbean	12,507	802 (-23-1516)	6.4 (−0.2-12.1)
USA	672	69 (-2-131)	10.2 (−0.3-19.5)
Canada	50	5 (0–10)	10.8 (−0.3-20.5)
South America	**13,231**	**747 (-21–1443)**	**5.7 (-0.2–10.9)**
Europe	**4446**	**605 (-18–1126)**	**13.6 (-0.4–25.3)**

[a] Annual number of deaths attributed to long-term exposure to $PM_{2.5}$ derived from fossil fuel combustion.
[b] Mean proportion of deaths due to long-term exposure to $PM_{2.5}$ generated by fossil fuel combustion. CI is the confidence interval.

4. Discussion

We used the chemical transport model GEOS-Chem to quantify the global mortality attributed to $PM_{2.5}$ air pollution from fossil fuel combustion. Using the updated concentration response relationship between relative mortality and airborne $PM_{2.5}$, we estimated global premature mortality in 2012 of 10.2 million per year from fossil fuel combustion alone. China has the highest burden of 3.91 million per year, followed by India with 2.46 million per year. These estimates carry large uncertainty (e.g., 95% CI of −47.1 to 17.0 million for the global estimate) from the concentration-response curve, as it is an improved function that provides a more realistic picture of the health consequences of $PM_{2.5}$ compared to previous studies.

Our estimate is for the year when fossil fuel emissions in China peaked and so predates large and dramatic reductions in fossil fuel emissions due to strict mitigation measures. These reductions led to a 30–50% decline in annual mean $PM_{2.5}$ across the country from 2013 to 2018 (Zhai et al., 2019). If we apply a 43.7% reduction in GEOS-Chem $PM_{2.5}$ concentrations from the simulation with all emission sources, premature mortality in China decreases from 3.91 million to 2.36 million. India has recently imposed controls on pollution sources, but there is not yet evidence of air quality improvements in densely populated cities like Delhi (Vohra et al., 2020). Consideration of the 2012–2018 decrease in $PM_{2.5}$ exposure in China reduces the total global premature mortality due to fossil fuel $PM_{2.5}$ from 10.2 million premature deaths each year to 8.7 (95% CI: −1.8 to 14.0) million.

In 2012, the population-weighted $PM_{2.5}$ is 72.8 μg m^{-3} for China and 52.0 μg m^{-3} for India from all sources and 9.9 μg m^{-3} for China and 9.0 μg m^{-3} for India without fossil fuel emissions. The low value of non-fossil fuel $PM_{2.5}$ is reasonable for southern India (Dey et al., 2012) but may be an underestimate in the Indo-Gangetic Plain where crop residue burning contributes to high levels of $PM_{2.5}$ (100–200 μg m^{-3}) during the post-monsoon season (Ojha et al., 2020). An increase in the concentration of non-fossil-fuel $PM_{2.5}$ would decrease our estimate of the number of premature deaths due to fossil fuel $PM_{2.5}$ in India and China, as this would decrease the risk of premature mortality with a unit change in

$PM_{2.5}$ (Figure S5).

4.1. Comparison with previous estimates of global mortality attributable to outdoor $PM_{2.5}$

Previous estimates of the GBD for 2015 suggest that exposure to total $PM_{2.5}$ causes 4.2 million deaths (Cohen et al., 2017), whereas here we estimate more than double (10.2 million) the number of premature deaths from fossil fuel combustion alone in 2012. Differences between the current study and the 2015 GBD lower estimates are related mainly to the choice of the shape of the concentration-response function and the relative risk estimate. First, to provide information about exposure response at higher concentrations, the 2015 GBD study used the integrated exposure–response (IER) model in which active and second-hand smoking exposures were converted to estimated annual $PM_{2.5}$ exposure equivalents using inhaled doses of particle mass (Burnett et al., 2014). Recent cohort studies from Asia indicate that this substantially underestimates the CRF at high concentrations. In contrast, in the current study we applied a CRF that was directly estimated from $PM_{2.5}$ studies alone, as described in a recent meta-analysis that included estimates from studies in countries like China with higher $PM_{2.5}$ concentrations than are included in previous derivations of CRFs (Vodonos et al., 2018). The CRF from this recent meta-analysis flattens out at higher concentrations, as does the IER curve. However, this flattening is not as great as in the IER, as Asian cohort studies at high $PM_{2.5}$ concentrations report larger effects than would be expected from the IER. Hence estimates of the global attributable fraction of deaths due to air pollution using the function from the recent meta-analysis are higher than the estimates using the IER function. In addition, at much lower concentrations (<10 $\mu g\ m^{-3}$), we applied higher slopes than assumed in the IER function. Recent studies at very low concentrations similarly show that the IER underestimated effects in this range (Pinault et al., 2016). Since GEOS-Chem estimated quite low concentrations in developed countries in Europe and North America, the number of premature deaths from $PM_{2.5}$ in these countries is greater than previous estimates.

Following an approach similar to the recent meta-analysis (Vodonos et al., 2018), Burnett et al. (2018) modeled the shape of the association between $PM_{2.5}$ and non-accidental mortality using data from 41 cohorts from 16 countries with GEMM. In that study, the uncertainty in a subset (15 cohorts) was characterized in the shape of the concentration-response parameter by calculating the Shape-Constrained Health Impact Function, a prespecified functional form. These estimated shapes varied across the cohorts included in the function. GEMM predicted 8.9 million (95% CI: 7.5–10.3) deaths in 2015 attributable to long-term exposure to $PM_{2.5}$ from all sources; 120% higher excess deaths than previous estimates, but still lower than our estimate of mortality from exposure to fossil-fuel derived $PM_{2.5}$ for 2012. Lelieveld et al. (2019) estimated the global and regional mortality burden of fossil fuel attributable $PM_{2.5}$ by applying the GEMM CRF to a global chemistry-climate model that is overall coarser (~1.9° latitude and longitude) than the model used in this work. The authors reported 3.61 million deaths per year attributable to pollution from fossil fuel combustion and 5.55 million deaths per year due to pollution from all anthropogenic sources. The estimated deaths from fossil fuel combustion are much lower than those in the current study for several reasons. First, the meta-analysis function used in our work includes 135 coefficients of all-cause mortality for adults aged 14–64 years old, together with cause-specific mortality and all-cause mortality among adults aged 65 and older, thus incorporating many more studies in a meta-regression framework than the 41 cohorts and coefficients in the GEMM function. Second, the approach used to estimate the CRF in Vodonos et al. (2018) allows for additional flexibility in the shape of the function because of its use of penalized splines. In contrast, the GEMM pooled CRF integrates a set of 26 log-linear functions and 15 functions characterized by three parameters governing the shape of the function. Third, while Cohen et al. (2017), Lelieveld et al. (2019) and Burnett et al. (2018) accounted for mortality from five specific causes (ischemic heart disease, stroke, chronic obstructive pulmonary disease, lung cancer and acute respiratory infections), in the current analysis we estimated changes in deaths from all causes. Fourth, some of the difference in the mortality estimates may come from differences in the age range. Our approach considers a wider population age range of over 14 years old (Vodonos et al., 2018) compared to the other studies, which considered a population age range of over 25 years (Burnett et al., 2018; Cohen et al., 2017; Lelieveld et al., 2019). Our approach has wider age range since the age range for the studies in the meta-analysis (Vodonos et al., 2018) included people younger than 25 years old (Hart et al., 2011; Pinault et al., 2016). Finally, the finer spatial resolution that GEOS-Chem utilizes over much of the globe improves co-location of PM hotspots and population centers, yielding higher estimates of excess mortality compared to Lelieveld et al. (2019).

4.2. Limitations

There are a number of limitations that must be acknowledged. First, vulnerability to $PM_{2.5}$ exposure may vary by population characteristics such as ethnicity, socio-economic status (SES), risk behaviors such as smoking and underlying comorbidities (Krewski et al., 2000; Pope et al., 2004; Wang et al., 2017) and by different exposure characteristics. We were limited in our ability to undertake a comprehensive analysis of factors influencing the association between $PM_{2.5}$ and mortality since the global mortality data were not available by detailed age, ethnicity, SES, lifestyle, and underlying disease strata. In addition, the 95% CI of our estimates reflect the lower and upper bound of the CRF, which flattens out at higher concentrations. Regions with very high concentrations (>50 $\mu g\ m^{-3}$) are beyond the data range in the meta-analysis; thus, the lower limit of the CI for those regions (China, West and North Africa; Table 1) are much less than zero. Second, for LRI in children, we have restricted our analysis to developed countries with annual $PM_{2.5} < 25\ \mu g\ m^{-3}$, in accordance with the geographical locations of the studies included in the meta-analysis by Mehta et al. (2013). Developing countries have much higher LRI mortality rates, and this restriction doubtless results in an underestimate. Finally, GEOS-Chem estimates of $PM_{2.5}$ concentrations almost certainly contains errors in estimates of emissions of pollution precursors, meteorological effects on air quality, and representation of the complex physical and chemical formation pathways. In the absence of systematic bias, such model error may not produce large aggregate errors in the mortality burden of $PM_{2.5}$, but bias may be present as well. In any event, it is challenging to estimate the true size of this error.

5. Conclusions

The effects of CO_2-driven climate change on human health and welfare are complex, ranging from greater incidence of extreme weather events, more frequent storm-surge flooding, and increased risk of crop failure (Duffy et al., 2019). One consequence of increasing reliance on fossil fuel as an energy source that has thus far received comparatively little attention is the potential health impact of the pollutants co-emitted with the greenhouse gas CO_2. Such pollutants include $PM_{2.5}$ and the gas-phase precursors of $PM_{2.5}$. This study demonstrates that the fossil fuel component of $PM_{2.5}$ contributes a large global mortality burden. By quantifying this sometimes overlooked health consequence of fossil fuel combustion, a clear message is sent to policymakers and stakeholders of the co-benefits of a transition to alternative energy sources.

Author contribution

K. Vohra and A. Vodonos carried out the health impact calculations guided by J. Schwartz. E. A. Marais and M. P. Sulprizio performed GEOS-Chem simulations. L. J. Mickley oversaw the project. All authors contributed to writing the manuscript.

Data availability

GEOS-Chem code and output are available at the GEOS-Chem website (http://acmg.seas.harvard.edu/geos_chem.html) and upon request.

Declaration of competing interest

The authors declare that they have no known competing financial interests or personal relationships that could have appeared to influence the work reported in this paper.

Acknowledgments

This study was funded by the Wallace Global Fund, the Environment and Health Fund (EHF) Israel, and a University of Birmingham Global Challenges Fund PhD studentship awarded to KV. This publication was made possible by USEPA grant RD-835872. Its contents are solely the responsibility of the grantee and do not necessarily represent the official views of the USEPA. Further, USEPA does not endorse the purchase of any commercial products or services mentioned in the publication.

Appendix A. Supplementary data

Supplementary data to this article can be found online at https://doi.org/10.1016/j.envres.2021.110754.

References

Apte, J.S., Marshall, J.D., Cohen, A.J., et al., 2015. Addressing global mortality from ambient $PM_{2.5}$. Environ. Sci. Technol. 49, 8057–8066. https://doi.org/10.1021/acs.est.5b01236.

Atkinson, R.W., Butland, B.K., Dimitroulopoulou, C., et al., 2016. Long-term exposure to ambient ozone and mortality: a quantitative systematic review and meta-analysis of evidence from cohort studies. Bmj Open 6. https://doi.org/10.1136/bmjopen-2015-009493.

Bateson, T.F., Schwartz, J., 2008. Children's response to air pollutants. J. Toxicol. Environ. Health A 71, 238–243. https://doi.org/10.1080/15287390701598234.

Brauer, M., Freedman, G., Frostad, J., et al., 2016. Ambient air pollution exposure estimation for the global burden of disease 2013. Environ. Sci. Technol. 50, 79–88. https://doi.org/10.1021/acs.est.5b03709.

Brook, R.D., Rajagopalan, S., Pope, C.A., et al., 2010. Particulate matter air pollution and cardiovascular disease an update to the scientific statement from the American heart association. Circulation 121, 2331–2378. https://doi.org/10.1161/CIR.0b013e3181dbece1.

Burnett, R., Chen, H., Szyszkowicz, M., et al., 2018. Global estimates of mortality associated with long-term exposure to outdoor fine particulate matter. P Natl Acad Sci USA 115, 9592–9597. https://doi.org/10.1073/pnas.1803222115.

Burnett, R., Pope, C.A., Ezzati, M., et al., 2014. An integrated risk function for estimating the global burden of disease attributable to ambient fine particulate matter exposure. Environ. Health Perspect. 122, 397–403. https://doi.org/10.1289/ehp.1307049.

Canada, S., 2018. Government of Canada. https://www150.statcan.gc.ca/n1/en/type/data.

CIESIN, Center for International Earth Science Information Network - Columbia University, 2018. Gridded Population of the World, Version 4 (GPWv4): Population Count Adjusted to Match 2015 Revision of UN WPP Country Totals, Revision 11. NASA Socioeconomic Data and Applications Center (SEDAC), Palisades, NY. https://doi.org/10.7927/H4PN93PB.

Cohen, A.J., Brauer, M., Burnett, R., et al., 2017. Estimates and 25-year trends of the global burden of disease attributable to ambient air pollution: an analysis of data from the Global Burden of diseases study 2015. Lancet 389, 1907–1918. https://doi.org/10.1016/S0140-6736(17)30505-6.

Dedoussi, I.C., Barrett, S.R.H., 2014. Air pollution and early deaths in the United States. Part II: attribution of $PM_{2.5}$ exposure to emissions species, time, location and sector. Atmos. Environ. 99, 610–617. https://doi.org/10.1016/j.atmosenv.2014.10.033.

Dey, S., Di Girolamo, L., van Donkelaar, A., et al., 2012. Variability of outdoor fine particulate ($PM_{2.5}$) concentration in the Indian Subcontinent: a remote sensing approach. Remote Sens. Environ. 127, 153–161. https://doi.org/10.1016/j.rse.2012.08.021.

Di, Q., Wang, Y., Zanobetti, A., et al., 2017. Air pollution and mortality in the medicare population. N. Engl. J. Med. 376, 2513–2522. https://doi.org/10.1056/NEJMoa1702747.

Drury, E., Jacob, D.J., Spurr, R.J.D., et al., 2010. Synthesis of satellite (MODIS), aircraft (ICARTT), and surface (IMPROVE, EPA-AQS, AERONET) aerosol observations over eastern North America to improve MODIS aerosol retrievals and constrain surface aerosol concentrations and sources. J. Geophys. Res. Atmos. 115 https://doi.org/10.1029/2009jd012629.

Duffy, P.B., Field, C.B., Diffenbaugh, N.S., et al., 2019. Strengthened scientific support for the Endangerment Finding for atmospheric greenhouse gases. Science 363, 597–+. https://doi.org/10.1126/science.aat5982.

Ford, B., Heald, C.L., 2013. Aerosol loading in the Southeastern United States: reconciling surface and satellite observations. Atmos. Chem. Phys. 13, 9269–9283. https://doi.org/10.5194/acp-13-9269-2013.

Forouzanfar, M.H., Afshin, A., Alexander, L.T., et al., 2016. Global, regional, and national comparative risk assessment of 79 behavioural, environmental and occupational, and metabolic risks or clusters of risks, 1990-2015: a systematic analysis for the Global Burden of Disease Study 2015. Lancet 388, 1659–1724. https://doi.org/10.1016/S0140-6736(16)31679-8.

Hart, J.E., Garshick, E., Dockery, D.W., et al., 2011. Long-term ambient multipollutant exposures and mortality. Am J Resp Crit Care 183, 73–78. https://doi.org/10.1164/rccm.200912-1903OC.

Heald, C.L., Collett, J.L., Lee, T., et al., 2012. Atmospheric ammonia and particulate inorganic nitrogen over the United States. Atmos. Chem. Phys. 12, 10295–10312. https://doi.org/10.5194/acp-12-10295-2012.

IHME, 2017. Institute for Health Metrics and Evaluation. http://ghdx.healthdata.org/gbd-results-tool.

Katanoda, K., Sobue, T., Satoh, H., et al., 2011. An association between long-term exposure to ambient air pollution and mortality from lung cancer and respiratory diseases in Japan. J. Epidemiol. 21, 132–143. https://doi.org/10.2188/jea.JE20100098.

Koplitz, S.N., Mickley, L.J., Marlier, M.E., et al., 2016. Public health impacts of the severe haze in Equatorial Asia in September-October 2015: demonstration of a new framework for informing fire management strategies to reduce downwind smoke exposure. Environ. Res. Lett. 11 https://doi.org/10.1088/1748-9326/11/9/094023.

Krewski, D., Burnett, R.T., Goldberg, M.S., et al., 2000. Special Report Reanalysis of the Harvard Six Cities Study and the American Cancer Society Study of Particulate Air Pollution and Mortality Part II: Sensitivity Analyses Appendix C. Flexible Modeling of the Effects of Fine Particles and Sulphate on Mortality. Health Effects Institute. https://www.healtheffects.org/system/files/SR-PartIIAppC.pdf.

Lacey, F.G., Marais, E.A., Henze, D.K., et al., 2017. Improving present day and future estimates of anthropogenic sectoral emissions and the resulting air quality impacts in Africa. Faraday Discuss 200, 397–412. https://doi.org/10.1039/c7fd00011a.

Leibensperger, E.M., Mickley, L.J., Jacob, D.J., et al., 2012. Climatic effects of 1950-2050 changes in US anthropogenic aerosols - Part 1: aerosol trends and radiative forcing. Atmos. Chem. Phys. 12, 3333–3348. https://doi.org/10.5194/acp-12-3333-2012.

Lelieveld, J., Klingmuller, K., Pozzer, A., et al., 2019. Effects of fossil fuel and total anthropogenic emission removal on public health and climate. P Natl Acad Sci USA 116, 7192–7197. https://doi.org/10.1073/pnas.1819989116.

Lim, S.S., Vos, T., Flaxman, A.D., et al., 2012. A comparative risk assessment of burden of disease and injury attributable to 67 risk factors and risk factor clusters in 21 regions, 1990-2010: a systematic analysis for the Global Burden of Disease Study 2010. Lancet 380, 2224–2260, 628-628, ://WOS:000315189300032.

Lin, J.T., van Donkelaar, A., Xin, J.Y., et al., 2014. Clear-sky aerosol optical depth over East China estimated from visibility measurements and chemical transport modeling. Atmos. Environ. 95, 258–267. https://doi.org/10.1016/j.atmosenv.2014.06.044.

Marais, E.A., Jacob, D.J., Guenther, A., et al., 2014a. Improved model of isoprene emissions in Africa using Ozone Monitoring Instrument (OMI) satellite observations of formaldehyde: implications for oxidants and particulate matter. Atmos. Chem. Phys. 14, 7693–7703. https://doi.org/10.5194/acp-14-7693-2014.

Marais, E.A., Jacob, D.J., Jimenez, J.L., et al., 2016. Aqueous-phase mechanism for secondary organic aerosol formation from isoprene: application to the southeast United States and co-benefit of SO_2 emission controls. Atmos. Chem. Phys. 16, 1603–1618. https://doi.org/10.5194/acp-16-1603-2016.

Marais, E.A., Jacob, D.J., Wecht, K., et al., 2014b. Anthropogenic emissions in Nigeria and implications for atmospheric ozone pollution: a view from space. Atmos. Environ. 99, 32–40. https://doi.org/10.1016/j.atmosenv.2014.09.055.

Marais, E.A., Silvern, R.F., Vodonos, A., et al., 2019. Air quality and health impact of future fossil fuel use for electricity generation and transport in Africa. Environ. Sci. Technol. 53, 13524–13534. https://doi.org/10.1021/acs.est.9b04958.

Marais, E.A., Wiedinmyer, C., 2016. Air quality impact of diffuse and inefficient combustion emissions in Africa (DICE-Africa). Environ. Sci. Technol. 50, 10739–10745. https://doi.org/10.1021/acs.est.6b02602.

Mehta, S., Shin, H., Burnett, R., et al., 2013. Ambient particulate air pollution and acute lower respiratory infections: a systematic review and implications for estimating the global burden of disease. Air Qual Atmos Hlth 6, 69–83. https://doi.org/10.1007/s11869-011-0146-3.

Nair, H., Nokes, D.J., Gessner, B.D., et al., 2010. Global burden of acute lower respiratory infections due to respiratory syncytial virus in young children: a systematic review and meta-analysis. Lancet 375, 1545–1555. https://doi.org/10.1016/S0140-6736(10)60206-1.

Ojha, N., Sharma, A., Kumar, M., et al., 2020. On the widespread enhancement in fine particulate matter across the Indo-Gangetic Plain towards winter. Sci Rep-Uk 10. https://doi.org/10.1038/s41598-020-62710-8.

Perera, F., 2018. Pollution from fossil-fuel combustion is the leading environmental threat to global pediatric health and equity: solutions exist. Int. J. Environ. Res. Publ. Health 15. https://doi.org/10.3390/ijerph15010016.

Pinault, L., Tjepkema, M., Crouse, D.L., et al., 2016. Risk estimates of mortality attributed to low concentrations of ambient fine particulate matter in the Canadian community health survey cohort. Environ Health-Glob 15. https://doi.org/10.1186/s12940-016-0111-6.

Pope, C.A., Burnett, R.T., Thurston, G.D., et al., 2004. Cardiovascular mortality and long-term exposure to particulate air pollution - epidemiological evidence of general

pathophysiological pathways of disease. Circulation 109, 71–77. https://doi.org/10.1161/01.Cir.0000108927.80044.7f.

Protonotariou, A.P., Bossioli, E., Tombrou, M., et al., 2013. Air Pollution in Eastern Mediterranean: Nested-Grid GEOS-CHEM Model Results and Airborne Observations. Advances in Meteorology, Climatology and Atmospheric Physics. Springer Atmospheric Sciences, Springer, Berlin, Heidelberg, pp. 1203–1209.

Shaddick, G., Thomas, M.L., Green, A., et al., 2018. Data integration model for air quality: a hierarchical approach to the global estimation of exposures to ambient air pollution. J R Stat Soc C-Appl 67, 231–253. https://doi.org/10.1111/rssc.12227.

Shindell, D., Faluvegi, G., Seltzer, K., et al., 2018. Quantified, localized health benefits of accelerated carbon dioxide emissions reductions. Nat. Clim. Change 8. https://doi.org/10.1038/s41558-018-0108-y.

Tseng, E., Ho, W.C., Lin, M.H., et al., 2015. Chronic exposure to particulate matter and risk of cardiovascular mortality: cohort study from Taiwan. BMC Publ. Health 15. https://doi.org/10.1186/s12889-015-2272-6.

Ueda, K., Nagasawa, S., Nitta, H., et al., 2012. Exposure to particulate matter and long-term risk of cardiovascular mortality in Japan: NIPPON DATA80. J. Atherosclerosis Thromb. 19, 246–254. https://doi.org/10.5551/jat.9506.

Veefkind, J.P., Boersma, K.F., Wang, J., et al., 2011. Global satellite analysis of the relation between aerosols and short-lived trace gases. Atmos. Chem. Phys. 11, 1255–1267. https://doi.org/10.5194/acp-11-1255-2011.

Vodonos, A., Abu Awad, Y., Schwartz, J., 2018. The concentration-response between long-term $PM_{2.5}$ exposure and mortality; A meta-regression approach. Environ. Res. 166, 677–689. https://doi.org/10.1016/j.envres.2018.06.021.

Vohra, K., Marais, E.A., Suckra, S., et al., 2020. Long-term trends in air quality in major cities in the UK and India: a view from space. Atmos. Chem. Phys. Discuss. https://doi.org/10.5194/acp-2020-342.

Wang, Y., Shi, L.H., Lee, M., et al., 2017. Long-term exposure to $PM_{2.5}$ and mortality among older adults in the southeastern US. Epidemiology 28, 207–214. https://doi.org/10.1097/Ede.0000000000000614.

WHO, World Health Organization, 2006. Principles for Evaluating Health Risks in Children Associated with Exposure to Chemicals. https://apps.who.int/iris/handle/10665/43604.

WHO, World Health Organization, 2016. Ambient Air Pollution: A Global Assessment of Exposure and Burden of Disease. https://www.who.int/phe/publications/air-pollution-global-assessment/en/.

Wong, C.M., Lai, H.K., Tsang, H., et al., 2015. Satellite-based estimates of long-term exposure to fine particles and association with mortality in elderly Hong Kong residents. Environ. Health Perspect. 123, 1167–1172. https://doi.org/10.1289/ehp.1408264.

Wong, C.M., Tsang, H., Lai, H.K., et al., 2016. Cancer mortality risks from long-term exposure to ambient fine particle. Cancer Epidem Biomar 25, 839–845. https://doi.org/10.1158/1055-9965.Epi-15-0626.

Xing, J., Mathur, R., Pleim, J., et al., 2015. Can a coupled meteorology-chemistry model reproduce the historical trend in aerosol direct radiative effects over the Northern Hemisphere? Atmos. Chem. Phys. 15, 9997–10018. https://doi.org/10.5194/acp-15-9997-2015.

Xu, Z.W., Sheffield, P.E., Hu, W.B., et al., 2012. Climate change and children's health-A call for Research on what works to protect children. Int. J. Environ. Res. Publ. Health 9, 3298–3316. https://doi.org/10.3390/ijerph9093298.

Yin, P., Brauer, M., Cohen, A., et al., 2017. Long-term fine particulate matter exposure and nonaccidental and cause-specific mortality in a large national cohort of Chinese men. Environ. Health Perspect. 125 https://doi.org/10.1289/Ehp1673.

Zhai, S.X., Jacob, D.J., Wang, X., et al., 2019. Fine particulate matter ($PM_{2.5}$) trends in China, 2013-2018: separating contributions from anthropogenic emissions and meteorology. Atmos. Chem. Phys. 19, 11031–11041. https://doi.org/10.5194/acp-19-11031-2019.

Zhang, L., Jacob, D.J., Knipping, E.M., et al., 2012. Nitrogen deposition to the United States: distribution, sources, and processes. Atmos. Chem. Phys. 12, 4539–4554. https://doi.org/10.5194/acp-12-4539-2012.

CDC, 2016. Centers for Disease Control and Prevention Wide-ranging ONline Data for Epidemiologic Research https://www.cdc.gov/nchs/data/nvsr/nvsr64/nvsr64_02.pdf.